Regional scale impacts of changing anthropogenic emissions on aerosols

Author(s):
Knote, Christoph

Publication Date:
2012

Permanent Link:

https://doi.org/10.3929/ethz-a-007179320 →

Diss. ETH No. 20227

Regional scale impacts of changing anthropogenic emissions on aerosols

A dissertation submitted to
ETH ZURICH

for the degree of
Doctor of Sciences

presented by
CHRISTOPH KNOTE
Dipl. Umweltwiss., Univ. Trier
born 13 January 1981
citizen of Germany

accepted on the recommendation of
Prof. Dr. Ulrike Lohmann, examiner
Dr. Dominik Brunner, co-examiner
Dr. Martijn Schaap, co-examiner

2012

Contents

Abstract **v**

Zusammenfassung **vii**

1 Introduction: aerosols in the troposphere **1**
1.1 Tropospheric chemistry . . . 1
1.2 Atmospheric aerosols . . . 6
1.3 3D numerical modeling of atmospheric aerosols . . . 20
1.4 Dissertation overview . . . 31

2 Towards an online-coupled regional chemistry climate model: evaluation of trace gases and aerosols in COSMO-ART **33**
2.1 Abstract . . . 34
2.2 Introduction . . . 34
2.3 Methods . . . 36
2.4 Evaluation . . . 41
2.5 Discussion of aerosol characteristics . . . 60
2.6 Conclusions . . . 63
2.7 Appendix: INT2COSMO-ART . . . 64
2.8 Appendix: transmission functions . . . 65
2.9 Acknowledgements . . . 65

3 An advanced scheme for wet scavenging and liquid-phase chemistry in a regional online-coupled chemistry transport model **67**
3.1 Abstract . . . 67
3.2 Introduction . . . 68
3.3 Methods . . . 69
3.4 Idealized 2D simulations . . . 74
3.5 Realistic application . . . 75
3.6 Limitations of the current implementation . . . 85
3.7 Comparison with other model systems . . . 85
3.8 Computational demand . . . 86
3.9 Conclusions . . . 86
3.10 Acknowledgments . . . 87

4 Contributions of different emission reductions to changes in aerosol chemical composition in Europe within the last two decades **89**
4.1 Introduction . . . 89
4.2 Methods . . . 90
4.3 Trend estimation from measurements and reported emissions . . . 93

4.4 Contributions of changes in different precursor emissions to observed trends 97
4.5 Conclusions 107
4.6 Acknowledgments 108

5 Summary and outlook **109**
5.1 Summary 109
5.2 Future work 110

A Supplement to 'Towards an online-coupled regional chemistry climate model: evaluation of trace gases and aerosols in COSMO-ART' (Chapter 2) **111**

B Emissions preprocessor documentation **117**
B.1 Introduction 117
B.2 Description of input data 117
B.3 Description of the modeling system 118
B.4 Emissions preprocessor 118
B.5 Usage and output 121

C INT2COSMO-ART documentation **125**
C.1 Introduction 125
C.2 Methods 125
C.3 Data format 127
C.4 Usage 127
C.5 Memory considerations 129
C.6 Combining multiple datasets 130
C.7 External parameters 131
C.8 Output files 132

Curriculum vitae **163**

Acknowledgments **165**

Abstract

Man-made emissions of air pollutants and their precursors have decreased substantially in Europe over the last decades, owing to emission reduction measures as part of programs to reduce air pollution and the anthropogenic contribution to climate change. The reactions of the atmospheric system to such measures are complex, non-linear, sometimes counter-intuitive and still not fully understood. Dynamics, radiation, clouds, trace gases, and particles interact in numerous ways, which makes estimates on the outcome of a certain measure difficult. Besides gaseous pollutants, particles in the atmosphere are a major concern. They are a health issue, lead to acidification and eutrophication of the environment, and interact with the climate system through their influence on radiation and clouds. Therefore, aerosols represent a direct link between air pollution and climate.

The steps to set up a comprehensive numerical modeling system which describes the major source, transport, transformation and removal processes are outlined. A comprehensive evaluation of the system against a large number of measurement datasets in all seasons shows that the model is well able to represent concentrations, spatial distribution and diurnal evolution of the major gaseous tropospheric air pollutants under current conditions. Averaged bulk mass, time evolution of particle mass, and time-averaged number concentration size distributions of ambient aerosols are reasonably represented. Notable differences to observations are found for sulfate (underestimation) and nitrate (overestimation) aerosol components. It is concluded that two missing processes, namely wet scavenging of gases and aqueous-phase chemistry, are responsible for these discrepancies.

A detailed coupling to a wet scavenging and aqueous-phase chemistry scheme is presented, with the focus on a description of the scavenging process that is consistent with the cloud microphysics module of the driving meteorological core. The online-coupling of the model system used, i.e. the simultaneous integration over time of meteorological together with chemistry and aerosol processes, allows for a explicit description of the transport of the chemical composition of cloud liquid and rain water content, and further makes the inclusion of cloud and rain droplet evaporation, including a description of aerosol processing, possible. Aerosol processing by clouds refers to the collection and combination of several aerosol particles, including newly oxidized mass from the gas-phase, in a single particle on evaporation of the cloud or rain droplet, and is associated with a net shift of the observed particle size distributions towards larger diameters. This is clearly observed in the simulations with the extended system. It is found that the newly oxidized mass contributes substantially to the mass of the newly formed particles. Sulfate aerosol mass is on average increased through aqueous-phase oxidation in droplets, while nitrate mass is reduced due the inclusion of wet deposition for nitric acid, its gaseous-phase precursor, in the new scheme. Comparison with measurements of precipitation chemical composition reveals considerable scattering for the short period investigate, however, on average very good agreement is found for nitrates and ammonium, while sulfate wet deposition is underestimated.

Changes in aerosol composition are investigated with the extended system over the domain of Europe for the years 1990 and 2009. A statistical assessment of the observed trends in wet deposition of nitrate, ammonium and sulfate within the EMEP measurement network is conducted. Sulfate aerosol mass decreased significantly at almost all stations investigated for this periods which is consistent with an uniform decrease in sulfur dioxide emissions over Europe. While also nitrates and ammonium show statistically significant decreases of wet deposited mass at a number of stations, the trend and its spatial variability is much less uniform than that of sulfates due to a more heterogeneous development of the respective precursor emissions over Europe. Lower absolute reductions also lead to a worse signal-to-noise ratio which decreases statistical significance of trends found. Sensitivity simulations considering only changes in selected air pollutant precursor emissions give insight into the contributions of each component to the composition changes observed. Reductions in sulfur dioxide are, as expected, responsible for the majority of changes in sulfate aerosols. For the other components interactions between different emission changes were observed. Particularly interesting was the role of changes in nitrogen oxide emissions, which were found to counteract reductions in aerosol mass due to reductions in other precursor emissions in very polluted regions like the Po basin.

Zusammenfassung

Die vom Menschen verursachten Emissionen von Luftschadstoffen und deren Vorläufern haben sich in den vergangenen Jahrzehnten durch Programme zur Reduktion der Luftverschmutzung und zur Verringerung des menschgemachten Beitrags zum Klimawandel stark reduziert. Wie die Atmosphäre auf solche Veränderungen reagiert ist komplex, nicht-linear, teilweise entgegen den Erwartungen und noch nicht vollständig verstanden. Dynamik, Strahlung, Wolken, Spurengase und Partikel interagieren über eine Vielzahl von Prozessen, was die Vorhersage des Einflusses einer bestimmten Massnahme sehr schwierig macht. Neben Spurengasen sind Partikel in der Troposphäre, sog. Aerosole, von grosser Wichtigkeit. Sie können gesundheitsschädlich sein, führen zu Versauerung und Eutrophierung der Umwelt, und beeinflussen das Klima durch ihre Interaktionen mit Strahlung und Wolken. Aerosole stellen damit eine direkte Verbindung von Luftqualität und Klima.

Die nötigen Schritte zum Aufbau eines numerischen Modellsystems das alle wichtigen Emissions-, Transport-, Konversions- und Senkenprozesse zur Beschreibung atmosphrischer Aerosole und Spurengase beinhaltet werden beschrieben. Ein Vergleich des Systems mit einer grossen Anzahl verschiedener Beobachtungsdaten in allen Jahreszeiten zeigt die Fähigkeit, die mittleren Konzentrationen, räumlichen Verteilungen und Tagesgänge der wichtigsten gasförmigen Luftschadstoffe darzustellen. Die gemittelten Partikelmassenkonzentrationen und ihre zeitliche Entwicklung, sowie eine zeitlich gemittelte Verteilung der Partikelanzahlkonzentrationen werden gut wiedergegeben. Ein Vergleich mit Messungen der chemischen Zusammensetzung der Aerosole zeigt jedoch eine Überschätzung von Nitrat und eine Unterschätzung von Sulfat. Verantwortlich dafür sind zwei fehlende Prozesse im Modell, die Auswaschung von Gasen und die Nassphasenchemie.

Eine detaillierte Kopplung mit einem Schema zur Beschreibung dieser Prozesse wurde realisiert, mit Fokus auf einer Darstellung des Auswaschungsprozesses die konsistent mit dem existierenden Wolkenmikrophysikmodul des meteorologischen Kerns ist. Die “online”-Kopplung des verwendeten Modells, das heisst die simultane Integration der meteorologischen sowie Chemie- und Aerosolprozesse über die Zeit, erlaubt eine explizite Beschreibung des Transports der chemischen Zusammensetzung des Wolken- und Niederschlagswassers, sowie die Beschreibung der Wolkenprozessierung von Aerosolen über eine Darstellung der Evaporation von Wolken- und Niederschlagströpfchen. Mit Wolkenprozessierung von Aerosolen ist das Sammeln und Zusammenführen von mehreren Aerosolteilchen, und zusätzlich von frisch oxidierter Masse aus der Gasphase, innerhalb eines einzelnen Tropfens gemeint, welche bei der Evaporation des Tropfens nur ein einziges Partikel hinterlässt. Dieser Prozess ist verbunden mit einer Verschiebung der Partikelmassenkonzentrationen hin zu grösseren Teilchendurchmessern, was in den Simulationen mit dem erweiteren Modell sehr gut beobachtet werden konnte. Es zeigte sich ausserdem dass die Oxidation gasförmiger Vorläufersubstanzen in den Tropfen merklich zur Masse der neu-formierten Teilchen beiträgt. Generell erhöhte sich in der Simulation mit dem neuen Schema der Schwefelanteil im Aerosol durch Ox-

idation in der Nassphase, während der Nitratanteil als Folge der Auswaschung von Salpetersäure, dem Vorläufer von Nitrat in der Gasphase, zurückging. Der Vergleich einer Simulationsperiode mit Messungen der nassen Deposition zeigt zwar eine merkliche Streuung, welche jedoch im Mittel eine sehr gute Übereinstimmung für Nitrat und Ammonium ergibt. Die Sulfatdeposition wird im Mittel unterschätzt.

Mit dem nun erweiteren Modellsystem wurden Veränderungen in der chemischen Zusammensetzung der Aerosole zwischen 1990 und 2009 untersucht. Die beobachteten Trends für Nitrat, Ammonium und Sulfat in der nassen Deposition gemessen von Stationen des EMEP Netzwerks wurden statistisch analysiert. Die Abnahme von Sulfat ist an fast allen Stationen signifikant nachzuweisen, was mit einer Abnahme der Schwefeldioxidemissionen während der Untersuchungsperiode in ganz Europe übereinstimmt. Während eine Reihe von Stationen ebenfalls signifikant negative Trends für Nitrat und Ammonium zeigt sind die Trends und ihre räumliche Verteilung hier sehr viel variabler, was auf eine heterogenere Entwicklung der Emissionen ihrer Vorläufersubstanzen zurückzuführen ist. Die geringeren absoluten Trends führen zusammen mit einer Variabilität die ähnlich der von Sulfat ist zu einem schlechteren Signal-Rausch-Verhältnis, was das Aufzeigen eines statistisch signifikanten Trends erschwert. Sensitivitätsstudien bei denen nur die Veränderungen in den Emissionen bestimmter Vorläufersubstanzen berücksichtigt wurden geben Aufschluss über die jeweiligen Beiträge zu den beobachteten Veränderungen im Aerosol. Die Reduktionen der Emissionen von Schwefeldioxid erwiesen sich wie erwartet als die Hauptverantwortlichen für die Reduktionen von Sulfat. Für die anderen Komponenten wurden Interaktionen zwischen den Veränderungen der Emissionen der einzelnen Vorläufersubstanzen entdeckt. Besonders interessant war die Rolle der Stickstoffemissionen und der Auswirkungen ihrer Veränderungen zwischen 1990 und 2009. Es zeigte sich dass diese Veränderungen in stark verschmutzten Regionen wie der Po-Ebene den Reduktionen in der Aerosolmasse aufgrund Veränderungen in anderen Emissionen entgegenwirkten.

Chapter 1

Introduction: aerosols in the troposphere

In this chapter the major processes associated with the creation, transport, conversion and removal of atmospheric aerosols are presented, including an outline of tropospheric chemistry and environmental impacts. In the first part a theoretical description of the processes is given, in the second their translation into numerical models is explained with a focus on the modeling system used throughout this thesis.

1.1 Tropospheric chemistry

Atmospheric aerosols are intimately intertwined with tropospheric gas- and aqueous-phase chemistry. Before concentrating on aerosols we need to set the stage by shortly reviewing the main processes.

1.1.1 Daytime photochemistry

Daytime gas-phase chemistry in the troposphere consists mainly of oxidation and photolysis reactions. Crutzen (1970) and Chameides and Walker (1973) showed the central role of nitrogen oxides. Nitric oxide (NO), nitrogen dioxide (NO_2) and ozone (O_3) are in constant interaction:

$$NO + O_3 \xrightarrow{k} NO_2 + O_2 \tag{1.1}$$

$$NO_2 + h\nu \rightarrow NO + O(^3P) \tag{1.2}$$

$$O(^3P) + O_2 + M \rightarrow O_3 + M \tag{1.3}$$

with $k = 1.4 \cdot 10^{-12}\, exp(-1310/T)$ $[cm^3\ molecule^{-1}\ s^{-1}]$ (Atkinson et al., 2004) being the rate constant at temperature T. Depending on the incoming solar radiation (J_{NO2} is the photolysis rate of NO_2), the *photo-stationary-state* defines the O_3 concentration in equilibrium:

$$[O_3] = \frac{J_{NO_2}[NO_2]}{k[NO]}. \tag{1.4}$$

The above reaction cycle is in constant interaction with a second cycle involving volatile organic compounds (VOC). Their interplay can be imagined as "two wheels" (Staehelin et al., 2000): the reactions of NO_x ($NO + NO_2$) outlined above represent the first wheel, and reactions where VOC are involved the second wheel (Fig. 1.1). The interactions between both (the "turning of the wheels") are instrumental for tropospheric chemistry as they alter the photo-stationary state and hence influence O_3 concentrations.

VOC-involving reactions are initiated by the hydroxyl radical (OH), which is generated e.g. from the photolysis of O_3:

$$O_3 + h\nu_{(\lambda<330nm)} \rightarrow O_2 + O(^1D) \tag{1.5}$$
$$O(^1D) + H_2O \rightarrow 2OH \tag{1.6}$$

Once OH exists it will oxidize VOC, exemplified here for ethane (C_2H_6):

$$CH_3 - CH_3 + OH \rightarrow CH_3 - CH_2' + H_2O \tag{1.7}$$
$$CH_3 - CH_2' + O_2 \rightarrow CH_3 - CH_2 - O_2 \tag{1.8}$$
$$CH_3 - CH_2 - O_2 + NO \rightarrow CH_3 - CH_2 - O' + NO_2 \tag{1.9}$$
$$CH_3 - CH_2 - O' + O_2 \rightarrow CH_3 - CHO + HO_2 \tag{1.10}$$

As a by-product, this reaction oxidizes NO to NO_2 and provides an additional hydroperoxyl radical (HO_2), which can react with NO to form NO_2:

$$NO + HO_2 \rightarrow NO_2 + OH. \tag{1.11}$$

Another OH is provided by this reaction, which can start again to oxidize VOC - the "wheels are turning".

Lack of solar radiation lets the sources of OH run dry and the wheels begin to stop. Further reactions terminate the oxidation cycle: on the VOC "wheel", the reaction of HO_2 with itself forms hydrogen peroxide (H_2O_2)

$$HO_2 + HO_2 + M \rightarrow H_2O_2 + M. \tag{1.12}$$

The hydroperoxy radical HO_2 can also combine with an organic peroxyl radical in general (RO_2, with R an arbitrary organic chain). Both remove HO_2 and hence inhibit the oxidation of NO.

In the view of aerosol processes the termination reaction on the NO_x wheel,

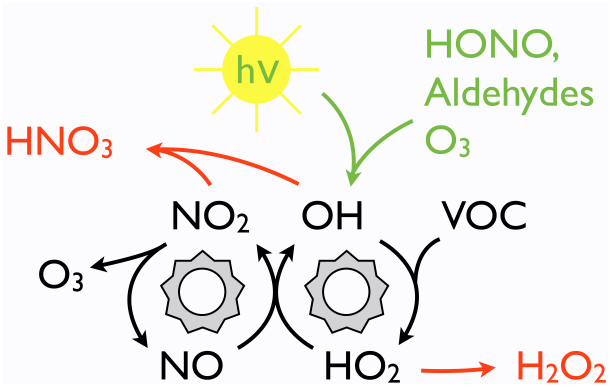

Figure 1.1: Schematic of the major daytime tropospheric gas-phase chemistry processes. Simplified from Staehelin et al. (2000).

$$NO_2 + OH + M \rightarrow HNO_3 + M, \tag{1.13}$$

bears significance as it creates nitric acid (HNO_3), which is the direct gas-phase precursor of ammonium-nitrate aerosols (NH_4NO_3).

As this thesis is focused on the effect of emission changes it is highlighted that from the mechanisms outlined above the complex relationship of emission reduction measures and air pollutant concentrations can already be observed: Dodge (1977) devised the so-called EKMA (empirical kinetic modeling approach) diagram which shows that the daily maximum O_3 concentrations depend on both NO_x and VOC concentrations (Fig. 1.2) in a non-intuitive way: simply reducing NO_x or VOC concentrations (through emission reductions) does not necessarily result in a reduction in O_3 concentrations. As can be seen in the figure, depending on the NO_x and VOC concentrations, O_3 concentrations are more sensitive to changes in nitrogen oxides (NO_x-*limited regime*) or to changes in volatile organic compounds (VOC-*limited regime*) (Sillman, 1995; Kleinman et al., 1997). Typically, urban regions are VOC-limited, while rural areas are NO_x-limited (Sillman and He, 2002).

1.1.2 Nighttime chemistry

Daytime photochemistry as outlined above is initiated through photolysis of selected compounds by sunlight and the creation of OH radicals. At night and without a NO_2 source from photolysis, O_3 concentrations are reduced through *titration* by NO via

$$NO + O_3 \rightarrow NO_2 + O_2 \tag{1.14}$$

which may proceed until all NO or all O_3 are used up. Other sources need to provide radicals to oxidize VOC. The ozonolysis e.g. of alkenes (Atkinson et al., 1992) can form OH without sunlight. More important though is the role of the nitrate radical (NO_3), formed through

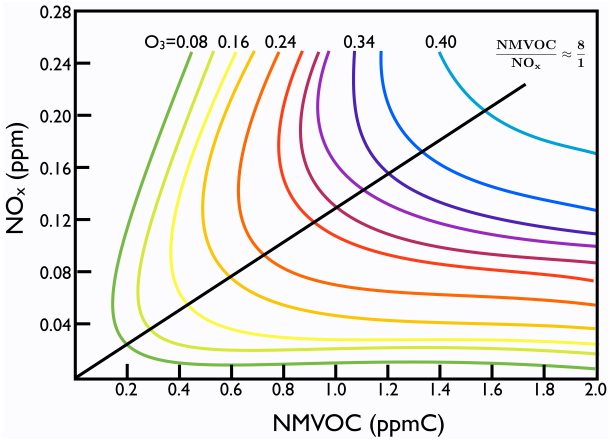

Figure 1.2: Dependence of daily maximum O_3 concentrations (colored contours, concentrations in ppmv) on the NO_x / VOC precursor concentrations. NMVOC are all VOC except methane ("non-methane volatile organic compounds"). At a proportion of about 8 to 1 (solid black line), O_3 shows equal sensitivity to NMVOC and NO_x reductions. Adapted from Dodge (1977).

$$NO_2 + O_3 \rightarrow NO_3 + O_2. \tag{1.15}$$

While this reaction also takes place at daytime it is less important then, as NO_3 is quickly destroyed by photolysis. At night however, NO_3 is the most important oxidant and thereby "drives the wheels" then (Platt and Heintz, 1994; Brown et al., 2004). The importance of nighttime chemistry now stems from the reactions

$$NO_3 + NO_2 + M \leftrightharpoons N_2O_5 + M \tag{1.16}$$

$$N_2O_5 + H_2O \rightarrow HNO_3. \tag{1.17}$$

NO_3 is in thermal equilibrium with dinitrogen pentoxide (N_2O_5), which heterogeneously (e.g. on aerosol surfaces or droplets) reacts to HNO_3 - again providing precursors for NH_4NO_3 aerosols (Brown et al., 2007b). It was shown that this heterogeneous process can lead to substantial contributions to ambient nitrate aerosol mass (Dentener et al., 1996; Riemer et al., 2003b).

1.1.3 Aqueous-phase chemistry

Clouds are ubiquitous in the atmosphere, and their aqueous-phase facilitates a number of aerosol-relevant reactions. The major types of reactions are acid-base, complexation and reduction-oxidation (RedOx) reactions (Jacobson, 1994). In the following we briefly outline the gas-to-droplet transfer mechanism and present an important reaction chain in the aqueous-phase.

Trace gases are transferred into droplets through dissolution. Given enough time, the concentration of a substance x in air and droplet will reach equilibrium, where the partial pressure in air p_x is proportional

to the molality of the dissolved gas in the solution $\mathbf{m}_{\mathrm{x}}$ (*Henry's law*, Jacobson, 1994):

$$\frac{m_x\ \gamma_{\mathrm{x}}}{p_x} = K_{eq}(T) \tag{1.18}$$

The temperature dependent constant of proportionality $\mathrm{K_{eq}(T)}$ above is called *Henry constant*, and γ_{x} is the *solute activity coefficient*. For a dilute solution like a droplet, γ_{x} is 1 and can be neglected (Jacobson, 2005).

Once in the droplet, many substances will *dissociate* into a conjugand base and a hydrogen ion, for example sulfuric acid ($\mathrm{H_2SO_4}$) by

$$H_2SO_4(g) \leftrightharpoons H_2SO_4(aq) \tag{1.19}$$
$$H_2SO_4(aq) \leftrightharpoons H^+ + HSO_4^-. \tag{1.20}$$

The amount of dissociation is a function of the acidity of the solution (concentration of the hydrogen ion ($\mathrm{H^+}$)), the strength of the electrolyte and the concentrations of other dissolved ions (Seinfeld and Pandis, 2006).

It is important to note that through the dissolution and subsequent dissociation, the equilibrium constant depends on the concentration of $\mathrm{H^+}$, hence on all other dissolved species in solution. In the example above, matters are further complicated by that fact that also the HSO_4^- anion will again dissociate.

The concentration of $\mathrm{H^+}$ is represented by the pH value:

$$pH := -log_{10}([H^+]). \tag{1.21}$$

From a practical point of view, this implies that one has to calculate (or estimate) the dissociation for soluble species, and derive an estimate of the pH of the droplet before Henry's law equilibrium with the gas-phase can be inferred. This new equilibrium constant which takes into account the dissociation is called *effective Henry's law constant*. Yin et al. (2001) show an efficient method to estimate it.

An important reaction chain in the context of atmospheric aerosols is the (irreversible) oxidation of sulfur to create sulfate aerosols ($\mathrm{SO_4}$). The first part is reversible: sulfur dioxide ($\mathrm{SO_2}$) is dissolved, converted to sulfurous acid ($\mathrm{H_2SO_3}$) which then dissociates:

$$SO_2(g) \leftrightharpoons SO_2(aq) \tag{1.22}$$
$$SO_2(aq) + H_2O(aq) \leftrightharpoons H_2SO_3(aq) \tag{1.23}$$
$$H_2SO_3(aq) \leftrightharpoons H^+ + HSO_3^- \tag{1.24}$$
$$HSO_3^- \leftrightharpoons 2H^+ + SO_3^{2-}. \tag{1.25}$$

The irreversible second part can take, depending on pH and availability of reaction partners, different forms. The most important ones are the oxidation by $\mathrm{H_2O_2}$ for $\mathrm{pH} \leq 6$

$$HSO_3^- + H_2O_2(aq) + H^+ \rightarrow SO_4^{2-} + H_2O(aq) + 2H^+, \tag{1.26}$$

and by O_3 in case pH is above 6:

$$SO_3^{2-} + O_3(aq) \rightarrow SO_4^{2-} + O_2. \tag{1.27}$$

Sulfur can further be oxidized by OH, by molecular oxygen (O_2) if transition metals are available, and under certain conditions by carbonyl compounds (Jacobson, 1994). All these reactions are of lesser importance than oxidation by H_2O_2 and O_3, but can contribute around 10 % to total sulfate production under atmospheric conditions (Alexander et al., 2009).

Besides the oxidation of sulfur there is evidence (Lim et al., 2010; Ervens et al., 2011) that the oxidation of organic substances within cloud droplets can contribute to the formation of aerosols.

1.2 Atmospheric aerosols

This section begins with a general description of the chemical and physical characteristics of aerosols and the associated processes. The remainder of the section elaborates further on selected aerosol processes that are of importance within the scope of this thesis.

1.2.1 Physical and chemical characterization

The technical definition of *aerosol* is "a suspension of fine solid or liquid particles in a gas" (Seinfeld and Pandis, 2006). Atmospheric scientists refer to aerosol as being (only) the particles within the suspension, and hence it is often used in plural - *aerosols* being "liquid or solid particles within the atmosphere".

Physical processes acting upon the aerosol

Figure 1.3 shows a schematic overview of the processes affecting aerosols. Single aerosol particles are subject to a number of *dynamical processes* (Seinfeld and Pandis, 2006):

- Drag forces due the flow of the surrounding molecules
- Gravitational settling (*sedimentation*)
- Electric fields
- Brownian motion
- Phoretic effects, like thermo-, photo- or diffusophoresis

Whole aerosol populations are further subject to *coagulation*, which is the term for the net change in the concentration size distribution due to the collision and combination of single particles facilitated through

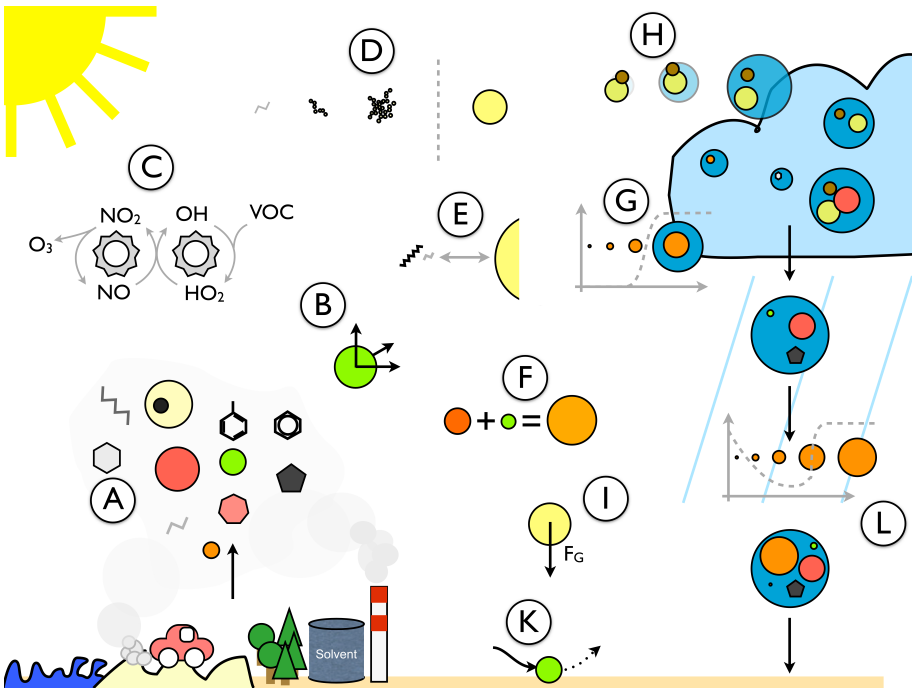

Figure 1.3: Schematic overview of the processes affecting aerosols during their lifetime in the atmosphere: emissions (A), transport (B), gas-phase chemistry (C), nucleation (D), condensation/evaporation (E), coagulation (F), activation/scavenging (G), evaporation/cloud processing (H), sedimentation (I), dry deposition (K), wet deposition (L).

different processes (hydrodynamical, electrical, gravitational or Brownian motion). Coagulation results in a loss in smaller and a gain in larger particle number concentrations. *Nucleation* is the formation of new particles out of stable molecule clusters from gas-phase precursors. *Condensation* is the deposition of low volatility gas-phase oxidation products on existing particles. Aerosols are removed from the atmosphere by *sedimentation* and *deposition*. *Sedimentation* refers to the gravitational settling of particles. *Dry deposition* is the sticking and adherence of particles to a surface which they came in contact with due to their transport within the atmospheric flow. *Wet deposition* is the sum of all removal processes in which hydrometeors are involved, and is also referred to as the sum of *washout* and *rain out*, or as *wet scavenging*.

Physical characterization

Aerosols span a size range from several nanometers (nm) up to hundreds of micrometers (μm). Size-resolved measurements of mass, number and surface area concentration show that often a number of distinct maxima, so called *modes*, exist (Fig. 1.4), which are the result of the different processes acting upon it. Aerosols are distinguished by their source: *primary* particles have been emitted directly as particles into the atmosphere, *secondary* particles have gas-phase precursors (nucleation, condensation). In the *nucleation* mode, with very small particles below 10 nm in diameter, freshly nucleated molecule clusters dominate number concentrations. They quickly grow by condensation and coagulation into the *Aitken* mode with diameters between 10 and 100 nm. The Aitken mode already has some contributions

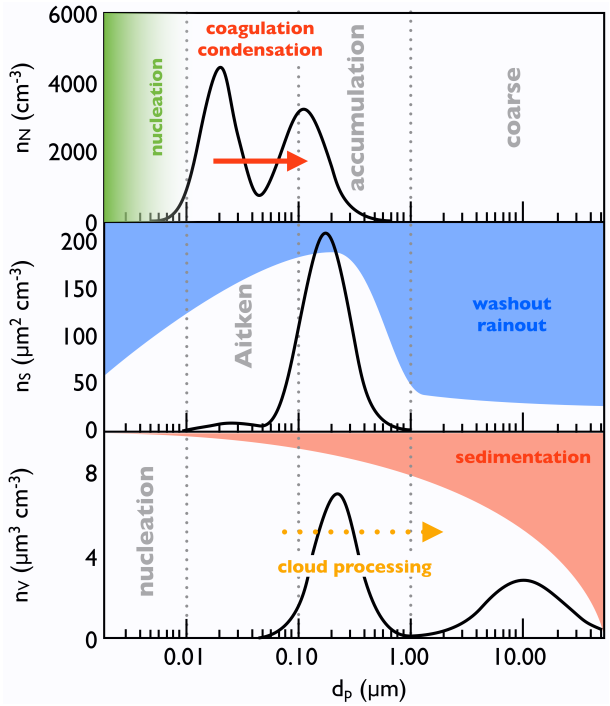

Figure 1.4: Schematic of aerosol size ranges and associated processes. Black solid lines: number (top), surface area (middle) and volume (bottom) concentration size distributions of an aerosol population typically found at remote continental sites. Grey dashed lines delineate approximately the different *modes* (see text). Processes acting upon the aerosol and their size-dependent efficiency are shown as shaded areas / arrows, and annotated with the processes' names. Figure modified from Fig. 7.18 in Seinfeld and Pandis (2006).

from primary particles. The size range between 100 nm and 1 μm is called *accumulation* mode, due to the fact that loss processes are least effective in this region. Above 1 μm, further growth becomes increasingly difficult as coagulation is less effective, condensation is limited due to diffusion, and wet deposition and sedimentation become more effective (see Fig. 1.4). The *coarse* mode, with diameters above 1 μm, is dominated by primary particles like dust, pollen, bacteria and sea salt, but has also contributions from secondary mass that condensed on / coagulated with these particles. Figure 1.4 schematically shows the influence of these processes on an aerosol population.

Measurements of aerosols often represent only a fraction of the total particulate matter (PM) due to the use of size-selective inlet systems and loss within the instrumentation. For mass measurements, the use of the upper cut-off diameter to identify the fraction is common: PM below 10 μm (PM_{10}), below 2.5 μm ($PM_{2.5}$), or below 1 μm (PM_1).

Chemical characterization

Depending on their origin, aerosols may have very different chemical composition. Aerosols can be *externally mixed* (aerosols of different composition are mixed in the same volume of air), or *internally mixed* (each aerosol is a mixture of many chemical species).

Fig. 1.5 shows the annually averaged measured chemical composition of PM_{10}. There, *organic aerosol (OA)* and *black carbon (BC)* make up the total carbonaceous fraction. A chemically more accurate classification is *organic carbon (OC)* and *elemental carbon (EC)*. OC is the carbon mass fraction of OA. Optical measurement techniques determining carbon by its absorption properties lead to the introduction of BC, which consists (chemically) of EC plus contributions from OC (Andreae and Gelencsér, 2006). Such particles when created by combustion are also referred to as *soot* (Seinfeld and Pandis, 2006). The organic aerosol itself is comprised of condensed organic precursors, called *secondary organic aerosols (SOA)*, and primary contributions - *primary organic aerosols (POA)*, made up e.g. of both biogenic (bacteria, pollen, spores and plant debris) and anthropogenic (combustion products e.g. from traffic) compounds. Ammonium, nitrate, sulfate and other inorganic ions are summarized as *secondary inorganic aerosol (SIA)*. Further mass-relevant primary contributors are mineral dust and sea salt. Note that a substantial fraction of the aerosol in Fig. 1.5 is labeled "unaccounted", indicating that there is mass which cannot be determined by the measurements. Putaud et al. (2004) suggest that water and additional organic mass are potential species contributing to this fraction. A number of species are only found in trace concentrations. Although their mass is negligible they can have profound effects e.g. on human health, like lead and other heavy metals, radioactive isotopes, or persistent organic pollutants (POP).

Particles can be of *geogenic* (mineral dust, sea salt) *biogenic* (plant debris, bacteria, etc.) or *anthropogenic* origin, with both *primary* (emitted as particles) and *secondary* (condensed from gas-phase precursors) creation pathways. The nucleation, Aitken and accumulation modes are mostly of secondary origin, while the coarse mode consists predominantly of primary particles.

1.2.2 Secondary aerosol formation

The representation of secondary aerosols is a major challenge for any aerosol model, as they are on the one hand representing a substantial part of ambient aerosol mass, and on the other are products of

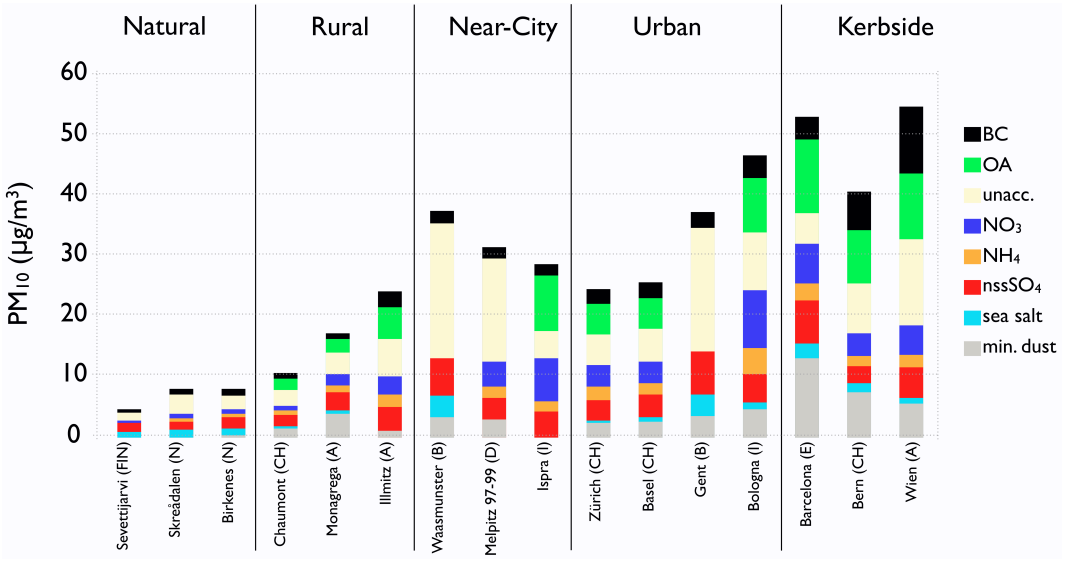

Figure 1.5: Annual average chemical composition of $PM_{2.5}$ mass at selected stations in Europe. Figure modified from Fig. 3 in Putaud et al. (2004).

complex gas-phase chemistry and gas-to-particle transfer processes. Hence the basic processes of gas-to-particle transfer are outlined in the following. The first part covers nucleation, followed by a description of secondary inorganic aerosols (SIA) and then secondary organic aerosols (SOA).

Nucleation

Gas molecules can, under certain conditions, form clusters sufficiently stable to be deemed aerosols. This formation process is called *nucleation*. One framework to understand nucleation is the *classical nucleation theory (CNT)*. According to this theory, nucleation is the result of the competition between surface tension and saturation ratio (Fig. 1.6), and usually expressed in terms of change in *Gibbs free energy (*G*)*

$$\Delta G = 4\pi r_p^2 \sigma_p - \frac{4}{3}\pi r_p^3 \rho_p \frac{RT}{m} ln S_q \tag{1.28}$$

(Jacobson, 2005) with r_p the cluster radius, σ_p its surface tension, ρ_p the cluster density, R the universal gas constant, T temperature, m the molecular weight of the condensing gas and S_q the supersaturation ratio of the substance (ratio of actual to saturation vapor pressure). The first term represents the effect of surface tension - it hinders the addition of new molecules to the cluster, as work is needed to increase the cluster area. The second term, the saturation ratio effect, favors the addition in case of a supersaturation of the substance with respect to the cluster. By plotting ΔG as a function of the radius of the cluster (Fig. 1.6), CNT now allows to derive a critical cluster size as the maximum in change in Gibbs free energy.

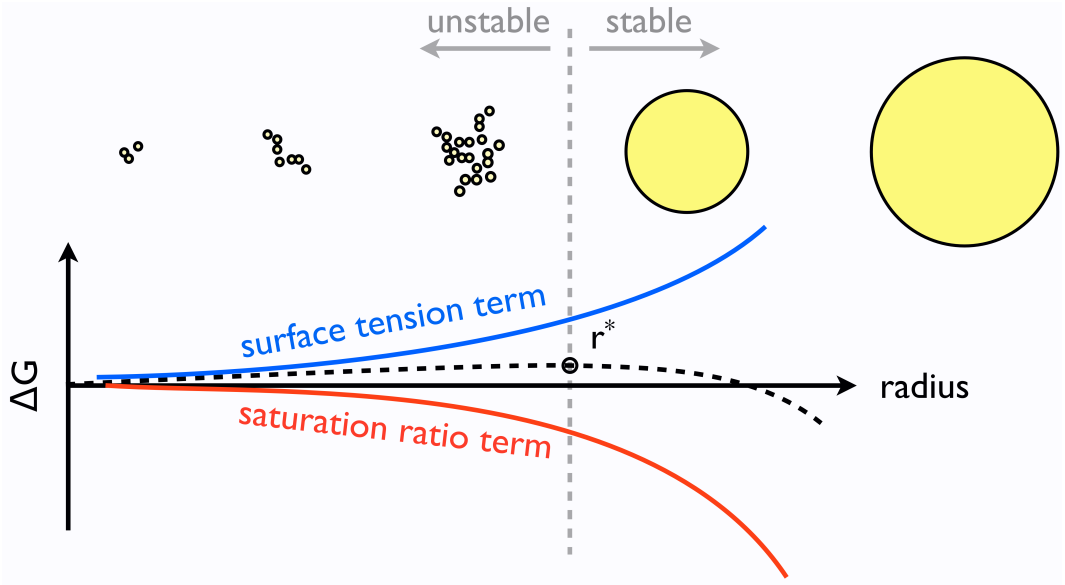

Figure 1.6: Illustration of the classical nucleation theory (CNT). The surface tension (blue curve) and the saturation-ratio (red curve) terms compete with each other, forming the black curve. The local maximum in the change in Gibbs free energy ΔG (intersection of the black curve with the dashed gray line) determines the critical radius r*, above which the cluster is stable and further growth is not limited by nucleation any more. Surface tension, saturation-ratio and sum term calculations based on Fig. 14.3 in Jacobson (2005).

For larger clusters, the addition of a molecule is energetically favorable, hence the cluster will continue to grow. From the critical cluster size, nucleation rates can be derived. Assuming an interaction between two different substances leads to *homogeneous bi-molecular nucleation* rates (Jacobson, 2005). Sulfuric acid and water have been shown to be the major species responsible for this kind of nucleation under atmospheric conditions (Kulmala et al., 2000).

The problem with CNT arises from the fact that it cannot represent nucleation rates observed in the atmosphere. The reasons for this are still not completely understood (Kanakidou et al., 2005). Proposed additional / alternative nucleation mechanisms are *ternary nucleation* with ammonia (NH_3) (Korhonen et al., 1999)), *ion-induced nucleation* (Lovejoy et al., 2004; Kirkby et al., 2011) or *heterogeneous nucleation* (Zhang and Wexler, 2002).

There is an ongoing debate whether organic molecules participate in nucleation directly, or whether they are merely responsible for subsequent particle growth by condensation (Kanakidou et al., 2005, and references therein). Studies conducted in smog chambers with very high concentrations of organic precursor gases repeatedly see nucleation events, though under atmospheric conditions no conclusive evidence is found (Kulmala et al., 2004).

Secondary inorganic aerosols (SIA)

SIA represent the liquid or solid phase of a mixture of inorganic salts of Na^+, Cl^-, SO_4^{2-}, NO_3^-, NH_4^+, K^+, or Mg^{2+} and other ions. Fig. 1.5 shows that they make up a substantial fraction of ambient aerosols. Inorganic species partition into the gas and particle phase and may exist in different ionic forms in the particle phase. SIA are assumed to be in thermodynamic equilibrium with the surroundings as outlined in the following.

Derivation of equilibrium constants $K_{eq}(T)$

Thermodynamic equilibrium of a set of species is a temperature-dependent stable state in the partitioning of their mass between all participating phases. It can be calculated by minimizing the *change in Gibbs free energy (*ΔG*)*. The reader is referred to text books on atmospheric chemistry for a complete description (Jacobson, 2005; Seinfeld and Pandis, 2006).

The resulting equation for the equilibrium constant $K_{eq}(T_0)$ at a reference temperature T_0, e.g. for the dissociation of a salt in a solution like

$$NH_4NO_3(s) \leftrightharpoons NH_4^+ + NO_3^- \tag{1.29}$$

is given as

$$K_{eq}(T_0) = exp\left(-\frac{1}{RT_0}\sum_i k_i \nu_i \Delta_f G_i^0\right). \tag{1.30}$$

$\Delta_f G_i^0$ is the *standard molal Gibbs free energy of formation* of substance i, ν_i a stochiometric normalization coefficient, and k_i a prefactor with $k_i = +1$ if the species is a reaction product and $k_i = -1$ if the species is a reactant. Values of $\Delta_f G_i^0$ can be derived experimentally and are tabulated (e.g. in Jacobson (2005)).

Including the *van't Hoff* equation allows to account for the temperature dependence of the equilibrium:

$$K_{eq}(T) = K_{eq}(T_0)\, exp\left\{-\sum_i k_i \nu_i \left[\frac{\Delta_f H_i^\circ}{R^* T_0}\left(\frac{T_0}{T}-1\right) + \frac{c_{p,i}^0}{R^*}\left(1-\frac{T_0}{T}+ln\frac{T_0}{T}\right)\right]\right\}. \tag{1.31}$$

$\Delta_f H_i^\circ$ is the *standard molal enthalpy of formation* and $c_{p,i}^0$ the *standard molal heat capacity at constant pressure*. Both can be derived experimentally and are again tabulated (Jacobson, 2005).

Equation 1.31 allows to calculate the equilibrium constant for a species in a sufficiently dilute solution. The Henry's law constant presented in Section 1.1.3 is one example of such a $K_{eq}(T)$.

Solute activity coefficients

Unfortunately liquid aerosols are not ideal solutions. When the solution is concentrated enough the ions interfere with each other, the behavior becomes non-ideal and the equilibrium constants change. The concentrations of substances in relation to the water content are so high that the assumption of activity coefficients γ_x being 1 no longer holds. This in consequence requires the calculation of γ_x for the mixture at hand.

Hydrochloric acid (HCl) for example has the following dissociation equilibrium in solution

$$\frac{\mathbf{m}_{H+}\gamma_{H+}\mathbf{m}_{Cl^-}\gamma_{Cl^-}}{\mathbf{m}_{HCl}\gamma_{HCl}} = K_{eq}(T) \tag{1.32}$$

Activity coefficients for single ions (like γ_{H+},γ_{Cl^-}) cannot be measured, but equation 1.32 can be reordered to

$$\frac{\mathbf{m}_{H+}\mathbf{m}_{Cl^-}\gamma_{H+,Cl^-}^2}{\mathbf{m}_{HCl}\gamma_{HCl}} = K_{eq}(T). \tag{1.33}$$

γ_{H^+,Cl^-} is called a *mean binary solute activity coefficient*. Given a pure HCl solution it can be experimentally derived or even theoretically calculated, e.g. using *Pitzer's method* (Pitzer, 1973). Atmospheric aerosols, however, are a mixture of several electrolytes, hence activity coefficients for these solutions must be found which are more complex and measurements are prohibitively difficult. *Mixing rules* have been developed to estimate them from binary solute activity coefficients (Bromley, 1973; Kusik and Meissner, 1978; Zaveri et al., 2005b).

Aerosol water content and hysteresis

The aerosol water content is important, as it critically affects its optical properties and, through the change in size, also its physical and chemical aerosol processes (like deposition, washout, sedimentation). Like any other component, aerosol water is assumed to be in thermodynamic equilibrium with respect to its environment.

Over a solution, the saturation water vapor pressure can be reduced (*Raoult's law*) and allows particles to contain water even if the relative humidity is below 100 %. The water content of a given mixture of salts can be substantially different from the content of the water content of pure solutions. Here, the

Zdanovskii-Stokes-Robinson (ZSR) relation (Stokes and Robinson, 1966; Clegg et al., 2003)

$$\sum_i \frac{\mathbf{m}_{i,m}}{\mathbf{m}_{i,a}} = 1, \tag{1.34}$$

where the molality in a solution of pure i is $m_{i,a}$ and the molality of i in the mixed solution is $m_{i,m}$, can help. It hypothesizes that the total water content of the mixed solution is very close to the sum of the water contents of each pure solution (Jacobson, 2005). As the pure solution activities are known or can be calculated (see above), the water content can be determined.

Note that a pronounced *hysteresis* effect exists when exposing the aerosol to varying degrees of relative humidity. Fig. 1.7 shows measurements of Tang (1997) where they observed changes in aerosol size (due to *hydration*, i.e. take-up of water) for sodium-chloride, sodium-sulfate and mixtures of these compounds when exposed to rising or falling relative humidities. At low relative humidities, all electrolytes are solid. Each salt has a certain relative humidity at which the saturation water vapor pressure is (above the particle) sufficiently lowered such that it is dissolved, the aerosol takes up water. This *deliquescence relative humidity (DRH)* is not the same for all electrolytes. It has been found that the DRH for mixtures of compounds is always lower than the minimum of all DRH of the single compounds (Wexler and Seinfeld, 1991). This lower DRH is called the *mutual deliquescence relative humidity (MDRH)*.

Starting with a liquid aerosol and lowering the humidity, a similar behavior is observed, with different relative humidities at which a certain dissolved compound crystallizes - the *crystallization relative humidity (CRH)*, also called *efflorescence relative humidity*. The aerosol can be supersaturated with respect to water, hence the mentioning of hysteresis. In general the CRH is always lower than the DRH (Wexler and Seinfeld, 1991; Tang and Munkelwitz, 1993). The point where the complete particle is crystallized is subsequently called *mutual crystallization relative humidity (MCRH)* (Zaveri et al., 2005a).

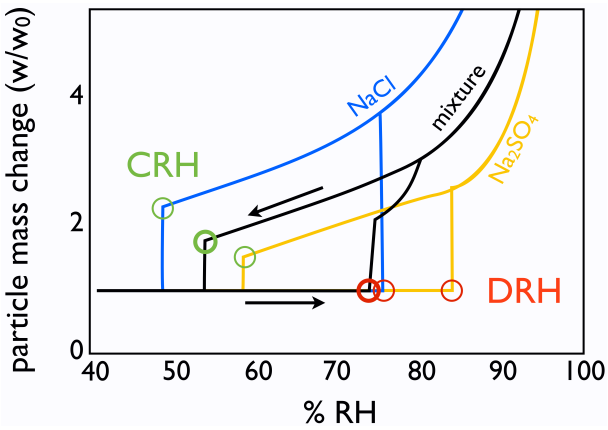

Figure 1.7: Particle growth rates as a function of relative humidity for a mixed sodium-chloride (NaCl) - sodium-sulfate (Na_2SO_4) particle. Figure based on Fig. 1 in Tang (1997). Solid black lines show the growth and evaporation curves for the mixed particle, blue lines for pure NaCl and orange lines for pure Na_2SO_4. Note the hysteresis between growth (particle grows once the deliquescence relative humidity (DRH) is reached) and evaporation (particle crystallizes only once the crystallization relative humidity (CRH) is reached). DRH and CRH are marked with circles, the mutual DRH / CRH with bold circles.

Interactions with organic species which further complicate the behavior of salts in solution (Marcolli et al., 2004; Ciobanu et al., 2009) but are out of scope for this description.

Conclusions for typical secondary inorganic aerosol components

The major inorganic compounds are ammonium, nitrate and sulfate, often found as ammonium-nitrate and ammonium-sulfate salts respectively. While the equilibrium partitioning of ammonium-sulfate under atmospheric conditions is such that it resides completely in the aerosol phase, this is not always the case for ammonium-nitrate. Its $K_{eq}(T)$ is sensitive to typical mid-latitude temperature and relative humidity ranges, resulting in annual and also diurnal cycles in the partitioning of

$$HNO_3(g) + NH_3(g) \leftrightharpoons NH_4NO_3(s). \tag{1.35}$$

The hysteresis effect mentioned poses a problem for the simulation of atmospheric aerosols, as it requires knowledge about the history of the particle to estimate its current phase state (Colberg et al., 2003).

Secondary organic aerosols (SOA)

Organic aerosols make up a considerable fraction of ambient aerosols (Fig. 1.5). Evaluation of measurement data (De Gouw et al., 2005; Lanz et al., 2007; Jimenez et al., 2009; Lanz et al., 2010) shows that most of the organic mass found is made up of secondary formed components (Fig. 1.8). Source apportionment of organic aerosols is difficult due to the large number of compounds involved, chemical transformations and analytical problems (Turpin et al., 2000; Kanakidou et al., 2005). Current techniques employ either laboratory analysis of PM filter samples, which allow detailed chemical analysis with the drawback of poor temporal resolution (days to weeks), or the use of an *aerosol mass spectrometer (AMS)* (Canagaratna et al., 2007). There, the fraction of sub-micron aerosol that can be vaporised (*non-refractory* PM_1 *(*$PM_{1,NR}$) is analyzed by mass spectrometry, which allows to derive a quantitative estimate of the mass of organics and major inorganic ions with high temporal resolution (minutes to seconds). Sources and types of OA are then inferred from statistical analysis (Zhang et al., 2005b,a; Lanz et al., 2007). Analyzed in such a way it was proposed that organic aerosol mass can be discerned into *hydrocarbon-like (HOA)*, *biomass burning (BBOA)*, *low-volatile (LV-OOA)* and *semi-volatile (SV-OOA) oxygenated organic aerosols*. HOA and BBOA are related to primary emissions, while the OOA part is considered secondary. These secondary contributions constitute the majority of total OA at most stations in Fig. 1.8, though with notable exceptions (e.g. Mainz, and New York, Tokyo in winter).

Which precursor species had been oxidized, and how, can only be guessed from these measurements. That VOC can be oxidized by radicals available in the atmosphere (OH, O_3 and NO_3), and that these products can have low enough volatilities (saturation vapor pressures) so they can condense to aerosols is well established (Went, 1960; Andreae and Crutzen, 1997; Griffin et al., 1999). Smog chamber experiments under controlled conditions serve as basis. These results are then extrapolated to atmospheric conditions. It is known that both anthropogenic and biogenic VOC contribute, but biogenic VOC have been found to be more reactive and hence of higher importance for SOA formation (Atkinson, 2000). Isoprene (2-methyl-1,3-butadiene), the most abundant *biogenic* VOC (BVOC) has been recently found to contribute to SOA formation as well (Claeys et al., 2004; Carlton et al., 2009), although with very low yields.

There are, however, multiple processes at work. Fig. 1.9 gives a schematic overview: *oligomerization*

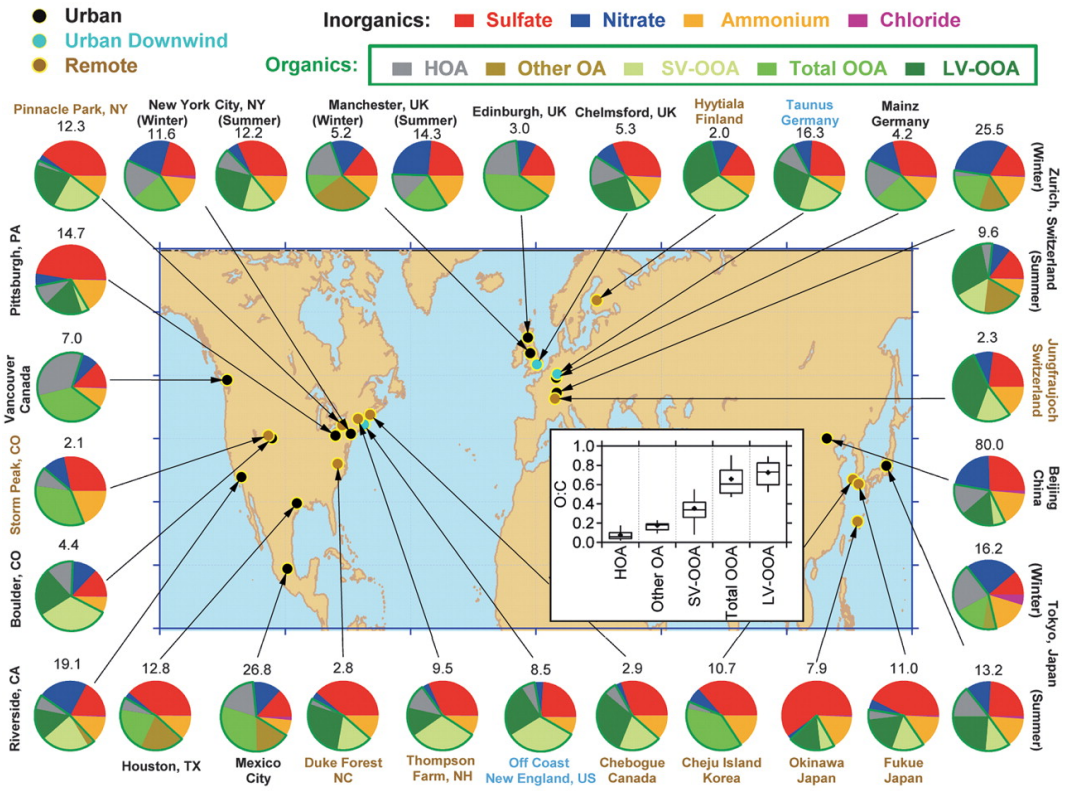

Figure 1.8: Fig. 1 in Jimenez et al. (2009): mass concentrations and chemical composition of non-refractory PM_1 ($PM_{1,NR}$) as measured by an aerosol mass spectrometer (AMS) during field campaigns at stations in the Northern Hemisphere. Statistical analysis was used to determine the fractions of primary (HOA + Other OA) and secondary organic aerosols (SV-OOA, LV-OOA)). In the inset the oxidation state of the different components is shown as the oxygen to carbon atoms ratio.

forms stable oligomers and polymers (Kalberer et al., 2004), *functionalisation* adds polar functional groups containing oxygen ("oxidation"), and *fragmentation* splits up organic substances in parts by cleavage of C-C bonds (Kroll et al., 2009). Dilution is influencing the gas-particle partitioning as well through the associated change in vapor pressure (Robinson et al., 2007), which indicates that also primary emissions of organic material must be considered as potentially volatile or *semi-volatile (SV-OOA)*.

In summary: a range of intermediate or semi-volatile organic species exist which partition between gas- and aerosol-phase depending on current environmental conditions (Donahue et al., 2006). A framework connecting gas-phase precursors to SOA mass observed including the correct reactions and processes is still outstanding.

1.2.3 Interaction with clouds and precipitation

Aerosols are instrumental for the formation of clouds. They serve as *cloud condensation / ice nuclei (CCN/IN)* which make condensation at supersaturations observed under atmospheric conditions possible in the first place. Evaporating cloud and rain droplets leave aerosols with substantially different characteristics behind - this is termed *aerosol processing by clouds*. Finally, precipitation is the major removal

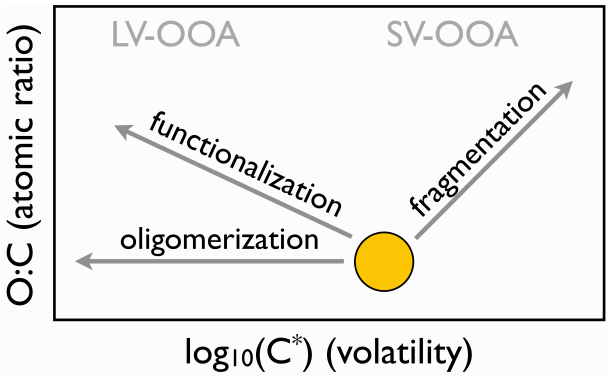

Figure 1.9: Schematic representation of the 2D-volatility basis set (2D-VBS), with the volatility on the x-axis and the oxidation state as y-axis. An arbitrary organic compound is shown with possible directions of movement through the different processes oligomerization, functionalisation and fragmentation. Further noted are regions of LV-OOA and SV-OOA. Fig. modified from Fig. 4c in Jimenez et al. (2009).

mechanism for aerosols from the atmosphere. The interactions with clouds have already been mentioned in the section explaining aqueous-phase chemistry for trace gases (1.1.3). In the following the activation of aerosols as liquid cloud droplets is explained followed by an outline of aerosol processing and the removal through precipitation. Interactions with the ice-phase in clouds are important (Lohmann and Feichter, 2005), though not topic of this thesis.

Activation

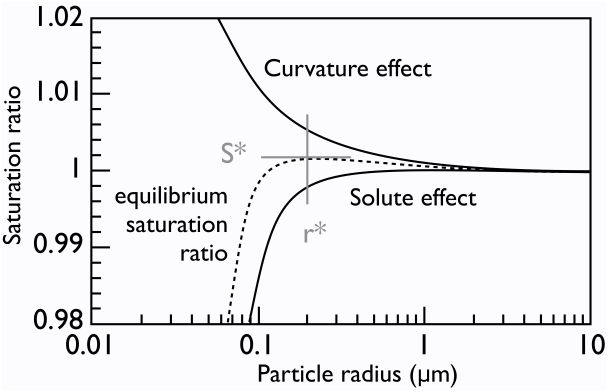

Figure 1.10: Effects of curvature and solutes on the critical saturation ratio S^* and the associated critical radius r^*. The dashed line represents the saturation ratio, i.e. a measure for the relative humidity necessary for activation. Fig. modified from Fig. 16.1 in Jacobson (2005).

Activation of aerosols as cloud condensation nuclei is of major importance for climate applications. This process describes the take up of water by an aerosol particle and subsequent growth by condensation of water to cloud droplet size. The basic idea is to understand under which conditions the saturation vapor pressure of water over the surface of an aerosol particle is sufficiently low that it will take up water and

grow into a cloud droplet. This is summarized by the Köhler equation (Köhler, 1936)

$$S' = \frac{p'_s}{p} \approx 1 + f_{curvature} - f_{solute} \tag{1.36}$$

where a relation is made between the water saturation vapor pressure p' over a curved surface of an solute-containing particle with the vapor pressure p over a flat surface without solute (Köhler, 1936). The saturation ratio S' is a function of two effects: Firstly, the *curvature* or *Kelvin effect*

$$f_{curvature} = \frac{2\sigma_p m_p}{rRT\rho_p}, \tag{1.37}$$

with σ_p the surface tension of the particle, m_p the molecular weight of the particle, r its radius, R the universal gas constant, T temperature and ρ_p the particle density. The Kelvin effect increases the saturation vapor pressure over smaller particles, as molecules are more likely to desorb from a curved surface than from a flat one. Note that the surface tension σ depends on the chemical composition of the aerosol particle.

Secondly, the *solute* or *Raoult effect*

$$f_{solute} = \frac{3m_v i_v M_s}{4\pi r^3 \rho_w m_s} \tag{1.38}$$

decreases the saturation vapor pressure if the particle is a solution. This is due to the fact that on the surface of a solution droplet both solute and solvent molecules can be found and hence the number of solvent (in our case water) molecules that can evaporate is lower compared to an identical droplet of pure water. m_v is the molecular weight of water, i_v a factor representing the number of ions created from the dissolution of a species, M_s the mass of solute in the particle, ρ_w the density of water, and m_s the molecular weight of the solute.

The *Köhler curve* as presented in Fig. 1.10 shows the combined effect of both processes on the saturation water vapor pressure as a function of particle size. A distinct maximum saturation ratio, the critical saturation ratio $S*$ can be inferred. The corresponding particle diameter is called critical diameter r^*. All particles that are larger than r^* with an equilibrium saturation ratio lower than the ambient saturation ratio will take up water, and continue to do so as the necessary equilibrium saturation ratio is always lower as the ambient saturation ratio for the - now larger - particles. Also particles smaller than r^* can be activated, given that the ambient saturation ratio exceeds their critical saturation ratio S^*.

1.2.4 Aerosol processing

Not all the mass that is incorporated into droplets is also removed from the atmosphere, but released back upon cloud / rain evaporation. Pruppacher and Jaenicke (1995) estimated that each particle is on average subject to 3 condensation / evaporation cycles before being removed. However this figure has considerable uncertainty and the actual number of cyclings could be much higher due to a substantial fraction of non-precipitating clouds. The aerosol population released back into the atmosphere might be

substantially altered compared to what had been scavenged, due to two processes: firstly, additional mass is scavenged from gas-phase precursors that is oxidized within the droplet (Section 1.1.3) and becomes part of the aerosol-phase once the cloud evaporates. The released particles will be larger than the scavenged ones. Secondly, a cloud droplet and even more so a rain droplet is likely to scavenge more than one aerosol particle. Due to dissolution and adherence upon evaporation, a cloud droplet will release only one aerosol consisting of the summed masses of all scavenged particles. Measurements in clouds indicate that this results in a net shift in aerosol size distributions towards larger diameters (Wurzler et al., 2000) and that even a bimodal distribution will develop (Hoppel et al., 1990), with particles never activated making up the lower mode, and cloud processed aerosols the larger one.

Wet deposition

From the air quality modeling perspective, clouds and rain are sinks for aerosols which remove them from the atmosphere. This process, the incorporation into hydrometeors and subsequent transport to the surface by precipitation, is called *wet deposition*. Often it is split into *rain out* and *washout*, where the former means the activation of a particle as cloud condensation nucleus and subsequent removal by precipitation, while the latter refers to the removal of particles by collision with already existing cloud or rain droplets and subsequent precipitation (Gong et al., 2011).

The activation as cloud condensation nuclei has been explained above, and *rain out* is the subsequent removal via precipitating droplets. The *washout* of aerosols by collision with rain droplets is a size-dependent process as well, and can be subdivided into three separate physical processes: *Brownian motion*, i.e. the collision of the particle with the rain droplet due to its random motion; *inertial impaction*, the collision of a particle with a rain droplet as it is unable to follow the streamlines around the droplet; and *interception*, the collision due to the fact that the particle is indeed following the streamline around the particle, but, due to its size, comes into contact with the droplet (Seinfeld and Pandis, 2006). Andronache (2003, 2004) give an overview and evaluation of commonly used parameterisations for these processes in atmospheric models.

The incorporation of a particle into a liquid droplet either through washout or rain out is termed *(wet) scavenging*. It is often separated into *in-cloud* and *below-cloud* scavenging, where the former refers to interactions (rain out or washout) with cloud droplets while the latter only refers to the washout by rain droplets which are assumed to fall out from the cloud above, although this is a loose terminology. Rain droplets exist within a cloud as well and the process of collecting aerosols is also active in there.

The combination of all the above mentioned processes leads to characteristic scavenging coefficient curves over particle radius (e.g. Fig. 1.11 for impaction scavenging), with a distinct minimum just below 1 μm. This is called the *scavenging or Greenfield gap*, and is one of the reasons for the existence of a pronounced accumulation mode in aerosol concentration size distributions.

1.2.5 Environmental impact

The environmental impact of ambient aerosols is divided into two major areas: climate change and health concerns.

Climate effects of aerosols are typically divided into *direct*, *semi-direct* and *indirect* effects. The direct effect (Albrecht, 1989) is the influence of aerosols on incoming radiation. Depending on their size, shape and chemical composition, particles either scatter or absorb light substantially altering the energy budget.

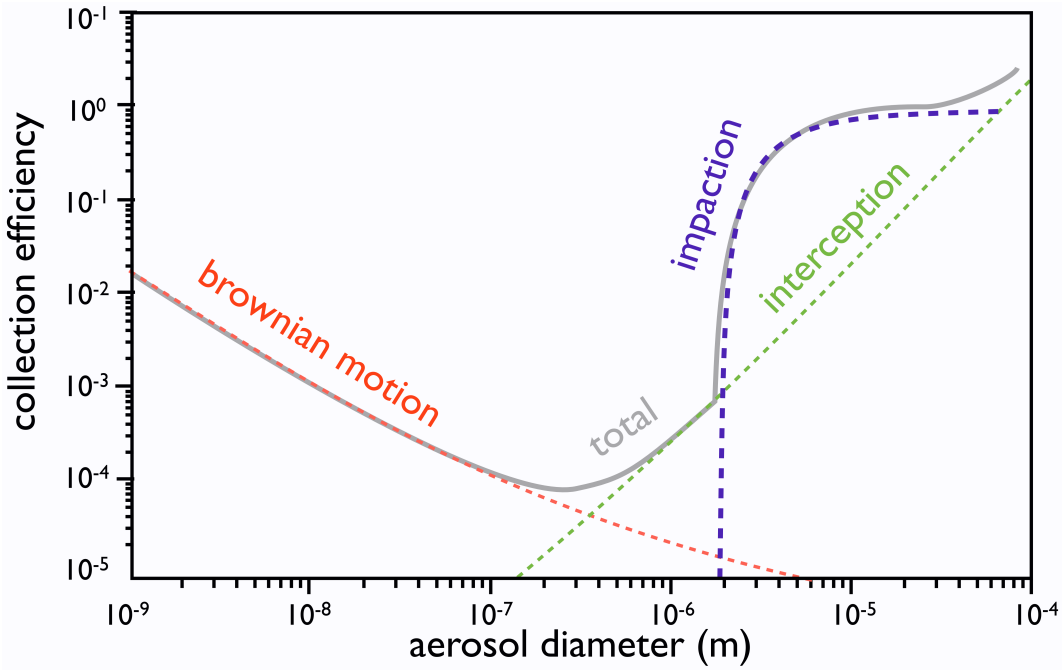

Figure 1.11: Collection efficiency for impaction scavenging as used in SCAV. The different participating processes are shown as dashed lines (red is Brownian motion, green interception and violet impaction). The gray solid line shows the resulting total collection efficiency. Figure modified from Tost et al. (2006).

The indirect effects concern the development and lifetime of clouds, and consist of an increase in cloud albedo due to more but smaller cloud droplets (1st indirect effect, Twomey, 1974), suppressed drizzle, increased cloud height (Pincus and Baker, 1994) and presumably increased cloud lifetime (2nd indirect effect, Albrecht, 1989), and further the glaciation indirect effect for ice and mixed-phase clouds (Lohmann, 2002). Finally, the semi-direct effect of aerosols (Ackerman et al., 2000) is the induced change in relative humidity and atmospheric stability through changes in the radiation budget by absorption of shortwave radiation.

The efficacy and efficiency of a certain aerosol to contribute to each of these effects is a function of its size (direct: scattering behavior, absorption cross-section; indirect: activation supersaturation), shape (direct: scattering behavior) and chemical composition (direct: optical properties, indirect: hygroscopicity, activation supersaturation).

Aerosols are also a health concern. Particles are inhaled, traverse the respiratory tract and reach the lungs, where they cause inflammations and can also be further redistributed to other organs (Donaldson et al., 2005). While a large number of studies clearly link air pollution to health problems and increased mortality (e.g. Dockery and Pope, 1996; Wichmann et al., 2000), the inner workings of these effects are sometimes only poorly understood. Bernstein et al. (2004) give a short summary on the health effects of particulate matter exposure and highlight that chemical composition plays a key role in these effects. Relatively well understood are the health effects of combustion-derived particles (Donaldson et al., 2005). Besides chemical working mechanisms, also “mechanics” can be important, as the research into respiration of asbestos fibers, long needle-like particles, showed: in the lung, macrophages - cells with the duty to “clean up foreign objects” - try to swallow these fibers. They fail as the fiber is too long and non-digestible

for them, which leads them to releases toxic substances (Donaldson and Tran, 2004). Current research (Brown et al., 2007a; Poland et al., 2008) into health effects of carbon nanotubes - essentially oddly-shaped nucleation mode aerosols - suggests that similar mechanisms might be active for these compounds.

How aerosols affect human health therefore also depends on size (ability to reach the lungs and further organs), shape (ability of the body to remove them from the lungs) and chemical composition (general toxicity).

1.3 3D numerical modeling of atmospheric aerosols

In the last section the relevant chemical and physical processes have been treated in a general, theoretical manner. This section now shows how these findings are represented in numerical models. In this thesis, numerical models are *regional* or *mesoscale Eulerian-type* models with typical horizontal grid dimensions on the order of 100 down to 1 kilometers (meso-β to meso-γ scale after Orlanski (1975)). Such models are called *limited area* models as they do not cover the whole globe. Historically the model representing meteorology and the one for aerosols and chemistry were separated. The difference in *coupling* with meteorology is explained in the following section. Then a description of the treatment of emissions is given which is followed by the representation of chemical reactions, aerosols and feedback processes. Wet removal processes are not explained here as a complete chapter is dedicated to the implementation of such a scheme in the modeling system used in this thesis.

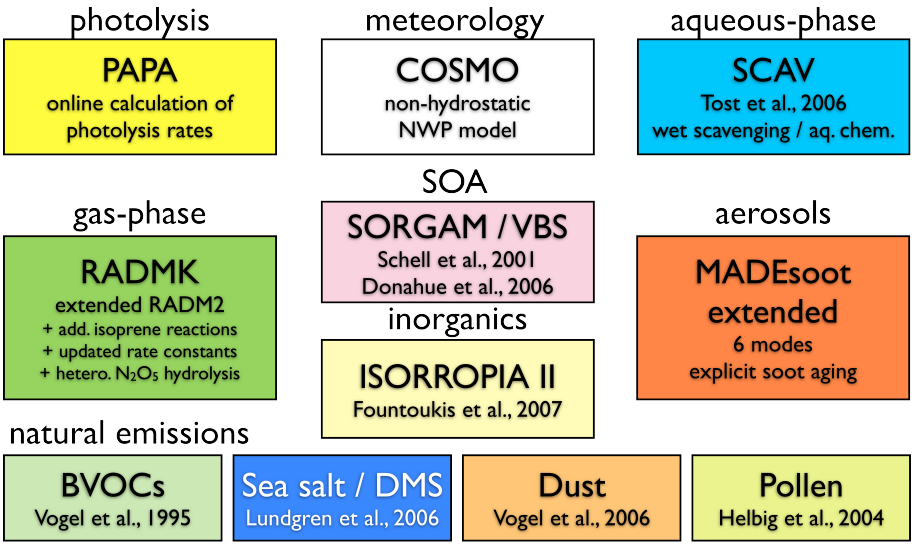

Figure 1.12: The components of the COSMO-ART (Vogel et al., 2009) modeling system, including the scavenging and wet-phase chemistry module added during this thesis (SCAV).

The model system used throughout this thesis is the model of the Consortium on Small-scale Modeling (COSMO, Baldauf et al., 2011) with Aerosols and Reactive Trace gases (COSMO-ART, Vogel et al., 2009). Examples for different processes given in the following are hence taken from the implementations in COSMO-ART. Figure 1.12 gives an overview of the model components.

1.3.1 Coupling to meteorology

Numerical weather prediction (NWP) and air quality models evolved in different communities. This led to the historical distinction between a *meteorological core* and a *chemistry transport model (CTM)* for the representation of trace gases and aerosols (Grell and Baklanov, 2011). Meteorological cores used are NWP systems like the fifth-generation Penn State/NCAR mesoscale model (MM5, Grell et al., 1994) and its successor, the Weather Research and Forecasting model (WRF, Skamarock et al., 2008), or COSMO. Commonly used CTMs including both a description of aerosols and gas-phase chemistry are the community multiscale air quality model (CMAQ, Byun and Ching, 1999), the comprehensive air quality model with extensions (CAMx, ENVIRON, 2004), CHIMERE (Schmidt et al., 2001; Vautard et al., 2001, 2003; Bessagnet et al., 2004) or LOTOS-EUROS (Schaap et al., 2008). Modeling systems which feature a tighter integration with meteorology are WRF with Chemistry (WRFChem, Grell et al., 2005), COSMO-ART or ENVIRO-HIRLAM (Korsholm et al., 2008). The difference in coupling with meteorology is described in the following:

The rate of change of the concentration c_x of a trace gas or particle x is governed by its continuity equation

$$\frac{\partial c_x}{\partial t} + \nabla \cdot (\vec{v} c_x) = (\nabla K_h \nabla) c_x + \sum_i^n S_i \tag{1.39}$$

with $\vec{v}$ the wind vector, K_h the eddy-diffusion coefficient for heat and S_i the sum of all source and sink processes acting upon the species, like emissions, chemical reactions, deposition, or washout (Jacobson, 2005). Wind vector, eddy-diffusion coefficients and other environmental quantities that are used in the source/sink terms, like temperature (BVOC emissions), friction velocity (deposition) etc., must be provided to the CTM, and two general methods have evolved to accomplish that. The first, traditional method is the *offline* approach. A NWP model simulation for a certain period is made, and three-dimensional representations of important quantities like the wind vector, temperature, pressure and humidity at given intervals in time (like every 3 hours) are saved. The offline CTM then uses these fields as input to its internal numerical representation of equation 1.39. The CTM hence solves advection, diffusion, convection and all other meteorological processes needed for the transport of trace gases and aerosols itself, with its own methods and approximations. The second, newer method is called *online* coupling. There, meteorological core and CTM are tightly coupled, such that equation 1.39 is implemented with a single set of approximations and parameterisations, which is then used for both scalar meteorological quantities (e.g. humidity), as well as trace gas and aerosol concentrations. All temporary variables (Eddy-diffusion coefficients, friction velocity, turbulent kinetic energy, etc.) are provided to the CTM by the meteorological core.

Both methods have advantages and drawbacks. Offline models are usually faster, as meteorological input data is often already available hence only chemistry and aerosols need to be calculated. They have been in use for tens of years and have matured during that time. Two major drawbacks of the offline approach lead to the development of the second type: as offline models use their own set of equations and approximations, inconsistencies deteriorate the representation of meteorology. Often also a different grid representation is employed by the CTM part resulting in interpolation errors. Even more importantly: feedback processes on meteorology (e.g. direct and indirect aerosol effects) are not feasible with such systems. Online-coupled models have been developed to overcome these problems. The major drawback of online models is that they are computationally more expensive, as the meteorology has to be calculated for every simulation

(compared to the possibility with an offline-model to do sensitivity studies e.g. with changed emissions more efficiently). Climate applications with transient simulations over decades are not yet possible with these systems. The reader is referred to Zhang (2008) for an overview of the state of recent online-coupled modeling systems and their benefits.

1.3.2 Initial and boundary conditions

Meteorology

Simulation of aerosols and trace gases with a limited area model is an initial and boundary values problem. Both *initial and lateral boundary conditions (IC/BC)* need to be provided, for both meteorological and aerosol/chemistry quantities. For meteorology this is solved by using the results of a global NWP simulation, like data from the Integrated Forecasting System (IFS) of the European Center for Midrange Weather Forecasts (ECMWF), or the Global Forecasting System (GFS) of the National Centers for Environmental Prediction (NCEP). These simulations are made operationally, i.e. on a daily / hourly basis, and provide data on resolutions up to 10 - 20 km horizontal grid cell size.

Chemistry and aerosols

Initial and boundary conditions for gas-phase and aerosol species can be derived from systems where such a global NWP model is coupled to a global CTM, like the MOZART-NCEP system presented in Emmons et al. (2010). A description of gas-phase chemistry and aerosols, however, requires a much larger number of variables (inorganic, organic trace gas concentrations, aerosols composition number and mass concentrations etc.), which makes finding a match between a regional model simulation and a global model output for every species more difficult. Often mean vertical profiles are given as (IC/BC) for aerosols and chemistry instead of realistic boundaries in that case.

In the course of this thesis the meteorological preprocessor INT2COSMO, which is the part of software that converts the output of the global NWP simulation to an input of a COSMO simulation, has been extended by the ability to interpolate and prepare data from global CTM simulations to COSMO-ART. It is described in Appendix C.

Emissions

Emissions are the main driver for tropospheric chemistry. Both man-made (*anthropogenic*) and natural (*biogenic*) sources for reactive gases and their precursors exist. Sources can be further distinguished into *point* (e.g. a stack), *line* (e.g. a road) and *area* sources (e.g. a forest). They can be singular / very irregular events (e.g. a volcanic eruption, forest fires) or rather continuous, though with diurnal, weekly, yearly cycles and a multi-year trend component (e.g. traffic).

All these sources need to be included in a modeling system, which for an Eulerian-type model relies on the discretization of space and time into a regular grid / time-step. Two major methods have been developed for this purpose. On the one hand *parameterisations* for emissions which can be inferred from variables known at model run-time, on the other hand *inventories* as gridded description of emissions prepared already before the start of the simulation.

Emission parameterisations are mostly used to describe biogenic emissions. Usually represented in

mesoscale models are: biogenic VOC from vegetation (Vogel et al., 1995; Guenther et al., 2006), PM, NMVOC, CO and NO_x from wildfires (van der Werf et al., 2010), lightning NO_x (DeCaria et al., 2005; Price et al., 1997; Schumann and Huntrieser, 2007), dimethyl sulfate (DMS) and sea salt from the oceans (Andreae et al., 1985; Bates et al., 1987), and mineral dust in deserted regions (Choi and Fernando, 2008; Marticorena and Bergametti, 1995). An example will outline the workings of such a parametrization: Vogel et al. (2006) parametrized dust emissions from deserted regions in COSMO-ART. The basic idea is that a threshold friction velocity exists above which dust particles become airborne. This velocity depends on soil water content and surface roughness. How much and which particle sizes are emitted depends on additional characteristics of the soil. Stanelle et al. (2010) give references for equations and datasets used. Friction velocity and soil moisture can be retrieved from the meteorological core (COSMO). Soil properties (e.g. roughness, size distributions, fraction of erodible surface) are derived from an external dataset which is interpolated to match the simulation grid in the extended INT2COSMO-ART. The emission flux is calculated each time-step and additional aerosol modes have been implemented that match the emissions. The module is hence independent of the simulated time-frame and model resolution, and - given the parametrization is scientifically valid for the whole globe, and the input data covers it - can be applied in any simulation setup.

The creation of *emission inventories* usable in models is laborious and requires a large number of input data and computation. Emission inventories are therefore developed by specialized groups rather than by each individual modeling team. The basic idea of an emission inventory is to split up emissions into a (gridded) representation of emission amounts and a description of the temporal evolution. The description of both can differ greatly in complexity between different emission inventories. As an example, the inventory used in the European Monitoring Atmospheric Composition and Climate (MACC) project developed by TNO (Netherlands) (Visschedijk et al., 2007; Denier van der Gon et al., 2010) is described. There, emission amounts are available as yearly emission totals (2003-2007) on a 0.125° x 0.0625° horizontal grid over the greater European domain for NO_x, SO_2, NMVOC, CO, NH_3, PM_{10} and $PM_{2.5}$. The emissions cover anthropogenic sources, and are divided into 10 different source categories according to the *Selected Nomenclature for Air Pollution (SNAP)*, like industrial combustion (SNAP 3), road traffic (SNAP 7) or agriculture (SNAP 10). Activities are available as daily, weekly and yearly cycles, with different sets for each country and source category.

The TNO/MACC dataset is used for the simulations in this thesis. Model specific adaptations have to be made to use such an inventory in COSMO-ART (and other models as well). In case of the TNO/MACC datasets these were:

- *Speciation* of total NMVOC for the representation of organic compounds in the chemical mechanism
- Distribution of total $PM_{2.5}$ onto the chemical components available in the aerosol module including an assumption about emitted particle diameters
- Split of total NO_x into NO and NO_2
- Vertical distribution (especially for stack emissions)
- Spatial interpolation of the emissions grid onto the model grid

Appendix B contains a detailed description of the steps taken in the emissions preprocessing module developed during this thesis. The implementation of additional interpolation routines for emissions into the preprocessing software INT2COSMO is presented in Appendix C. Here only the effects on the simulation

are noted: the speciation of NMVOC depends on the use of source specific composition profiles (Derwent et al., 1996; Passant, 2002; Theloke and Friedrich, 2007), and can influence the reactivity of the resulting model species, and hence its influence on O_3 and chemistry in general, as well as its SOA creation potential. The split of NO_x into NO and NO_2 is changing over time especially for traffic, the largest source of NO_x (Grice et al., 2009), which can have important effects on O_3 and inorganic aerosols - a fact that will be discussed in Chapter 4. For the emissions of particulates a diameter needs to be assumed, as only mass is given in the inventory. While there are studies implying that this can be done in a very simple manner (Elleman and Covert, 2010), others show that this should be studied more carefully (Spracklen et al., 2010). Emitting particles in the wrong dimensions affects the aerosol size distribution with all its subsequent effects on conversion, cloud processing and deposition.

1.3.3 Chemical reactions

A number of *mechanisms* (sets of equations) representing tropospheric gas-phase chemistry are used in current air quality models. They include the description of the photo-stationary equilibrium, the major VOC reactions and a connection to radiation to estimate photolysis rates. Typically such a set includes about 150 reactions and 50 species. Current examples are the second generation regional acid deposition model (RADM2 , Stockwell et al., 1990) (used in COSMO-ART), the carbon bond mechanism version 5 (CB05, Yarwood et al., 2005), or the mechanism of the (former) statewide air pollution research center (SAPRC07, Carter, 2010). While the reactions involving only inorganic species are usually included explicitly in such mechanisms, reactions including organic compounds are often more or less strongly simplified due to the large number of such species and reactions found in the atmosphere. Current mechanisms simplify their treatment by *lumping* organic species. The *lumped molecules* approach represents chemically similar species by a surrogate species, e.g grouped according to the reactivity with the OH radical (like in SAPRC07, RADM2). The *lumped structure* approach represents organic species as a combination of functional groups (CB05). Using a different photochemical mechanism can result in differences up to 10 % (Dodge, 2000), with largest differences in VOC-limited regions where the representation of organics has more weight.

The main difficulty in integrating a system of chemical equations over time lies in the fact that there are reactions that are very fast, yet others are very slow, which translates to a stiff system of ordinary differential equations (ODE). The numerical solver hence needs to be accurate enough to represent the fast reactions reasonable, though computationally efficient for use in 3D air quality models. Types of solvers used are the older quasi steady state approximation (QSSA) (Hov et al., 1978; Hesstvedt et al., 1978) and Gears-type (Hindmarsh, 1972), and newer Runge-Kutta-Rosenbrock (Rosenbrock, 1963; Hairer and Wanner, 2010) or LSODE (Radhakrishnan et al., 1993). Sandu et al. (1997b) and Sandu et al. (1997a) present benchmarking results for a number of solvers.

Typical air quality modelers are not necessarily experts in the development of numerical solvers for ODE systems, though, due to the advances in science, it often happens that new reactions or species are introduced into the system. Hence several packages have been developed that allow to paraphrase the system of reactions to solve in a simple language, which is then translated into computer source code that allows to integrate the reaction system over time. The numerical solver is hence decoupled from the actual system to solve and allows for much greater flexibility in the use in model systems. Both commercial (e.g. Facsimile, `http://www.mcpa-software.com/facsimile/`, accessed Dec. 2011) and freely available systems (e.g. the Kinetic PreProcessor in Sandu and Sander (2006)) have been developed to accomplish

this task. COSMO-ART has been adapted to use KPP to solve the gas-phase chemistry mechanism. The cloud chemistry scheme (Tost et al., 2006) coupled to COSMO-ART in this thesis makes use of KPP for aqueous-phase reactions as well.

1.3.4 Representation of atmospheric aerosol

Representing aerosols in numerical models is a challenging task. Typical concentrations of hundreds to several tens of thousands of particles per centimeter cubed, each potentially having a unique chemical composition with tens of different species, make an explicit representation of each particle not feasible. Instead, most current models represent aerosols in a simplified manner, with two commonly used approaches: *modal* and *sectional*.

In the modal approach, the fact is exploited that the concentration size distributions can be approximated by a superposition of a number of (e.g.) log-normal distribution functions (Seinfeld and Pandis, 2006; Binkowski and Shankar, 1995; Whitby and McMurry, 1997), e.g. for the number density size distribution of a mode as

$$n(d_p) = \frac{N}{\sqrt{2\pi} d_p \, ln\sigma_g} exp\left(-\frac{(lnd_p - lnd_{pg})^2}{2ln^2\sigma_g}\right) \tag{1.40}$$

with $n(d_p)$ the number concentration at diameter d_p, N the total number concentration, σ_g the geometric standard deviation, and d_{pg} the geometric mean diameter. One can now employ the concept of moments to conveniently derive surface and volume concentrations, the k-th moment of the distribution $n(d_p)$ being defined as

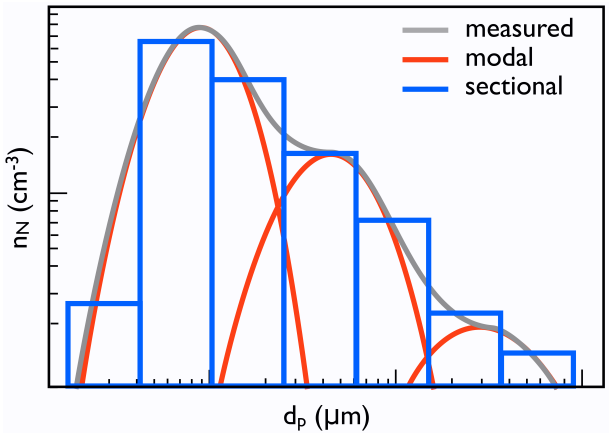

Figure 1.13: Schematic of typically used methods to represent a given (measured) aerosol distribution (gray solid line). For the modal approach: red solid lines show three log-normal distributions whose superposition is used to approximate the given distribution. For the sectional approach: blue boxes represent size bins.

$$M_k = N d_{pg}^k exp\left(\frac{k^2}{2} ln^2 \sigma_g\right) \tag{1.41}$$

(Binkowski and Shankar, 1995). Under the assumption that the aerosols are spherical, surface area S and volume V are proportional to the 2nd and 3rd moment of the distribution function with the constants of proportionality being

$$S = \pi M_2 \tag{1.42}$$

$$V = \frac{\pi}{6} M_3 \tag{1.43}$$

(Riemer, 2002). Knowing the density of the aerosol, the total mass of each mode can be derived. It is now possible to fully describe the system by deriving prognostic equations for three moments, e.g. in MADE as developed in Binkowski and Shankar (1995); Ackermann et al. (1998) with equations for the zeroth (total number concentration), third (total volume concentration) and sixth moment. Also, all processes acting on the aerosols can be translated into a form applicable to log-normal distributions (e.g. in Ackermann et al., 1998).

An alternative to the modal approach is the sectional approach like it is used for example in Gong et al. (2003) or Bessagnet et al. (2004). Gelbard and Seinfeld (1980) cover the basics of this approach: the density function of a size range covering most observed aerosols (e.g. 10 nm to 40 μm in Bessagnet et al. (2004)) is discretized into m not necessarily equally-spaced bins. $n(\nu, t)$ is the size distribution function, with ν representing particle size. The total mass of aerosols Q_l in bin l as interval $[\nu_{l-1}, \nu_l]$ is then

$$Q_l = \sum_{k=1}^{s} Q_{l,k} = \int_{\nu-1}^{\nu_l} \nu n(\nu, t) d\nu \tag{1.44}$$

for an aerosol of s different components. Coagulation kernels are set up defining the intra-bin mass transfer (see Gelbard and Seinfeld, 1980). Using a reasonable number of bins (e.g. 6 in (Bessagnet et al., 2004)) requires a substantial amount of equations to solve for the aerosol dynamical processes, and a number of prognostic variables that is often larger than for modules based on the modal approach. Hence the sectional approach tends to be more expensive in terms of computational demand.

Both approaches are used in current modeling systems, e.g. M7 (Vignati et al., 2004) or MADE (Ackermann et al., 1998) as examples for the modal approach, and CAM (Gong et al., 2003), the UCD module in CMAQ (Zhang et al., 2008), MOSAIC (Zaveri et al., 2008) or the aerosol module of the CHIMERE modeling system (Bessagnet et al., 2004). Sectional and modal approaches are only the two most often used approaches, though other methods exist as well, e.g. the stochastic particle-resolved approach of Riemer et al. (2009b).

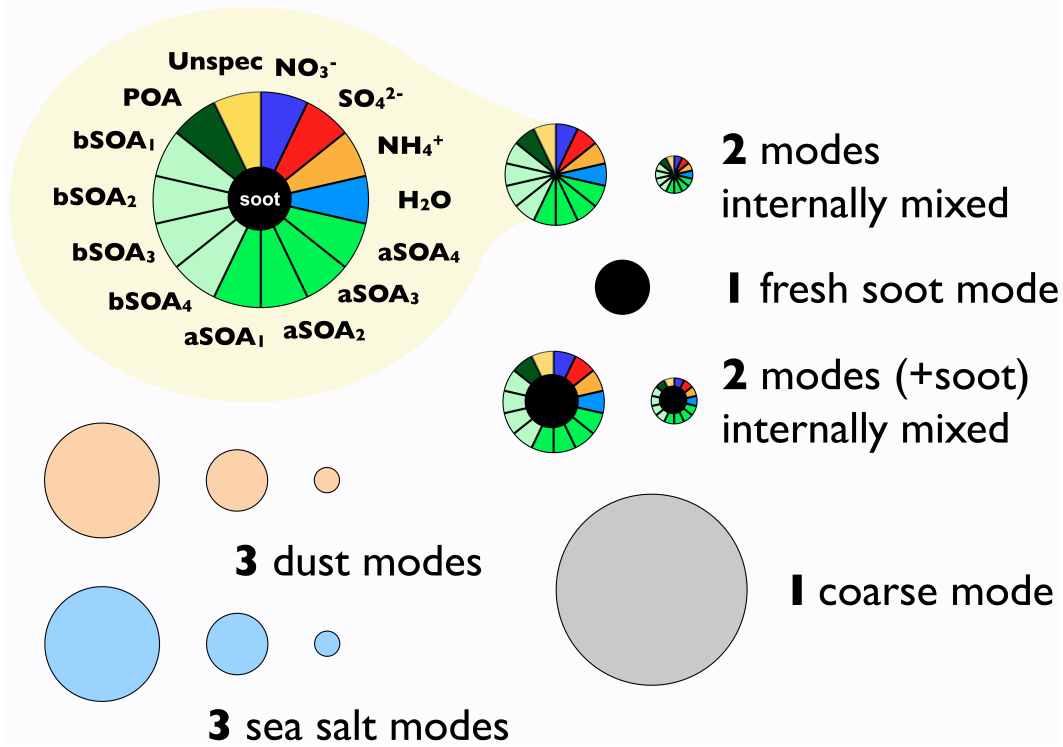

Figure 1.14: Representation of aerosols in COSMO-ART: MADEsoot extended (Riemer et al., 2004; Vogel et al., 2009). 2 pairs of Aitken and accumulation modes, one with and one without soot core, a fresh soot mode, a primary coarse mode, 3 modes for mineral dust and 3 for sea salt.

Representation of aerosols in COSMO-ART

COSMO-ART employs a modified version of the MADE, MADEsoot extended (Vogel et al., 2009) which explicitly considers the aging (coating with secondary substances) of soot particles (Riemer et al., 2003a). 5 modes represent secondary substances (a pair of Aitken and accumulation mode without soot core, a fresh soot mode, and a pair of Aitken and accumulation modes with soot core), and additionally 3 modes for mineral dust, and 3 for sea salt exist (Fig. 1.14).

1.3.5 Secondary inorganic aerosols

Several parameterisations for the representation of inorganic aerosol-/gas-phase thermodynamics exist. Very detailed calculations based on directly minimizing the Gibbs free energy, like AIM (Wexler and Clegg, 2002) or AIOMFAC (Zuend et al., 2008), and models with different simplifications like MESA (Zaveri et al., 2005a), ISORROPIA (Nenes et al., 1998; Fountoukis and Nenes, 2007) or EQSAM (Metzger et al., 2002, 2011). The latter are computationally efficient enough to be included in three-dimensional atmospheric simulations. These models simplify for example by dividing the problem into subsets based on the availability of certain species, and subsequently only using those species in the solution that are important in that case, which reduces the number of equations to solve and hence computational demand. This is done in ISORROPIA. The precalculation of look-up tables for the mutual deliquescence relative

humidity for a certain mixture is another possibility to reduce complexity. MESA (Zaveri et al., 2005a) uses sophisticated numerical techniques to speed up the numerical integration process of the otherwise rigorous equation system.

Current thermodynamic modules are distinguished not only by the accuracy of the solution for a given set of species, but also by the number of species considered. ISORROPIA in its first version of Nenes et al. (1998) for example did consider NH_4^+, SO_4^{2-}, NO_3^-, Na^+, and Cl^- in the aerosol and ignored other electrolytes, although they influence the deliquescence properties of the aerosols. Fountoukis and Nenes (2007) extended the module by crustal material species K^+, Ca^{2-}, and Mg^{2+}. The effect of organics on the solution is not considered so far.

In COSMO-ART, ISORROPIA in version 2 (Fountoukis and Nenes, 2007) is used, though crustal species, sodium and chloride are not considered as the representation in the aerosol module is missing.

1.3.6 Secondary organic aerosols

Accurate modeling of SOA is a topic of current research. Although parameterisations have been available for more than ten years (Schell et al., 2001) correlation with measured SOA is still insufficient, in general the models tend to underestimate mass substantially (Volkamer et al., 2006; Hallquist et al., 2009; Hodzic et al., 2009).

The work of Odum et al. (1996) sets the basis for most SOA parameterisations and is outlined briefly in the following. Therein, *yields* (mass of SOA produced per amount of reactive precursor) are used to estimate SOA production.

Assuming equilibrium between gas- and aerosol-phase implies that in the case where the actual vapor pressure of a given VOC oxidation product exceeds its saturation vapor pressure, the excess amount will partition into the aerosol phase (i.e. condense on existing particles or nucleate forming new ones). Odum et al. (1996) now stated that, based on the work of Pankow (1994), additionally to this condensing mass due to supersaturation, even more available low-volatility VOC oxidation product mass will partition into the aerosol-phase, depending on the amount of already available organic mass in the particle:

$$K_{om,i} = \frac{F_{i,om}}{A_i, M_o}, \tag{1.45}$$

with $K_{om,i}$ the partitioning coefficient for species i, $F_{i,om}$ the concentration of species i in the aerosol-phase, A_i its gas-phase concentration and M_o the total organic mass in the aerosol (eqn. 3 in Odum et al., 1996).

As VOC are comprised of a large number of species and numerous reactions take place, the total SOA mass yield Y is then the sum of all partitionings:

$$\sum_i Y_i = M_o \sum_i \left(\frac{\alpha_i K_{om,i}}{1 + K_{om,i} M_o} \right) \tag{1.46}$$

where α_i relates the total concentration of VOC i to the total amount of product formed (eqn. 7 in Odum et al., 1996).

From the comparison with a number of different smog chamber studies Odum et al. (1996) derived that two photochemical oxidation products ($i = 2$), one with low and one with higher volatility, are sufficient to reproduce the yields for various concentrations of organic aerosol mass and hence SOA production for different species can be described solving Equation 1.46 with parameters that can be estimated from smog chamber experiments.

Schell et al. (2001) implemented these findings into an operational SOA mechanism for three-dimensional air quality models - the *Secondary ORganic Aerosol Model (SORGAM)*. This is the mechanism used in COSMO-ART throughout this dissertation. In SORGAM, eight SOA classes are considered, four anthropogenic (2 from higher alkenes precursors, 2 from higher alkanes) and four biogenic (2 from α-pinene, 2 from limonene). Isoprene is not considered in SOA formation. The precursors can be oxidized by OH, O_3 and NO_3, which generates low-volatile gases that are then subject to a partitioning based on the work of Pankow (1994) and Odum et al. (1996).

From 1.46 they derived the aerosols concentration $C_{aer,i}$ for a species i as

$$C_{aer,i} = C_{tot,i} - C^*_{sat,i} \frac{C_{aer,i}/m_i}{\sum_{j=1}^{n}(C_{aer,j}/m_j) + C_{init}/m_{init})} \tag{1.47}$$

where $C_{tot,i}$ is the total concentration of compound i in both gas and aerosol, $C^*_{sat,i}$ is the saturation concentration for the pure species i, m_i its molecular weight, n the number of absorbing organic compounds (i.e. 8 for SORGAM), further are $C_{aer,j}$ and m_j the aerosol mass and molecular weight of each of them, and C_{init} and m_{init} the aerosol mass and mean molecular weight at the start of the calculation.

This system then needs to be solved iteratively, as the total absorbing mass (the denominator in Eqn. 1.47) is not known initially.

A lot of research has been conducted since the formulation of SORGAM. An example of a current representation of SOA formation (which is also currently being implemented in COSMO-ART) is the *volatility basis set (VBS)* approach of Donahue et al. (2006). Rather than assuming that volatile substances form very low volatile precursors by a one-step oxidation, which then partition into the aerosol-phase, the VBS approach groups organic substances according to their volatility into volatility "bins" (Fig. 1.15). Once applying such a VBS scheme, processes like dilution, chemical reactions and mixing do not further impact the partitioning between gas and aerosol, but rather a set of distribution matrices are applied which reshuffle the organic mass distribution within the bins. Recently, also the VBS approach has been extended owing to the finding that besides volatility, also the oxidation state of the aerosol is important as it allows an improved description of the oxidation chemistry and a better comparison with measurements. Here, additionally to the volatility, the O:C ratio is added as second dimension and the new approach is called *2D volatility basis set (2D-VBS)* accordingly (Donahue et al., 2011).

1.3.7 Feedback processes

Online-coupled modeling systems allow the inclusion of (climate) feedback processes. *Radiation feedbacks* require a coupling to the scheme that calculates short- and longwave radiation in the underlying meteorological model. These modules typically partition the electromagnetic spectrum in a number of bands in the short- and longwave range in such a way that the major absorption and transmission features of atmospheric constituents can be represented in a computationally efficient manner. GRAALS (Ritter

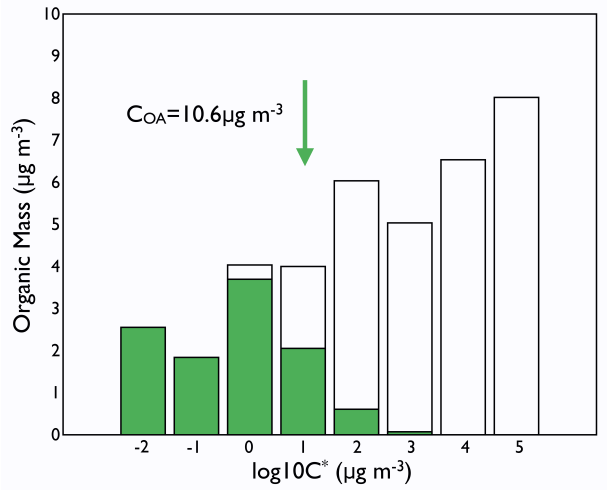

Figure 1.15: The VBS, adapted from Fig. 1a of Donahue et al. (2006). "Partitioning of a collection of semi-volatile compounds, with total loadings (in $\mu g\,m^{-3}$) shown with full bars and the condensed-phase portion with filled (green) bars. Compounds are distributed according to their mass-equivalent effective saturation concentration (C*, also in $\mu g\,m^{-3}$), which is presented as a logarithmically distributed basis set. $C_{OA} = 10.45\ \mu g\,m^{-3}$, shown with an arrow, and so that bin is evenly split between the two phases" (Donahue et al., 2006).

and Geleyn, 1992) is used in COSMO-ART, McRad (Morcrette et al., 2008) in the ECMWF IFS, and the combination of the Goddard scheme (Chou et al., 1998) (shortwave) and the rapid radiative transfer model (RRTM, Mlawer et al., 1997) (long-wave) in WRFChem. The inclusion of aerosols requires detailed calculations of the scattering properties according to Mie-theory which is usually not feasible within air quality applications. The required input parameters are (in case of GRAALS) extinction coefficient τ, single scattering albedo (SSA), and asymmetry factor γ, and these parameters are a function of aerosol size distribution, chemical composition and water content. In COSMO-ART this problem is solved by relying on precalculations of these parameters with a detailed model of Mie-theory for a range of ambient aerosol conditions. The resulting values are then arranged as functions of wet mass or mass fractions. In the operational application, the values for τ, SSA, γ are the interpolated output of the precalculated look-up tables (Vogel et al., 2009). All this is done for a large number of single wavelengths and the results are weighted according to Bäumer et al. (2007), with special considerations for soot aerosols (Vogel et al., 2009). A comparable coupling in WRFChem has been achieved by Fast et al. (2006).

Implementation of *cloud feedbacks* are usually more involved than radiation feedbacks. The basis of the feedback is that for the nucleation of cloud droplets, cloud condensation nuclei (CCN) are required, which are those aerosols that can activate to cloud droplets under the given supersaturation. How many cloud droplets exist is a function of the number of suitable aerosol particles. Which of them are suitable is still a matter of current research. Soluble, hygroscopic aerosols are favorable for activation, while hydrophobic substances like fresh soot are not. It is further complicated by the fact that water not only exists as vapor and cloud droplets but also in the ice phase as crystals, snow flakes, and hail, and combinations like graupel. A particle is either an efficient cloud condensation nucleus or an efficient ice nucleus (IN) and vice versa. CCN are liquid, while IN are solid. For the first indirect or cloud albedo effect the optical properties of the cloud has to be calculated which is only feasible if the number and size distribution

of the cloud droplets is known. Most operational cloud microphysics schemes treat the water content in each species as a bulk quantity (e.g. COSMO), hence do not represent the size distribution of cloud droplets. It is therefore necessary to first include a more detailed cloud microphysics scheme into the meteorological model itself, before the aerosols as calculated by aerosol module can be used as CCN/IN. Radiative calculations for clouds are then (in the shortwave) very similar to the methods outlined above. Also the second indirect effect depends on a representation of droplet number and size distribution in the meteorological model. Bangert et al. (2011) included such a coupling into COSMO-ART, which requires the exchange of the operational cloud microphysics scheme in COSMO with a more detailed representation by Seifert and Beheng (2006). Chapman et al. (2009) recently evaluated the coupling as it has been achieved in WRFChem.

1.4 Dissertation overview

In this dissertation the effects of changing anthropogenic emissions on ambient aerosol characteristics over the European continent during the last decades are investigated by the online-coupled regional chemistry-climate model COSMO-ART. Considerable efforts have been taken to setup a modeling system with state-of-the-art components and input datasets, which resulted in an emissions and initial and boundary conditions data preprocessing system (Appendices B and C). The first chapter presents a comprehensive evaluation of the model system against various kinds of measurement datasets to understand to which extend the system is able to represent current ambient aerosol characteristics, as this is a prerequisite for further investigations on the effect of changes in emissions on the aerosol. From the results of this chapter it became clear that an aqueous-phase chemistry and wet scavenging scheme was necessary to remedy discrepancies found in the comparison of aerosol chemical composition with measurements. Chapter 3 presents the implementation of such a scheme in COSMO-ART. The improved system is then used in chapter 4 to investigate the effects of different emissions reduction measures, and the contributions of reductions in single precursor species onto changes in aerosol chemical composition.

Chapter 2

Towards an online-coupled regional chemistry climate model: evaluation of trace gases and aerosols in COSMO-ART

Published in Geoscientific Model Development, 4, 1077-1102, 2011.
The supplement mentioned in the text is found in Appendix A.

Authors: Christoph Knote[1,2], Dominik Brunner[1,2], Heike Vogel[3], James Allan[4], Ari Asmi[5], Mikko Äijälä[5], Samara Carbone[6], Hugo Denier van der Gon[7], Jose L. Jimenez[8], Astrid Kiendler-Scharr[9], Claudia Mohr[10], Laurent Poulain[11], André S. H. Prévôt[10], Erik Swietlicki[12], and Bernhard Vogel[3]

[1] Laboratory for Air Pollution / Env. Technology, Empa Materials and Science, 8600 Duebendorf, Switzerland
[2] C_2SM Center for Climate Systems Modeling, ETH, Zurich, Switzerland
[3] Institute for Meteorology and Climate Research, Karlsruhe Institute of Technology, Karlsruhe, Germany
[4] School of Earth Atmospheric, and Environmental Sciences, National Centre for Atmospheric Science, University of Manchester, Manchester, UK
[5] Department of Physics, University of Helsinki, Helsinki, Finland
[6] Air Quality Research, Finnish Meteorological Institute, Helsinki, Finland
[7] TNO Princetonlaan 6, 3584 CB Utrecht, The Netherlands
[8] CIRES and Dept. of Chemistry and Biochemistry, Univ. of Colorado, Boulder, CO, USA
[9] Institut IEK-8, Troposphäre, Forschungszentrum Jülich, Jülich, Germany
[10] Laboratory of Atmospheric Chemistry, Paul Scherrer Institute, Villigen, Switzerland
[11] Leibniz Institute for Tropospheric Research, Leipzig, Germany
[12] Division of Nuclear Physics, Department of Physics, Lund University, Lund, Sweden

2.1 Abstract

The online-coupled, regional chemistry transport model COSMO-ART is evaluated for periods in all seasons against several measurement datasets to assess its ability to represent gaseous pollutants and ambient aerosol characteristics over the European domain. Measurements used in the comparison include long-term station observations, satellite and ground-based remote sensing products, and complex datasets of aerosol chemical composition and number size distribution from recent field campaigns. This is the first time these comprehensive measurements of aerosol characteristics in Europe are used to evaluate a regional chemistry transport model. We show a detailed analysis of the simulated size-resolved chemical composition under different meteorological conditions. Mean, variability and spatial distribution of the concentrations of O_3 and NO_x are well reproduced. SO_2 is found to be overestimated, simulated $PM_{2.5}$ and PM_{10} levels are on average underestimated, as is AOD. We find indications of an overestimation of shipping emissions. Time evolution of aerosol chemical composition is captured, although some biases are found in relative composition. Nitrate aerosol components are on average overestimated, and sulfates underestimated. The accuracy of simulated organics depends strongly on season and location. While strongly underestimated during summer, organic mass is comparable in spring and autumn. We see indications for an overestimated fractional contribution of primary organic matter in urban areas and an underestimation of SOA at many locations. Aerosol number concentrations compare well with measurements for larger size ranges, but overestimations of particle number concentration with factors of 2 - 5 are found for particles smaller than 50 nm. Size distribution characteristics are often close to measurements, but show discrepancies at polluted sites. Suggestions for further improvement of the modeling system consist of the inclusion of a revised secondary organic aerosols scheme, aqueous-phase chemistry and improved aerosol boundary conditions. Our work sets the basis for subsequent studies of aerosol characteristics and climate impacts with COSMO-ART, and highlights areas where improvements are necessary for current regional modeling systems in general.

2.2 Introduction

Aerosols affect climate through changes in the radiation budget (direct effect), the subsequent changes in atmospheric stratification (semi-direct effect, Haywood and Boucher, 2000) and through changes in cloud development and lifetime due to the differences in available cloud condensation / ice nuclei (indirect effects, Lohmann and Feichter, 2005). Aerosols also constitute a health concern if they are small enough to traverse the human respiratory tract (Laden et al., 2006; Dockery et al., 1996). Once in the lungs their toxicity depends on size (Donaldson et al., 2000) and chemical composition (Aktories et al., 2009; Hoek et al., 2002). Within the climate system, their influence on the radiation budget depends on their optical properties, and how they affect clouds is a function of size and hygroscopicity. Size, chemical composition, and optical properties are therefore indispensable parameters that need to be well represented if any study of aerosol effects should be accurate.

Up to now, climate modeling studies including aerosols often lack a comprehensive description of aerosol characteristics, due to the high computational demand of such a complex effort. Approaches range from simple bulk mass aerosol schemes with only externally mixed aerosols, up to multi-component, size-resolving aerosol modules including explicit aging of aerosols and interactions with radiation and clouds. Often these modules lack parts (or all) of the interaction between gas- and aerosol-phase. Nucleation of ammonium-sulfate particles is represented in most models, and also the condensation of organics onto

particles is included in some. Nitrates, which can represent up to 50% of ambient aerosol mass in polluted regions (Putaud et al., 2004), were missing for example in all but two models participating in the Fourth Assessment Report of the Intergovernmental Panel on Climate Change (IPCC, Meehl et al., 2007). This was probably due to the lack of the necessary, but computationally expensive, gas-phase chemistry leading to nitrate formation.

Current efforts try to bridge the gap between accurate representation of all aerosol components while retaining the ability to model climatic timescales. To reach this goal it is necessary to couple climate and air quality models. One such modeling system which focuses on the regional scale combines the numerical weather prediction model of the Consortium for Small Scale Modeling (COSMO, Baldauf et al., 2011) with an extension for Aerosols and Reactive Trace gases: COSMO-ART (Vogel et al., 2009). It is based on state-of-the-art components for the description of meteorology, chemistry and aerosols and features an integrated approach to couple them. Such an "online"-coupling allows for consistent treatment of all components by the same parameterization (e.g. advection, diffusion, convection) and avoids unnecessary interpolation steps. Additionally, simulation of feedbacks between chemistry, aerosols and meteorology becomes possible. Grell and Baklanov (2011) showed the importance of this approach and its benefits compared to traditional "offline" models, and Zhang (2008) gave a comprehensive overview of the available modeling systems. COSMO-ART is in its composition very similar to the Weather Research and Forecasting model (WRF) extended by chemistry and aerosols: WRF/chem. Grell et al. (2005) presented a comprehensive evaluation for this modeling system. Most of the components of COSMO-ART are well known and tested. However, their interplay and integration into the modeling system lacks a thorough evaluation.

In this work we analyse COSMO-ART regarding its ability to represent ambient concentrations of gaseous and particulate matter constituents over Europe under different meteorological conditions. Through a detailed analysis of aerosol size distributions and chemical composition we set the basis for subsequent analyses of aerosol-climate interactions in COSMO-ART. We have collected an extensive evaluation dataset of satellite-derived NO_2 and aerosol optical depth (AOD), long-term station measurements for gas-phase tracers, bulk aerosol mass and optical properties, as well as aerosol mass spectrometer (AMS) measurements of aerosol chemical composition and measurements of aerosol size distribution. The comprehensive datasets of aerosol characteristics have been created during recent field campaigns of the European integrated Project on aerosol cloud climate air quality interactions (EUCAARI, Kulmala et al., 2009), during intensive measurement campaigns of the European Monitoring and Evaluation Programme (EMEP, `http://www.emep.int`) and in coordinated measurements of the European Supersites for Atmospheric Aerosol Research (EUSAAR, `http://www.eusaar.net`) and the German Ultrafine Aerosol Network (GUAN, Birmili et al., 2009).

Our simulations employ full gas-phase chemistry and aerosol dynamics. Spatial and temporal resolution of input data (meteorology, anthropogenic emissions) and model setup is on the top end of currently possible simulations. While the modeling system is currently still too expensive to be used for climate simulations, the results of our evaluation efforts can be seen as a benchmark for what degree of accuracy in simulation gas and aerosol characteristics can be expected in future fully-coupled regional chemistry-climate models, and identify model deficiencies which would need to be remedied before such simulations can be made.

We begin with a description of the system, its setup and the measurement datasets used in evaluation. The second chapter describes the findings of our evaluation against the different datasets and discusses the results. The last chapter provides a more in-depth discussion of simulated aerosol characteristics. We conclude with implications for future studies and give directions for further developments of the modeling

system.

2.3 Methods

2.3.1 Modeling system

COSMO-ART is a regional chemistry transport model, online-coupled to the COSMO regional numerical weather prediction and climate model (Baldauf et al., 2011). COSMO is operationally used for numerical weather prediction (NWP) purposes by several European national meteorological services and research institutes. In its climate version (Rockel et al., 2008) it has been used in several studies of regional climate impact assessment (e.g. Jaeger and Seneviratne, 2010; Suklitsch et al., 2008; Hohenegger et al., 2008) and participated in the IPCC fourth assessment report modeling ensemble (Christensen et al., 2007). The extension for Aerosols and Reactive Trace gases (ART) contains a modified version of the Regional Acid Deposition Model, Version 2 (RADM2) gas-phase chemistry mechanism (Stockwell et al., 1990). It has been extended by a more sophisticated isoprene scheme of Geiger et al. (2003) for a better description of biogenic volatile organic compounds (VOC), but does not include recent findings regarding formation of secondary organic aerosols and OH recycling due to isoprene chemistry (e.g. Paulot et al., 2009). Aerosols are represented by the modal aerosol module MADE (Modal Aerosol Dynamics Model for Europe, Ackermann et al., 1998), improved by explicit treatment of soot aging through condensation of inorganic salts (Riemer et al., 2003a) and additional modes for mineral dust (Stanelle et al., 2010) and sea salt. Nucleation of new particles is formulated according to Kerminen and Wexler (1994) allowing for binary homogeneous nucleation of sulfuric acid. The condensation of vapours from biogenic and anthropogenic VOCs is parametrized with the Secondary Organic Aerosol Model (SORGAM) of Schell et al. (2001). This is still a commonly used module, although Fast et al. (2009) showed that this scheme underpredicts SOA concentrations by up to a factor of 10 in very polluted regions. Biogenic VOC emission fluxes, considering isoprene, α-pinene, other monoterpenes and a class of unidentified compounds, are calculated online with a Guenther-type model presented in Vogel et al. (1995), using land use data from the Global Land Cover 2000 (GLC2000) dataset (Bartholomé and Belward, 2005). Seasalt emissions follow Lundgren (2006), and mineral dust is parameterized as described in Vogel et al. (2006). Dry deposition is modeled by a resistance approach (Baer and Nester, 1992). Washout of aerosols is included by a parameterization of Rinke (2008). Wet removal of gases and aqueous-phase chemistry are currently not considered. COSMO-ART is fully online-coupled, and currently allows for feedbacks of aerosols on radiation (direct / semi-indirect effects). Cloud feedbacks (indirect effects) have been included in a research version (Bangert et al., 2011) but were not used in this work. A complete description of the modeling system can be found in Vogel et al. (2009) and references therein. In our study, COSMO-ART based on COSMO version 4.17 is used.

For meteorology we used initial and boundary conditions from the European Centre for Medium-Range Weather Forecasts (ECMWF) Integrated Forecast System (IFS) model, with an update frequency of 3 h. For runs on climatic timescales boundary data could e.g. be provided by the ECHAM-HAM (Stier et al., 2005) or (for past episodes) by ERA-40 (Uppala et al., 2005) / ERA-Interim (Simmons et al., 2007) reanalyses, which are all based on the IFS and would therefore deliver comparable meteorology. Boundary data for gas-phase species, including most of the lumped NMVOC compounds, were provided through simulations of the Model for Ozone and Related chemical Tracers (MOZART) driven by meteorological data from the National Center for Environmental Prediction (NCEP) presented in Emmons et al. (2010),

with an update frequency of 6 h. No boundary data for aerosol components were available from MOZART or other models that matched our aerosol mechanism. Therefore, we took the output of a previous (otherwise identical) simulation of COSMO-ART and chose one point in the Northern Atlantic (8.7°W, 47.4°N, see Fig. 2.1). We averaged the simulated aerosol characteristics over the complete simulation period, and used this vertical column as lateral boundary conditions for all aerosol variables. While this gives more realistic aerosol concentrations at the boundaries, the total inflow will still be underestimated. In this work we will show that simulated particulate matter concentrations are often underestimated, which will also be the case for boundary conditions based on such a simulation.

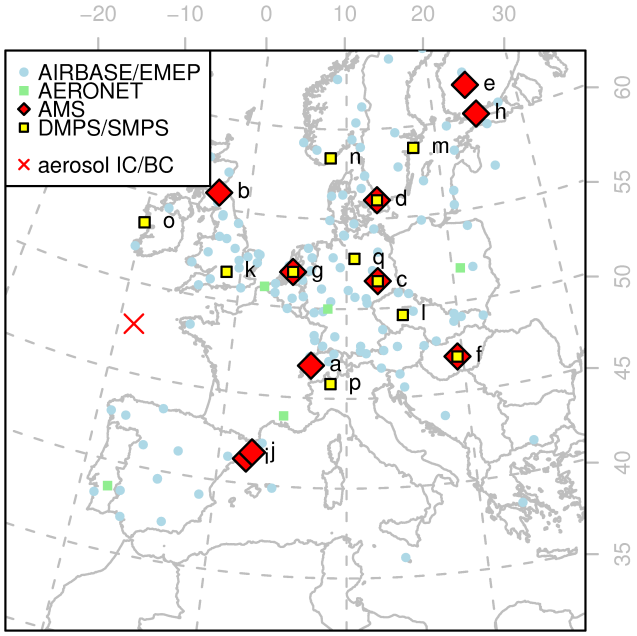

Figure 2.1: Model domain and measurement station positions. AIRBASE/EMEP: gas-phase and bulk aerosol mass, AMS: aerosol chemical composition (EIMP/EUCAARI/EUSAAR), DMPS/SMPS: aerosol size distribution (EUSAAR/GUAN), AERONET: aerosol optical depth. The position of the column used for aerosol boundary conditions is marked with a red cross (aerosol IC/BC). Stations with AMS and/or DMPS/SMPS measurements: [a] Payerne (CH), [b] Aucencorth/Bush (UK), [c] Melpitz (DE), [d] Vavihill (SE), [e] Hyytiälä (FI), [f] K-Puszta (HU), [g] Cabauw (NL), [h] Helsinki (FI), [i] Barcelona (ES), [j] Montseny (ES), [k] Harwell (UK), [l] Kosetice (CZ), [m] Aspvreten (SE), [n] Birkenes (NO), [o] Mace Head (IE), [p] Ispra (IT), [q] Waldhof (DE). Several named stations measured both chemical composition and size distribution.

The emission inventory for Europe developed by TNO (Netherlands) within the Monitoring Atmospheric Composition and Climate (MACC) project (TNO/MACC, Kuenen et al., 2011; Denier van der Gon et al., 2010) provides anthropogenic emissions. This is a follow-up and improvement of the earlier TNO-GEMS emission database (Visschedijk et al., 2007). Therein, emissions from 10 different SNAP (Selected Nomenclature for sources of Air Pollution) source categories are represented by a spatial pattern of annual emission totals for the years 2003 - 2007, and statistical time functions for species, country and source category dependent monthly, weekly and daily cycles. Our speciation of non-methane volatile organic compounds (NMVOC) mass totals is done using composition information from Passant (2002)

and a translation matrix to RADM2 (J. Keller, PSI, Switzerland, personal communication, 2009). Aerosol emissions are provided as mass totals of particulate matter below 10 μm (PM_{10}) and below 2.5 μm ($PM_{2.5}$) in diameter. We distribute them onto the different MADE modes following Elleman and Covert (2010), with a disaggregation into chemical components using a split table from TNO (Table 2.1). Emission country totals per SNAP category from the International Institute for Applied Systems Analysis (IIASA, PRIMES09 scenario) serve to extrapolate TNO/MACC emissions to years after 2007. With its spatial resolution of about 8 km (0.125 x 0.0625°), the description of the time evolution of emissions and the comprehensive set of emitted species this dataset is one of the most detailed currently available emission inventories for Europe. Preparation of all input datasets for COSMO-ART is done using INT2COSMO-ART (Appendix 2.7).

Our modeling domain (Fig. 2.1) covers the greater European region, with a horizontal resolution of 0.17° and a grid of 200 x 190 points. Vertically, the model is discretized into 40 terrain-following hybrid sigma levels, with the lowest level at 10 m (layer thickness: 20 m) and ranging up to approx. 24 000 m (20 hPa). A Runge-Kutta time integration scheme is employed with time steps of 40 s. Tracers are advected horizontally via a semi-lagrangian method conserving mass over the total domain ("globally mass-conserving"). The overall model configuration closely follows the current operational setup of COSMO-EU of the German Meteorological Service (DWD).

2.3.2 Measurement data

Meteorological parameters have been taken from the operational surface synoptic observations (SYNOP) network, providing measurements for temperature, dew point temperature, wind speed and direction at or in the vicinity of most measurement points of chemical composition. In the EMEP programme a number of stations throughout Europe report quality-controlled, long-term measurements of gaseous precursor substances and aerosol variables. AIRBASE (European AIR quality dataBASE, `http://airbase.`

Table 2.1: Contributions (in % mass) to $PM_{2.5}$ emissions as used in the TNO/GEMS emission inventory. Sodium (Na) is not used directly in the simulations, but added to the "other primary" category, representing the remaining, non-carbonaceous primary $PM_{2.5}$ part (including e.g., minerals, metal oxides, product emissions). Sulfate contributions have been calculated assuming 2% of total emitted SO_2 mass (IIASA RAINS emissions for 2000) is H_2SO_4 for all SNAP categories except SNAP 1 and 3. There, measured compositions of coal fly ash (as dominant contributor to source category) as reported by Lipsky et al. (2002) and Senior et al. (2000) are used as basis. OC depicts organic carbon, a ratio of 1.3 has been used to convert OC to organic aerosol (OA).

SNAP	Description	SO_4^{2-}	OC	BC	Na	other primary
1	Energy transformation	15.0	2.0	1.0	1.5	80.0
2	Small combustion sources	2.0	35.0	18.0	1.0	44.0
3	Industrial combustion	10.0	3.0	1.0	1.0	84.0
4	Industrial process emissions	3.0	3.0	5.0	1.5	88.0
5	Extraction of fossil fuels	0.0	0.0	0.0	0.5	99.5
6	Solvent and product use	0.0	0.0	0.0	0.0	0.0
7	Road transport	1.0	32.0	49.0	0.1	17.0
8	Non road transport (e.g. international shipping)	3.0	31.0	41.0	0.2	26.0
9	Waste handling and disposal	0.0	31.0	20.0	0.0	49.0
10	Agriculture	0.0	48.0	15.0	0.0	37.0

eionet.europa.eu/) provides measurements at a much larger number of stations, but with heterogeneous quality and mostly at rather polluted locations not representative for the model grid size of 0.17° (approx. 19 km at model domain center). While AIRBASE, in its recently published version 5, provides data up to the end of 2009, EMEP data were only available until 2008. As one of our simulation periods is in 2009, we settled on the following method to provide a homogeneous dataset of measurements for gas-phase species and aerosol mass for all periods: We retrieved data from AIRBASE, but restricted the stations used to those which also report to EMEP. As discrepancies between modelled and measured values might be related to the type and location of a measurement station, we have additionally disaggregated the selected stations into categories based on the representativeness study done by Henne et al. (2010), which includes a more comprehensive analysis of the surroundings of each station. Therein, stations are classified regarding their pollution burden and usability in a model evaluation. We have used the "alternative classification" described in the supplement S3 in Henne et al. (2010), which gives classes ranging from very clean stations ("rural/remote"), stations with very variable pollution levels ("rural/coastal"), and stations representative for a larger area ("rural"), up to stations with a strong influence of large urban areas in their vincinity ("suburban/urban"). Most EMEP stations are found in the "rural" and "rural/coastal" classes, and are seen as the most representative when evaluating model results.

The Aerosol Robotic Network (AERONET) (Holben et al., 1998) provides measurements of aerosol optical depth (AOD) for analysis of the optical properties. Aerosol mass spectrometer (AMS) measurements give quantitative measurements of the chemical composition of submicron non-refractory aerosol mass ($NR - PM_1$) with high temporal resolution (Canagaratna et al., 2007). AMS data collected at several sites throughout Europe during measurement campaigns of the EMEP/EUCAARI project in October 2008 and March 2009 were used, as well as from an EMEP intensive campaign in June 2006. No evaluation of elemental carbon has been made, as the different measurement techniques used make even inter-station comparison difficult (Andreae and Gelencsér, 2006), and devising a homogenized dataset was out of scope for this work. Homogenized measurements of aerosol size distribution from scanning mobility particle sizer (SMPS) and differential mobility particle sizer (DMPS) instruments were provided in Asmi et al. (2011) as a result of the EUSAAR project and data from the GUAN network (Birmili et al., 2009), with 24 measurement sites in Europe. Figure 2.1 shows the locations of ground-based stations used in our evaluation.

Finally, satellite-derived datasets provide a vertically integrated view on model performance. In our analysis, tropospheric columns of NO_2 from the Ozone Monitoring Instrument (OMI) were used for gas-phase comparison. The NO_2 columns are based on the Empa OMI NO_2 retrieval (EOMINO) which includes several improvements as compared to operational products in particular regarding a better representation of topography and surface reflectance using high-resolution data sets (Zhou et al., 2009, 2010). To estimate the accuracy of the spatial distribution of simulated aerosol loadings aerosol optical depth (AOD) retrieved from the Moderate Resolution Imaging Spectrometer (MODIS) (Levy et al., 2007, MOD04_L2 product) were used.

2.3.3 Investigation periods

The selection of the investigation periods was driven by two goals: to evaluate model performance under typical weather conditions and in all seasons, and to have AMS measurement data available for comparison. Apart from the campaign measurement data, AIRBASE and satellite data were available for all simulations. The following periods were chosen:

"Winter case": 23 January - 11 February 2006

A stable high pressure system with very low surface temperatures was present over Europe from 23 January onwards, with only minor disturbances on 5 - 7 February. Over Switzerland and Eastern Europe, this resulted in an episode with strong temperature inversions and exceptionally high particulate matter (PM) concentrations. The Swiss legislative limit for daily mean PM_{10} (particulate matter below 10 μm in diameter) of 50 $\mu g/m^3$ was exceeded every day between 27 January and 5 February at several measurement stations. This episode represents a typical winter situation where high pollution levels are building up through strong inversions and local emissions are the strongest contributors to pollution levels (Holst et al., 2008).

"Summer case": 10 - 29 June 2006

This episode was characterized by dry, sunny and warm conditions due to a stable high pressure system from 10 - 24 June, and a transient low pressure system with embedded thunderstorms on 25 to 29 June. Such a situation is associated with strong photochemistry and high O_3 levels, representing a typical "summersmog" episode. AMS instruments were deployed in Payerne (CH), Harwell and Auchencorth (UK) during this period in the context of an EMEP intensive measurement campaign. We used data from Payerne and Auchencorth in our analysis.

"Autumn case": 1 - 20 October 2008

A low pressure system over Scandinavia brought polar airmasses towards Europe at the beginning of the month. From 5 - 20 October generally mild and sunny conditions prevailed. On 16 October a low pressure disturbance passed, bringing rain to Central Europe. Frequent disturbances by mesoscale systems gradually change a summertime atmosphere towards a wintertime one in this simulation. During this period, an EMEP/EUCAARI measurement campaign took place, from which we received AMS data for Payerne (CH), Melpitz (DE), Vavihill (SE), Hyytiälä (FI) and K-Puszta (HU). EUSAAR size distribution data were available for this period.

"Spring case": 1 - 20 March 2009

A low pressure system originating over the North Atlantic brought cold weather on 1 and 2 March. It was followed by spring-like conditions from 13 - 18 March, and a cold surge from NE on 20 March. We regard this situation as typical of spring, with first warm days including the initial onset of BVOC emissions, intermitted by "cleansing" periods with clouds, precipitation and strong mesoscale forcing. Another EMEP/EUCAARI campaign took place during this period, from which we present data from AMS instruments deployed in Payerne (CH), Melpitz (DE), Vavihill (SE), Hyytiälä (FI), Cabauw (NL), Helsinki (FI), Barcelona (ES), and Montseny (ES). EUSAAR size distribution data were available for this period.

2.4 Evaluation

The following section contains a description of the results of our evalution efforts, starting with meteorology, then trace gases and finally aerosol characteristics. Each section is accompagnied by a figure / table summarizing the results for the species discussed. Section 2.5 then further elaborates on the results for aerosol characteristics.

2.4.1 Meteorology

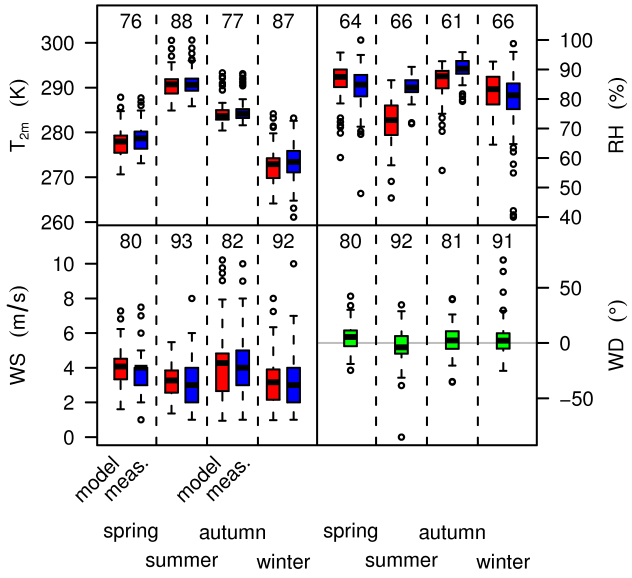

Figure 2.2: Boxplots of modelled (red) and measured (blue) median values of 2 m temperature (T_{2m}) and relative humidity (RH), and 10 m wind speed (WS). Note that 10 m wind direction (WD) are mean biases (green). Station RH was calculated from T_{2m} and Td_{2m}. Used are measurements from the SYNOP station nearest to each AIRBASE/EMEP station used in Figure 2.3. The number of stations used is shown at the top of each comparison. Simulations are ordered to represent an annual cyle: spring 2009, summer 2006, autumn 2008 and winter 2006.

COSMO-ART is in its meteorological core code identical with the NWP model COSMO, and its performance is continuously verified by several European weather services and in more detail also within field campaigns like e.g. in Barthlott et al. (2011). Meteorological evaluation has therefore been limited in this work to surface parameters. In all periods, the comparison of simulated temperature, dew point temperature, wind direction and wind speed show very good agreement with SYNOP measurement data both in terms of temporal variability and average values (Figure 2.2). Sometimes the (diurnal) variability is underestimated by the simulations (not shown), which is not unexpected for such coarse grid simulations due to the averaging onto a 0.17° grid box (e.g. Schlünzen and Katzfey, 2003; Heinemann and Kerschgens, 2005). The means of temperature, wind speed and direction are well reproduced (Table 2.2). Except for the summer 2006 period, where the model shows a negative bias (Figure 2.2), also relative humidity is realistically represented. The negative bias in summer 2006 might be related to an unrealistic initialization of soil moisture. Further investigation is needed to remedy this deficiency.

Table 2.2: Normalized mean biases (%) in spring, summer, autumn and winter (SP,SU,AU,WI) for SYNOP and AIRBASE datasets, satellite comparisons and aerosol datasets. Satellite biases are the mean over all grid points, only land points and only sea points. AERONET comparison shows biases model - AERONET (AER), model - MODIS (MOD) at AERONET station, and MODIS - AERONET (DIF). AMS and EUSAAR biases are the mean over all stations presented in the evaluation, the number of stations in each period is given in the notes.

	SP	SU	AU	WI	note
Meteorology (SYNOP)					
T_{2m}	0	0	0	0	
WS_{10m}	3	3	6	-1	
WD_{10m}	6	3	3	3	
RH	6	-15	-4	10	
Gas-phase tracers and aerosol bulk mass (12-18 LT)					
O_3	-12	-15	2	-22	rural
	-16	-3	2	-22	remote
	-17	-13	-1	-23	coastal
NO_2	-2	-10	18	11	rural
	7	-39	44	-3	remote
	10	49	44	14	coastal
NO	-2	-14	-21	-40	rural
	69	19	75	36	remote
	-41	-48	-37	-30	coastal
SO_2	108	0	49	39	rural
	60	72	324	-11	remote
	155	203	473	75	coastal
PM_{10}	-35	-48	3	-43	rural
	8	-39	15	-25	remote
	16	-25	43	-7	coastal
$PM_{2.5}$	-2	-55	-11	1	rural
	13	21	43	27	remote
	-26	-36	101	-2	coastal

	SP	SU	AU	WI	note
Satellite observations					
NO_2	31	1	56	59	all
(OMI)	10	-11	38	40	land
	66	28	108	121	sea
AOD	-58	-56	-55	-49	all
(MODIS)	-50	-58	-31	-44	land
	-61	-55	-65	-51	sea
AOD at stations (AERONET/MODIS)					
AOD	-22	-61	-14	-46	AER
	-30	-57	-27	-41	MOD
	14	19	2	-10	DIF
Aerosol chemical composition					
NO_3^-	39	-48	47	-	8,3,5,-
NH_4^+	-33	-72	-34	-	8,3,5,-
SO_4^{2-}	-86	-84	-81	-	8,3,5,-
OA	1	-61	-17	-	8,2,5,-
Aerosol number concentrations					
N_{30to50}	149	-	97	-	9,-,10,-
N_{50}	71	-	53	-	9,-,10,-
N_{100}	64	-	76	-	9,-,10,-
N_{250}	139	-	257	-	9,-,10,-

IFS analysis data were used to initialize and force the model at the lateral boundaries. Within the model domain COSMO runs freely, creating its own dynamics. This is not the best possible setup. Constant data assimilation from observations like it is done for operational analysis (e.g. nudging), or a reinitialization of meteorology after one or two days could further improve meteorology. However, using simple comparison with SYNOP data we found no significant loss in accuracy of the simulation over the whole integration period when compared against several SYNOP stations, suggesting that the lateral forcing provides a sufficiently strong constraint for the meteorology within the model domain. Some of the underestimated (diurnal) variability found would likely be improved at increased resolution.

The modest deficiencies found such as an underestimated diurnal variability are well known to NWP modellers and represent problems such models are currently faced with in general (e.g. Schlünzen and Katzfey, 2003; Heinemann and Kerschgens, 2005). Mean wind speeds simulated by the model, for example, are below 5% biases at nearly all stations in all periods (Table 2.2), and temperatures show essentially no bias. Overall, meteorology is well represented and these findings set the basis for a successful air quality simulation. They also highlight one of the key benefits of this modeling system: Its direct coupling to an operational weather prediction model.

2.4.2 Gas-phase

Mean concentrations

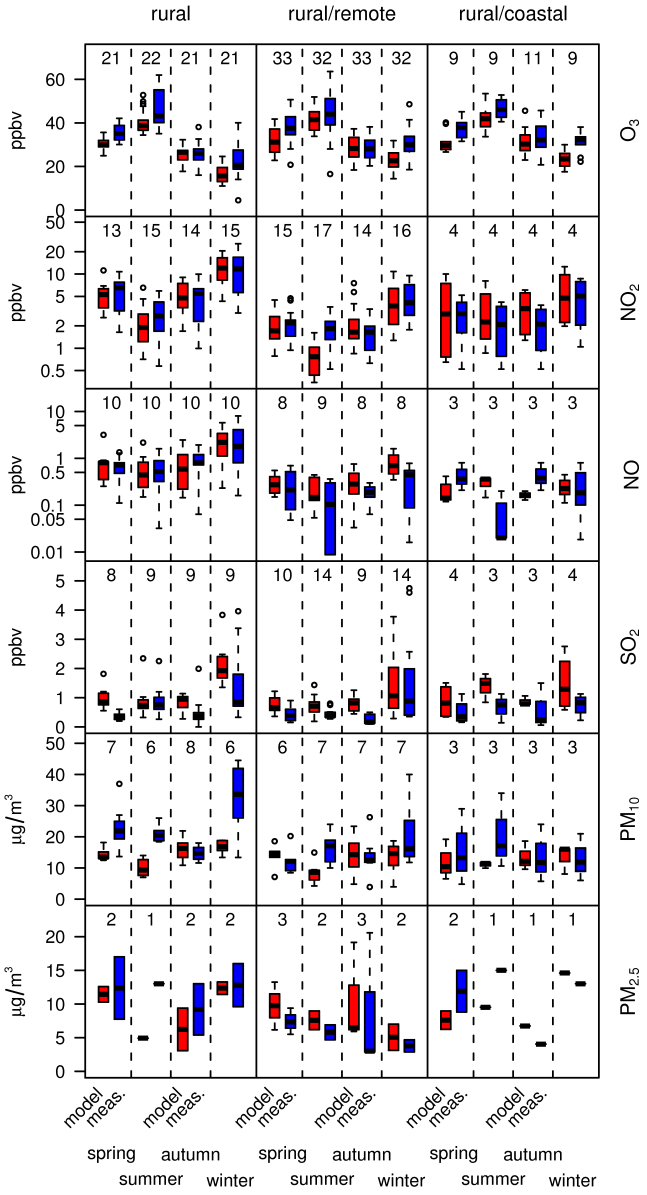

Figure 2.3: Boxplots of modelled (red) and measured (blue) median concentrations for afternoon hours (12 - 18 LT) of several compounds, classified after Henne et al. (2010). The number of stations used is shown at the top of each comparison. Note that values for NO and NO_2 are on a logarithmic scale. Simulations are ordered to represent an annual cyle: spring 2009, summer 2006, autumn 2008 and winter 2006.

We have calculated the distribution of median pollutant concentrations at all stations in the model domain over each simulation period. Shown in Figure 2.3 are the distributions of O_3, NO_2, NO, SO_2, PM_{10} and

$PM_{2.5}$ for different station classes. They are presented by boxplots of the distribution of measured and modelled median values during each season (afternoon values of hours 12 - 18 local time) and allow to evaluate accuracy and potentially existing biases in our simulations. Table 2.2 gives a summary of the mean biases found.

O_3 is the measure air quality models often have been "tuned" for. COSMO-ART is no different from other models in its ability to represent this quantity very well. A small but consistent underestimation is visible, but seasonal differences are well captured. In winter 2006 largest (negative) biases are observed, while autumn 2008 matches measurements best (Table 2.2). Overall biases in the median never exceed 10 ppbv and are often below 5 ppbv. Variability within the distributions is comparable with observations. Overall, a correlation of 0.7 (r) with hourly station values shows that the performance of our O_3 simulations are in the same range as results from simulations with comparable modeling systems like WRF/Chem in Grell et al. (2005).

The O_3 precursors NO and NO_2 measured within the AIRBASE network show a much larger variability than O_3 itself. The differences between rural and rural/remote stations in concentrations of NO and NO_2 are well reproduced by the model. Spring 2009, summer 2006 and autumn 2008 concentrations are in a similar range, while values more than twice the median of the other seasons were measured during the high pollution episode of winter 2006. The model reproduces this finding very well. NO_2 concentrations vary strongly between station types and season, which the model also represents. However, a comparably strong underestimation is found in summer 2006. Steinbacher et al. (2007) and Dunlea et al. (2007) showed that the often used molybdenum converter based NO_2 measurements are biased high due to the additional conversion of other oxidized nitrogen compounds. This will influence the comparison especially during this period, which is characterized by the high oxidative capacity of the atmosphere due to warm, sunny conditions. "Rural/coastal" stations show an overestimation throughout all simulation periods (Table 2.2), a first indication that shipping emissions might be overestimated.

SO_2 levels are generally overestimated, again especially at coastal stations. Only during the summer 2006 period, "rural" stations compare well to modelled results. The increase in SO_2 concentrations during the polluted winter 2006 episode is reproduced, though exaggerated. We argue that a missing parameterization in COSMO-ART for wet scavenging of gases, and the associated aq.-phase oxidation of SO_2 to particulate SO_4^{2-} can explain a large part of this SO_2 overestimation. A possible overestimation of SO_2 emissions in the TNO/MACC inventory can also contribute to the observed mismatch. Uncertainties in emission inventories for SO_2 have been shown to be generally large (de Meij et al., 2006), and even more so for their strongest contributor, international shipping (Endresen et al., 2005), consistent with the stronger overestimation at coastal stations. However, no other species shows a similar overestimation (over land) in our simulations.

Very few measurements were available for NH_3 (3 stations in the Netherlands). At those points, NH_3 levels are on average well represented, but show large variability throughout the simulation period (not shown).

NMVOCs, the components missing to assess the tropospheric chemistry as a whole, could not be thoroughly evaluated due to a lack of long-term, European-wide measurements. A preliminary comparison with total NMVOC measured at Duebendorf (CH) showed good agreement (not shown), which gave confidence that our NMVOC levels are in the correct range, but we could not assess the spatial distribution.

Spatial distribution

Maps of mean afternoon (hours 12 - 18 UTC) concentrations over the whole simulation period were produced, overlaid with point indicators of the same mean concentrations at each measurement station (Fig. 2.4 for summer 2006 and in the supplement for the other periods).

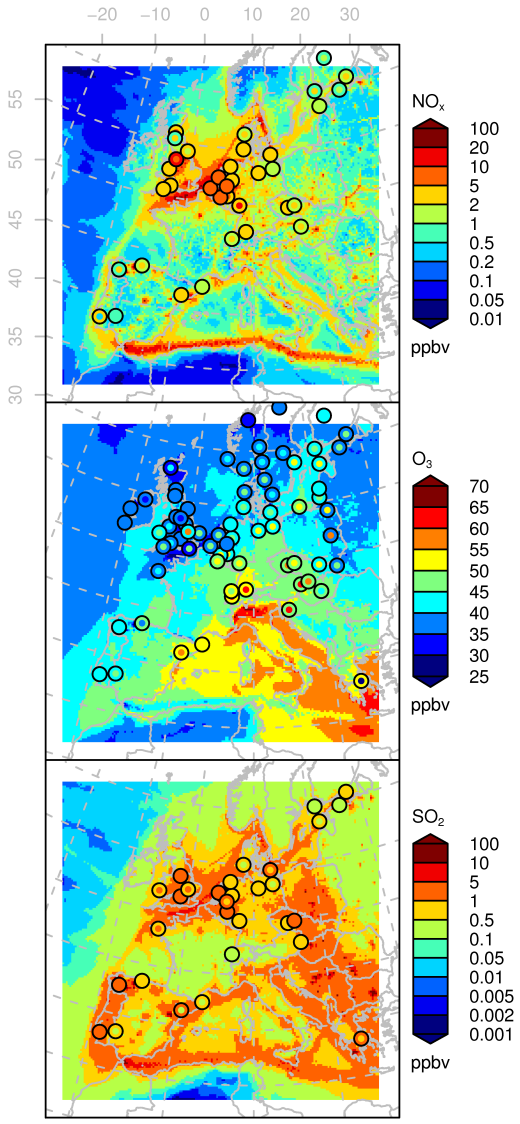

Figure 2.4: Maps of mean afternoon (12 -18) NO_x, O_3 and SO_2 concentrations for the summer 2006 period. Comparison with AIRBASE station concentrations is shown as points: Modelled mean in the outer ring and measured mean in the center.

The spatial distribution of O_3 and NO_x concentrations corresponds with observed values. Only minor differences are found, as for example a large inter-station variability of measured O_3 in Eastern Europe which is not seen in the model, and an underestimation of O_3 concentrations over the Iberian Peninsula

during the spring 2009 period. NO_x values show no region with exceptional biases over land. Striking, however, are the high modelled values of NO_x, but also of SO_2, over water, along shipping routes in the Mediterranean Sea and the English Channel. The general overestimation of SO_2 concentrations found in evaluation of the mean quantities is clearly visibile throughout Europe for the autumn 2008 period, but less so in the other periods. Modelled SO_2 concentrations at coastal stations in NE Spain are consistently too high, again point towards high shipping emission contributions. Apart from that no distinct spatial pattern of overestimation could be found.

Diurnal cycles

The representation of the diurnal cycle of atmospheric constituents was evaluated by means of ensemble plots. The ensemble consisted of all stations which had measurement data for the compound of interest, disaggregated by the classification of Henne et al. (2010). The distribution of concentrations was then calculated for each hour of day, over the whole simulation period. The median and the range covering 70 and 90% of all stations are shown in Fig. 2.5 (see supplement for plots of the other periods).

The simulated daily cycle of O_3 is accurate throughout most seasons and station types. The slight underestimation of mean O_3 concentrations found is visible as a shift of the diurnal cycle to lower values. Only in the autumn 2008 period the modelled diurnal amplitude is noticeably smaller than the measured one.

Simulated NO_2 diurnal cycles also correspond well with observations in most cases. Important aspects like the peaks during morning and evening hours ("rush-hour") visible in the spring 2009 and autumn 2008 periods are reproduced. NO_2 levels during nighttime are overestimated in spring 2009 for rural stations, and in autumn 2008 for rural and rural/remote stations. This overestimation at night could be a consequence of the fact that in reality the station is away from emission sources of NO_2, though in the model NO_2 is emitted directly into the grid box the station is located in. In spring 2009 (rural stations) and summer 2006 (rural and rural/remote), an exaggerated diurnal amplitude leads to underestimations of NO_2 concentrations during daytime. Here again, the positive measurement bias will have an influence on our comparison with high levels of oxidized nitrogen compounds such as peroxyacetylnitrates (PAN) and HNO_3 in the afternoon, leading to positive biases in the measured NO_2 concentrations (Steinbacher et al., 2007; Dunlea et al., 2007). Simulated inter-station-type variability is comparable with measurements.

Nitric oxide compares well to observations during daytime, but is underestimated at night. The relatively high measured concentrations at nighttime could be an indication for local sources affecting the measurement sites since NO_x is mostly emitted in the form of NO and then rapidly converted to NO_2 by reaction with ozone. This interpretation is supported by the comparatively high NO:NO_2 ratios of the measurements. The model, conversely, shows very low NO values as expected for truly remote sites (Carroll et al., 1992; Brown et al., 2004). Overall the diurnal cycle with low values during nighttime, a distinct peak during morning hours and a slow reduction towards evening is captured accurately in all simulated periods.

Only 3 measurement points were available to investigate the simulation quality of NH_3, and all were located in the (highly NH_3 loaded) Netherlands, making this comparison relatively uncertain. While NH_3 mean concentrations were comparable to measurements, the diurnal cycles were not (both not shown). The measured cycles were very variable throughout seasons and stations, and we see a clear deficiency of the modeling system to account for this variability. The main sources of NH_3 emissions are agricultural activities, especially livestock and manure. NH_3 concentrations are mostly dominated by local emissions.

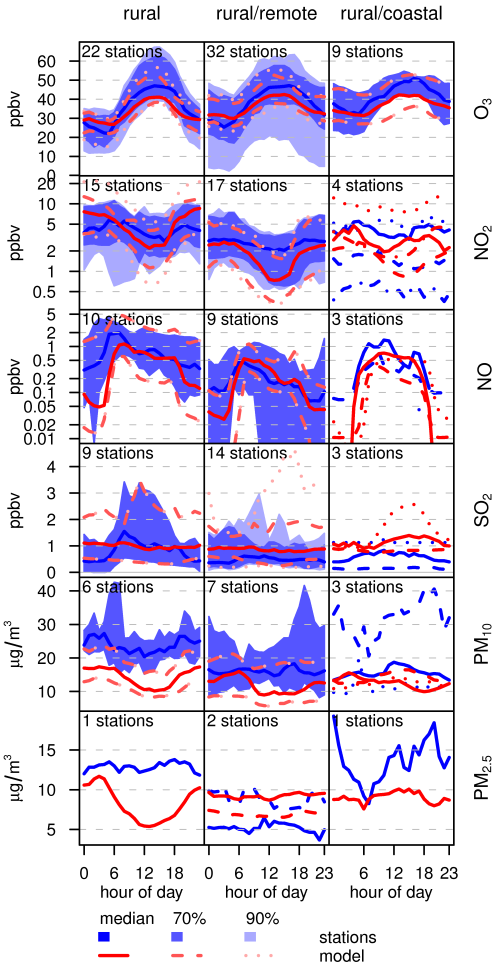

Figure 2.5: Modelled and measured (AIRBASE) mean diurnal cycles of several compounds during the summer 2006 period, disaggregated after Henne et al. (2010). Measured values are shown as colored areas, modelled parameters as lines. Light blue areas show 90% range of station values, the range between dotted lines the same for modelled values. Blue colored areas compare to the area between dashed lines (70% range). The median of measured values is a solid, dark blue line, the median of modelled values a solid red line. If less than 5 stations report data, measured and modelled medians are reported as blue and red line pair per station, with different line styles for each pair.

It is known that the diurnal cycle of NH_3 emissions strongly depends on the emission source (Reidy et al., 2009). Ellis et al. (2011) showed that bi-directional fluxes between the atmosphere and land surfaces might be needed to accurately simulate NH_3 (and associated aerosol) levels. All this makes modeling such emissions a major challenge which is currently not accurately addressed in most models (Zhang et al., 2008), as emission inventories based on spatially distributed emission totals and associated, statistically averaged time functions cannot capture such process-based emissions.

Satellite observations

For comparison with OMI satellite information, vertical tropospheric columns (VTCs) of NO_2 were calculated from model output for the hour of the satellite overpass (13:30 local time, approx. 12:30 UTC over Europe). The height of the troposphere was assumed to be fixed over all simulations at 10 km geometric height, the exact choice has little influence on the NO_2 columns. The comparison was made only where OMI data were available at each overpass and the conditions were nearly cloud-free (cloud radiance fraction reported by OMI retrieval $< 50\%$, corresponding to approx. $<20\%$ cloud coverage). The arithmetic mean over each simulation period was calculated and the results are shown in Fig. 2.6. The aggregated mean biases for all grid points, land points and sea points can be found in Table 2.2. We compared the model simulated NO_2 columns directly with the respective EOMINO columns without taking into account the averaging kernels which would remove the dependency of the result on the a priori NO_2 profiles used in the EOMINO retrieval. Not accounting for the averaging kernels might introduce biases of the order of 30% with EOMINO columns tending to be too high over remote locations and too low over polluted areas (Russell et al., 2011), while differences averaged over Europe are likely to be small (Huijnen et al., 2010).

Spatial distribution and magnitude of NO_2 is in good agreement with our modeling results. Highly polluted regions over the Netherlands and southern United Kingdom, as well as the Po Valley (Italy) are accurately captured. Plumes of large urban agglomerations (Paris, Madrid, Berlin, Warszaw) are comparable in extent and magnitude. Also, cleaner regions like for example southern France are reproduced. Notable differences are mostly found in polluted coastal areas, especially in the Mediterranean Sea, where the model tends to overestimate NO_2 concentrations over water, particularly in the autumn 2008 and spring 2009 period. This overestimation is also visible in the mean over all grid points over sea in Table 2.2. Emission estimates for ship traffic are known to have large error margins both in magnitude (Corbett and Koehler, 2003) and spatial allocation (Wang et al., 2008). From the magnitude of the error and the spatial correlation with main shipping routes an overestimation of ship emissions by the inventory used is likely. This would also explain the consistent overestimation of SO_2 concentrations at coastal stations in NE Spain. Seasonal differences are captured for spring, summer and autumn, only the model results for the winter 2006 period overestimate NO_2 columns noteably in Northern and Eastern Europe.

2.4.3 Aerosol characteristics

All comparisons of measured and modelled particulate matter were made in an as rigorous as possible manner. For PM_{10} and $PM_{2.5}$ bulk mass and $NR - PM_1$ AMS measurements, the modelled log-normal distribution functions were integrated over the respective size ranges, and size cut functions were employed to simulate the size-dependent transmission efficiency that is typically found in the measurement instruments used. See Appendix 2.8 for a description of the transmission functions used. For the AMS the modelled quantities were additionally converted to vacuum aerodynamic diameter (DeCarlo et al., 2004). No transmission functions were applied to number size distribution measurements, the modelled values are derived from integration over the exact intervals given: 30 to 50 nm, 50 to 500 nm, 100 to 500 nm and 250 to 500 nm respectively.

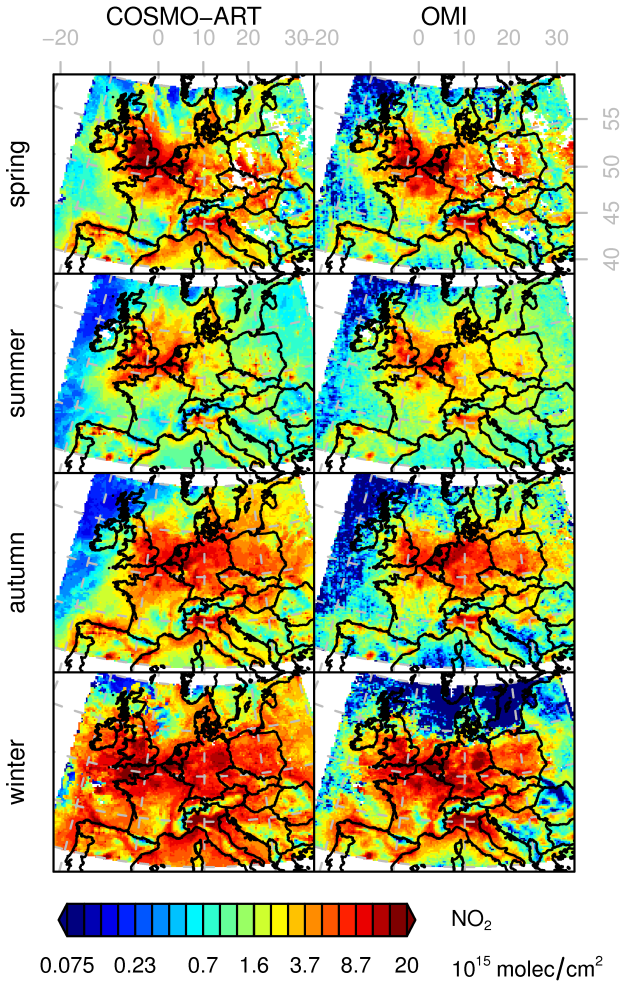

Figure 2.6: Comparison of modelled NO_2 VTCs against OMI satellite data for (from top) the spring 2009, summer 2006, autumn 2008 and winter 2006 periods. Modelled values are found in the left column, OMI observations in the right one. Not the whole simulation domain could be compared due to missing coverage of the EOMINO dataset.

Bulk mass

Continous bulk aerosol mass measurements are the least available within the measurement dataset, making the ensemble of stations for comparison very small (max. 8 stations). When looking at PM_{10} concentrations (Fig. 2.3, Table 2.2), our simulations match observations for rural stations in autumn 2008, and underestimate them in the other periods. Simulated concentrations for rural/remote stations are almost identical to those at rural stations in the model, while in reality large differences are found. In consequence, modelled values are above measurements in spring 2009 and autumn 2008, but below in summer and winter 2006. Rural/coastal station concentrations are underestimated in spring 2009 and summer 2006, match observations in autumn 2008 and are above measurements in winter 2006. All this makes autumn 2008 the period in which PM_{10} is simulated best, and worst in summer 2006 (Table 2.2).

"Rural"-type stations are deemed the most representative for such a model evaluation, and they show (except in autumn 2008) an underestimation typical for many regional models (see e.g. Stern et al., 2008), probably due to missing sources (e.g. resuspension, secondary organics, local mineral dust sources, missing aq.-phase conversion of SO_2 to SO_4^{2-}). Stations of type "rural/coastal", in contrast, have a tendency towards more positive biases, which is reasoned by the high amounts of seasalt aerosols found at these stations in the modeling results. The overestimation could also be an artefact of the limited model resolution: Coastal stations may be located in grid cells partly covered by sea where sea salt aerosols are therefore emitted directly. Further investigations, e.g. comparisons with filter samples, are needed to assess if the amount of seasalt from the parameterization in COSMO-ART is realistic. The very high PM_{10} concentrations in winter 2006 are not accurately represented in the model. There is in fact no visible increase in PM_{10} concentrations in the model results compared to the other seasons at all.

The diurnal cycles for PM_{10} show that simulated concentrations are often in the same order as the measured values, both in variability and evolution in time, although overall the simulated values are mostly too low. Winter 2006, the period with very high PM levels, has no observable diurnal cycle. In spring 2009 and summer 2006, the diurnal cyles at rural stations show a PM_{10} maximum during night and a minimum at noon, which is - although shifted to lower values - reproduced by the model. The diurnal cycle for rural stations in autumn 2008 is characterized by high but constant PM_{10} levels during nighttime and a drop in concentrations during the day. The model reproduces this finding to a certain degree, although the amplitude of the drop is underestimated.

Only 7 stations, from 3 different categories, had measurements for $PM_{2.5}$ for our simulation periods. From this uncertain data basis we see equally large disagreements as have been found for PM_{10}. McKeen et al. (2007) compared $PM_{2.5}$ measurements with several air quality forecast models in North America and concluded that, while most of the models are able to accurately represent daily average $PM_{2.5}$ concentrations, there are substantial inconsistencies in representing the diurnal cycle. Most models show a negative bias and exaggerate the diurnal variability, something we can observe also for the (single) rural $PM_{2.5}$ station in our comparison (Fig. 2.5).

The errors are in a similar range as found in other model simulations. Vautard et al. (2007) showed similar performance problems in simulating PM_{10} in Europe. Stern et al. (2008) saw better agreement with measurements (i.e. less underestimation) for $PM_{2.5}$ simulations than for PM_{10}, which we could not confirm with the dataset mentioned above.

Aerosol optical depth

For comparison with MODIS AOD data, a similar procedure was employed as for OMI NO_2 vertical tropospheric columns, only using grid points for which satellite data were available and which were cloud-free also in the model. The whole vertical column in the model was used in the calculation of aerosol optical depth with the method described in Vogel et al. (2009). All aerosol categories (internally and externally mixed Aitken and accumulation modes, soot, mineral dust and sea salt modes) contribute to calculated AOD. Then, the median was calculated over the whole simulation period. We chose the median instead of the mean to be more robust against outliers. Figure 2.7 presents the results. Furthermore, as for the comparison with OMI NO_2 VTCs, aggregated biases have been calculated and can be found in Table 2.2.

For all AERONET stations in the model domain, timelines of AOD at 550 nm were calculated from model output and compared against measured values. AERONET data were interpolated (if no direct

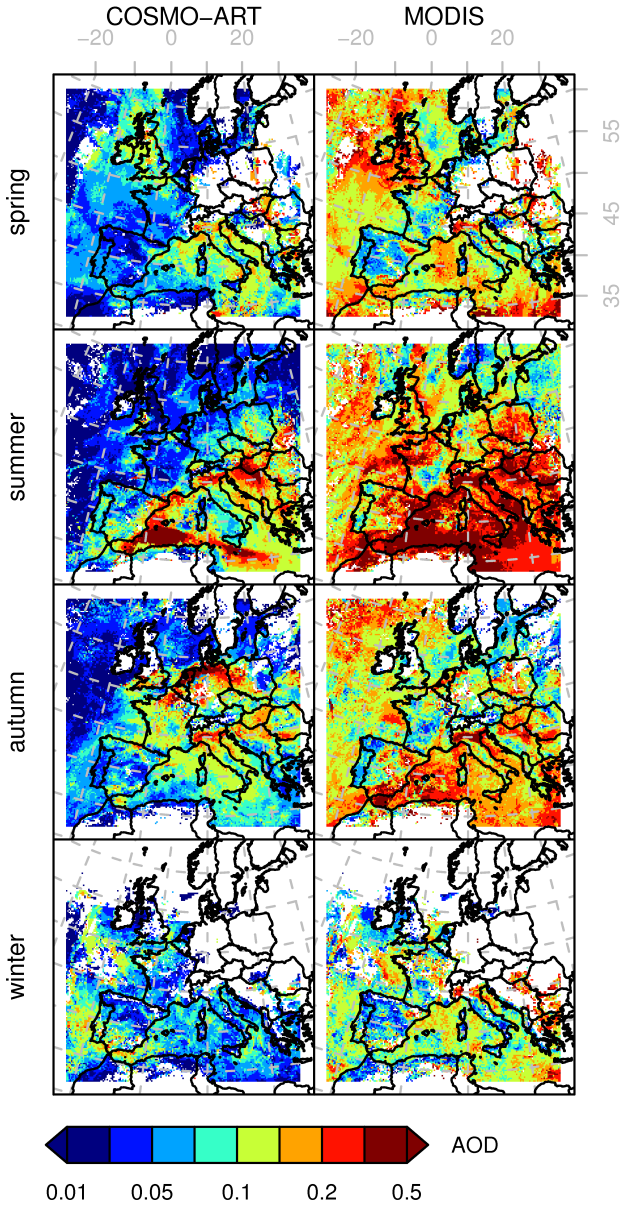

Figure 2.7: Comparison of modelled AOD (550 nm) against MODIS satellite data for (from top) the spring 2009, summer 2006, autumn 2008 and winter 2006 periods. Modelled values are found on the left, MODIS observations on the right hand side.

measurement at 550 nm was available) linearly in log-log space. In case MODIS data were available also this information was added to the plots. The results for selected stations are shown in Figure 2.8, plots for the remaining stations can be found in the supplement, and Table 2.2 shows the mean biases for these comparisons.

The comparison against these two independent sets of AOD measurements leaves a mixed picture: com-

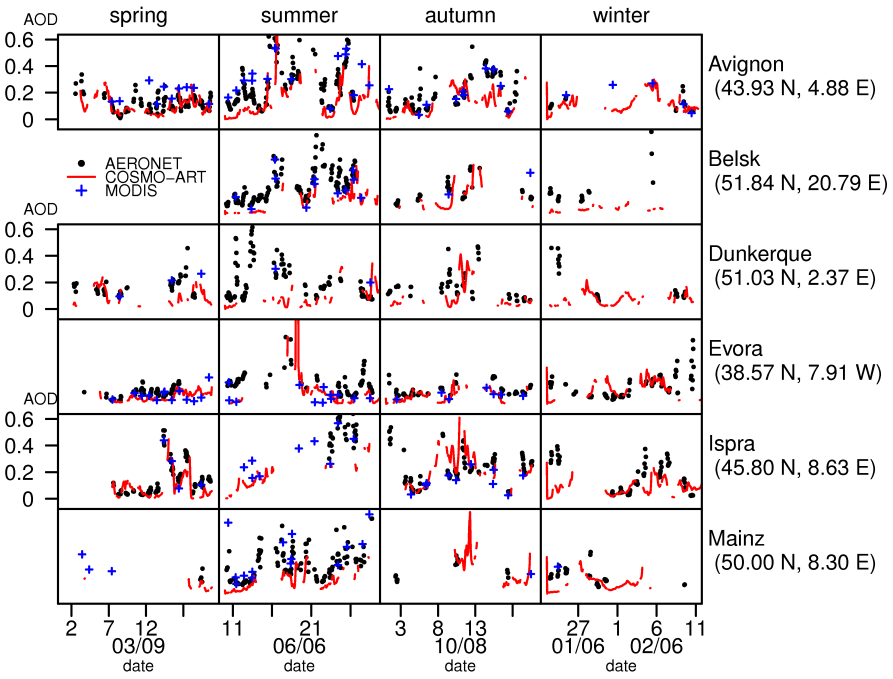

Figure 2.8: Timelines of aerosol optical depth (AOD) at selected AERONET stations in Europe for the different periods. Shown are AERONET measured values (black circles), MODIS derived AOD (blue asterisks) and the simulated AOD values (red lines). AERONET data has been cloud-screened by the data provider. MODIS data is also cloud screened. Modelled values are masked if simulated total cloud cover was above 25 %.

pared with MODIS, the model shows consistently lower values than derived from the satellite. We can capture regions with continuously high AOD values like the Po valley (northern Italy) or Saharan dust events like e.g. in the summer 2006 period over the western Mediterranean Sea. The magnitude of the dust event is underestimated, which might be explained by the fact that modelled "dust" is only created within the region of the model domain which covers only a small part of the Sahara. At the boundaries only very low dust concentrations are prescribed due to the way aerosol boundaries are treated (see Section 2.3.1). Contribution of sea salt to AOD is visible over the Atlantic ocean, but the absolute values are much lower than MODIS derived values, except for winter 2006. Some very polluted regions in south-eastern Europe are captured in location and magnitude (e.g. in Northern Croatia / Southern Hungary), while several other "hot-spots" visible from the satellite (e.g. Eastern UK coast) are missed.

Comparison with AERONET station data reveals additional details. Although the absolute levels are often too low, which is consistent with our comparison with MODIS data, the temporal evolution is often well represented and most high AOD events visible in station data are also observed in our simulations. Differences between MODIS and AERONET derived AOD on the other hand are at several occasions as big as the differences between model and AERONET, and non-negligible on average (up to 10% compared to up to 60% difference between model and measurements, see Table 2.2). We suggest that the role of water in the aerosol (both simulated and in reality) will play a major role in the differences found. Both MODIS and AERONET data are "cloud-screened", i.e. data points contaminated by clouds were removed, as they give erroneously high AOD values. Capturing the onset of a cloud is difficult, so some increase in

AOD due to aerosol water might be left in the dataset. These effects are visible within the satellite data shown in Figure 2.7 (e.g. over Germany in autumn 2008 or west of Ireland in spring 2009) near regions with missing (cloud-screened) pixels. Also in several AERONET stations the sudden steep increase of AOD just before measurements are filtered (for clouds) can be found. While we tried to remove this error by using median values instead of the arithmetic mean to calculate the MODIS-model comparison, we probably could not exclude all of those situations. As the effect is non-linear and acts towards very high AOD values, this will probably bias AOD results. Secondly, differences in simulated and real aerosol chemical composition will also have an effect on AOD. The next section addresses a comparison of aerosol chemical composition.

A clear negative bias in absolute AOD is seen in our model when compared with two independent measurement datasets which appears to be consistent with the too low simulated PM_{10} and $PM_{2.5}$ levels. Fair correlation of the evolution in time is visible from the AERONET comparison. Performance of our AOD simulations is well in range of results for comparable modeling systems (e.g. Zhang et al., 2010; Aan de Brugh et al., 2011). We argue that both missing aerosol mass at the lateral boundaries and inaccuracies of simulated aerosols within the domain contribute to the underestimated AOD. Especially for aerosol components from natural sources (Saharan dust) the missing lateral contribution could be substantial. Although we tried to remedy this by using averaged profiles from a previous run, we could not - especially for those categories - represent the absolute mass contributions correctly. The impact of the missing pathway to form sulfate in clouds and the known too small yield of SOA in the SORGAM model are additional sources of error that impact the overall accuracy of the comparison.

Chemical composition

Aerosol chemical composition was evaluated by comparison with AMS data. In summer 2006, AMS measurements were available at Payerne (CH) and Bush (UK) (Lanz et al., 2010). Several AMS instruments were deployed during the 2008 (autumn) and 2009 (spring) periods at stations throughout Europe. Timelines of the composition of $NR - PM_1$ are presented for both measurement and simulation at these stations. Shown in Figures 2.9, 2.10a, and 2.10b are the timelines for the autumn 2008 and spring 2009 periods. The comparison for summer 2006 (3 stations) can be found in the supplement. In the figures, colors typically used in the AMS community are used to represent each species: ammonium (NH_4) in orange, sulfate (SO_4) in red, and nitrate (NO_3) in blue. Organic aerosols (OA) are represented as shades of green. Charges are omitted intentionally for the AMS in the figure legends, as also contributions from organosulfates, organonitrates are included which are not ions (Farmer et al., 2010). In case of modelled values, a distinction can be made between anthropogenic primary organics (aPOA), secondary organics from anthropogenic (aSOA) and biogenic (bSOA) sources. Table 2.2 presents the mean biases for each species over all stations in each season.

At all stations the time evolution of $NR - PM_1$ is represented well by our simulations, sometimes however for the wrong reasons due to a mismatch in chemical composition. Single events with higher aerosol concentrations (e.g. in Vavihill, 2008, Fig. 2.9) correspond in time and magnitude with the observations in most cases. Several model deficiencies can also be seen throughout the comparison, namely an overestimation of nitrate components and an underestimation of sulfate and, sometimes, organic mass. In the following we will briefly discuss the result for each station.

In Switzerland, measurements at Payerne were available for three periods. The time evolution of total aerosol mass corresponds best in spring 2009, and worst in the summer 2006 period. The weak correlation

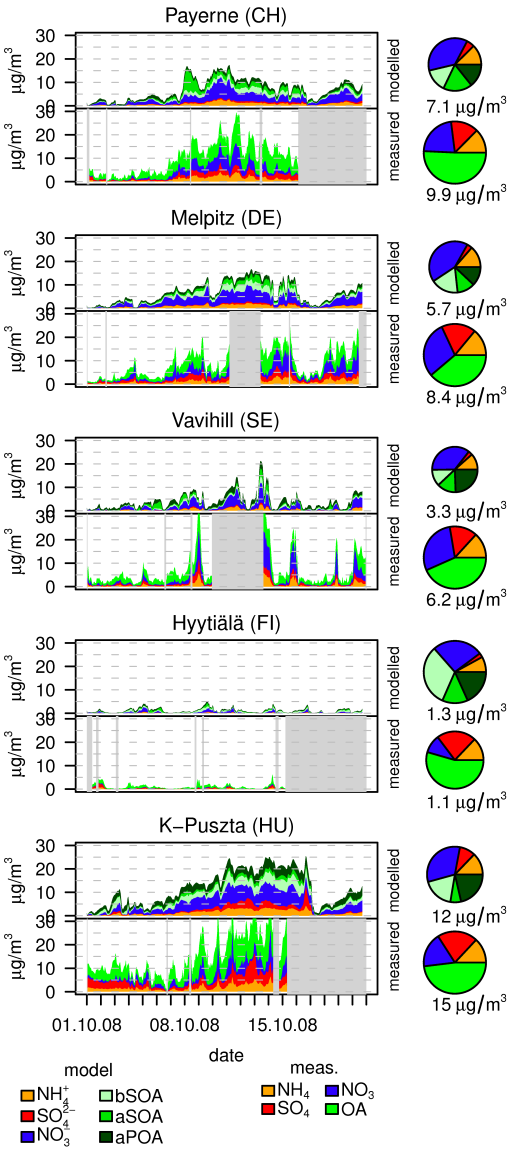

Figure 2.9: Timeline of chemical composition of NR − PM_1 (top: modelled, bottom: measured by AMS) during autumn 2008. Pie charts give mean over time period (size of pie relates total mass). Measured OA should be compared with the sum of modelled aPOA, aSOA and bSOA. Gray shaded areas mask times without measurement data.

in summer 2006 is mostly due to a severe underestimation of OA, especially during daytime hours, and an overestimation of nitrate during nighttime. In spring 2009, several abrupt changes in aerosol mass concentrations were observed. Although the timing is not the same each time, the model reproduces those changes. A tendency to retain too much nitrate in the aerosol phase during daytime is apparent. Sulfate is underestimated. During autumn 2008, an episode of high aerosol concentrations is observed in the middle of the observation period. This is also reported by the model. OA are, however, underestimated, and nitrate aerosols overestimated. Here also, modelled aerosol nitrate shows a persistence to remain in the

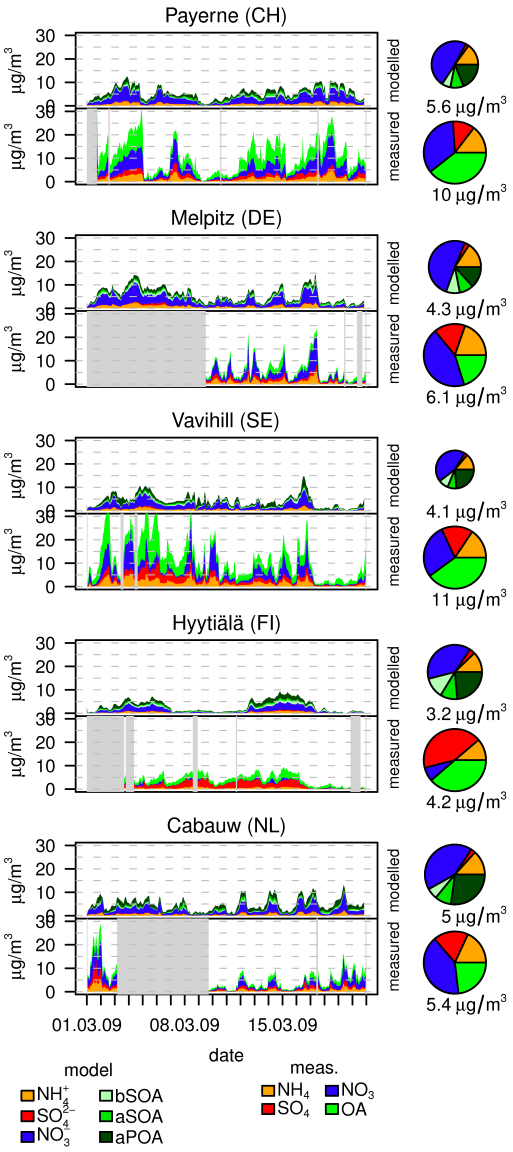

Figure 2.10a: Timeline of aerosol chemical composition as in Figure 2.9 but for stations measuring during the spring 2009 period (1 of 2).

aerosol phase during daytime that is not found in the observed values. Melpitz in Germany differs from Payerne in a generally higher sulfate content. Otherwise those stations report similar aerosol composition. Striking is the stronger overestimation of nitrate aerosols at Melpitz, compared to Payerne, in both periods. Simulated sulfate is in the same range as in Payerne, and therefore even more strongly underestimated. The concentrations of organics are lower in Melpitz, and simulated values are comparable here. The third station with more than one period of measurements is Vavihill (SE). Generally low aerosol concentrations alternate with isolated peaks in aerosol mass with high contents of inorganic secondary components. This burst pattern is captured in our simulations, and also the timing fits mostly well. Especially in spring

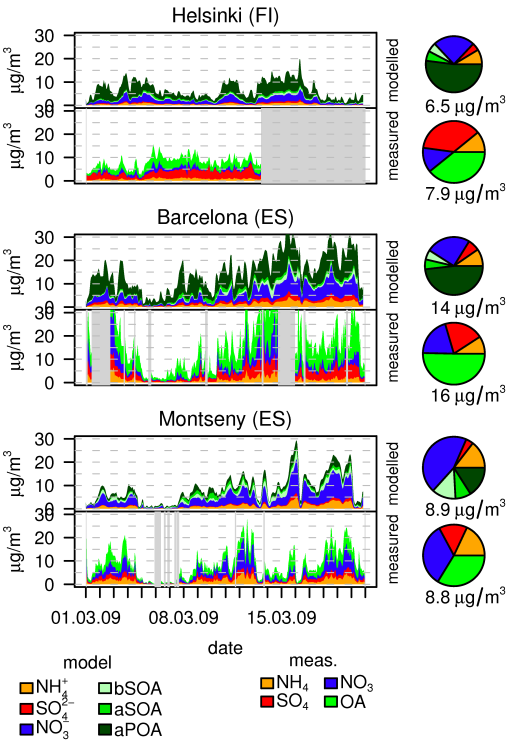

Figure 2.10b: Timeline of aerosol chemical composition as done in Figure 2.9 but for stations measuring during the spring 2009 period (2 of 2).

2009 the model lacks, though, the OA mass necessary to fit the measurements. While ammonia levels are comparable in autumn 2008, they are above measured levels in spring 2009. The AMS deployed at Hyytiälä reports very low $NR - PM_1$ concentrations, with large contributions by sulfate and OA, and, in spring 2009, almost no nitrate. The model can represent the overall level of aerosol concentration. However, the simulations significantly underestimate sulfate and overestimate nitrate.

All other stations only report data for one period. In autumn 2008, measurements of aerosol chemical composition were also available for K-Puszta, Hungary. The station reported high aerosol concentrations with levels up to 30 μg/m^3 total mass. While the model represents the build-up of aerosols towards the middle of the observation period, the overall mass is underestimated. Too high nitrate levels are simulated. Organics and ammonium match observations better, but sulfate tends to be understimated also at this location. Four more stations reported data during spring 2009: Cabauw (NL), Helsinki (FI), Barcelona (ES) and Montseny (ES). Cabauw (NL) has lower concentrations than e.g. Payerne or Melpitz, and a big gap in measurements during the first half of our simulations. There is some resemblence in the peaks of aerosol mass during the second half of the simulation between model and station values. Nitrates are overestimated while ammonium and sulfate are too low. Organics are well captured. Helsinki (FI), an urban background station is, like Hyytiälä (FI) characterized by a strong contribution from sulfate. The simulated total aerosol loadings are comparable to the observed concentrations but do not match in composition. We can tentatively explain this difference by looking beyond the border of the model domain: both stations are in the vicinity of large sources of SO_2 on the Kola peninsula in Russia (Tuovinen et al.,

1993) which are still found to be underestimated in current emission inventories (Prank et al., 2010). Additionally, due to the setup of aerosol boundary conditions in our modeling system, we very likely underestimate direct sulfate inflow in this region. In Barcelona (ES), also an urban background location, a very variable time series is reported, with the highest absolute concentrations of all stations used in this analysis. Several peaks of aerosol concentration each day are common, containing relatively high sulfate levels compared to other stations. The model produces a similar variability, although it overestimates nitrate. Sulfate levels are comparable at this site with a large influence from shipping. OA concentrations are, in contrast to most other stations, overestimated at Barcelona and Helsinki. The largest contributor to simulated total organic mass at these stations is primary emitted organics. Statistical analysis of the organic fraction (positive matrix factorization (PMF), Paatero and Tapper, 1994) indicates that organics in urban stations are comprised of similar amounts of SOA and POA, while in the model it is almost exclusively POA. This points towards a strong underestimation of secondary organics in polluted regions as it has been found already by Fast et al. (2009). Finally, the AMS in Montseny (ES) measured a time-series with several periods with increased aerosol loadings, and during the first third a period where almost no aerosols were found due to an episode of strong Atlantic advection. The model captures this period well. Total organics are comparable throughout the simulation period, although a PMF analysis gives about 5% mass contribution from urban primary organics (Minguillón et al., 2011), instead of about 30% as given in the model. Nitrates are too high, and lacking the diurnal cycle visible in the measurement. Simulated sulfate is below measurements.

Number concentrations and size distributions

The dataset compiled by Asmi et al. (2011) provides a homogenized overview of the statistical characteristics of aerosol size distributions in Europe during the years 2008 and 2009. We evaluate different particle dry size separated subsets of the number concentrations, following Asmi et al. (2011). The number of particles from 50 (N_{50}) and 100 (N_{100}) nm up to 500 nm have been chosen as proxies to study climate effects. Health concerns are related to very small particles, which are assessed by comparing number concentrations of particles between 30 and 50 nm (N_{30to50}). This concentration can also serve as an indicator of new particle formation and emissions from combustion processes. Finally, the number of particles with diameters between 250 and 500 nm (N_{250}) are given to show the contribution of larger particles to total aerosol number concentrations. We have calculated the corresponding model values by integrating the aerosol modes over the respective intervals. Data were available in up to hourly resolution, so a direct comparison could be made between modelled and simulated values. Table 2.3 shows the resulting comparison for the autumn 2008 period, table 2.4 for spring 2009. Table 2.2 gives a summary overview of the mean biases over all stations.

We also studied the histograms (occurrence distribution) of logarithms of the number concentrations in the particle size ranges (not shown). The analysis was done in logarithmic concentration space as most of the aerosol number concentrations are log-normally distributed (Asmi et al., 2011). It shows the model's ability to produce similar distributions of number concentrations as measured and provides a more detailed way to analyze the differences. We also performed a Mann-Whitney U-test (Higgins, 2004) on the modelled and measured concentration distributions to see with what p-value they could be considered to be from the same distribution with similar mean and distribution shape.

The histograms of number concentrations show that the agreement is better in greater diameter size ranges (N_{100} and N_{250}) in comparison to concentrations in N_{30to50} size range. The model seems to overestimate

Table 2.3: Comparison of number concentrations in different size ranges after Asmi et al. (2011) for number size distributions during the autumn 2008 simulation. N_{30to50}: 30 to 50 nm, N_{50}: above 50 nm, N_{100}: above 100 nm, N_{250}: above 250 nm. Note that the N_{250} parameter has a larger uncertainty than the others due to very low sampling rates.

station name	category	N_{30to50}		N_{50}		N_{100}		N_{250}	
		meas.	mod.	meas.	mod.	meas.	mod.	meas.	mod.
Birkenes (NO)	rural/remote	133	374	250	517	96	171	6	42
Cabauw (NL)	suburban	2787	2605	4649	4048	1170	1706	63	250
Harwell (UK)	rural	705	2181	1097	2247	410	713	51	92
Ispra (IT)	suburban	1732	4915	7172	6293	3829	2632	373	423
K-Puszta (HU)	rural	597	2698	4626	4247	2609	2013	390	313
Mace Head (IE)	rural/remote	48	29	158	124	104	95	41	59
Melpitz (DE)	rural	1031	1377	2386	3447	1306	1650	312	305
Kosetice (CZ)	rural/remote	508	866	2346	2724	1423	1340	262	265
Vavihill (SE)	rural	577	1314	1187	2761	365	1010	51	146

Table 2.4: Comparison of number concentration comparisons, like in Table 2.3, but for the spring 2009 simulation.

station name	category	N_{30to50}		N_{50}		N_{100}		N_{250}	
		meas.	mod.	meas.	mod.	meas.	mod.	meas.	mod.
Aspvreten (SE)	rural/coastal	201	1084	645	1932	302	808	63	152
Cabauw (NL)	suburban	1466	2780	1894	3399	433	1248	20	187
Harwell (UK)	rural	746	2517	1453	2285	634	762	103	125
Ispra (IT)	suburban	904	2341	2921	2136	1451	776	157	116
K-Puszta (HU)	rural	855	2133	3104	3890	1673	1670	203	267
Mace Head (IE)	rural/remote	324	542	779	1199	418	569	108	127
Melpitz (DE)	rural	508	1380	1343	2868	762	1279	219	242
Kosetice (CZ)	rural/remote	467	1342	2032	3748	1282	1751	210	319
Vavihill (SE)	rural	402	1272	1496	2850	607	1266	171	236
Waldhof (DE)	rural/remote	652	1209	1744	2678	935	1241	227	248

the number concentrations in the smaller size ranges by a factor of two to five, especially in Harwell (UK), Ispra (IT) and the two Swedish stations (Aspvreten and Vavihill). This overestimation could be explained by a relatively low fraction of new particle formation in the modelled environment. COSMO-ART uses the nucleation parametrization from Kerminen and Wexler (1994), which does not generally produce the observed amounts of nucleated particles in the European boundary layer. Thus the overestimation could be due to a disproportioned amount of emitted sulphur to be considered as primary Aitken particles, which have a much higher lifetime in the atmosphere compared to newly nucleated particles in these regions. For the larger particle sizes (N_{100} and N_{250}), the model-measurement comparison is more successful. At Central European stations the modelled and measured concentration distributions are generally of similar shape and median, which is well demonstrated by p-values ranging from 0.31 to 0.66 in the U- test test parameter for Kosetice and Melpitz. The overall shapes of the concentration histograms are generally similar in all the stations, although some discrepancies in lower-concentration regions are visible. The agreement is generally poorer in lower-concentration regions of Northern Europe, but also in Cabauw (NL) and Harwell (UK) N_{250} concentrations, where the model overestimated the concentrations by a factor of 2 in 2008.

A second dataset available from Asmi et al. (2011) is seasonal statistics of aerosol number size distributions.

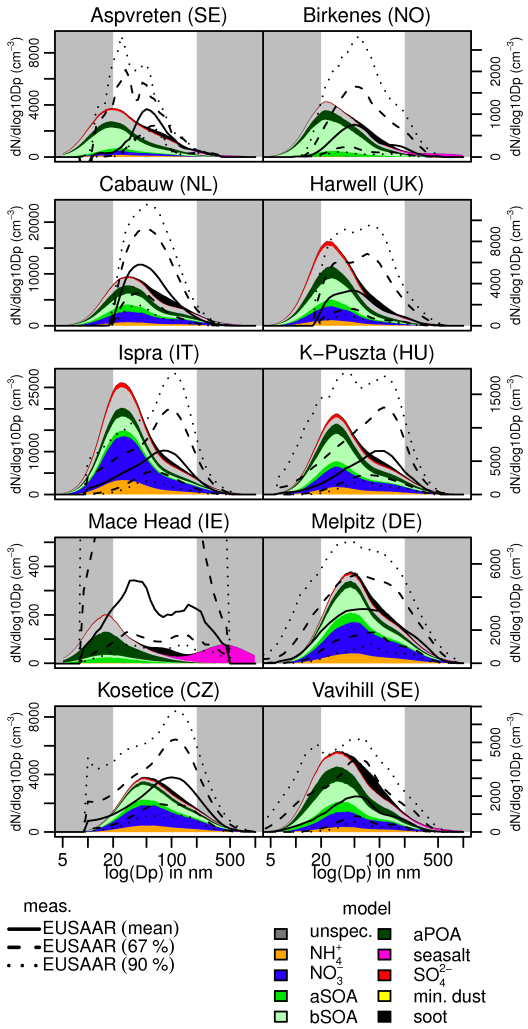

Figure 2.11: Modelled and measured aerosol size distributions at EUSAAR stations for the autumn 2008 period. Modelled distributions are shown as area shaded by mass contributions of different species, calculated as median over the simulation period. Measured values are a statistical size distribution from data of the whole season and are shown as lines. Solid lines depict median values, dashed lines the 67 % and dotted lines the 90 % percentile range. Grey background denotes areas with higher measurement uncertainty (Wiedensohler et al., 2010).

We have calculated a distribution function as mean over all modelled values in each simulation period, and compared it against the measured distribution statistics of the corresponding season (Fig. 2.11 for autumn 2008, plots for spring 2009 can be found in the supplement. Note that there is no exact match between the time periods covered by the measurements and the simulations (3 weeks out of the 3 months). Overall, the modelled size distributions are at several stations close to the observed ones. At most stations, simulated size distributions were within the central 67% percentiles of the values reported by Asmi et al. (2011) when comparing the 20 to 200 nm size range, for which the instruments were reported to compare the best (Wiedensohler et al., 2010). Concerning the shape of the size distributions, stations with the best match between model and measurements were Melpitz (DE), Waldhof (DE) and Kosetice (CZ), with only very

small deviances in both years. Aerosol number size distributions at the rather polluted sites Ispra (IT) and K-Pustza (HU) show distribution functions with comparable peak values but opposite skewness. While model values lean towards smaller diameters, measurements have their peak in number concentration at much larger aerosol diameters. For Ispra (IT) this is probably due to the influence of the Milan urban agglomeration. Due to the coarse horizontal resolution, fresh emissions (with smaller diameter) contribute much more to aerosol composition at Ispra in the model than in reality, where the aerosol had more time to age. This ageing would shift the size distribution towards larger diameters via coagulation as observed in the measured distributions. A similar explanation might hold for K-Puszta (HU), which is located near Budapest, the capital of Hungary. Cloud processing of aerosols is missing in COSMO-ART and might be responsible in general for a bias towards small peak diameters. Cabauw (NL) and Vavihill (SE) show comparable shape but model and measurements disagree in number concentration. Both, Birkenes (NO) and Harwell (UK) show a tendency towards a bimodal size distribution, which is captured by the model in 2008, but missed in the 2009 case. Finally, Mace Head (IE), with its large variability in number concentrations reasoned by the stations setting at the coast in western Ireland, representing mostly clean maritime air masses, occasionally interrupted by continental influences, shows acceptable agreement in terms of total number concentrations, but no clear agreement in size distribution.

In general the model has an acceptable representation of the variability of number concentrations between stations (Table 2.3). In most cases the model overestimates number concentrations throughout the size range covered. The station with the best agreement was Aspvreten (SE) in autumn 2008 and Birkenes (NO) in spring 2009, while Ispra (IT) compared worst in 2008, K-Pustza in 2009. Several stations showed acceptable agreement for number concentrations, for example Melpitz (DE) and Birkenes (NO) in 2008 or Waldhof (DE) and Vavihill (SE) (except for the N30to50 range) in 2009. The agreement found was generally better during the autumn 2008 than during the spring 2009 period.

2.5 Discussion of aerosol characteristics

2.5.1 Sulfate

This aerosol species is virtually always underestimated. Several factors contribute to this error: Besides some minor direct emissions of sulfate particles, most of the aerosol sulfate is secondary, created from oxidation of SO_2 in the gas-phase and within the aqueous-phase in cloud droplets. Studies have shown that the amount of sulfate produced in clouds is substantial and even dominating (Walcek and Taylor, 1986; Rasch et al., 2000). COSMO-ART currently lacks a parameterization for this pathway. Therefore, especially during periods with cloudy conditions, the underestimation of SO_4^{2-} is likely explained by this missing process. The missing conversion of SO_2 to SO_4^{2-} is also consistent with too high levels of SO_2 in our model. Aksoyoglu et al. (2011) simulated the summer 2006 period with another modeling system including in-cloud oxidation of SO_2 and found better agreement. Whether this can be attributed to in-cloud sulfur oxidation is unclear. In addition to the oxidation issue it was shown that the regional (e.g. Wagstrom and Pandis, 2011) and even intercontinental (e.g. Liu and Mauzerall, 2007) contributions to sulfate aerosol mass are higher than for other aerosol categories like nitrate. Inflow of aerosol concentrations at the lateral boundaries is realized by a smooth transition to values from a given profile or a coarser grid model, this is called relaxation. While we do relax our model at the lateral boundaries against data from a global chemistry transport model (CTM) for gas-phase species, we could not provide similar boundary conditions for aerosol species. Instead we relax against a mean profile from a previous run

(which is also low in sulfate). Therefore, only very little long-range transport of sulfate is simulated (approx. 0.2 to 0.4 $\mu g/m^3$ surface concentration), contributing to this underestimation. A sensitivity study with strongly increased lateral sulfate showed a noticeable but insufficient increase of sulfate at the grid boxes of the AMS measurement stations. Finally, oceanic emissions of dimethyl sulfate (DMS) have also been shown to contribute to aerosol SO_4^{2-} levels (Gondwe et al., 2003). A parameterization has recently been included (Lundgren, 2010) in COSMO-ART but was not yet used in our studies. Sensitivity studies showed, though, that sulfate originating from maritime DMS emissions has no substantial influence over continential regions, which again indicates the importance of cloud processing of SO_2. Oxidation of sulfates in clouds will be included via a comprehensive wet scavenging and aqueous-phase chemistry scheme, currently under development at Empa.

2.5.2 Organics

Often also organic aerosol contributions are underestimated. This is a well-known problem of current CTMs (Volkamer et al., 2006; Hodzic et al., 2009; Hallquist et al., 2009), in our case reasoned by the use of an older parameterization of the conversion of condensable organic vapours to secondary organic aerosols (SOA) (Schell et al., 2001), based on the two-product method by Odum et al. (1996).

Our total OA underestimations are substantial and reach factors of 2. Underestimations for SOA alone by a factor of 10 or more were summarized by Volkamer et al. (2006) and Hodzic et al. (2010) for multiple polluted regions in 3 continents using SOA modules similar to ours. Compared to the current state of knowledge our SOA parameterization has too low yields, and is lacking the description of semi-volatile and intermediate volatility species as implemented in e.g. the volatility basis set approach (Donahue et al., 2006; Murphy et al., 2011). The particular SOA module used in this work (MADE/SORGAM) has been shown to underpredict SOA formation by about a factor of 10 in the Mexico City region (Fast et al., 2009). Thus it is very likely that a strong underprediction of pollution-related SOA is compensated by an overprediction of anthropogenic POA (De Gouw and Jimenez, 2009), to result in a lower underprediction of total OA. The comparisons with the AMS deployed in Barcelona/Helsinki further support this hypothesis: these two stations were located within an urban area. There, the model overestimates total organics, and attributes the large majority of the mass to primary organics, while the measurements show a major fraction of secondary organics, as is typical of most urban areas (Zhang et al., 2007; Jimenez et al., 2009). Furthermore, emissions from forest fires were not included in our simulations, althought it is known that they can be a major OA contributor (e.g. Aiken et al., 2010). Emissions of biogenic SOA precursors, and the effectiveness of the conversion pathways, are still in discussion and will also contribute to the discrepancies found. Finally, domestic wood burning has been shown to release substantial amounts of OA in wintertime (Alfarra et al., 2007), but also these emissions were not included. Work is currently underway to integrate all these recent developments in SOA and emissions modeling in COSMO-ART.

2.5.3 Nitrate

The most substantial bias found in our simulations is an overestimation of nitrate aerosol components. This is not a new phenomenon and seen also in other model evaluations (e.g. Stern et al., 2008). Accurately modeling this species is challenging (Dentener and Crutzen, 1994), as it represents the result of a dynamic, coupled system between gas- and aerosol-phase, depending on the amount of gas-phase precursors, temperature, relative humidity and aerosol composition (cf. Chapter 9 in Seinfeld and Pandis,

2006). We have tested several hypotheses to understand this deficiency in our model. We could exclude an erroneous nighttime or daytime chemistry (e.g. providing too much HNO_3) and emission sources (too high levels of NO_x). Evaluation against nitrate totals (daily averages of gas-phase HNO_3 + particulate NO_3^- from impregnated filter packs at the station Payerne (CH)) showed some high bias, but the overestimation is much smaller than for nitrate alone. Three hypotheses seem likely: the lack of sulfate, missing wet deposition of HNO_3 and inaccuracies in the model's ability to reproduce relative humidity and temperature well enough.

In experiments, available ammonia is first neutralized by sulfuric acid and only if no more sulfuric acid is available, nitric acid serves as a replacement to form NH_4NO_3 aerosols (Seinfeld and Pandis, 2006). Suppose now that ammonia is limited, then the mass of nitrate found in the aerosol depends also on the amount of sulfate substantially. As our simulations currently underestimate sulfate, the higher amount of available NH_3 will combine to "excess" NH_4NO_3. As mentioned earlier, we could not assess the accuracy of the modeling system regarding NH_3 concentrations due to the lack of measurements. If ammonia is overestimated this will strongly influence this system as well.

Secondly, due to the missing wet scavenging of gases, HNO_3 is not removed from the atmosphere as effectively as in reality. As HNO_3 is a very hydrophilic substance it will easily transfer to the aqueous-phase and is therefore efficiently scavenged. This coud lead to the observed too high levels of total nitrate, which are then subject to gas-aerosol partitioning.

Thirdly, the gas-aerosol partitioning for nitrates has a strong temperature dependence. If our model cannot represent daytime temperature maxima and minima to a high degree of accuracy, this will lead to errors in the partitioning. It is also known that the phase-state solid/liquid is a strongly non-linear function of aerosol chemical composition and relative humidity (see Figs. 2, 5 and 7 in Nenes et al., 1998), consequently changing the partitioning behaviour between gas and aerosol phase. As the lifetime of gas-phase HNO_3 is much shorter than for particulate NH_4NO_3, too strong partitioning to the aerosol phase results in too strong survival of total HNO_3 + nitrate in the atmosphere, which contributes to overpredictions of nitrate at later times.

In summary: firstly, if the model underestimates sulfate more ammonia is available to form nitrate aerosols, which leads to an overestimation. Secondly, if not enough HNO_3 is removed more total nitrate is available for partitioning. Thirdly, even small differences in modelled temperature and relative humidity compared to the situation at the instrument could change the nitrate gas/aerosol partitioning. Finally, if NH_3 concentrations are overestimated themselves, even more NH_3 is available to neutralize NO_3^-, and even more ammonium-nitrate is formed. We think those processes together explain a large part of our overestimation of nitrate aerosols. Other models are better able to simulate mean nitrate concentrations, for example the Comprehensive Air quality Model with extensions (CAMx) / particulate matter CAMx (PMCAMx) (e.g. Aksoyoglu et al., 2011; Andreani-Aksoyoglu et al., 2008) or WRF/Chem (e.g. Li et al., 2010), but once the diurnal cycle of gas-/aerosol partitioning of nitrate is looked at, also these modeling systems exhibit problems.

We have seen that there are substantial model deficiencies to accurately describe nitrate aerosols and that this is a general problem also for other, comparable model systems. One straightforward way to improve the situation will be to increase the horizontal resolution of the simulations to better represent the variability in temperature and relative humidity. A better knowledge on NH_3 emissions and concentrations is needed. The impact of the implementation of a comprehensive wet phase chemistry scheme will be investigated in a future study.

2.5.4 Number size distributions and concentrations

The evaluation showed a small but consistent high bias of modelled number concentrations in both periods. As it can be seen from comparison with the number size distributions this is often caused by overestimated particle numbers in smaller diameter regions, pointing towards either a too high number of particles emitted in the Aitken mode, overestimated nucleation rates, or underestimated coagulation. We consider the nucleation scheme of Kerminen and Wexler (1994) used to contribute to these differences. No explicit nucleation mode exists in COSMO-ART, hence secondary generated sulfate particles are transferred directly into the Aitken mode. A fixed factor is applied here to reasonably reduce number concentrations that get lost through coagulation during the growth from freshly nucleated clusters to Aitken-mode-size particles. In case the number of existing particles (e.g. in strongly polluted regions) does not match the assumptions made for this conversion factor, formation rates of Aitken-mode-sized particles through nucleation of SO_4^{2-} are under-/overestimated.

The distribution of emitted particle mass on accumulation and Aitken mode follows a recent publication of Elleman and Covert (2010), which used a similar aerosol module. They did not find high variability in used emission diameters for different categories in North American simulations, and therefore allowed a very simple description of the size distribution of emitted particles (a time and emission source category invariant split based on total emitted mass). However, their study did not consider modern new particle formation parametrizations. As a result they could have considered at least some of the particle precursors as primary emissions. A study by Spracklen et al. (2010) over Europe came to a different conclusion, indicating substantial variability in emitted number size distributions and high importance of adequate representation of new particle formation.

Even though COSMO-ART does not consider some of the more recent findings on new particle formation or nucleation (e.g. Kerminen et al., 2010), the overall ability of the model to reproduce the measured size distributions was adequate. We consider this to be an evidence that using properly derived emission factors, the overall transformation from emissions to CCN sized particles can be somewhat captured using mostly primary-emission based methodologies. However, the overall agreement between modelled and measured values were in general poorer in N_{30to50} range in comparison to larger size ranges, especially in more remote areas, suggesting a need for a better mechanism to account for the differences between primary and secondary formation. We did not assess, however, the relative contributions of nucleation (and condensation) versus primary emissions (and condensation) to number concentrations in smaller diameters, so these findings will need further study. Finally, the missing description of cloud processing will influence number size distributions and likely shift the distribution to larger diameters. This could explain part of the overestimation for small particles found.

We conclude for the number size comparison that the approach used is comparable with methods currently taken by other modeling groups, but that there is considerable uncertainty that needs to be better understood for future simulations. The overall acceptable agreement between modelled and measured N_{100} and N_{250} concentrations suggests that the pool of CCN-sized particles simulated in these periods are generally well captured in comparison with measurements.

2.6 Conclusions

Our goal has been to thoroughly evaluate the online-coupled, regional-scale chemistry-transport-model COSMO-ART for its ability to simulate trace gas concentrations and aerosol characteristics. The evalua-

tion dataset we have collected allows for a comprehensive assessment of model performance at the surface throughout Europe. Comparison with only recently available measurements of aerosol chemical composition (AMS) and aerosol size distribution data were particularly valuable. Not included in our work has been an evaluation of vertical profiles and upper-air variables of chemical and meteorological parameters with aircraft or radiosonde measurements.

Surface meteorological conditions are very well simulated in all periods investigated without any need for tuning. However, there is room left for improvements through data assimilation and nudging. Results for gas-phase tracer and bulk aerosol mass concentrations are encouraging, also for rather difficult periods like winter 2006. Both, temporal and spatial distributions of O_3 and NO_x are in good agreement with observations. The lack of a coordinated, european-wide measurement network for NH_3 and NMVOC impairs our ability to wholly evaluate gas-phase chemistry, and a missing homogenized elemental carbon dataset hinders evaluation of this aerosol component. From the more advanced datasets, aerosol chemical composition and size distributions, we can conclude that the modeling system is able to represent those quantities with an acceptable degree of accuracy, although nitrate aerosols tend to be overestimated and sulfate underestimated. Not only is the temporal evolution of aerosol mass correctly reproduced, including distinct peaks seen on several occasions and places, but also the chemical composition is quite comparable to reality though some deficiencies have been found. In addition, we could show that the modeling system is able to represent these quantities in an acceptably size-resolved manner - a quantity that is indispensable for correct quantification of climate and health effects. Some deficiencies have been identified in the model system. Most of them will be adressed in the near future by already ongoing developments. These are:

- wet scavenging for gases and wet-phase chemistry / parameterization of in-cloud oxidation of SO_2 to SO_4^{2-}
- update of the representation of secondary organic aerosol components
- realistic lateral boundary conditions for aerosol species
- representation of number size distribution and concentrations in primary emissions of aerosol particles
- inclusion of forest fire emissions

Some discrepancies found are more likely related to the simulation setup rather than the model system itself. An increase in horizontal resolution will be key to address those issues. Continuous assimilation of meteorological measurement data is another method which will likely result in improvements.

The coupling to a meteorological core that is actively used and developed for both short-term weather forecasting as well as climate simulations is regarded as a key benefit. We conclude that the model is suitable for air-quality assessments and the framework is set to evaluate the accuracy of aerosol-climate interactions. Only after our evaluation results are known, more complex studies of e.g. climate impacts, can be conducted reliably.

2.7 Appendix: INT2COSMO-ART

INT2COSMO (formely known as INT2LM, see Schättler, 2009) is the official preprocessor for COSMO which, among other tasks, interpolates initial and boundary conditions (IC/BC) for meteorology to a

given COSMO grid. We have extended this preprocessor by the ability to interpolate and combine several emission and boundary data sets for gas-phase and aerosol species. Additional boundary conditions for parameterized emissions can now also be interpolated. The interpolation procedures are mass-conserving on the total domain.

COSMO-ART thereby gained the ability to be used easily for different domain and grid setups, with different kinds of chemistry IC/BC and emission datasets. Additionally, operational usage is now made feasible. This addition is called INT2COSMO-ART and is available for other users of COSMO-ART.

2.8 Appendix: transmission functions

A correction for the size cut / transmission characteristics of the inlet system for the AIRBASE/EMEP bulk mass and the AMS measurements was performed. For measurements within the AIRBASE/EMEP network (PM_{10}, $PM_{2.5}$ bulk mass) we could not determine the inlets used at each measurement station separately. Therefore we settled on applying the transmission characteristics of typically used inlets for such instruments. In case of $PM_{2.5}$ we used the transmission characteristics of the United States Environmental Protection Agency (US EPA) $PM_{2.5}$ Well Impactor Ninety-Six (WINS) as described in Peters et al. (2001). We could not find studies on transmission functions for any PM_{10} inlet used. Instead we applied a function that resembles the maximum allowed tolerances for a PM_{10} measurement method that would be accepted as US EPA reference method (Table D-3 in 53.43, Part 53, Title 40, Electronic Code of Federal Regulations, `http://www.gpoaccess.gov/ecfr/`). For the AMS, additionally to the correction for vacuum aerodynamic diameter, whe applied a transmission function which consists of:

- 0% transmission below 40 nm d_{va}
- linear increase in transmission vs $\log(d_{va})$, from 0% at d_{va} = 40 nm to 100% at d_{va} = 100 nm
- 100% transmission from d_{va} = 100 nm up to d_{va} = 550 nm
- linear decrease in transmission vs $\log(d_{va})$, from 100% at 550 nm to 0% at d_{va} = 2 μm

This transmission function is an average of the transmission curves used in several AMS studies (DeCarlo et al., 2004; Cross et al., 2007; Vaden et al., 2011; Park et al., 2004).

2.9 Acknowledgements

We acknowledge the EBAS team at NILU, Norway, for providing measurement data through their web interface. Pirmin Kaufmann, MeteoSuisse, made SYNOP measurement data available. The Swiss National Supercomputing Center (CSCS) and the Ipazia-team at Empa provided computing ressources for our simulations. The Swiss National Science Foundation is acknowledged for partly financing the IPAZIA computational cluster (project 206021_128754). We thank the AERONET PI investigators and their staff for establishing and maintaining the 36 sites used in this investigation. Louisa Emmons provided MOZART-NCEP output which we have used as initial and boundary conditions in our simulations, and we are also thankful for advice and help she gave us via email. The work of the AMS measurement group from Manchester has been funded by ACCENT and the UK Natural Environment Research Council (NERC). The Colorado AMS group was supported by NSF ATM-0919189 and NOAA NA08OAR4310565. The

AMS measurements at Melpitz were supported by the Umweltbundesamt (UBA) grants n^o 351 01 031 and n^o 351 01 038, and UFOPLAN contract 3703 43 200.

Chapter 3

An advanced scheme for wet scavenging and liquid-phase chemistry in a regional online-coupled chemistry transport model

Authors: C. Knote[1,2], D. Brunner[1,2]

in preparation for publication

3.1 Abstract

Clouds and precipitation are a major sink for atmospheric trace gases and aerosols. They also provide an environment for additional chemical reactions and physical processes through mixing and recombination of aerosols within droplets. The regional chemistry-climate model COSMO-ART has been lacking a description of wet scavenging of gases and aqueous-phase chemistry. In this work we present a coupling of COSMO-ART with a state-of-the-art wet scavenging and aqueous-phase chemistry scheme. We focus on a coupling that is consistent with the cloud microphysics scheme of the underlying meteorological model, yet based on the standard version of COSMO-ART so it can be used without modifications. First we give details to understand the coupling methods, then present results from idealized flow-over-hill experiments in a 2D model setup and finally present results from a realistic 3D simulation. Comparison against measurement data shows that the scheme efficiently reduces SO_2 trace gas concentrations while leaving O_3 and NO_x unchanged. PM_{10} aerosol mass, which has been overestimated previously, is now in much better agreement with measured values due to a stronger scavenging of coarse particles. While total $PM_{2.5}$ changes only little, chemical composition and also aerosol size distributions change notably. Over-

[1]Laboratory for Air Pollution / Env. Technology, Empa Materials and Science, 8600 Duebendorf, Switzerland
[2]C_2SM Center for Climate Systems Modeling, ETH, Zurich, Switzerland

estimations of nitrate aerosols are reduced while sulfate mass is increased. The effect of cloud processing of aerosols on its size distribution, i. e. a shift of towards larger diameters, is seen.

3.2 Introduction

Clouds are reaction chambers for trace gases and aerosols in the atmosphere. Their aqueous-phase facilitates chemical reactions like the oxidation of sulfur (Hegg and Hobbs, 1978; Walcek and Taylor, 1986) or reactions of organic compounds (Altieri et al., 2006; Carlton et al., 2007; Sorooshian et al., 2006) which contribute substantially to gas-to-particle transfer (Feichter et al., 1996; Zhang et al., 1999; Rasch et al., 2000). Aerosols are on average subject to about 3 condensation/evaporation cycles before being removed from the atmosphere (Pruppacher and Jaenicke, 1995). This cloud processing of aerosols influences size distribution and chemical properties (Wurzler et al., 2000; Lim et al., 2005; Ervens et al., 2008), and therefore their effects on cloud formation (Feingold and Kreidenweis, 2000). The associated precipitation leads to vertical redistribution of gases and aerosols, and represents through wet deposition a major removal mechanism for air pollutants from the atmosphere.

Numerical chemical transport models (CTMs) are used to describe the chemical composition of the atmosphere and are invaluable tools to improve our understanding of atmospheric processes, for the analysis of past air pollution events, for chemical weather forecasting, or for estimating the efficiency of emission reduction measures. These models are either driven offline by meteorological output from a numerical weather prediction / climate model, or they include a meteorological core and are then called "online-coupled". CTMs typically contain modules for aerosol dynamics and gas-phase chemistry, as well as parametrized / prescribed descriptions of anthropogenic and biogenic emission and removal processes. COSMO-ART is a recently developed online-coupled regional CTM which currently includes wet scavenging of aerosols but lacks a parametrization of aqueous-phase chemistry and wet deposition of gases. Previous evaluation efforts (Knote et al., 2011) showed the necessity to include these processes.

Comparable regional modeling systems already have such parameterisations, though with varying degree of explicitness and differences in the number of processes treated (Gong et al., 2011). In particular, they largely differ in the complexity of the description of aerosol scavenging and the number of aqueous-phase chemical reactions considered.

In this work we describe the coupling of the comprehensive wet scavenging and aqueous-phase chemistry scheme SCAV (Tost et al., 2006) with COSMO-ART. SCAV includes descriptions of the scavenging of both gases and aerosols, liquid-phase chemistry and a simple cloud processing of aerosols (in the sense of a mass transfer from smaller to larger particles). Several adaptations had to be made to use this scheme in COSMO-ART, as it had been originally developed for global models making assumptions that are not reasonable for kilometer-scale regional modeling. Adaptations include the prognostic treatment of cloud and precipitation chemical composition, and a linkage to the COSMO grid-scale clouds and precipitation scheme. We show results of idealized two-dimensional simulations of the flow over a hill and present a comparison of a realistic 3D simulation over the European domain with results obtained in a previous evaluation study of COSMO-ART without aqueous-phase chemistry.

3.3 Methods

3.3.1 Modeling system

COSMO-ART (Vogel et al., 2009) is an online-coupled regional chemistry transport model (CTM) developed at KIT Karlsruhe, Germany. It is based on the numerical weather prediction (NWP) system of the Consortium for Small-Scale Modeling (COSMO model, Baldauf et al., 2011). COSMO has been extended to optionally simulate Aerosols and Reactive Trace gases (ART). Aerosols are represented by the modal aerosol module MADEsoot extended (Ackermann et al., 1998; Riemer et al., 2003a) employing five different interacting modes (2 Aitken, 2 accumulation, 1 fresh soot) for the description of fine particulate matter and explicit aging of soot particles. One pair of Aitken and accumulation modes is called "fresh", as it has no soot core, while the other pair, the "mixed" Aitken and accumulation modes, includes soot. Additional modes describe coarse particles (1 mode), dust (3 modes) and sea salt (3 modes). The Regional Acid Deposition Model, Version 2 (RADM2, Stockwell et al., 1990) is used for gas-phase chemistry in a modified version (RADMKA) that has been extended to include the more comprehensive isoprene chemistry of Geiger et al. (2003). Condensation of organic species onto aerosols is realized using the SORGAM module (Schell et al., 2001), with an update to a volatility basis set (Donahue et al., 2006) method currently under development. ISORROPIA II (Fountoukis and Nenes, 2007) is used to calculate thermodynamic equilibrium of the $NH_4^+ - SO_4^{2-} - NO_3^- - H_2O$ aerosols system. New particle formation is simulated according to Kerminen and Wexler (1994) considering binary homogeneous nucleation of H_2SO_4. A washout scheme for aerosols is included based on the work of Rinke (2008). The model has been thoroughly evaluated in Knote et al. (2011), where an overestimation of SO_2 concentrations compared to surface station observations was determined. From a comparison against aerosol mass spectrometer (AMS) data it was found that nitrate aerosol concentrations were overestimated while the concentrations of sulfate aerosols were too low.

3.3.2 Scavenging scheme

The SCAVenging submodel (Tost et al., 2006) of the Modular Earth Submodel System (MESSy, Jöckel et al., 2005) contains a comprehensive description of the transfer of gases and particulate matter between air, cloud droplets and rain drops. It has been developed for global chemistry transport models. Transfer of gases between air and droplet can be described in SCAV either by (effective) Henry's law equilibrium coefficients (Lawrence and Crutzen, 1998) or by explicitly calculating the transport processes through a system of coupled ordinary differential equations. Liquid-phase chemistry is solved using the Kinetic PreProcessor (KPP, Damian et al., 2002) allowing for a flexible adaptation of the chemistry scheme. The chemical mechanism used is based on MECCA (Sander et al., 2005) with some extensions from the CAPRAM mechanism of Ervens et al. (2003), and comprises sulfur oxidation, halogen and transition metal chemistry and a number of inorganic and organic acid-base equilibria. Depending on the application the mechanism can be reduced to the reactions that are of interest. Aerosol scavenging is divided into *nucleation* scavenging by cloud droplets, and *impaction* scavenging by rain droplets. *Nucleation* scavenging employs an empirical function to describe nucleation and growth of cloud droplets (Tost et al., 2006), but also considers Brownian motion following Seinfeld and Pandis (2006). This activation parametrization is only applied to aerosols tagged as being "soluble". *Impaction* scavenging by rain droplets is realized according to Slinn (1984) taking into account both particle and rain droplet size. No distinction is made between in-cloud and below-cloud scavenging, hence scavenging by rain droplets (impaction scavenging)

can be active also within clouds, and seeder-feeder type clouds are more realistically represented. All scavenging processes are only applied to the cloud covered fraction of a grid cell. Upon evaporation, dissolved gases that have not been converted to ions are released back into the gas-phase. Aerosols (and the newly created ions) can be either released back into the mode they originated from, or into the largest soluble mode. This "cloud processing", that is the transfer of mass into the largest soluble mode, is based on the assumption that upon evaporation of a cloud droplet all (small) particles that might have been scavenged during the lifetime of the cloud by a single cloud droplet will stick together and form one single particle upon release.

The module makes use of current environmental quantities (temperature, pressure, water vapor content, cloud liquid water content, rain water content, rain flux) as given by the driving meteorological model. In its original formulation it is assumed that the complete cloud life-cycle (condensation, scavenging, aqueous-phase chemistry, washout by precipitation, evaporation) takes place at each time-step.

3.3.3 Coupling and adaptations

Several simplifications in the original SCAV version are not reasonable for high-resolution regional simulations. It was assumed that the lifetime of a cloud is shorter than a model time-step, and in consequence, complete condensation and evaporation of cloud liquid water was simulated each time-step. This avoided the need to make the chemical composition of the liquid-phase transported quantities and greatly improved the computational efficiency of the scheme. The COSMO-ART modeling system is operated on the meso-γ scale (Orlanski, 1975), with mesh sizes up to 1 kilometer. On this scale, the lifetime of a cloud (10-30 minutes for shallow cumuli (Zhao and Austin, 2005) and thunderstorm cells (Cotton et al., 2011), up to several hours for stratiform clouds (Albrecht, 1989)) is well above typical model time-steps (several seconds to minutes). This made the simplification of simulating a complete cloud life-cycle in one time-step obsolete and required the inclusion of the transport of quantities within the aqueous-phase, in cloud and rain droplets separately, and further the calculation of fractional condensation and evaporation as described in the following.

Transport in cloud and rain water

In COSMO-ART the transport of chemical quantities is consistent with meteorological scalars (humidity, hydrometeors). As COSMO-ART is an "online-coupled" model system, this means that exactly the same advection, diffusion and convection operators are used for both cloud liquid water and the chemical constituents. The choice of the scheme therefore depends on the preferences of the user. Current operational setups (and the simulations in this work) employ a Runge-Kutta type time integration scheme and Bott advection, both methods are described in Doms (2011). We have extended these schemes and included the transport of the chemical composition in cloud liquid water and rain water. COSMO-ART has the ability to relax the boundaries of the simulation domain against a coarser grid simulation of COSMO-ART or a simulation of a global model. We have provided this possibility of a "one-way nesting" into another COSMO-ART simulation also for the transported quantities in cloud and rain water.

Partial condensation and evaporation of clouds

Aerosols are scavenged by nucleation scavenging during cloud formation and released back to the atmosphere during dissipation of the cloud. In order to represent these processes more realistically, we extract

the necessary information out of the treatment of liquid-phase species within COSMO. There, grid-scale clouds and precipitation are described by a bulk water-continuity model, where the total water content of a grid cell is distributed across a number of reservoirs, and budget equations are solved to redistribute mass between these reservoirs. In the current operational formulation (Doms et al., 2011), the "two category cloud-ice scheme", 5 types of water are accounted for: water vapor (qv), cloud liquid water (qc), cloud ice (qi), rain (qr) and snow (qs). Each reservoir has a budget equation of its source and sink terms (Eqn. 5.95 in Doms et al. (2011)), e.g. for cloud liquid water it is given as

$$S^c = S_c - S^c_{au} - S_{ac} - S^c_{frz} + S^i_{melt} - S_{rim} - S_{shed}, \tag{3.1}$$

where S_c is condensation and evaporation of cloud water, S^c_{au} the autoconversion of cloud water to form rain, S_{ac} the accretion of cloud water by raindrops, S^c_{frz} the nucleation of cloud ice due to homogeneous freezing of cloud water, S^i_{melt} the melting of cloud ice to form cloud water, S_{rim} the collection of cloud water by snow (riming), and S_{shed} the collection of cloud water by wet snow to form rain (shedding). All terms are given in $\frac{\mathrm{kg}}{\mathrm{kg \cdot s}}$.

We are now interested in the total transfer between the reservoirs water vapor qv, cloud liquid water qc, and rain water qr. As there might be several processes contributing to each transfer, we generalize and introduce summary variables: for the transfer between water vapor and cloud liquid water we use $\mathrm{S_{v2c}}$, for the transfer between cloud liquid water and rain $\mathrm{S_{c2r}}$, and for the transfer from rain to water vapor $\mathrm{S_{r2v}}$.

The cloud water condensation/evaporation tendency S_c is calculated in COSMO with a saturation-adjustment technique, where temperature and cloud liquid water in a grid-cell are isobarically adjusted, taking latent heating into account, until saturation is reached. Decreases / increases in specific humidity (qv) then define the amount of condensation / evaporation (chapter 5.6 in Doms et al., 2011). As several processes act upon the water reservoirs in COSMO (advection, precipitation, relaxation, nudging), this saturation adjustment is applied several times per time-step. All other terms in Eqn. 3.1 are calculated once per time-step in a dedicated subroutine in the microphysics scheme.

We extended the saturation-adjustment routine to save the summed condensation/evaporation tendency $\mathrm{S_c}$ over all calls to it per time-step ($\mathrm{n_{satad}}$). As this is the only process transferring mass between water vapor and cloud liquid water, we get

$$S_{v2c} = \sum_{i=1}^{n_{satad}} S_c \tag{3.2}$$

Depending on the direction of change ($\mathrm{S_{v2c}} > 0$ is condensation, $\mathrm{S_{v2c}} < 0$ is evaporation), we calculate the fractional change in cloud water due to condensation, $f_{qc,cond}$, as

$$f_{qc,cond} = min\left[1.0, max\left(0.0, \frac{S_{v2c} \cdot \Delta t}{qc(t = t_0 + \Delta t)}\right)\right], \tag{3.3}$$

and in case of evaporation as

$$f_{qc,evap} = min\left[1.0, max\left(0.0, \frac{S_{v2c} \cdot \Delta t}{qc(t = t_0)}\right)\right] \tag{3.4}$$

where t_0 represents the beginning and $t_0 + \Delta t$ the end of the current time-step.

In case of condensation ($S_{v2c} > 0$), the nucleation and growth parametrization in SCAV (Eqn. 9 in Tost et al. (2006)) is applied, but only to the freshly condensed fraction of the aerosol. This fraction is equal to $f_{qc,cond}$, assuming a linear relationship between the fraction of condensed cloud liquid water and aerosols acting as cloud condensation nuclei. Note that *nucleation* scavenging in Tost et al. (2006) comprises scavenging due to Brownian motion and the nucleation and growth parametrization. While the latter is subject to the application restriction above, the former is not, as Brownian motion scavenging is active also within the cloud. All scavenging processes are only applied to the cloud covered part of the grid cell (f_{CLC}), hence, from the example above, the fraction of the grid box mean aerosol concentration considered in the nucleation and growth parametrization is

$$f_{grid\ box,cond} = f_{CLC} \cdot f_{qc,cond}. \tag{3.5}$$

In case of evaporation, not all components evaporate at the end of a time-step, but only a fraction (equal to $f_{qc,evap}$), while the remainder is kept and advected as liquid-phase concentration. If no cloud liquid water is left in the grid cell, everything is evaporated.

Precipitation

Precipitation is a prognostic quantity in COSMO as well. For grid cell sizes less than 10 km, the assumption of independent columns is unrealistic, as precipitation can be displaced horizontally during fallout by more than the size of a grid cell. It has been shown that the prognostic treatment is beneficial in the representation of certain (i.e. lee-side) precipitation patterns (Baldauf and Schulz, 2004).

To describe the removal of aerosols by precipitation, we need to extract information from the COSMO model on the conversion S_{c2r} of cloud to rain water, the fraction $f_{qr,sed}$ of rain water sedimenting out of a grid box during a time step, and the fraction $f_{qr,evap}$ of rain water evaporating during a time step, which is closely related to the rate S_{r2v}.

The total change of rain water over a time-step Δt is given by

$$\Delta qr_{tot} = \Delta qr_{dyn} + \Delta qr_{sed} + \Delta qr_{mp}, \tag{3.6}$$

with Δqr_{mp} the contribution by microphysics, Δqr_{dyn} and Δqr_{sed} the contributions by dynamics (advection, diffusion) and sedimentation, respectively.

As for cloud liquid water (Eqn. 3.1), also rain water (qr) has a balance equation describing the tendency due to all microphysical processes,

$$S^r = S^c_{au} + S_{ac} - S_{ev} + S_{shed} - S^r_{cri} - S^r_{frz} + S^s_{melt}, \tag{3.7}$$

with the additional terms S_{ev} for evaporation of rain water, S^r_{cri} and S^r_{frz} for freezing of rain due to collection of cloud ice / heterogeneous nucleation forming snow, and S^s_{melt} representing melting of snow.

The conversion rate S_{r2v} is directly given by the term S_{ev}, and the rate S_{c2r} is given by the sum of all terms converting cloud water to rain water, that is

$$S_{c2r} = S^c_{au} + S_{shed} + S_{ac}. \tag{3.8}$$

The different aerosol tendencies due to rain processes are now given as follows:

Impaction scavenging of aerosols in SCAV is a function of the rain rate prr, which can be extracted from the COSMO microphysics scheme for each model level.

The rain production per time-step is used to estimate the amount of aerosol mass dissolved in cloud water which is transferred to rain water. It is calculated as the integral of S_{c2r} over Δt, given as

$$\Delta qr_{prod} = S_{c2r} \cdot \Delta t. \tag{3.9}$$

The fraction of aerosol mass in rain water that evaporates per time-step is derived from the evaporation tendency as given by the microphysics scheme as

$$f_{qr,evap} = \frac{S_{r2v} \cdot \Delta t}{qr'}, \tag{3.10}$$

where qr′ is the amount of precipitation after the dynamical tendencies have been updated:

$$qr' = qr(t = t0) + \Delta qr_{dyn}. \tag{3.11}$$

Finally the fraction of aerosol mass contained in rain water which sediments out of the grid cell per time step is

$$f_{qr,sed} = \frac{prr \cdot \frac{\Delta t}{\rho}}{qr'}, \tag{3.12}$$

the relation between rain rate (converted to mass per time-step) and rain water content.

In conclusion, our coupling transports the chemical composition of cloud liquid and precipitating water consistently with the respective quantities in the meteorological part. Evaporation, condensation and (in case of rain) sedimentation tendencies from the meteorological core are used to describe the respective scavenging / evaporation processes.

3.3.4 Cloud processing of aerosols

Under the assumption that each cloud droplet will form a single aerosol particle upon evaporation, the aerosol size distribution may be substantially altered as compared to the size distribution upstream of the cloud. The question that arises is how to represent this process in a modal scheme like MADE. There, a number of log-normal modes exist which represent Aitken, accumulation and coarse mode particles. If now cloud processing creates an additional mode, a “from-cloud” mode, and one does not intend to represent this new mode in the aerosol-phase additionally to the existing ones, mass and number released from cloud droplets need to be redistributed onto the existing modes. SCAV in its original formulation had the options to put mass back into the originating modes (i.e. no cloud processing), or into the largest soluble mode (in our case the “mixed” accumulation mode). We have used the second option, but refined it by distributing mass and number by equal fractions on the mixed Aitken (10 %) and accumulation

mode (90%). This is done to avoid unrealistic growth of the accumulation mode diameters, assuming that a small fraction of the cloud processed aerosol is smaller than the accumulation mode size range.

3.4 Idealized 2D simulations

To understand the interplay of the different components of the new scavenging scheme we have set up an idealized 2D simulation of the flow over a Gaussian hill with a precipitating cloud above. The model setup consists of 200 grid points in x direction with a grid spacing of dx = 0.0045° (≈ 500m) and 40 vertical hybrid sigma levels up to 20 hPa. Lateral meteorological forcing is provided by an atmospheric profile as used in Weisman and Klemp (1982), with a maximum wind speed of 20 m/s and relative humidities between 10 and 70 %. In the domain center a Gaussian shaped hill with a height of 2500 m and a half width diameter of 6000 m acts as distortion element to the flow field, resulting in cloud development and precipitation (see top and middle panel of Fig. 3.1). Chemical composition (gases and aerosols) at the lateral boundaries is prescribed using the vertical profile of a grid point from a previous 3D simulation. The composition represents typical conditions at Payerne, a rural site in the Swiss Plateau, at noon time, and is calculated as the mean of all 12 UTC profiles at Payerne during the 20 days of simulation (we used output from the "autumn" case in Knote et al. (2011)). Two simulations have been made, each integrated over 12 hours, which allowed the system to reach steady state, one without *any* scavenging as a reference simulation (REF), and one including the new coupling (SCAV). In the following plots, means (or differences of the mean) over this integration period are shown.

Figure 3.2 shows that SO_2 is efficiently scavenged after the air has passed the cloud, and that in turn total aerosol sulfate mass has increased by up to 30 %. The time an air parcel spends in the cloud in this setup is 250s (cloud with approx. 5 km diameter, 20 m/s wind speed), and the absolute difference in SO_4^{2-} in the wake of the cloud is +0.25 $\mu g/m^3$. This means that with an initial SO_2 concentration of about 5 $\mu g/m^3$ we generated approximately 1 ng/m^3 of SO_4^{2-} per second due to aqueous-phase chemistry. Figure 3.3 shows the distribution of mass between the different phases for sulfur and nitrogen compounds during passage of the cloud between grid cells 90 and 110. Wet deposition was negligibly small for mass calculations in this idealized simulation. Both, sulfur and oxidized nitrogen show increases in aerosol mass by 13 and 17 % column total respectively. Reduced nitrogen resides almost completely in the aerosol-phase and remains essentially unchanged. This makes this idealized simulation ammonia-limited. An increase in sulfate aerosols is notable, and would be even stronger if the time spent in the cloud were longer, as can be seen from the amounts of sulfate increase (200 %) in the realistic simulation described in the next section.

Clearly visible is that oxidized nitrogen (mostly HNO_3) transfers into the aqueous-phase rapidly, where it dissociates to create additional nitrate aerosols on evaporation. In a more realistic scenario with notable wet deposition, this fast transfer of nitrogen compounds into cloud (and rain) droplets actually leads to a decrease in nitrate aerosol mass (see next section). Also, note that the conversion of sulfur is irreversible, while (ammonium-)nitrate is in thermodynamic equilibrium with the environment. The cloud pH as presented in the lower panel of Fig. 3.1 shows simulated values between 5.0 and 5.8 (except at cloud edges where very low LWC disturbs the results). We can loosely compare this to measured values: the Duebendorf (CH) station of the Swiss Federal air quality network (NABEL) routinely measures rain pH, and the mean for the period in autumn 2008 we have used the boundary chemistry profile from is 5.9. Cloud processing of aerosols is implemented such that most aerosol mass released on evaporation is put into the mixed accumulation mode. Figure 3.4 shows that this happens very efficiently. Most of the

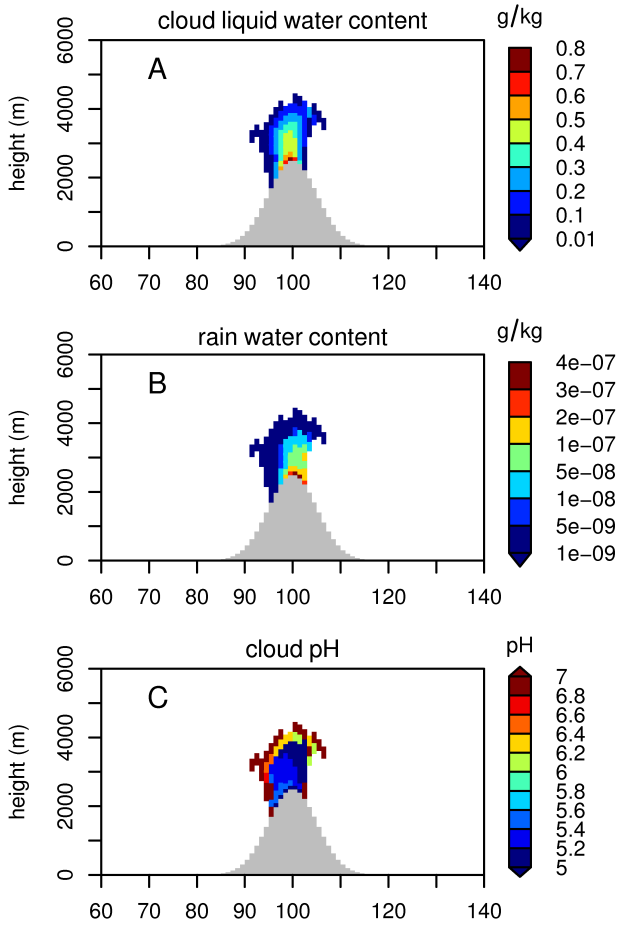

Figure 3.1: Cloud liquid water (A) and rain liquid water (B) concentrations (g/kg), and cloud pH (C).

sulfate mass originally in the Aitken mode is scavenged and placed (together with the newly oxidized sulfur) into the mixed accumulation mode. Starting half through the cloud evaporation already sets in, releasing aerosols from the cloud phase.

The idealized simulations provided useful insight into the workings of the new coupling and the results were physically and chemically plausible. Therefore the coupling has been applied to a realistic 3D simulation of air quality over Europe.

3.5 Realistic application

In Knote et al. (2011), COSMO-ART has been extensively evaluated against a number of observational datasets, including measurements of aerosol chemical composition by aerosol mass spectrometry (AMS). These datasets were available for two periods in autumn 2008 and spring 2009. While several parameters were simulated with good quality, a number of deficiencies were found as mentioned earlier. A wet-scavenging scheme that includes aqueous-phase chemistry should have a positive impact on these problems: firstly, the overestimation of ammonium-nitrate aerosols is expected to be reduced since the

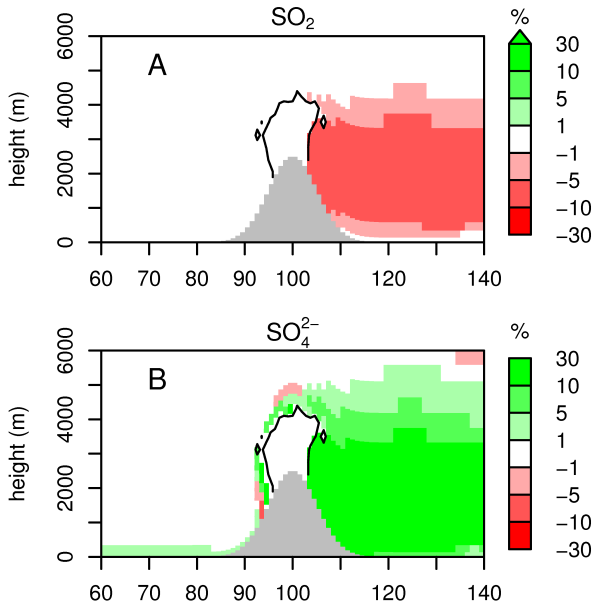

Figure 3.2: Changes in gaseous SO_2 (A) and total SO_4^{2-} (B) aerosol mass as percent change against the reference simulation.

gas-phase precursor / reservoir of ammonium-nitrate, HNO_3 and NH_3, readily transfer into the aqueous-phase and are therefore more efficiently scavenged than other components. Secondly aerosol sulfate was underestimated and is expected to increases since aqueous-phase conversion of SO_2 to SO_4^{2-} contributes substantially to measured aerosol sulfate (Walcek and Taylor, 1986; Rasch et al., 2000). To understand the impacts of our addition in a realistic setting we chose to re-simulate one of the evaluation periods from Knote et al. (2011). We picked the autumn 2008 period due to high cloudiness and frequent precipitation events. The setup of the new run is identical to the simulations in Knote et al. (2011) except that SCAV has now been included and switched on. The previous wet scavenging scheme for aerosols has been active in the reference simulation.

Figure 3.5 summarizes the impact of the coupling on concentrations of O_3, NO_x, SO_2, PM_{10}, and $PM_{2.5}$. Shown are the simulation period mean concentrations of a set of surface station observations throughout Europe from the EMEP network and the corresponding model concentrations for the reference simulation from Knote et al. (2011) and the new version including SCAV. The comparisons are subdivided according to the station classification of Henne et al. (2010), in which stations are categorized according to their representativeness.

Ozone and NO_x are virtually unaffected by the implementation, which was expected. SO_2 shows strong reductions (see Figure 3.6 A) and agrees better with measurements (Figure 3.5), although it is still above measured concentrations. PM_{10}, which has been overestimated during this period is visibly reduced, with the largest decreases at coastal stations. We attribute this to a more efficient scavenging of larger aerosol particles like sea salt, dust or coarse anthropogenic particles compared to the aerosol scavenging scheme used previously. $PM_{2.5}$ mass totals in contrast show only minor changes.

The spatial distribution of changes in SO_2, in the chemical composition of sulfate and nitrate aerosol mass

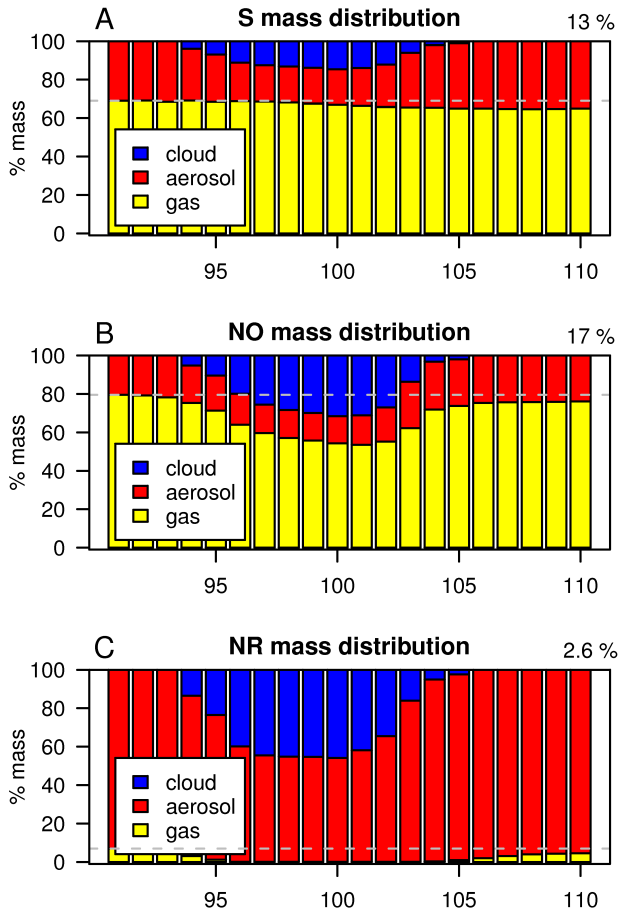

Figure 3.3: Distribution of of different groups of compounds between phases during passage of the cloud (between grid cells 90 and 110 of the idealized simulation). The three phases considered are gas (g), aerosol (a), and cloud water (l). The compound groups are sulfur "S" (plot A): SO_2 (g), H_2SO_4 (g), SO_4^{2-} (s), SO_2 (l), H_2SO_4 (l), HSO_4^- (l), SO_4^{2-} (l), HSO_3^- (l), SO_3^{2-}(l). Oxidized nitrogen "NO" (plot B): NO (g), NO_2 (g), HNO_3 (g), N_2O_5 (g), NO_3 (g), NO_3^- (s), HNO_3 (l), NO_3^- (l). Reduced nitrogen "NR" (plot C): NH_3 (g), NH_4^+ (s), NH_3 (l), NH_4^+ (l). Shown are column totals for grid columns above the mountain with its top at grid point 100. The percentage given at the top right shows the relative change in total aerosol mass between before (column total at grid point 90) and after cloud processing (at grid point 110).

are shown in Figure 3.6. Accumulated precipitation is given as reference as well. Presented are differences in the mean concentration over the simulation period between the reference and the simulation including SCAV relative to the reference case. SO_2 is reduced by up to 50 %, with the strongest reductions over the Northern Atlantic ocean, Norway, the Alps and North Africa. In large parts of Central and Eastern Europe strong reductions are found as well. Interestingly, sulfur dioxide reductions are smallest over the oceans in regions with strong emissions from shipping routes (North Sea, English Channel, coast of Portugal, Straight of Gibraltar), which is however only caused by the fact that due to the strong pollution in this region the *relative* reductions are small. Absolute differences are comparable to other regions. Sulfate aerosol mass increases over large parts of Europe, with increases up to 200 % over Central and North-Eastern European regions. Reductions in NO_3^- aerosol mass are substantial, with reductions between 20

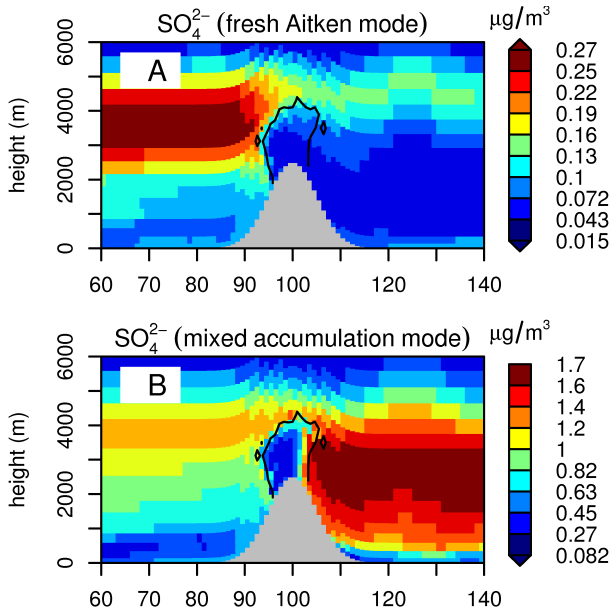

Figure 3.4: Changes in mass concentrations of sulfate aerosols in the fresh Aitken mode (A) and the mixed accumulation mode (B) showing the effect of cloud processing.

and 40 % over large parts of France, Germany, Poland and the Baltic region including Greece. Strong reductions are found in Northern European regions and over the Northern Atlantic. These were also the regions with highest cloudiness and most frequent precipitation events.

Information about the aerosol chemical composition with high temporal resolution (hourly and better) can be inferred for non-refractive particles below 1 μm (NR $-$ PM$_1$) using an aerosol mass spectrometer (AMS, Canagaratna et al., 2007). During the simulation period, several AMS instruments had been deployed at a number of stations throughout Europe within a EUCAARI/EMEP measurement campaign. These data allow for quantitative comparison of the mass of major inorganic species and organic contributions. Figures 3.7a and 3.7b show that the inclusion of SCAV has considerable impact on the chemical composition. While in Knote et al. (2011) the mass of non-refractive particles below 1 μm was used, which is the correct quantity to compare to the AMS, Figures 3.7a and 3.7b show a comparison with PM$_{2.5}$. The reason for that will be explained below.

The overestimation of nitrate compounds found in previous simulations is reduced, which is mostly due to the efficient washout of the HNO_3 precursor. Some discrepancy remains, like for example a tendency of the model to retain too much nitrate in the particle phase during daytime (e.g. in Payerne and Melpitz in Fig. 3.7a or K-Puszta in Fig. 3.7b). This might be due to small differences found between modeled (grid cell mean) and measured (at AMS location) temperature and relative humidity and the subsequent partitioning errors in the thermodynamic equilibrium calculations, as we already suggested in Knote et al. (2011). Sulfate aerosol mass increases substantially but we do not find a single station where it would be overestimated compared to measurements. The overestimation of SO_2 and the underestimation of sulfate points to a still too slow oxidation of SO_2 in the aqueous-phase: sulfur can be oxidized within droplets by H_2O_2, O_3 and OH, and further by O_2 if catalyzed by transition metals (Fe(III), Mn(II)). Smaller contributions come from the oxidation by formaldehyde and dichloride ions (Jacobson, 2005). Kreidenweis et al.

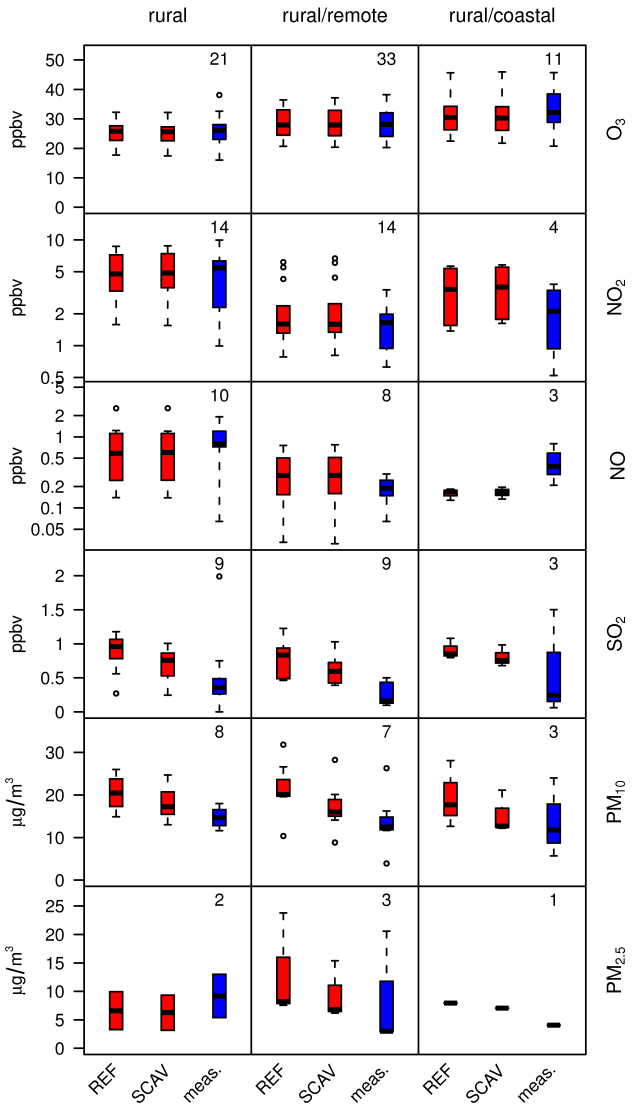

Figure 3.5: Boxplots of mean trace gas and particulate matter concentrations over the simulations period. Shown are results from the reference simulation in Knote et al. (2011) (REF), results from a new simulation including aqueous-phase chemistry (SCAV), and measurement data from the AIRBASE network (meas.). Stations classified according to their representativeness following (Henne et al., 2010).

(2003) showed that high uncertainties exist between different model formulations regarding the oxidation of sulfur by O_3 (less so for oxidation by H_2O_2), mostly due to the treatment of cloud pH which governs relative contributions and efficiency of these pathways. To accurately simulate pH a complete ion balance is needed. In our current implementation we lack the explicit representation of several potentially relevant ions (Mn, Fe, Ca, K). Therefore some error will be introduced in both the chemical environment (pH) and the oxidation pathways, possibly leading to an underestimation of sulfate formation and insufficient reduction of SO_2.

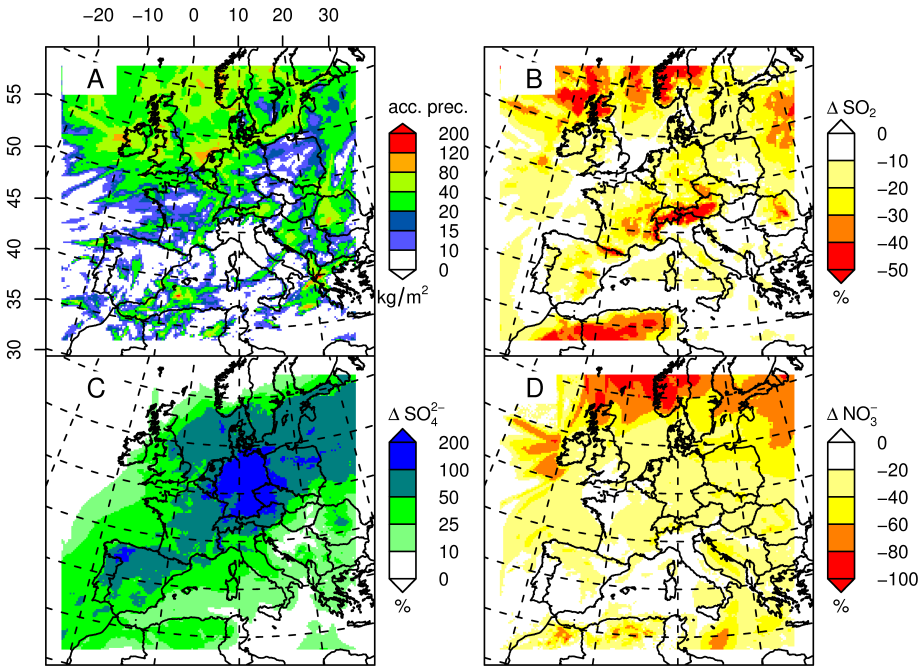

Figure 3.6: Accumulated precipitation (A), values below 10 kg/m^2 are masked out. Relative changes in SO_2 (B), and SO_4^{2-} (C) and NO_3^- (D) aerosol mass concentrations due to the inclusion of the new scavenging module. Shown are mean differences over the whole simulation period.

In contrast to the comparison with bulk $PM_{2.5}$ mass measurements (Fig. 3.5), total aerosol mass is reduced substantially when using the new scavenging scheme. To compare with AMS measurements, the AMS transmission function needs to be applied to the modeled aerosol mass size distribution to accurately represent the particle size range "visible" for the AMS. Doing so resulted in a notable reduction in total $NR - PM_1$ mass (not shown, about -25 % total mass). Analysis of the distribution of mass over the size ranges revealed that the underestimation of $NR - PM_1$ mass is caused by an efficient shift of mass to larger diameters and a somewhat stronger washout. The shift in diameters is due to the cloud processing and the addition of new mass through the oxidation of gaseous precursors, without an associated increase in aerosol number. This results in an increased fraction of mass in the accumulation mixed mode not being "seen" by the AMS due to the specific sampling efficiency cut-off of this instrument at about 1 μm, leading to the aforementioned underestimation. From comparison with $PM_{2.5}$ measurements we know however that the mass is not lost, rather only redistributed. We therefore compared against modeled $PM_{2.5}$ in Figures 3.7a and 3.7b.

In Knote et al. (2011) a homogenized dataset of observed number concentration size distributions (Asmi et al., 2011) has been used in evaluation. Therein, data for several stations throughout Europe is available. We have used the same station locations, but compared volume concentrations instead of number concentrations to better understand the effect of the new scavenging scheme on aerosol mass. As converting the measured number concentrations into volume concentrations would have made assumptions necessary which we could not reasonably justify we only show the modeled results here. Figure 3.8 presents the total volume concentrations for the reference case and the new modeling system as function of the particle

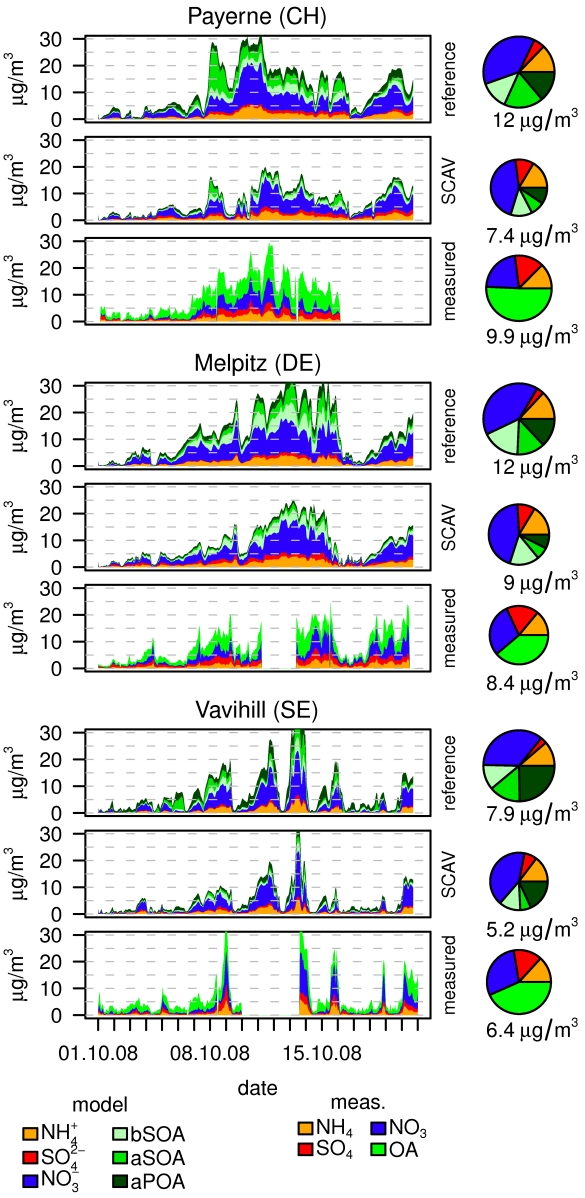

Figure 3.7a: Timeline of aerosol chemical composition (top: reference simulation (Knote et al., 2011), middle: simulation with SCAV, bottom: measured by AMS) during autumn 2008. Pie charts give mean over time period (size of pie relates total mass). Measured OA should be compared with the sum of modeled aPOA, aSOA and bSOA. Gray shaded areas mask times without measurement data. While AMS measures non-refractory PM below 1 μm, we compare here with modeled PM below 2.5 μm, due to effects of the changes in size distribution mentioned in section 3.5.

diameter over a range between 20 nm up to 10 μm. Typical transmission functions for an AMS, a $PM_{2.5}$ and a PM_{10} inlet system (as calculated in Knote et al. (2011)) are given in the figure for comparison.

At almost all stations shown in Figure 3.8, a shift of the size distribution towards larger diameters is

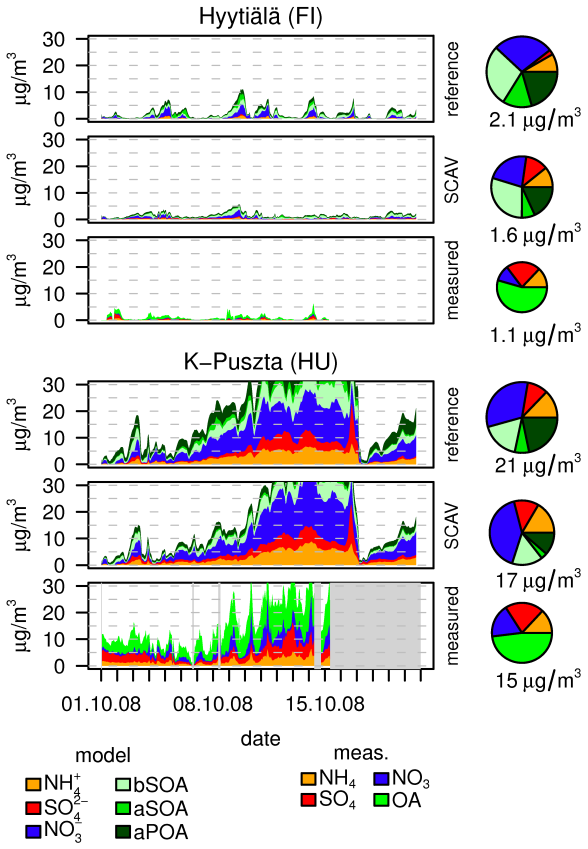

Figure 3.7b: As Figure 3.7a but for different stations.

visible, which is the expected result of the cloud processing of aerosols. Sensitivity simulations revealed that this shift is almost insensitive to the choice of the "cloud processing" option implemented in SCAV (distribute mass onto mixed Aitken / accumulation mode, or redistribute onto mode of origin). The reason for this insensitivity is a technical one: a substantial mass fraction of the Aitken and accumulation modes are inorganic ions ($NO3^-$, $SO4^{2-}$, and $NH4^+$) which are used in the liquid-phase chemistry in SCAV and therefore loose the information on their mode of origin on scavenging. Upon evaporation, all mass of chemically active ions is put into the accumulation mixed mode irrespective of the choice of "cloud processing". As this processing only adds mass - but does not create new particles - the existing particles grow in diameter.

Several stations in coastal regions (Aspvreten, Birkenes, Cabauw, Mace Head, Vavihill) show a pronounced bimodal distribution with a second peak at coarse diameters around 5 to 10 μm which is caused by strong contributions from sea salt. This peak is strongly reduced through the inclusion of SCAV. This is the reason for the improvement in the comparison with bulk mass measurements of PM_{10} in Figure 3.5 mentioned above.

To understand the quality of the aerosol and trace gas sink term due to wet scavenging, we compared our simulations against wet deposition station data from the European Monitoring and Evaluation Programme (EMEP, `http://www.emep.int`). 80 stations throughout Europe provided daily sums of wet deposited

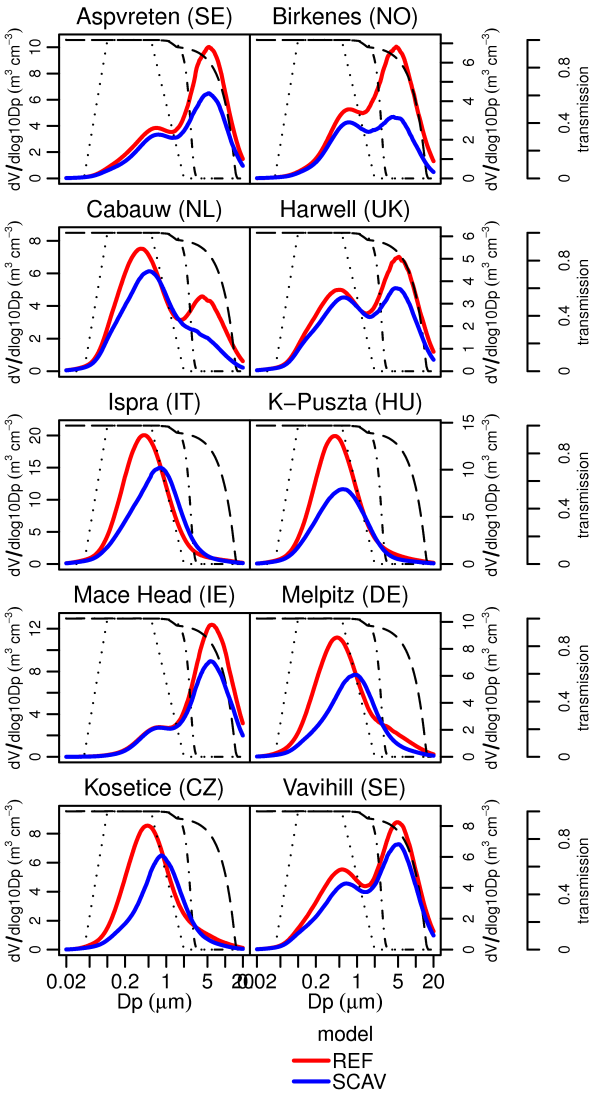

Figure 3.8: Modeled aerosol volume concentration size distributions at selected stations for the autumn 2008 period. Modeled results for the reference simulation (red) and a simulation including SCAV and cloud processing (blue) are shown as thick solid lines. For reference the transmission functions of an AMS (dotted line), a $PM_{2.5}$ (dash-dotted line) and a PM_{10} (dashed line) inlet system as calculated in Knote et al. (2011)) are given as well.

masses of $NO3^-$, $NH4^+$ and $SO4^{2-}$, usually measured by ion chromatography (Aas et al., 1996). Figure 3.9 shows a comparison of the wet deposited mass totals over the simulated period. Most of the comparisons with single station measurements lie within a factor of 5. Deposited nitrate and ammonia mass generally corresponds to measurements, only sulfate mass tends to be underestimated, which reflects the still somewhat too low sulfate aerosols concentrations. The stochastic characteristics of precipitation explain the strong scattering of the comparison of such a short period, and would be reduced by simulating

a longer time period. This probably also explains the observation that at a number of stations the model reports wet deposition, while the measurements do not: grid values are mean values, and (especially) a (convective) precipitation event does not necessarily have to comprise the location of the measurement station, while all observed precipitation events at the station should also lead to grid point mean precipitation. Also, very low precipitation intensities (drizzle) may not be registered by the instrumentation as precipitation event due to the measurement principle (opening of lid required (Aas et al., 1996)).

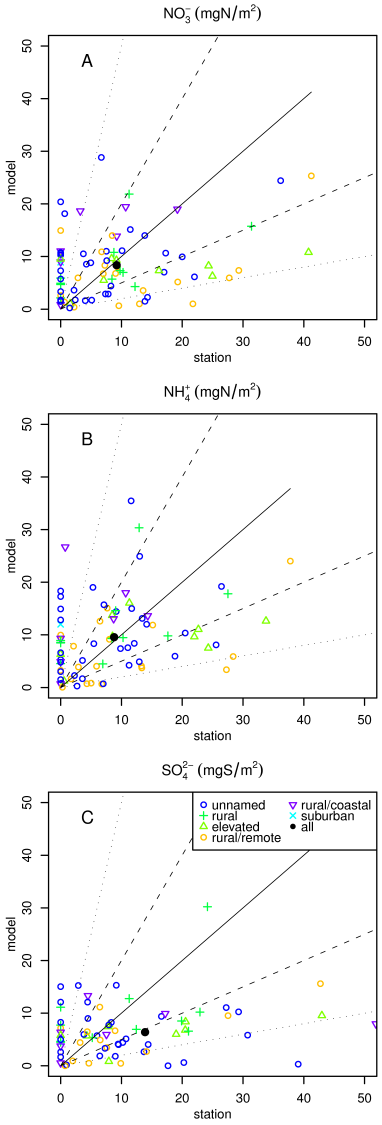

Figure 3.9: Scatterplots of wet deposited mass of NO_3^- (A), NH_4^+ (B), and SO_4^{2-} (C). Each hollow symbol represents the comparison between the measured mass total over the simulation period against the modeled one at a single station. Symbols are categorized according to a station representativeness classification by Henne et al. (2010), which is shown by different colors / symbols. Filled black circles represent the arithmetic mean deposited mass. Lines are drawn to help estimate over/underestimation factors: solid = 1:1 , dashed = 2:1 and dotted = 5:1.

One possibility to circumvent the problem of statistical undersampling which does not involve simulating longer periods is to calculate the mean deposition (as arithmetic mean over all stations, black circles in Figure 3.9), which can serve as a proxy for total wet deposition in Europe. There, $SO4^{2-}$ is underestimated by a factor of 2. Model and measurements show excellent agreement for $NO3^{-}$ and $NH4^{+}$.

3.6 Limitations of the current implementation

Despite the comparatively high degree of complexity of our scheme, three major omissions and the reasons need to be mentioned:

Firstly, no scavenging of aerosols or trace gases by ice crystals or snow flakes has been implemented so far, although SCAV does allow such a coupling. The species most affected by such a scavenging is HNO_3 (Chang, 1984; Baltensperger et al., 1991; Abbatt, 1997), and its magnitude can be substantial under free-tropospheric conditions. Neu and Prather (2011) recently highlighted the importance of this process for a correct description of HNO_3 lifetimes and subsequently of upper troposphere O_3 concentrations. For studies of the lower troposphere this is, however, of much lesser importance and arguably negligible. In the light of the additional computational demand of such a coupling (additional 35 fields to be transported, twice the transport processes and chemistry) we refrained so far to include this coupling, but it would be important for studies of the upper troposphere / polar regions.

Secondly, COSMO-ART has recently been coupled to the experimental two-moment microphysics scheme of Seifert and Beheng (2006) to simulate aerosol indirect effects on clouds (Bangert et al., 2011), which would allow a much more detailed description of the nucleation scavenging processes for aerosols. Currently, SCAV employs an empiric method derived from measurements of interstitial aerosol within clouds, which completely disregards variability in activation due to aerosol characteristics other than size. However we have chosen to couple SCAV with COSMO-ART in a way that is applicable in typical/operational COSMO-ART setups. As the parametrization of Bangert et al. (2011) requires the Seifert and Beheng (2006) two-moment microphysics scheme (itself experimental), this would not be the case. Such a coupling is nonetheless an important topic for future studies of aerosol cloud interactions.

Thirdly, the coupling to the convection parametrization is included but does not consider scavenging during up-/downdrafts. The default convection parametrization in COSMO is a modified Tiedtke-scheme and described in Doms et al. (2011). Aerosols and trace gases already took part in the vertical redistribution calculations of the convection scheme. We have extended this to include the redistribution of cloud and rain droplet composition as well. There is, however, no additional scavenging and liquid-phase chemistry taking place during this redistribution, as this coupling would be non-trivial and exceed the scope of this work.

3.7 Comparison with other model systems

The extensive review of cloud chemistry and scavenging representations in current regional model systems in Gong et al. (2011) facilitates a comparison of the new coupling with implementations in other modeling systems. Our coupling includes a kinetic description of the transfer processes between gas-phase and droplet and therefore does not assume equilibrium, neither for the transfer into cloud droplets nor into rain droplets. This is expected to be beneficial especially for high-resolution applications where the time-

steps drop below 10 seconds and equilibrium might not be achieved. Only one other model (AURAMS) uses such a physical approach. Nucleation scavenging of aerosols is parametrized by an empirically derived activation curve, which we have coupled with the condensation tendency derived from the microphysics module. This is a more realistic approach than models defining complete modes as activated fraction once a cloud is formed in a grid cell (CMAQ). However, models including a physically based activation scheme (WRF-Chem, GATOR) will be more realistic in their description of this process as they can take into account the size distribution and chemical composition of the aerosols. Impaction scavenging of aerosols in SCAV takes into account both the particle and an estimated droplet size distribution, as the COSMO microphysics scheme is a bulk scheme and cannot deliver a "real" droplet size distribution. We have seen from the review in Gong et al. (2011) that this method is one of the more detailed methods compared to what is implemented in other models, though can be improved with realistic cloud droplet size distributions. The aqueous-phase chemistry mechanism used in this study can be classified (according to Gong et al. (2011)) as a condensed mechanism focusing on sulfur oxidation. However, it is up to the user to choose the level of complexity, as the KPP-based chemistry allows for sufficient flexibility. When choosing the full mechanism as described in Tost et al. (2006) the coupled system can be ranked in the class of "more complete" mechanisms (Gong et al., 2011). The fact that the chemical composition of rain droplets is a prognostic quantity, and that these components can be released back to the atmosphere upon evaporation of the droplets is possible in our approach are to our knowledge unique features.

3.8 Computational demand

Simulations including the new aqueous-phase chemistry model typically double run-times. Profiling analysis showed that this is predominantly due to large load imbalances (SCAV acts only on cloudy grid points) in combination with the added transport load (additional fields for cloud and precipitation concentration for 35 species). Calculations in SCAV itself are only a minor fraction of the computational overhead. We expect speed improvements due to an ongoing project (HP2C, `http://www.hp2c.ch/projects/cosmo-cclm/`) focused on advances in the underlying structure of the COSMO model. Load imbalances are a typical problem associated with chemistry transport models (Elbern, 1997; Wolke et al., 2001) and methods for improvement have already been suggested (Lieber and Wolke, 2008; Sausen, 2010), focusing on (dynamic) restructuring of the domain decomposition. For COSMO-ART this should be done in a manner consistent with a restructuring of the meteorological part - an effort also ongoing within the HP2C project.

3.9 Conclusions

We have coupled COSMO-ART with SCAV, a scheme accounting for wet scavenging of gases and aerosols, and aqueous-phase chemistry. Adaptations had to be made to account for the use of a scheme originally developed for global models in a regional model with grid resolutions in the kilometer range and time-steps in the order of seconds. Tendencies for condensation and evaporation of cloud and rain droplets given in the COSMO microphysics scheme are used to link the scheme with the underlying meteorology. Cloud and rain chemical composition are now transported quantities. Results from a 2D flow-over-hill study show that the conversion of SO_2 to sulfate aerosols is efficient with up to 30 % increase in total sulfate leewards the mountain. Comparison of the results of a realistic simulation with measurements

indicate that SO_2 is efficiently reduced although the reductions are not large enough to reach measured concentrations. Reductions in PM_{10} due to a more efficient scavenging of coarse particles compared to the old wet scavenging scheme for aerosols are substantial and improve the agreement with measurements. The chemical composition of $NR - PM1$ changed substantially, mostly due to a reduction in nitrate components and an increase in sulfate, and now matches observations better. Inclusion of SCAV also resulted in a decrease in total $NR - PM1$ mass, which leads to stronger underestimations with respect to AMS measurements. This is due to a shift of mass from the sub-PM_1 diameter region to the region between PM_1 and $PM_{2.5}$. Deposition amounts are within a factor of 5 compared to measurements for most stations, with a number of station where wet deposition occurs in the model, but is not observed. This is assumed to be an artifact of the comparison of a point measurement against a grid box mean value. The mean wet deposition over all stations shows excellent agreement for nitrate and ammonium. Sulfate wet deposition is underestimated by a factor of 2. Limitations of the coupling have been mentioned which need to be taken into account in case the system is to be applied for different purposes. The implementation lays the groundwork for further studies of cloud processing, aqueous-phase production of secondary organic aerosols and wet deposition with COSMO-ART.

3.10 Acknowledgments

We thank Holger Tost, MPI Mainz, Germany, for his willingness to provide source code and updates for the SCAV module and his kindness in responding to our questions. The Swiss National Science Foundation is acknowledged for partly financing the IPAZIA computational cluster (project 206021_128754). The IPAZIA team is kindly acknowledge for their support.

Chapter 4

Contributions of different emission reductions to changes in aerosol chemical composition in Europe within the last two decades

4.1 Introduction

Substantial reductions in emissions of air pollutant precursors in Europe over the last two decades (Aas et al., 2011) resulted in strongly reduced ambient concentration of SO_2 (Vestreng et al., 2007) and moderate reductions in NO_x (Vestreng et al., 2009). Tropospheric O_3 concentrations did not follow this trend, to the contrary, median concentrations even increased slightly though maxima were indeed reduced (Jonson et al., 2006). The response of particulate matter to the reductions in precursors is even more complex. A number of long-term measurements (wet deposition, gas-aerosol totals, aerosol chemical composition) of inorganic aerosol components show that trends in sulfate closely follow the emission reductions (Putaud et al., 2004; Fagerli and Aas, 2008). For the other major inorganic ions (NO_3^-, NH_4^+) this is not the case. While there are regions where the observed reductions in NO_x emissions are reflected in likewise decreases in nitrate aerosols, reductions in other regions are smaller than the emission reductions or there is no reduction at all. This is a surprising finding, and has already been addressed by a number of authors for different European regions (Fowler et al., 2005; Hůnova et al., 2004; Zimmermann et al., 2003) and for whole Europe in Fagerli and Aas (2008).

Several hypotheses have been proposed to explain this finding: firstly that reductions in sulfate levels are responsible, as available ammonia would first neutralize available sulfate and only afterwards combine with nitrates (Seinfeld and Pandis, 2006). As sulfates have been reduced, more ammonia would be available to neutralize nitrate. A second hypothesis considers the lack of changes in the concentrations of ozone in combination with changes in the fraction of NO_x that is emitted as NO_2 (f_{NO_2}). The increase in f_{NO_2} led to almost constant ambient NO_2 levels since about 2000 despite decreases in total NO_x emissions (Hüglin et al., 2006; Guerreiro et al., 2011). This could lead to an increase in HNO_3 production both during daytime by an increase in NO_2 + OH, and during nighttime, as lower levels of NO lead to less titration

of O_3 and hence to an increase in the heterogeneous HNO_3 pathway via NO_3 and N_2O_5 (Fowler et al., 2005). Finally, although there are long-term measurements for (at a few stations) over 30 years (EMEP wet deposition data), the statistics for the data available might be insufficient to remove the influence of meteorological variability, which might mask trends. All these complex interactions also make it difficult to understand which emission reduction measure had which impact on aerosol characteristics.

In this work we conduct a first exploratory analysis of the non-linear effects of reductions in different precursors on ambient aerosol chemical composition using the online-coupled regional chemistry transport model (COSMO-ART, Vogel et al., 2009) employing full gas-phase chemistry and aerosol processes. Our work builds on the previous efforts of Fagerli and Aas (2008) who investigated trends on an European level, and tried to explain the changes based on relations between measured concentration and emission trends, taking trans-boundary transport into account. Fagerli and Aas (2008) also conducted a sensitivity study to assess the impact of the decreasing SO_2 emissions. We extend these assessments by investigating the contributions of the changes in a number of additional precursor emissions (NO_x, NH_3, NMVOC) and also which effect the changes in the fraction of NO_x emitted as NO_2 (f_{NO_2}) have on ambient aerosol characteristics. f_{NO_2} changed dramatically over the last decades for road traffic sources due to changes in vehicle fleet composition and exhaust after-treatment technologies (Grice et al., 2009).

Within a preliminary sensitivity study, two simulations were made for a winter period of one week, one using emission amounts of 1990, the other emissions of 2009. Both simulations employ the same meteorology (of 2009) to remove the effects of meteorological variability. A winter time frame has been chosen as this season is usually the largest contributor to annual mean particulate matter mass, and it further is a period where the ammonia/nitric acid - ammonium-nitrate equilibrium tends to the aerosol phase. We then conducted additional sensitivity simulations by only applying the changes in emissions observed for selected precursors. In the beginning we present wet deposition amounts, trends and their spatial distribution in Europe for the investigation period as observed within the EMEP measurement network. Then, the effects of the changes in the different precursors are analyzed both in their spatial distribution and as regionally averaged reduction totals which are then compared to changes in emissions and also the changes in measured wet deposition

4.2 Methods

4.2.1 EMEP measurement and emission data

In compliance with the Convention on Long-range Transboundary Air Pollution (CLRTAP) the European Monitoring and Evaluation Programme (EMEP) has been created, wherein European countries were required to measure inter alia the chemical composition of precipitation with a defined and comparable method (Aas et al., 1996). These wet deposition data have been acquired from the EMEP website (`http://www.emep.int`, accessed 10.11.2011). In total 233 stations reported data to EMEP regarding acidification / eutrophication, under which precipitation measurements are accounted for. Out of those, 38 stations reported more than 15 years of data between 1990 and 2009 for the major inorganic ions SO_4^{2-}, NO_3^-, and NH_4^+ (Fig. 4.1). The reported data (in $\mu g/l$) were converted to freights ($\mu g/m^2$) using the precipitation amounts also reported at those stations, and further aggregated to monthly freights.

As well as being required to monitor air pollution levels, European countries also report emission amounts for the major pollutants and its precursors to EMEP. Data on emissions as reported by the parties were

retrieved from the EMEP website (`http://www.ceip.at`, accessed 10.12.2011) for nitrogen oxides (NO_x), sulfur oxides (SO_x) and ammonia (NH_3), which were available for most species and countries since 1990. In the following we always relate SO_x emissions to SO_4^{2-} aerosols / wet deposition, NO_x to NO_3^-, NH_3 to NH_4^+, and volatile organic compounds (VOC) to secondary organic aerosols (SOA).

4.2.2 Modeling system

The model of the Consortium on Small-scale MOdeling (COSMO, http://www.cosmo-model.org, Baldauf et al., 2011) has been extended recently by a treatment of Aerosols and Reactive Trace gases (COSMO-ART, Vogel et al., 2009). It includes a description of gas-phase chemistry as a variant of the second generation Regional Acid Deposition Model (RADM2, Stockwell et al., 1990) which was extended by a more detailed description of isoprene (Geiger et al., 2003) and called RADMKA (Vogel et al., 2009). Aerosols are represented by a modal approach, with 5 log-normal distributions representing fine particulate matter, including an explicit description of soot aging (Riemer et al., 2003a), one mode for coarse anthropogenic primary particles, and description of sea salt and mineral dust (Stanelle et al., 2010) each employing 3 modes. This module is called MADEsoot extended (Vogel et al., 2009) and is based on the Modal Aerosol Dynamics for Europe (MADE Ackermann et al., 1998). Gas-phase and aerosols are coupled through ISORROPIA II (Fountoukis and Nenes, 2007) for thermodynamic equilibrium of inorganic species, and the condensation of organic species using SORGAM (Schell et al., 2001). New particle formation considers homogeneous nucleation of sulfuric acid and water following Kerminen and Wexler (1994). Aqueous-phase chemistry and wet scavenging of gases and aerosols is included using the recently developed coupling to the MESSy submodel SCAV (Chapter 3).

TNO in the Netherlands has developed a comprehensive dataset for anthropogenic emissions in Europe for the years 2003 - 2007 within the European Monitoring Atmospheric Composition and Climate (MACC) project (Visschedijk et al., 2007; Kuenen et al., 2011). Emissions of trace gases (SO_2, NO_x, NMVOC, NH_3, CO, CH_4) and particulate matter ($PM_{2.5}$ and $PM_{10-2.5}$) for 10 emissions categories (Selected Nomenclature for Air Pollutants, SNAP) are available on a grid with horizontal resolution of approx. 8 km (0.00625° x 0.0125°). Daily, weekly and monthly cycles per country and SNAP category allow for a detailed temporal description. The dataset is processed further by a preprocessor developed at Empa (Appendix B) which includes a speciation of NMVOC mass totals onto the surrogate species of the chemical mechanism, a vertical distribution of emissions, a split of particulate matter in chemical components, and a scaling to years outside the range 2003 - 2007. This is accomplished for years before 2003 by deriving scaling factors from per country emission totals as reported to EMEP (e.g. EMEP(1990)/EMEP(2003)). These factors are then used to scale the TNO/MACC emission data for 2003. Note that substantial uncertainties are introduced in the total emission amount, the time functions, and the spatial allocation through this extrapolation. Further, total NO_x is split into NO and NO_2 by a fixed ratio ($f_{NO_2} = 0.1$) for all source categories except traffic, where values for f_{NO_2} are derived from Grice et al. (2009), taking into account the different temporal evolution in the major European countries. Countries not considered in Grice et al. (2009) are assigned the evolution of f_{NO_2} of their geographically nearest neighbor.

4.2.3 Experiment setup

COSMO-ART has been set up with a 0.0125° x 0.0125° grid over the greater European domain (Fig. 4.1) with a rotated north pole at 38.0° N, 171.5° W, resulting in a grid with 300 x 350 points. The model is

discretized in 40 vertical terrain-following hybrid-sigma levels up to 20 hPa. Analyzes of the Integrated Forecasting System (IFS) of the European Centre for Medium-range Weather Forecasts (ECMWF) provide initial and 3 hourly updated lateral boundary conditions for meteorology. Initial conditions for trace gases are given as idealized vertical profiles, and typical (vertically constant) concentrations are used to relax the trace gas concentration fields at the boundaries. Boundary conditions for aerosols are provided as mean vertical profile from a previous COSMO-ART simulation (location marked in Fig. 4.1) as it has been done in Knote et al. (2011).

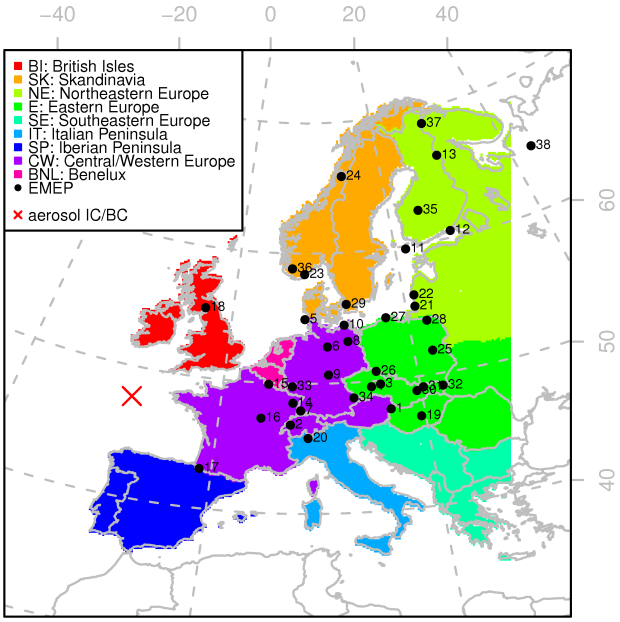

Figure 4.1: COSMO-ART model domain. A red X marks the position of the averaged vertical column that is used for initial and lateral boundary conditions for aerosols. Regions used in evaluation are color coded, see also Table 4.2. A frame of 30 grid points at the domain boundaries is not used as it is influenced by the relaxation against boundary values. EMEP stations used in analysis and their abbreviations (black circles): [1] Illmitz (AT02), [2] Payerne (CH02), [3] Svratouch (CZ01), [4] Kosetice (CZ03), [5] Westerland (DE01), [6] Langenbrügge (DE02), [7] Schauinsland (DE03), [8] Neuglobsow (DE07), [9] Schmücke (DE08), [10] Zingst (DE09), [11] Utö (FI09), [12] Virolahti II (FI17), [13] Oulanka (FI22), [14] Donon (FR08), [15] Revin (FR09), [16] Morvan (FR10), [17] Iraty (FR12), [18] Eskdalemuir (GB02), [19] K-puszta (HU02), [20] Ispra (IT04), [21] Rucava (LV10), [22] Birkenes (NO01), [23] Tustervatn (NO15), [24] Jarczew (PL02), [25] Sniezka (PL03), [26] Leba (PL04), [27] Diabla Gora (PL05), [28] Vavihill (SE11), [29] Chopok (SK02), [30] Stará Lesná (SK04), [31] Starina (SK06), [32] Deuselbach (DE04), [33] Brotjacklriegel (DE05), [34] Ähtäri (FI04), [35] Skreådalen (NO08), [36] Janiskoski (RU01), [37] Pinega (RU13).

The period January 2009 has been chosen for the experiment. The simulation setup for 1990 is identical to the one in 2009, except that different emissions are used. This means that the meteorology of 2009 is used for the 1990 simulation as well, so that we can eliminate the influence of meteorological variability. TNO/MACC emissions have been prepared for both simulation periods, and additionally for several sensitivity simulations: emissions for 1990 serve as basis and only fields for selected precursors are replaced by their respective 2009 counterparts. For the simulation with changing f_{NO_2}, the amount of NO_x equals the 2009 values, but the f_{NO_2} of traffic for 1990 is used. Table 4.1 lists all simulations made.

Table 4.1: Simulations made and abbreviations used. 1990 and 2009 always refer to the simulation time frame in January of these years. Note that Δf_{NO_2} uses 2009 emissions as basis, instead of the remaining sensitivity studies that use emissions of 1990.

Simulation	Description
W09	base simulation, emissions and meteorology of 2009
W90	base simulation, emissions of 1990, meteorology of 2009
ΔSO_2	like W90, but SO_2 emissions of 2009
ΔNO_x	like W90, but NO_x emissions of 2009
ΔNH_3	like W90, but NH_3 emissions of 2009
ΔVOC	like W90, but VOC emissions of 2009
Δf_{NO_2}	like W09, but traffic f_{NO_2} of 1990

4.3 Trend estimation from measurements and reported emissions

A linear trend has been fitted to the monthly aggregated wet deposition measurements at each EMEP station using least squares regression, and a Mann-Kendall test (Mann, 1945; Kendall, 1975) was employed to evaluate whether a statistically significant monotonic trend is observed. Changes in percent mass were then calculated as differences of the predicted values from the least squares regression between 2009 and 1990, relative to the predicted value of 1990. Figures 4.2 and 4.3 show the resulting evolution of yearly wet deposited mass of SO_4^{2-}, NO_3^-, and NH_4^+, and also the associated pH values as measure of the acidity of the precipitation for the stations analyzed. Stations were ranked according to average SO_4^{2-} deposition.

From panel A in Figure 4.2 it is obvious that sulfate mass has decreased substantially at almost all stations. 32 of 36 stations we looked at have a significant negative trend. For 31 this trend is significant on the 99.9% level. Only one station (RU13) shows a (non-significant) upward trend. This indicates that emission reduction measures for SO_2 were successful in reducing sulfate aerosol mass. 24 of 36 stations show a significant upward trend in precipitation pH towards less acidic conditions. A total of 8 stations with a negative trend towards more acidic precipitation are found, of which only 3 are statistically significant (Virolahti II (FI17), Iraty (FR12), and Janiskosi (RU01)).

The evolution of ammonium and nitrate deposition (panels A and B in Figure 4.3) is less clear: at 15 stations the wet deposition of ammonium as well as nitrate decreased significantly, whilst at 2 stations a statistically significant increase is found (ammonium: Eskdalemuir (GB02), and Janiskosi (RU01); nitrates: Revin (FR09), and Pinega (RU13)). Averaged over all stations, the deposition trends 1990 - 2009 for ammonium (-20%) and nitrate (-12%) are less pronounced than for sulfate (-61%). Together with a comparable inter-annual variability of SO_4^{2-}, NO_3^-, and NH_4^+ most probably due to meteorological variability, this leads to a worse signal-to-noise ratio which makes the detection of significant trends for ammonium or nitrate more difficult. Considering that one of the goals of the emission reduction measures in Europe at the end of the last century was to reduce ecosystem damage through acid rain, the trends in pH in panel B of Figure 4.2 together with the reductions in ammonium (panel A in 4.3, see next paragraph) support the statement that the measures were successful, at least in some regions.

Figure 4.4 shows the spatial distribution of measured trends and the corresponding trends in emissions of the main precursor. As expected, sulfur dioxide emissions and sulfate deposition both have a strong negative trend over almost all stations and countries, with the notable exception of Turkey, where emissions

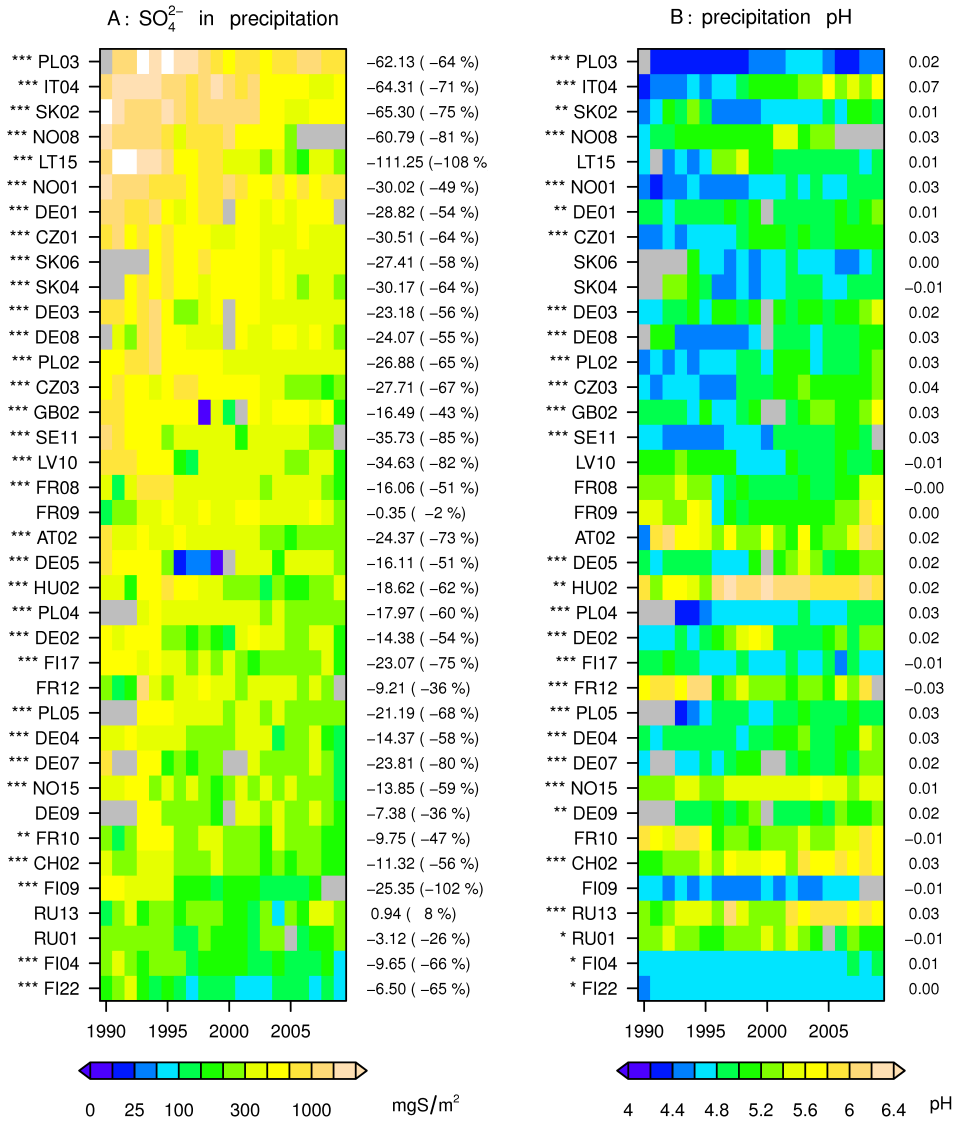

Figure 4.2: Observed yearly wet deposition (1990 - 2009) of SO_4^{2-} (A) and precipitation pH (B) for measurements within the EMEP network. Station abbreviations and statistical significance of the trend (*: 95%, **: 99%, ***: 99.9% level) at the left hand side of each row, mean yearly trends (mg S m^{-2} a^{-1}, pH a^{-1}) and total change between 1990 and 2009 (in % mass of 1990) as derived from least squares regression at the right-hand side of each row. Stations are sorted by mean wet deposition of SO_4^{2-}.

increased within the period investigated. The effects of this increase cannot be determined in this study however, as no measurements within Turkey or the immediate surroundings were available. One station in the center of Europe (Revin (FR09)) shows no significant reduction in sulfate concentrations, an exception we cannot explain so far. Note that the geographical distribution of the measurement stations is heavily biased towards central European and Skandinavian countries.

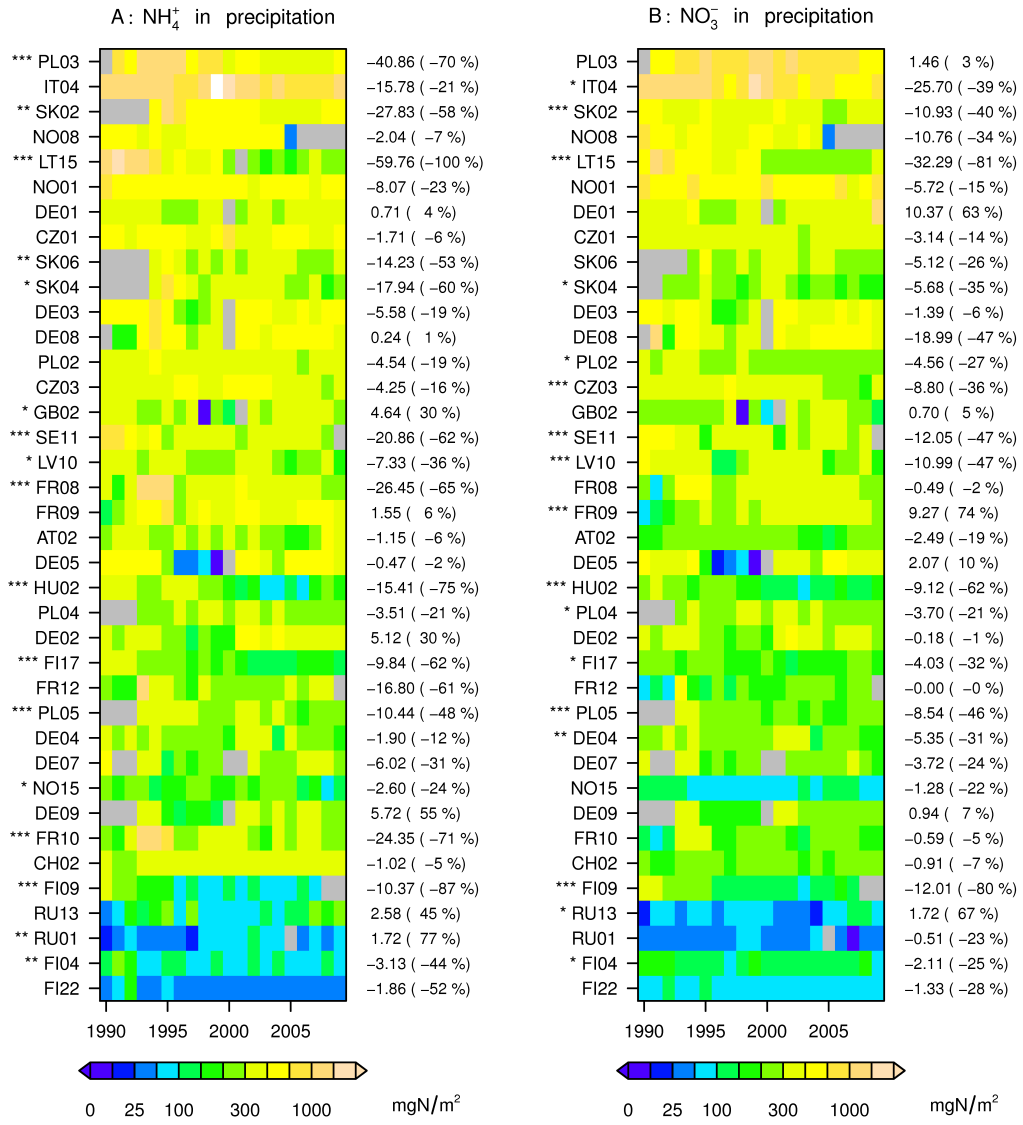

Figure 4.3: Like Figure 4.2, but for observed yearly wet deposition of NH_4^+ (A) and NO_3^- (B). Mean changes per year are mg N m^{-2} a^{-1} here. Stations are sorted by mean wet deposition of SO_4^{2-} (Fig. 4.2).

A surprising West-East gradient in reductions of NH_3 since 1990 is observed, with the highest reported reductions in Eastern European countries. In Western Europe, France and the United Kingdom report decreases as well (in the range of -5 to -25 %), which are however smaller than decreases in the range of 40 to 60 % in central and Eastern European countries. The reaction of ammonium wet deposition is partly consistent with these emission reductions, with a number of stations in Europe showing significant negative trends. There are however notable exceptions, two stations in Germany (Zingst, DE09, and Langenbrügge, DE02) even show increases by 30 and 55 % respectively. The reader should keep in mind that these stations have a large inter-annual variability (panel A in Fig. 4.3) and that their trends are in

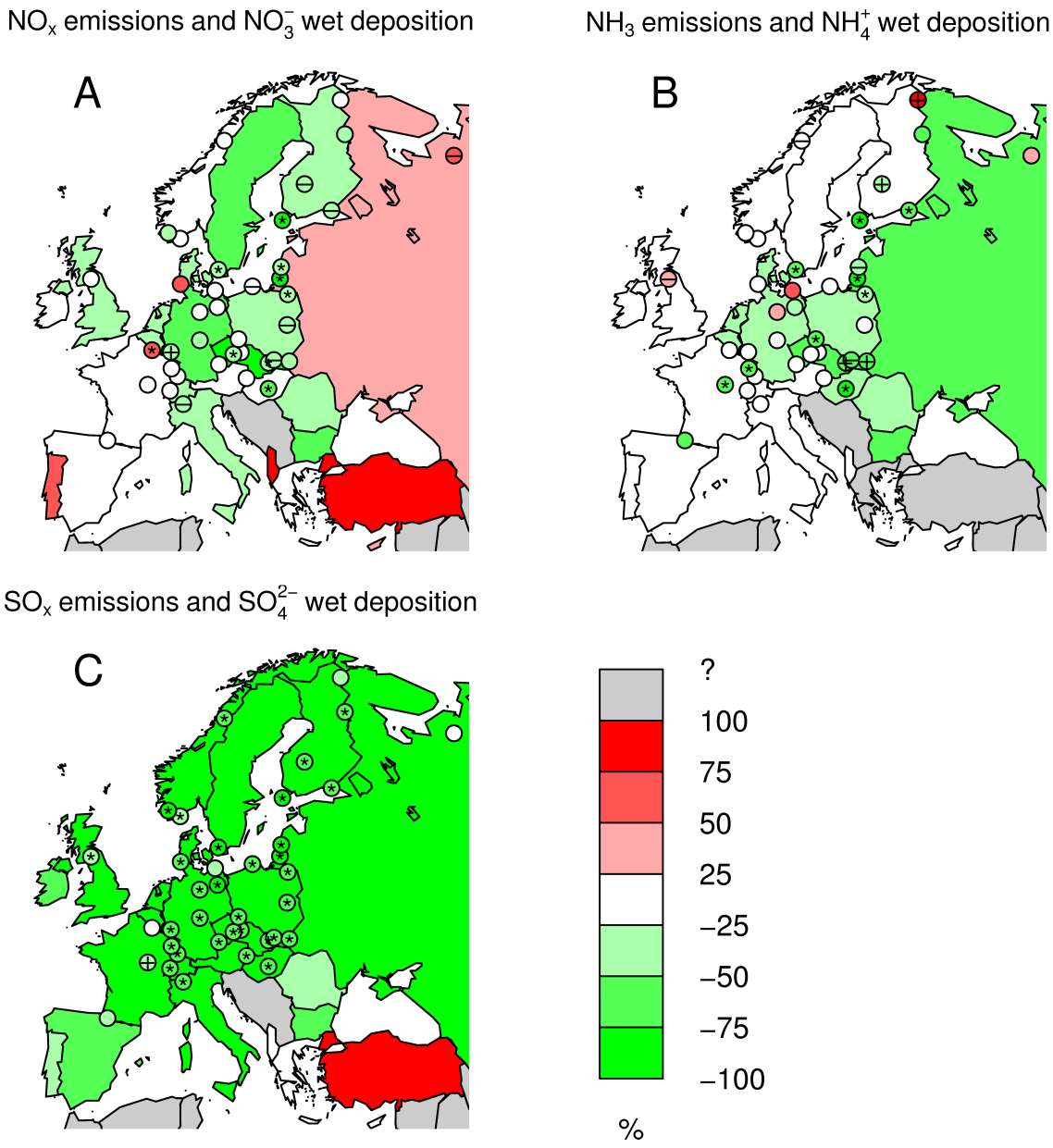

Figure 4.4: Trends in measured wet deposition of the major inorganic ions (filled circles), and trends in emissions of the respective precursors (country color) in Europe between 1990 and 2009 as percent mass differences for: NO_x emissions with NO_3^- wet deposition (A), NH_3 with NH_4^+ (B), and SO_2 with SO_4^{2-} (C). Measured trend estimated as linear regression on monthly aggregated data. Statistical significance of a monotonic trend (Mann-Kendall test, Mann, 1945; Kendall, 1975) marked by stars: significant on the 95% (-), 99% (+), or 99.9% (*) level.

consequence not statistically significant. Only 2 stations report significant upward trends in ammonium deposition: Eskdalemuir (GB02) in the UK, and Janiskoski (RU01) at the border to Norway. Janiskosi reports generally very low deposition amounts, which makes it susceptible to even small increases in

concentration. Whether the increase found is due to stronger long-range transport, additional local emissions or meteorological variability is unknown. Great Britain reported a decrease of -21 % in ammonia emissions. The changes at GB02 can therefore not be explained by a more polluted environment in general, and are more likely due to changes in local sources. The time-series in Fig. 4.3 also reveal a strong variability at this station with a period of very low concentrations between 1995 to 1999 of unknown origin.

Nitrogen oxide emissions are the ones with the least uniform pattern throughout Europe. While strong reductions are reported in Germany (-53 %), Sweden (-51%) and other central European countries, emissions of other countries like Portugal (1.5 %), Russia (-5 %), Norway (-6 %), Austria (-4 %) remained almost unchanged from 1990 to 2009. In the light of these findings, and considering the substantial transboundary transport of air pollutants, a trend in nitrate aerosols as clear as for sulfate aerosols cannot be expected. There are stations where significant reductions are observed. Most of them are found in Eastern Europe, in the Czech republic, Slovakia, Poland and Finland. In central and Western Europe, trends are much smaller, and seldom statistically significant. Revin (FR09) is again at odds with the remaining stations, with a highly significant increase of nitrate wet deposition of 74% between 1990 and 2009. Note here however that 1990 seems to be, relative to the rest of the period investigated, negatively biased (panel B in Fig. 4.3). In several countries with strongly reduced NO_x emissions like Germany or the United Kingdom, nitrate levels have *not* decreased significantly.

In summary we find that sulfate wet deposition closely follows emissions and significant negative trends are found at almost all stations. An interesting West-East gradient in reductions of ammonia emissions is observed. The majority of stations follow the emissions trend, however with notable exceptions. Trends in oxidized nitrogen emissions are non-uniform through Europe during the period investigate, which also results in a non-uniform response of the wet deposition measurements. Several countries with strong emission reductions do not observe associated decreases in nitrate wet deposition.

4.4 Contributions of changes in different precursor emissions to observed trends

In the next section we present the results of the preliminary sensitvity study conducted with the COSMO-ART modeling system. We investigate the contributions of changes in different precursors onto the changes in chemical composition of ambient aerosols in this period. The first part presents the spatial distribution of the changes observed, while the second part focuses on relating simulation results with reported emissions and observations for a number of selected regions within the model domain.

4.4.1 Spatial distribution of trends and contributions

Two simulations have been made using emissions of 1990 and 2009 respectively, and additional 5 sensitivity studies: 4 in which only the changes in emissions of a selected precursor are considered (ΔSO_2, ΔNO_x, ΔVOC, and ΔNH_3), and one to understand the effect of changes in vehicle technology, with traffic f_{NO_2} as proxy (Δf_{NO_2}). Figures 4.5, 4.6, 4.8, and 4.9 show the spatial distribution of the major secondary aerosol mass components (SO_4^{2-}, NO_3^-, NH_4^+, and secondary organic aerosols SOA), and the absolute influence that the changes in emissions had on each component.

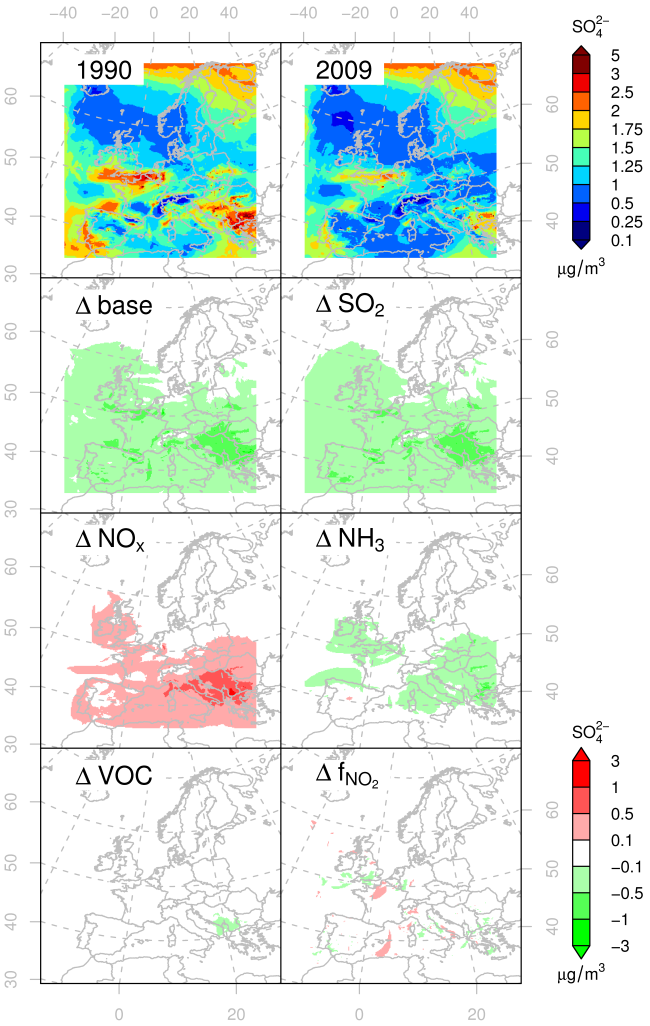

Figure 4.5: Maps of the mean mass concentrations of SO_4^{2-} for the simulation with emissions of 1990 and 2009 (top row), and maps of absolute changes in this component considering all emission changes (Δbase) as well as due to changes in emissions of a single precursor (ΔSO_2, ΔNO_x, ΔNH_3, ΔVOC) and the change in f_{NO_2} (Δf_{NO_2}). Absolute changes are mean concentrations of the respective study minus base case with 1990 emissions (ΔX - 1990), except for Δf_{NO_2}, where the 2009 case is the reference.

Sulfate

Highest concentrations of sulfate aerosols are simulated in the region of the English channel, the Bay of Biscay, southern Portugal / Straight of Gibraltar, and southeastern Europe (Figure 4.5). The high concentrations found at the northern model domain border are an artifact of the treatment of aerosols at the model domain boundaries. Highest absolute changes in the base case where all changes in emissions are considered (Δbase) are found in the regions of highest overall concentrations, and hence mostly in southeastern Europe. The impact of emission reduction measures (or forced reduction due to economic collapse) for sulfur dioxide emissions there is clearly visible and stronger than in Western Europe. Changes in sulfate mass observed in the sensitivity study in which only the changes in SO_2 emissions (ΔSO_2) are considered are almost identical to the base case, showing that the chemistry connecting sulfur dioxide

and sulfate is in this case straightforward. An interesting finding is the response of sulfate to changes in NO_x emissions (ΔNO_x) where increases in sulfate aerosol concentrations are found over southeastern Europe with similar magnitudes as the reductions observed in the other simulations. This might be due to a more efficient in-cloud sulfate formation pathway due to an increase in mean cloud pH and elevated O_3 concentrations as result of the reductions in NO_x. There are regions, again especially in southeastern Europe but also in the English Channel, where the changes in ammonia emissions resulted in substantial decreases of sulfate aerosols (ΔNH_3). Very minor changes in both directions are found due to changes in f_{NO_2} (Δf_{NO_2}) and due to VOCs (ΔVOC).

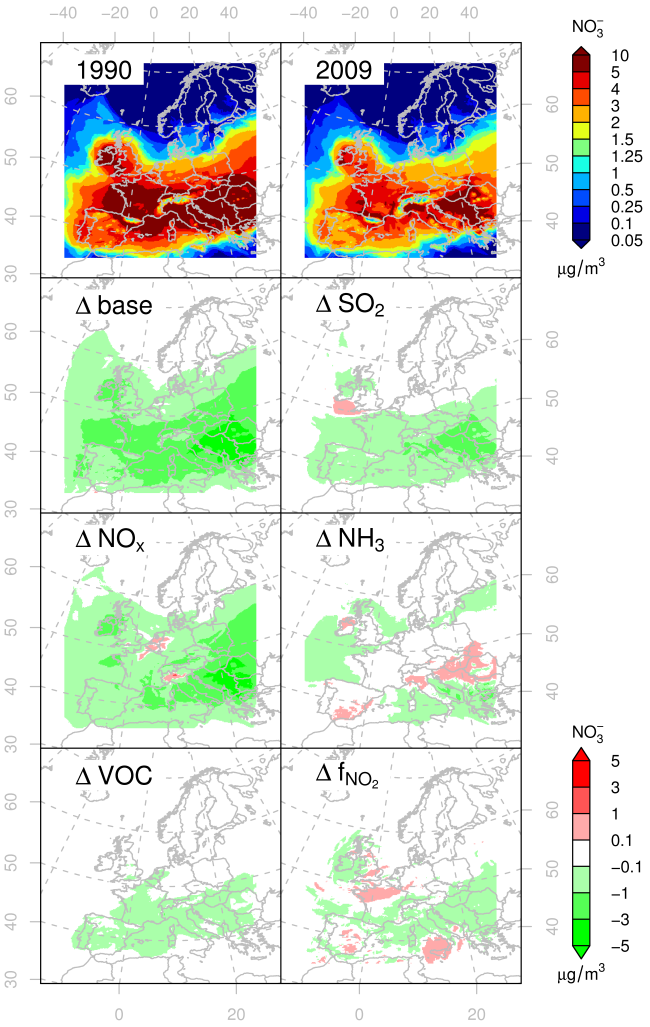

Figure 4.6: Like Figure 4.5, but for NO_3^-

Nitrate

In contrast to sulfate, nitrate aerosols are found to be dispersed over larger areas with less identifiable hot spots (Figure 4.6). Highest concentrations are found (in 1990) over Ireland, France, Italy and southeastern Europe. In 2009, concentrations have reduced in all regions, with the strongest reductions observed in

southeastern European countries (Δbase). Nitrate is found to be sensitive to SO_2 emission changes, with considerable reductions of nitrate over southeastern Europe (ΔSO_2). The mechanism mainly responsible for this sensitivity is found to be the following: HNO_3 is produced at night via heterogeneous hydrolysis of N_2O_5 on aerosol surfaces. The rate constant $k_{N_2O_5}$ for this reaction is parameterized in COSMO-ART (Riemer et al., 2003b) as

$$k_{N_2O_5} = 0.25 \cdot c_{N_2O_5} \cdot S \cdot \gamma_{N_2O_5}, \tag{4.1}$$

with $c_{N_2O_5}$ the mean molecular velocity of N_2O_5, S the aerosol surface density, and $\gamma_{N_2O_5}$ the reaction probability. $\gamma_{N_2O_5}$ was found to vary by orders of magnitude depending on the chemical composition of the aerosol (Riemer et al., 2003b, and references therein). In COSMO-ART it is a function of the nitrate to sulfate ratio and the abundance of organic material (Riemer et al., 2009a). The reductions in sulfate aerosol mass as observed between 1990 and 2009 reduced the aerosol surface density S, and increased the nitrate to sulfate ratio. Both effects decrease $k_{N_2O_5}$, hence the heterogeneous formation of HNO_3, and thereby nitrate aerosol mass. These effects are most pronounced in southeastern European countries as the strongest reductions in aerosol mass (and surface) occured there. Difference plots of aerosol surface density agree with these findings, and an increase in N_2O_5 concentrations in these regions is observed in the model results as well (Fig. 4.7). This increase in N_2O_5 is the result of an unchanged source term combined with a decreased heteorogeneous hydrolysis sink.

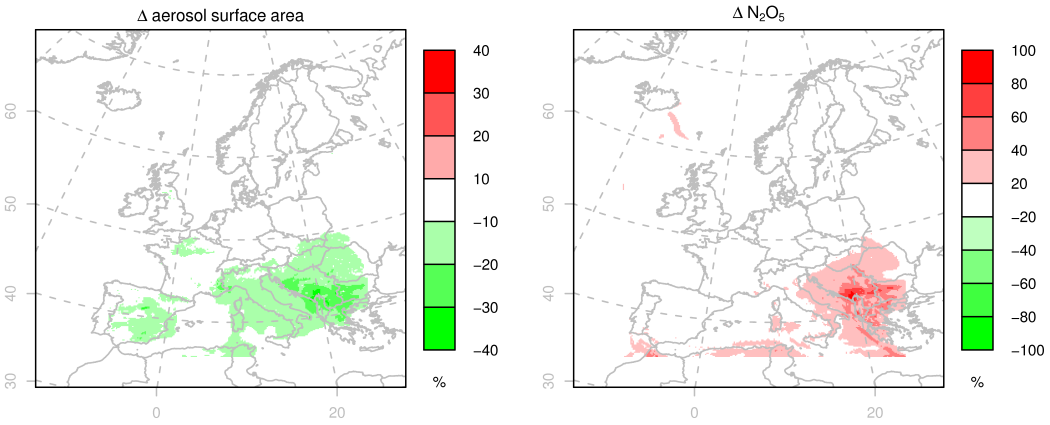

Figure 4.7: Differences in aerosol surface area density (left) and mean N_2O_5 concentration (right) between Δbase and ΔSO_2 in percent.

In contrast to the reaction of sulfate to SO_2 emission changes, the connections between NO_x and nitrate are less straightforward (ΔNO_x). While most of the model domain, and especially Ireland, central and southern Italy and the southeastern European countries, show reductions in nitrate as expected, the strongly polluted, ammonia-rich regions of the Po Basin and the Benelux (Belgium, Netherlands, Luxembourg) countries experience *increases* in nitrate aerosol concentrations although NO_x emissions were greatly reduced in these regions. This is likely the result of an increase in O_3 and OH radicals as a response to lower NO_x in these polluted and hence VOC-limited regions. While also other regions are possibly VOC-limited (e.g. southeastern Europe), no increases in nitrate are observed there. This is found to be due to an overcompensation of the positive effect of an increased oxidation capacity by a strong

total NO_x emissions reduction and hence a lower primary production of HNO_3 precursors. The reaction of nitrate to changes in ammonia emissions is noticeable (ΔNH_3), but smaller in magnitude than for ΔSO_2 or ΔNO_x, and both increases and decreases are observed. Changes in VOC emissions are associated with a decrease in nitrate mass over Portugal, Spain, France, Italy and the southern Balkans, and an increase over northern Italy and the northern Balkans, however again with smaller absolute values than in ΔSO_2 or ΔNO_x. Changes in f_{NO_2} disturbed nitrate with a magnitude of up to 1 $\mu g; m^{-3}$ in both directions, though no clear pattern is observed. The magnitude is comparable with the reaction of nitrate to changes in ammonia or VOC emissions.

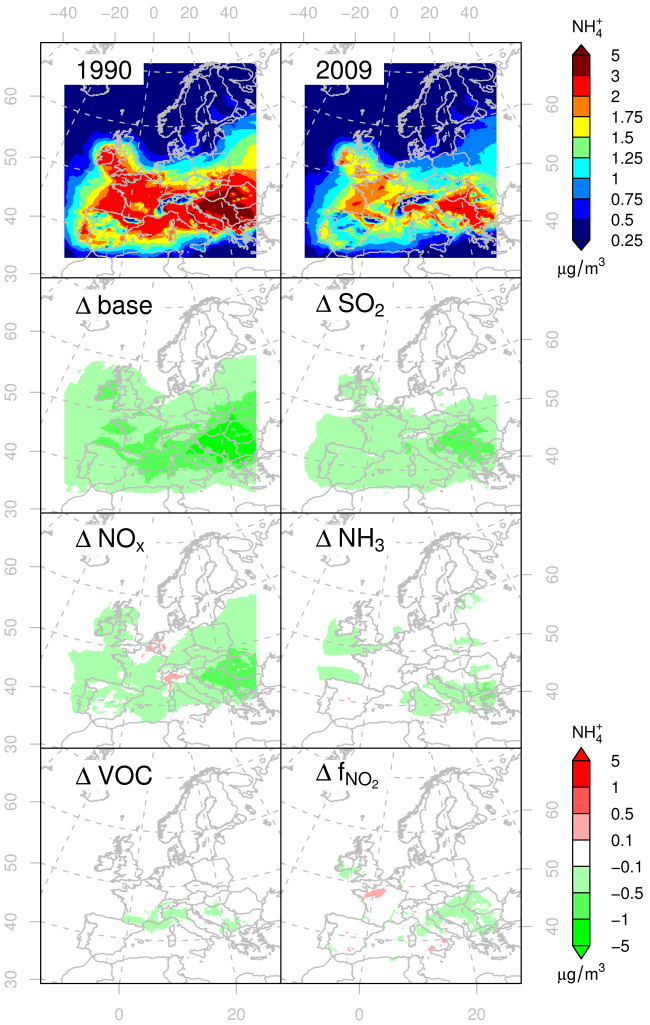

Figure 4.8: Like Figure 4.5, but for NH_4^+

Ammonium

Ammonium in the aerosol phase is the result of a combination with sulfate or nitrate. The observed pattern of ammonium concentrations is similar to the one of nitrates (Figure 4.8). Like for nitrates, large urban agglomerations (Barcelona, Madrid, Rome, and several cities in Romania) are distinct regions

with lower concentrations. Relative to the concentrations in the rest of Europe, lower concentrations are observed over the Iberian Peninsula both in 1990 and 2009 than for nitrate. Ammonium concentrations are sensitive to both changes in SO_2 and NO_x, and also here it is observed that reductions in NO_x actually increase ammonium concentrations over the Po Basin and the Benelux region (ΔNO_x). Changes in VOC had only minor effects on ammonium concentrations (ΔVOC), as had the changes in NH_3 themselves (ΔNH_3). The reader should keep in mind, though, that the evolution in ammonia emissions did not decrease as strongly and uniformly over the European continent as did the emissions of sulfur dioxide, on the contrary the changes were only moderate and not necessarily reductions at all. Hence one should refrain from concluding that NH_3 reductions would be inefficient to reduce ambient aerosol concentrations. Minor changes are observed when the fraction of NO_2 is altered (Δf_{NO_2}), especially in southeastern Europe.

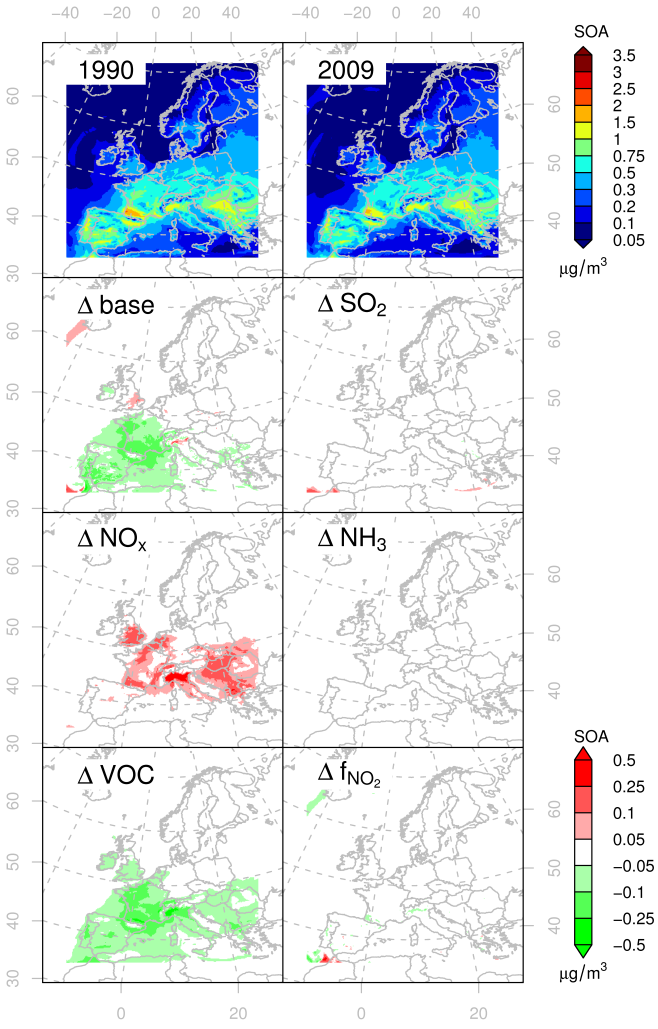

Figure 4.9: Like Figure 4.5, but for SOA

SOA

Simulated secondary organic aerosol mass (SOA) over Europe has its highest concentrations over the southern European regions in the simulations (Figure 4.9). Note that biogenic precursor emissions of SOA are considered, but kept constant between the simulations. The difference plots reveal that strongest reductions are found over France and Spain (Δbase), with distinct increases in concentration in the Po Basin (Italy) and no changes in the rest of the model domain. The sensitivity studies show no sensitivity of SOA to changes in SO_2. NO_x emission changes lead to increases in SOA mass, especially in the polluted Po Basin, but also in parts of northern France and the Benelux regions, and southeastern Europe as well - in summary in all regions where higher SOA concentrations are observed, with the exception of Spain (ΔNO_x). This is again attributed to increases in O_3 and OH concentrations as a result of NO_x reductions in VOC-limited regions. Changes in NH_3 emissions did have no visible effect on SOA concentrations. The reaction of SOA mass to changes in anthropogenic emissions of VOC shows almost the same spatial pattern and absolute reduction amounts as the base case, where all emissions are considered, with the exception of southeastern Europe, where reductions are stronger than in the base case. Also, the increase in SOA mass in the Po Basin is not visible in this case. Hence, the reductions of NO_x were responsible for an increase in SOA mass there, not changes in VOCs. Finally, the changes in f_{NO_2} result in only very small changes in SOA.

In summary, sulfate aerosols are most sensitive to emissions in SO_2 which is expected considering its formation pathways. A surprising response is found to changes in NO_x emissions. Although NO_x emissions were reduced considerably, sulfate mass increases as a response, especially over southeastern Europe. This response is not yet fully understood, but could be associated with the aqueous-phase formation pathway. The observed changes in nitrate aerosols are the result of the changes in NO_x emissions in most regions, except for the Po Basin and the Benelux region. There, NO_x emission changes would have actually led to an increase in nitrate aerosol mass (through changes in OH radical concentrations), which is however offset by the changes in the emissions of the other precursors. The heterogeneous formation pathway of HNO_3, and hence nitrate aerosol mass, was found to be sensitive to changes in SO_2 emissions due to the parameterization used in the model. Whether this effect is realistic could not be assessed. Ammonium mass is sensitive to both nitrate and sulfate changes, which is expected as it is the combination partner for both. An increase of mass in the strongly polluted regions northern Italy and Benelux is also observed for the ΔNO_x case. SOA finally changed only in France and Spain for the period investigated. The potential for reduction in other regions just considering the changes in VOC emissions did exist (ΔVOC), but was offset by the effect of the changes in NO_x.

4.4.2 Quantification of regional trends and contributions

In this section the qualitative changes observed in the last section are quantified and compared to emissions and observations. Therefore, the simulated changes in the different aerosol components are aggregated over a number of regions and percent changes relative to the 1990 level are calculated, as it has been made for the EMEP wet deposition measurements (percent designations in Figures 4.2 and 4.3). Compared are: changes in total emissions of the respective precursor in a region ("emiss." in Figures 4.10a and 4.10b), changes in total wet deposition of all stations in a region ("obs."), and the results from the simulations. The observed trend ("obs.") can be loosely compared with the trend of the Δbase simulation. The model is considered to accurately represent the reality if these are similar, however with the strong caveat that observations are only comprised of a very low number of stations and might therefore be substantially biased. Reported

emissions and observations are both annual and hence allow for a quantitative comparison, while the simulations only cover a week in January and hence can only give hints on important components and processes.

Each region is comprised of a number of countries (Fig. 4.1), listed in Table 4.2. Simulated relative differences are calculated as follows: the simulation period mean total mass $\bar{m}$ in each grid cell $n \in N_r$ of a region r is calculated for each component. Relative differences per region are then given as

$$\Delta_r = \left(\frac{\sum_{n=1}^{N_r} \bar{m}_{n,2009} - \sum_{n=1}^{N_r} \bar{m}_{n,1990}}{\sum_{n=1}^{N_r} \bar{m}_{n,1990}} \right) \cdot 100. \tag{4.2}$$

In the following the results shown in Figures 4.10a and 4.10b are discussed.

Sulfate

The main contribution to sulfate aerosol reductions comes indeed from the reduction in sulfur dioxide emissions. The changes observed in the SO_2 sensitivity study (yellow bars in Figures 4.10a and 4.10b) almost equal the changes found in the base case (red bars). NO_x emission changes (green bars), which are mostly downwards as well, would have actually increased sulfate aerosol mass, mostly in SE and IT. For most regions (BI, E, SE, IT) the changes in ammonia emissions (light blue bars) contributed substantially to sulfate reductions and hence offset the effects of NO_x. Neither VOC changes (dark blue bars) nor the differences in f_{NO_2} (pink bars) influenced sulfate. In general, the simulated changes in sulfate aerosols (-20 to -30 %) are smaller than the reductions in emissions (white bars), and also smaller than the observed reductions in wet deposited mass (gray bars, -40 to -80 %), indicating a lower sensitivity of the simulation to the changes in emissions than observed. From previous evaluation of the modeling system (Knote et al., 2011) it was found that total sulfate mass was underestimated. Although this greatly improved through the introduction of a new wet scavenging and aqueous-phase chemistry scheme (Chapter 3), the model still tends to be biased low rather than high, indicating that sulfate production within the model domain might still be too slow. In consequence, the boundary conditions for sulfate will have stronger influence on sulfate concentrations within the model domain. This influence of long-range transport needs to be

Table 4.2: Regions used in analysis, their abbreviations, and the countries they are comprised of. Figure 4.1 gives a graphical overview.

Region	Abbr.	Countries contained
British Isles	**BI**	Ireland, United Kingdom
Skandinavia	**SK**	Denmark, Sweden and Norway
northeastern Europe	**NE**	Byelarus, Estonia, Finland, Latvia, Lithuania, Russia
Eastern Europe	**E**	Czech Republic, Hungary, Moldova, Poland, Romania, Slovakia, Ukraine
southeastern Europe	**SE**	Albania, Bosnia and Herzegovina, Bulgaria, Croatia, Greece, Kosovo, Macedonia, Montenegro, Serbia, Slovenia
Italian Peninsula	**IT**	Italy
Iberian Peninsula	**SP**	Portugal, Spain
central/Western Europe	**CW**	Austria, France, Germany, Switzerland
Benelux	**BNL**	Belgium, Luxembourg, Netherlands

taken into account when judging these results: lateral boundary conditions for SO_2 as well as for SO_4^{2-} were kept the same over all simulations, and in consequence the influence of changes there is missing in our analysis.

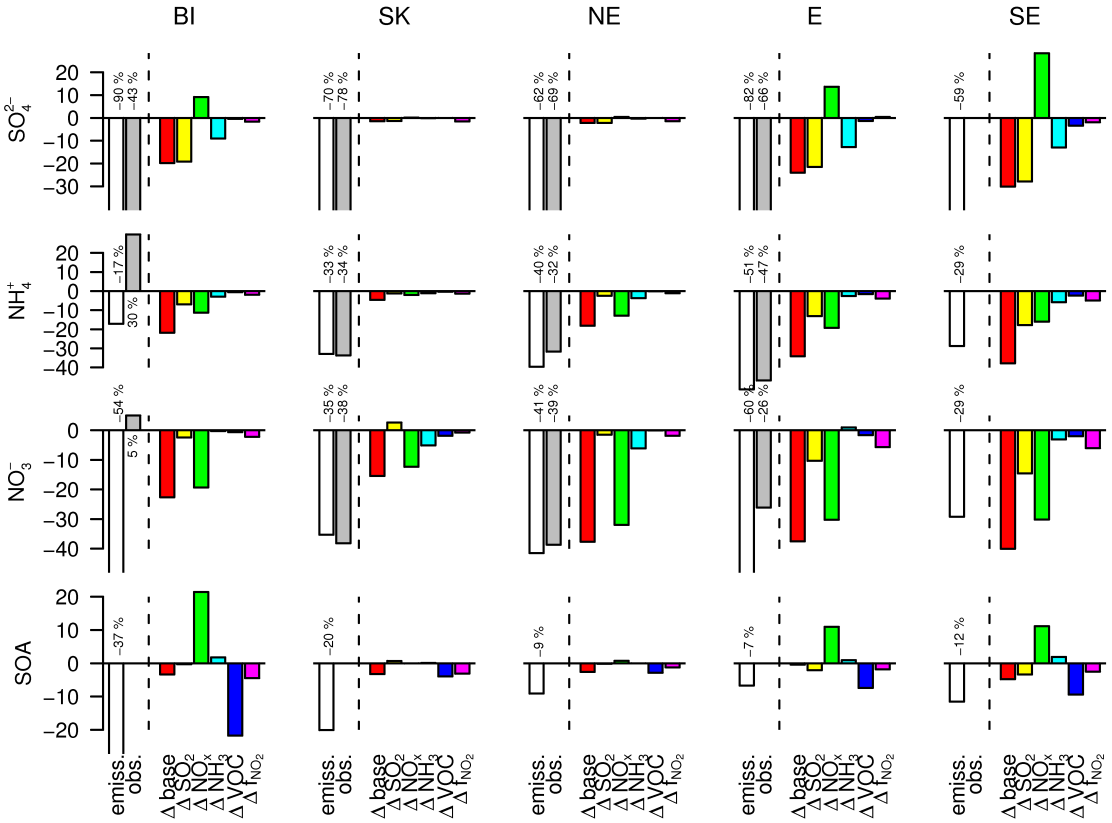

Figure 4.10a: Modeled changes in mass of inorganic (NH_4^+, NO_3^-, SO_4^{2-}) and secondary organic (SOA) aerosol components (colored bars) between January 2009 and January 1990, the changes in annual precursor emissions (leftmost, white bar) and the changes in average annual wet deposition of all EMEP stations in the region if available (second from the left, gray bar) between 2009 and 1990 for all regions shown in Fig. 4.1 and listed in 4.2. All values are given as change in percent (emitted/wet deposited/ambient aerosol) mass of (January) 1990.

Ammonium

Ammonium aerosols are the combination partner for both sulfate and nitrate aerosols components. In consequence, changes in these components also have the strongest influences on ammonium aerosols, with stronger contributions from nitrate in northern and Eastern European regions, while sulfate contributions outweigh nitrates in southern Europe. The influence of ammonia emissions themselves has only a minor influence on changes in ammonium aerosol concentrations. Considering such a case as ammonia-limited (the prerequisite for the hypothesis of sulfates being responsible for the lack of changes in nitrate aerosols) this influence would have to be much stronger. Changes in VOC and f_{NO_2} only have a minor influence on ammonia. Compared with observed changes in ammonium wet deposition, the simulated changes (-5

to -40 %) are well in the range of observed changes (+30 to -50 %). In several regions good agreement of modeled reductions is observed compared with changes in measured wet deposition (NE, E, IT, CW).

Nitrate

From the analysis of changes in nitrate aerosols it becomes clear that also here, emissions of its gaseous precursors have the dominant influence on ambient concentrations in the model. In the BI and CW regions, this is not the case for the observations. The reductions in NO_x emissions are exclusively responsible for the reductions in nitrate aerosols in BI, SK and NE, hence in the northern half of Europe. In central and southern Europe, reductions in SO_2 emissions begin to influence nitrate reductions and eventually reach almost equal share over the Italian Peninsula (IT). While the total reductions of nitrate in the Benelux (BNL) region were rather small (-10 %), its biggest contributor was changes in VOC rather than either SO_2 or NO_x emissions. Compared to measurements of wet deposition, we find reasonable agreement in several regions (NE, E, IT) and the overall range (modeled -10 to -40 %, measured +5 to -40 %) is similar.

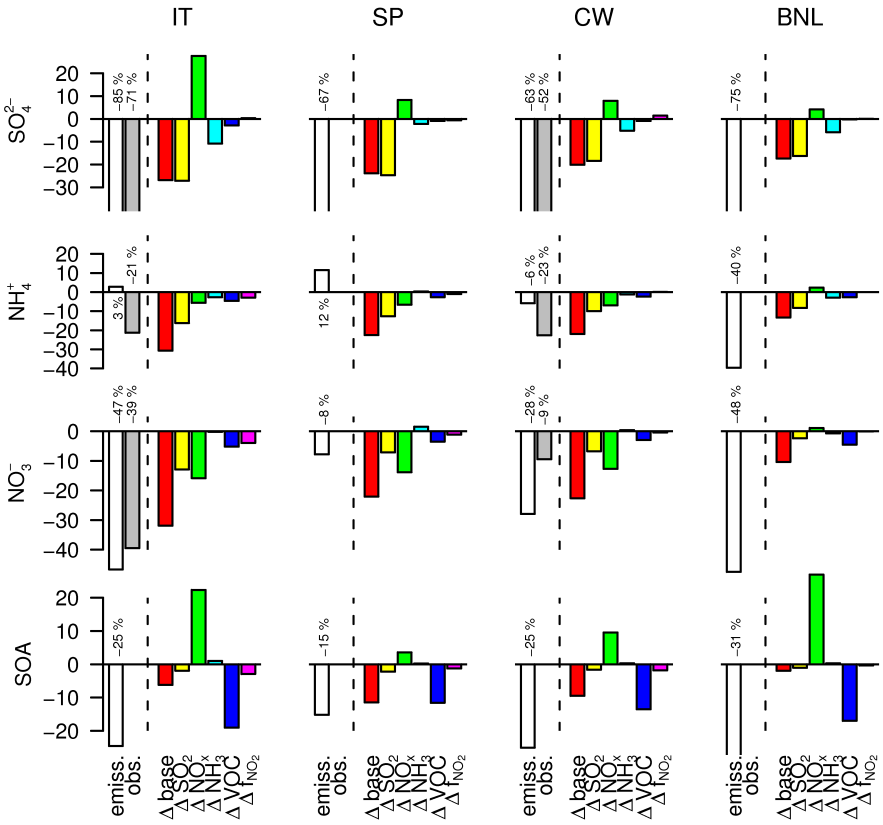

Figure 4.10b: Like Fig. 4.10a, but for the remaining regions.

SOA

Changes in only two components showed an influence on SOA concentrations, with opposite direction: changes in emissions of volatile organic compounds strongly reduced SOA concentrations in the BI, IT,

CW and BNL regions. In each of these regions, the changes in NO_x, being substantial reductions there, lead to an increase in SOA concentrations. This can again be attributed to the effect of decreasing NO_x levels on a polluted, VOC-limited region: the concentration of OH radicals increases which accelerates SOA generation. From the comparison with the total changes in SOA concentrations in these regions it can be seen that these effects cancel out each other in the simulation with all emission changes considered (Δbase): BI, E, and BNL see no change in SOA in the base simulation, while substantial changes would be found if only NO_x or VOC emissions are considered.

4.5 Conclusions

A statistical analysis of the trends and their spatial variability of annual wet deposition of the major inorganic ions found in ambient aerosols was conducted for the years 1990 to 2009, based on data from the EMEP network. The results were compared with the changes in emissions of the gaseous precursors of these aerosol components as reported to EMEP by the European countries.

Sulfate wet deposition was found to have decreased considerably and in accordance with the respective emission reductions. The picture was less clear for nitrate and ammonium aerosols. Only about half of the stations investigated showed a significant downwards trend, whilst some stations even found a (significant) increase in concentrations. Overall smaller trends in nitrate and ammonium associated with an inter-annual variability comparable to that of sulfate do not allow to derive statistically significant downwards trends as convincing as for sulfates. The more heterogeneous development of the precursor emissions for nitrates is considered to have contributed substantially to these findings. Mostly upward precipitation pH trends together with ammonia reductions showed that the environmental issue of acid rain could be efficiently tackled by the emission reduction measures at most stations.

A preliminary modeling study was conducted for a winter period to investigate the effects of the changes in emissions of selected precursors on aerosol composition. It was found that reductions in SO_2 were responsible for the reductions in sulfate aerosols observed. Nitrate aerosol mass decreased almost exclusively due to changes in NO_x emissions in northern and Eastern Europe, while in southern Europe reductions in SO_2 (and hence sulfate) contributed up to an equal share to the total reductions. This was found to be due to the parameterization of the heterogeneous formation pathway of HNO_3. Ammonium reductions observed are primarily the result of the changes in sulfates and nitrates. Changes in emissions of ammonia had only a minor effect on NH_4^+ aerosol mass, mostly due to the fact that these emission changes were relatively small. Secondary organic aerosols were mostly influenced by changes in emissions of VOC. Visible changes (reductions) were only observed over France and Spain. It was found that the changes in NO_x emissions played a key role in this period: their reductions led to considerable increases in the mass of the other aerosol components in very polluted regions (Benelux, Po Basin). The VOC-limited regime there reacts to a decrease in NO_x with an increase in OH radicals, which in turn increases the production of nitrate, sulfate and SOA components. The changes in the fraction of NO_x emitted as NO_2 showed in general less influence on aerosol concentrations in the period investigated than the other changes. For nitrate aerosols the changes due to f_{NO_2} however reached up to 5 % mass.

What do the results implicate regarding the hypotheses presented in the introduction? In the first hypothesis it is proposed that nitrate aerosol mass does not follow NO_x emission reduction trends as decreases in SO_2 emissions lead to excess nitric acid replacing sulfate as combination partner for ammonia. This hypothesis however is only valid if ammonia would be limiting, which is most probably not true for most

of the European continent considering the extent of agricultural (manure) activity in large parts of Europe (being the largest single source of ammonia emissions). Non-zero concentrations of ammonia are measured and modelled throughout the year, which contradict an ammonia-limitation. The results of the preliminary model study also support this finding, where only in a very limited region west of the British Isles an increase in nitrate aerosol mass can be observed when only SO_2 emissions are reduced. Hence we consider this hypothesis very unlikely due to the lack of ammonia limitation.

The second hypothesis considered changes in NO_x emissions and the associated increases in O_3 and the fraction of NO_2 emitted. The model study results show that NO_x emission reductions lead to an increase in the oxidative capacity of the atmosphere over VOC-limited regions and an increase in O_3 concentrations, which in turn increase the production of nitrate and secondary organic aerosols. In regions with strong absolute reductions in NO_x emission in Eastern Europe these processes can be overcompensated and decreases in nitrate aerosols are indeed observed. We therefore conclude that the effects of changes in NO_x emissions on the oxidative capacity of the atmosphere are indeed substantial and counteract decreasing trends due to total reduction in precursors. Changes in the fraction of NO_2 emitted could be shown to have only a minor effect on the atmospheric oxidative capacity, and cannot be considered substantial for the observed changes in nitrate aerosol mass according to our preliminary model study. Our findings therefore at least qualitatively support the hypothesis that increases in O_3 levels due to decreases in NO_x emissions are in part responsible for the lack of reductions in nitrate aerosol mass in the winter period investigated.

The third hypothesis stated that meteorological variability might mask existing trends. This study had not been designed to explicitly evaluate the meteorological influence, therefore only indirect evidence can be considered. Analysis of observed wet deposition found considerable interannual variability at all stations, similar in magnitude for all components, which can be attributed to a large extent to meteorology. As trends in nitrate and ammonium were found to be smaller than for sulfate in the period investigated, this results in a worse signal-to-noise ratio and could indeed point to an at least partial masking of trends in nitrate and ammonium by meteorology, as this leads to a lack of statistical significance of trends in nitrate and ammonium. A quantification of this effect is out of scope of this work.

4.6 Acknowledgments

The Swiss National Science Foundation is acknowledged for partly financing the IPAZIA computational cluster (project 206021_128754). The IPAZIA team is kindly acknowledged for their support.

Chapter 5

Summary and outlook

5.1 Summary

In this thesis the effects of changing anthropogenic emissions on aerosol characteristics are investigated by means of comprehensive regional numerical modeling of emissions, transport, conversion and removal of aerosols and trace gases in the atmosphere. A major part of the work was dedicated to the set up and improvement of a modeling system able to represent all processes necessary for an accurate description of ambient aerosols. In a first effort it was necessary to investigate the capability of the model to represent aerosols and trace gases under current conditions. A model evaluation study was conducted to show the performance of the model in all seasons for the domain of Europe when compared to a number of surface and satellite datasets. Both, the accuracy of the representation of trace gases as well as aerosol characteristics have been analyzed. It could be shown that the model is able to represent the main gaseous air pollutants with very good accuracy, and also for total aerosol mass and number concentrations reasonable agreement was found. Comparison with aerosol chemical composition data from a recent large field campaign revealed a tendency to overestimate nitrate components and underestimate sulfate. In the second part of this thesis the model system was extended by a treatment of wet scavenging of gases and aerosols, and a description of aqueous-phase chemistry within cloud and rain droplets. The deficiencies found in the evaluation of the original modeling system were supposed to be caused by a lack of these processes. For the coupling to the aqueous-phase chemistry module the focus was laid on a flexible method on the one hand, that allowed to facilitate the inclusion of additional species or aqueous-phase reactions, and on the other hand on a consistent coupling to the existing cloud microphysics module in the meteorological driver. The results of both idealized 2D and realistic 3D simulations with the new system showed that, as expected, sulfate mass increased due to aqueous-phase oxidation, and nitrate mass decreased due to strong washout of its gaseous precursor nitric acid. Aerosol processing of clouds had considerable influence on the mass concentration size distribution of the simulated aerosols, with a clearly visible shift of mass concentrations towards larger diameters. This was expected from theory and could be confirmed. Wet deposition as main removal process in the atmosphere was compared to measurements with reasonable agreement. The improved model system was then used in an analysis of the changes in aerosol composition over the last two decades in Europe for a selected winter period, and sensitivity studies were conducted to assess the influence changes in selected gaseous precursor emissions had on aerosols. While it was found that the reductions in sulfate observed are clearly linked to reductions in the emissions of sulfur dioxide, the changes in nitrate aerosols had a more complex background. Both,

reductions in nitrogen oxide and sulfur dioxide emissions influenced the reductions simulated. Ammonium components were sensitive to reductions of nitrogen oxides and sulfur dioxide as well, surprisingly however not to the changes in ammonia emissions. This indicates that the explanation of reductions in sulfate being solely responsible for the lack of changes in nitrates is not valid. A surprising finding was the role of nitrogen oxide emission reductions on the aerosol in heavily polluted regions like the Po basin in Italy or the Benelux (Belgium, Netherlands, Luxembourg) area: decreases of nitrogen oxides in these regions lead to an increase in aerosol mass of almost all components during the winter period investigated. An increase in oxidant concentrations associated with such a reduction in VOC-limited regions is suggested to be responsible, which increases secondary aerosol formation.

5.2 Future work

The next steps to continue the work presented are primarily focused on the extension of the analysis presented in Chapter 4 which is so far limited to an investigation of a single period in winter. This study can be extended in three ways which will lead to improvements in the reliability of the results, their validity for various meteorological conditions and the accuracy of the trends derived from measurements: firstly, the length of the simulation period can be extended. Simulations with COSMO-ART are computationally expensive, and especially for sensitivity studies with several parameters this is often a limiting factor. A time frame of 2 - 4 weeks however is a realistic value, and would improve the statistics for the calculation of simulated trends. Further, only a winter period was chosen for the analysis, which will have to be extended at least by a simulation during summer. The considerably different meteorological conditions will have important effects on tropospheric chemistry and aerosols which cannot be extrapolated from the results of the simulations during wintertime. Finally, the analysis of the measurement data presented can be improved and more information can be derived from the dataset. In the presented study only a rather simple linear regression was used to estimate trend and their significance. This should not de-emphasize the advantages of a simple method, but more sophisticated statistical methods would allow for example to remove meteorological variability also from the measured values, and hence allow for a more direct comparison with the simulated results. A proposed method would be to use a generalized additive model (GAM, Hastie and Tibshirani, 1990), which has already been used by a number of authors to investigate trends in ozone (Pearce et al., 2010), particulate matter (Barmpadimos et al., 2011) or NO_2 from satellite data (Hayn et al., 2009; Zhou et al., 2011). Thereby, the influences of meteorology could be quantified and removed, resulting in more reliable trend estimation.

Appendix A

Supplement to 'Towards an online-coupled regional chemistry climate model: evaluation of trace gases and aerosols in COSMO-ART' (Chapter 2)

Published in Geoscientific Model Development, 4, 1077-1102, 2011

Authors: Christoph Knote[1,2], Dominik Brunner[1,2], Heike Vogel[3], James Allan[4], Ari Asmi[5], Mikko Äijälä[5], Samara Carbone[6], Hugo Denier van der Gon[7], Jose L. Jimenez[8], Astrid Kiendler-Scharr[9], Claudia Mohr[10], Laurent Poulain[11], André S. H. Prévôt[10], Erik Swietlicki[12], and Bernhard Vogel[3]

[1] Laboratory for Air Pollution / Env. Technology, Empa Materials and Science, 8600 Duebendorf, Switzerland
[2] C_2SM Center for Climate Systems Modeling, ETH, Zurich, Switzerland
[3] Institute for Meteorology and Climate Research, Karlsruhe Institute of Technology, Karlsruhe, Germany
[4] School of Earth Atmospheric, and Environmental Sciences, National Centre for Atmospheric Science, University of Manchester, Manchester, UK
[5] Department of Physics, University of Helsinki, Helsinki, Finland
[6] Air Quality Research, Finnish Meteorological Institute, Helsinki, Finland
[7] TNO Princetonlaan 6, 3584 CB Utrecht, The Netherlands
[8] CIRES and Dept. of Chemistry and Biochemistry, Univ. of Colorado, Boulder, CO, USA
[9] Institut IEK-8, Troposphäre, Forschungszentrum Jülich, Jülich, Germany
[10] Laboratory of Atmospheric Chemistry, Paul Scherrer Institute, Villigen, Switzerland
[11] Leibniz Institute for Tropospheric Research, Leipzig, Germany
[12] Division of Nuclear Physics, Department of Physics, Lund University, Lund, Sweden

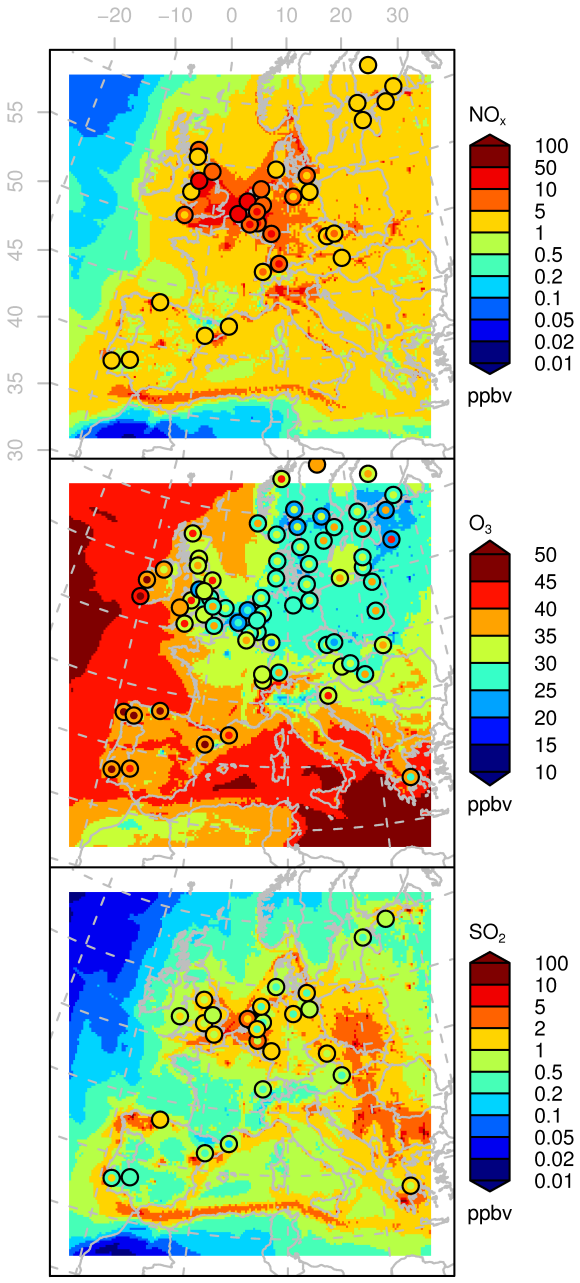

Figure A.1: Overview of mean afternoon (hours 12 - 18) NO_x, O_3 and SO_2 concentrations like in Figure 2.4 but for the spring 2009 period.

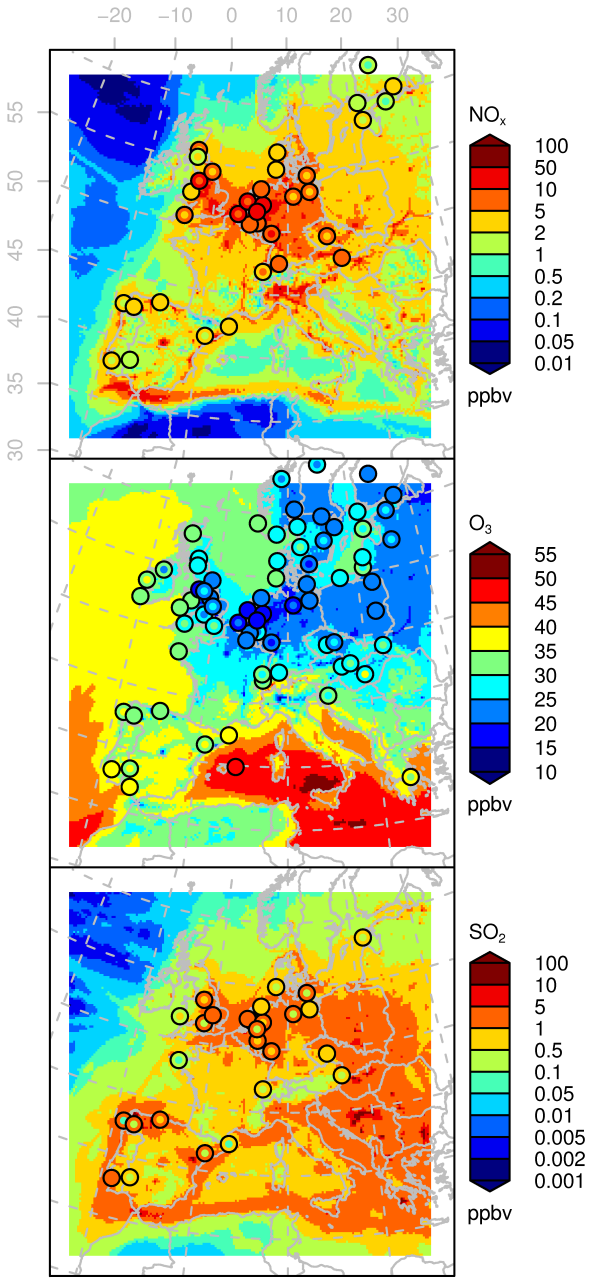

Figure A.2: Overview of mean afternoon (hours 12 - 18) NO_x, O_3 and SO_2 concentrations like in Figure 2.4 but for the autumn 2008 period.

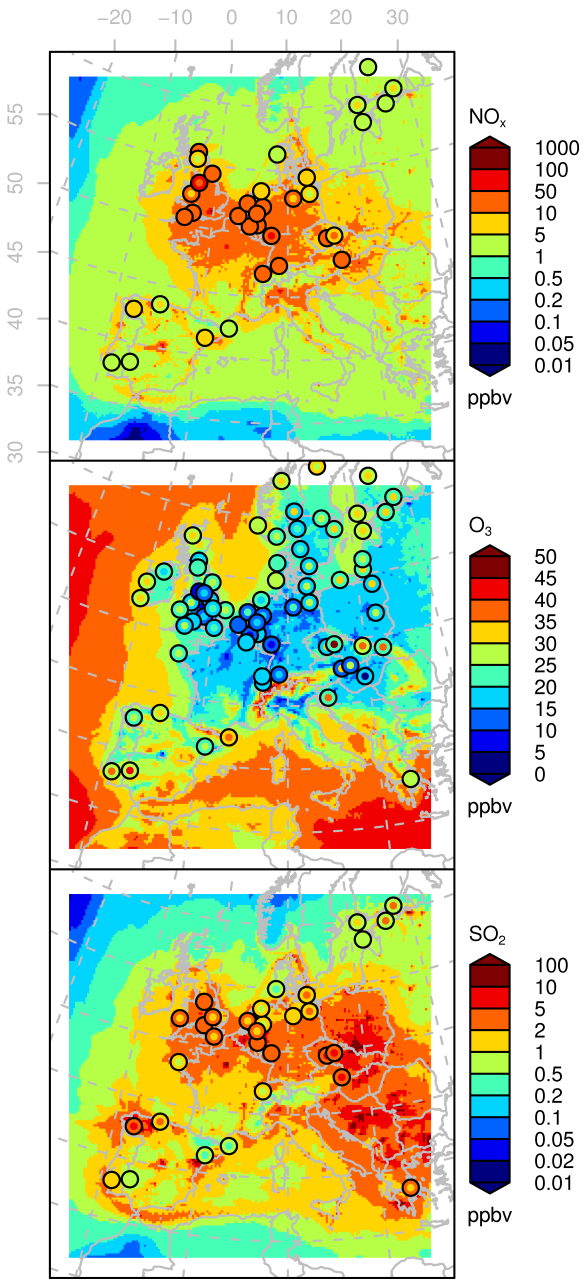

Figure A.3: Overview of mean afternoon (hours 12 - 18) NO_x, O_3 and SO_2 concentrations like in Figure 2.4 but for the winter 2006 period.

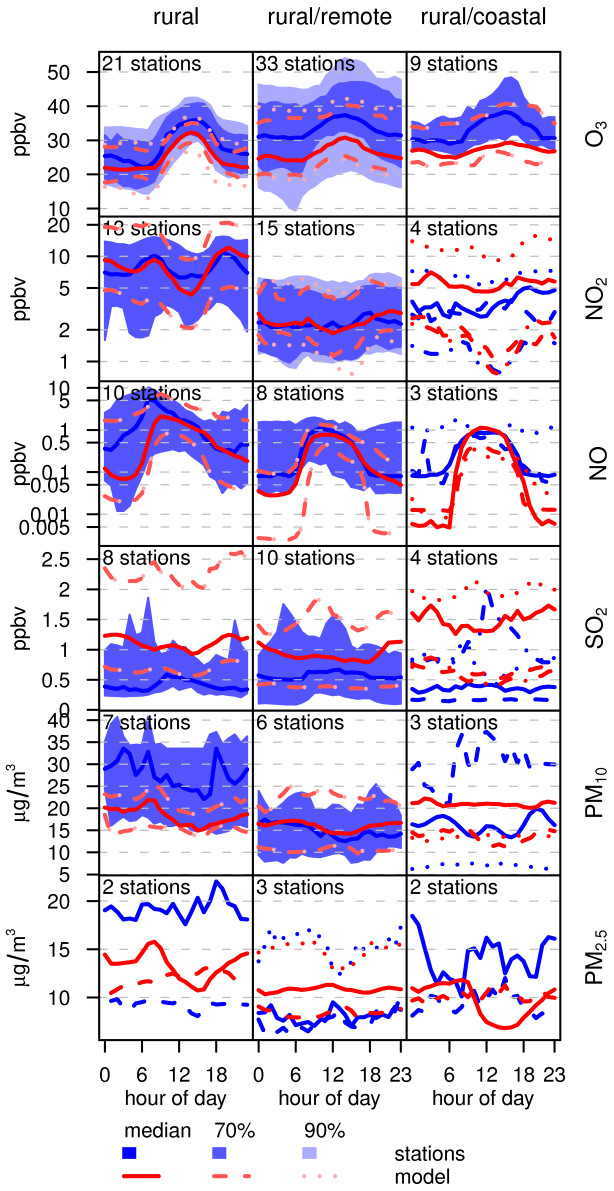

Figure A.4: Statistics of mean diurnal cycles of several compounds for model and AIRBASE data. Like Figure 2.5 but for the spring 2009 period.

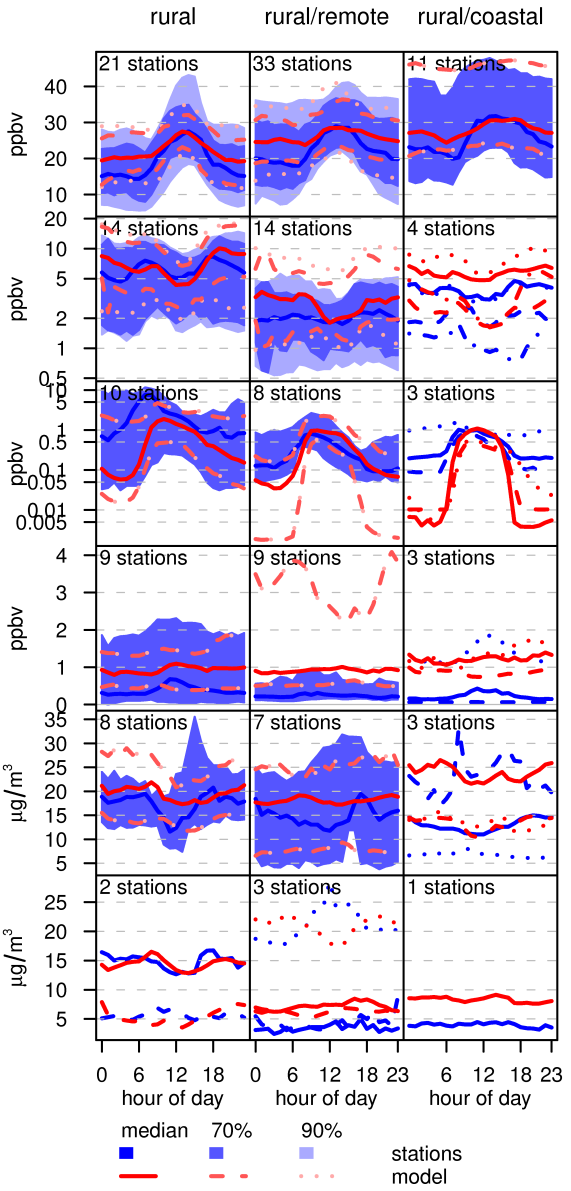

Figure A.5: Statistics of mean diurnal cycles of several compounds for model and AIRBASE data. Like Figure 2.5 but for the autumn 2008 period.

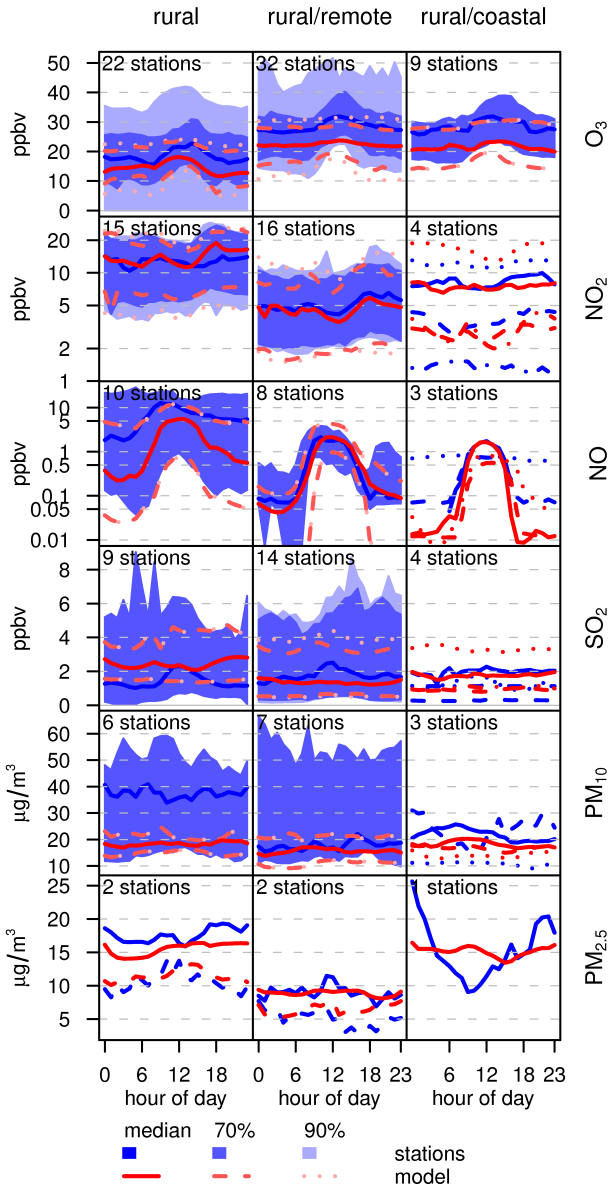

Figure A.6: Statistics of mean diurnal cycles of several compounds for model and AIRBASE data. Like Figure 2.5 but for the winter 2006 period.

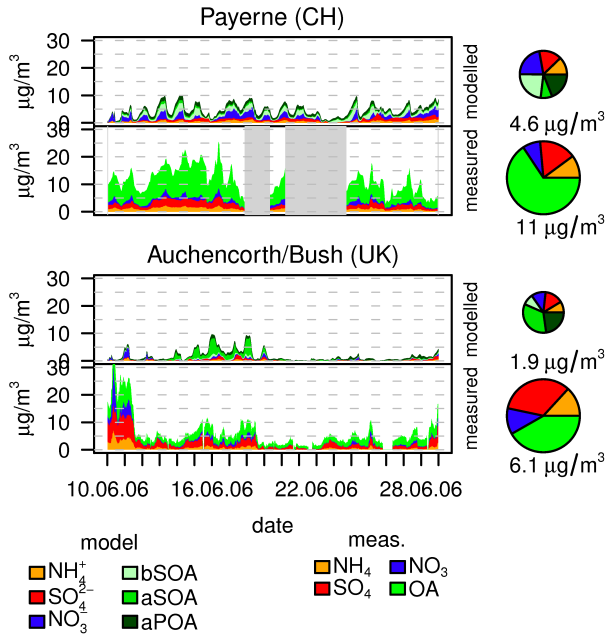

Figure A.8: Timeline of aerosol chemical composition. Like Figures 2.9 and 2.10a, 2.10a but for the summer 2006 period.

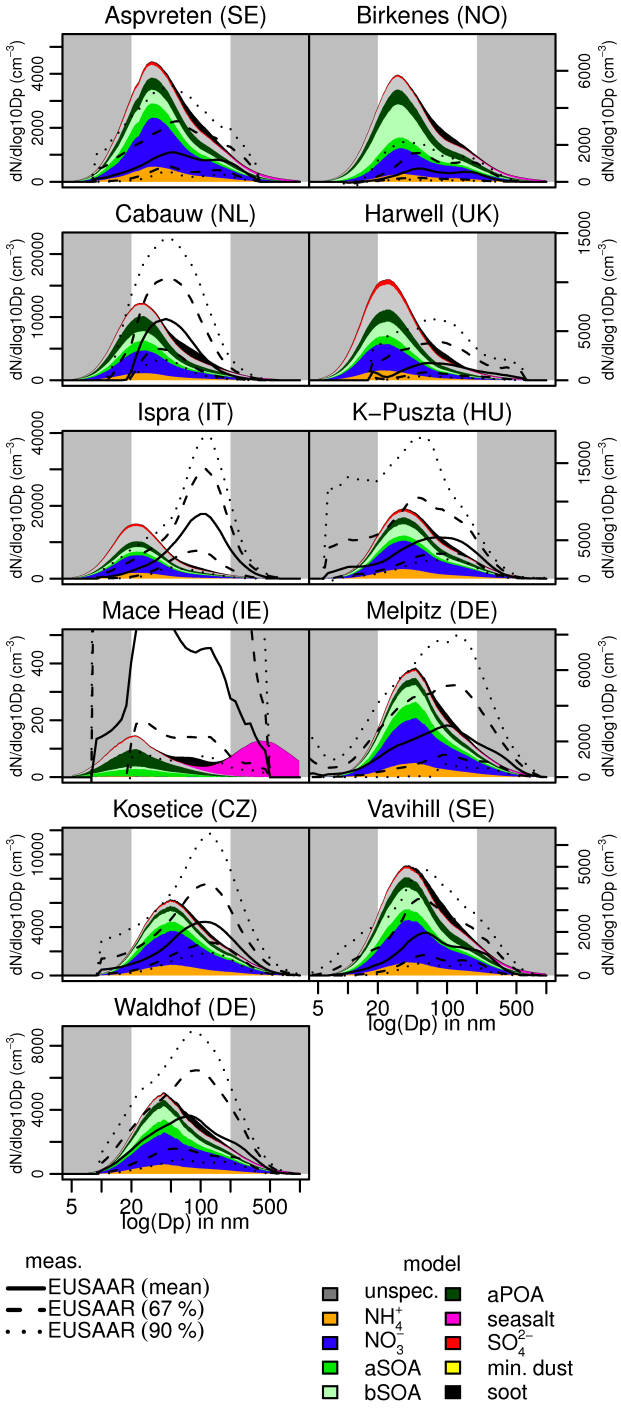

Figure A.9: Comparison of modelled and measured aerosol size distributions at EUSAAR stations. Like Figure 2.11 but for the spring 2009 period.

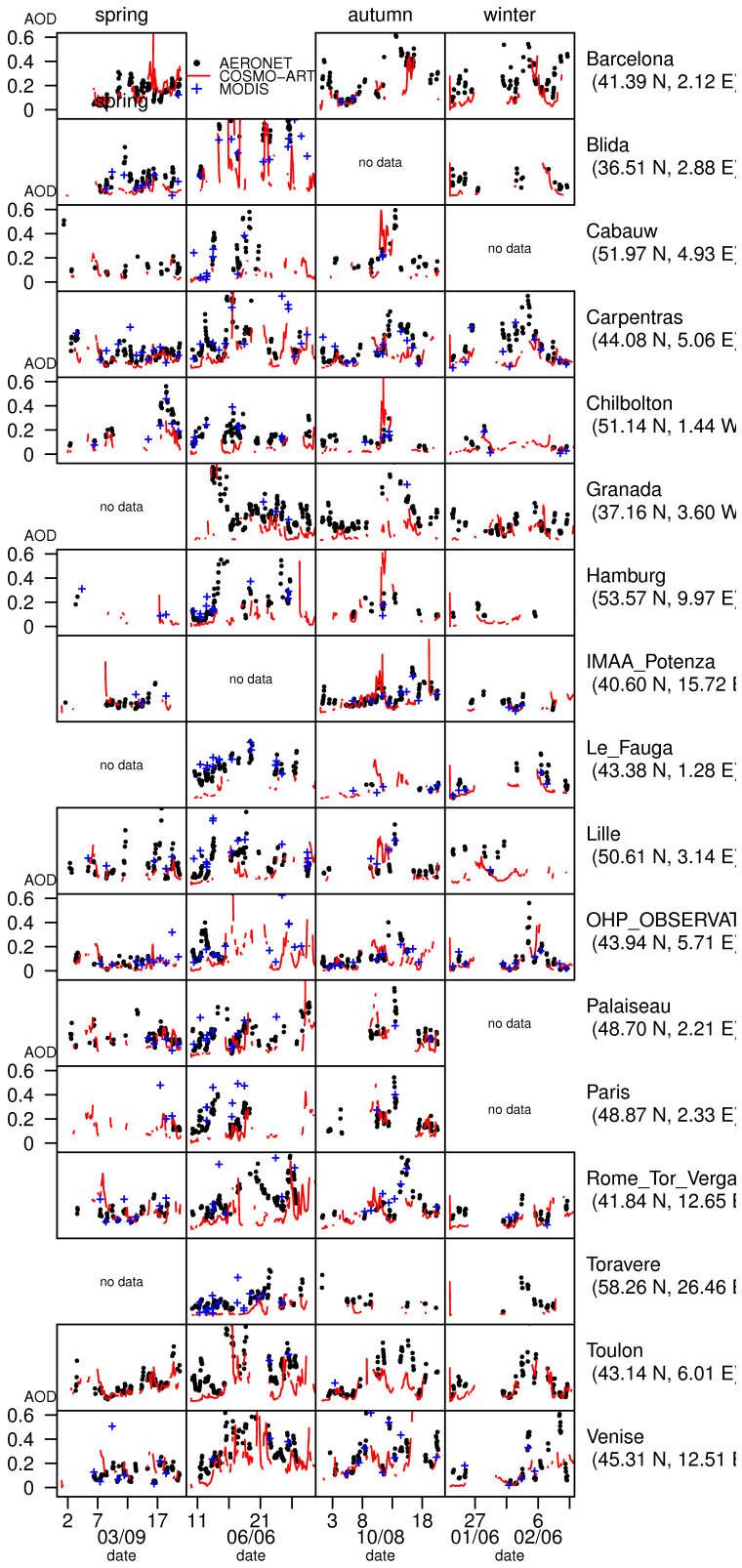

Figure A.7: Timelines of aerosol optical depth (AOD) at several AERONET stations in Europe. Like Figure 2.8 but for the remaining stations.

Appendix B

Emissions preprocessor documentation

B.1 Introduction

The scope of this document is to describe the processing steps taken to prepare the gridded emission data created by TNO (Netherlands) within the European Monitoring Atmospheric Composition and Climate (MACC) project (TNO/MACC, Denier van der Gon et al., 2010; Kuenen et al., 2011) for use in the regional chemistry transport model COSMO-ART (Vogel et al., 2009). The main parts are the speciation of organic precursor gases (NMVOCs) into model surrogates, disaggregation of total particulate matter into chemical components used in the model, application of a fractional distribution of total nitrogen oxides onto NO and NO_2 (f_{NO_2}), vertical distribution of the emission data and scaling to years different from the years the inventory has been created for.

B.2 Description of input data

The TNO/MACC data is delivered in two parts: firstly a spatial representation of the annual total of emissions of several gaseous and particulate compounds on a regular 0.125° x 0.0625° (about 8 km) grid covering the domain of Europe is provided for the years 2003 to 2007. Available are data for methane (CH_4), carbon monoxide (CO), ammonia (NH_3), non-methane volatile organic compounds (NMVOC), nitrogen oxides (NO_x), sulfur dioxide (SO_2), particulate matter mass of particles below 10 μm in diameter (PM_{10}) and below 2.5 μm ($PM_{2.5}$). The emission totals are subdivided into 10 source categories according to the Selected Nomenclature for Atmospheric Pollutants (SNAP) level 1 scheme (EMEP/CORINAIR, 2001). Covered are anthropogenic emission sources including an inventory of international shipping emissions. For road transport, additional subcategories for gasoline (7.1), diesel (7.2) and LPG powered vehicles (7.3) as well as volatilization (7.4) and road, brake and tire wear (7.5) emission estimates are available. Secondly, time functions for the calculation of emissions for a certain date and time are given in the form of daily, weekly and monthly cycles for each country and SNAP category for most species.

The data are delivered in ASCII text format.

B.3 Description of the modeling system

The model of the Consortium on Small-Scale MOdeling (COSMO, Baldauf et al., 2011) has been extended by a treatment of Aerosols and Reactive Trace gases (COSMO-ART, Vogel et al., 2009). Aerosols are described with a modal approach in an extended version of the Modal Aerosol Dynamics for Europe (MADE Ackermann et al., 1998) module, called MADEsoot extended (Riemer et al., 2004; Vogel et al., 2009). Fine particulate matter is represented by five overlapping log-normal distributions with constant standard deviation. Number and mass concentrations are prognostic quantities. A pair of Aitken and accumulation modes consists of secondary inorganic and organic components and primary emissions, another mode represents fresh soot, and another pair of Aitken and accumulation modes contains the same species as the first pair, though now with a soot core. Additional 7 modes represent coarse particles: 1 anthropogenic coarse mode, 3 modes for mineral dust, and 3 for sea salt. Trace gases are modeled with an extended version of the second generation regional acid deposition module (RADM2, Stockwell et al., 1990). While inorganic species are treated explicitly, organic compounds are grouped using the lumped species approach into surrogate species according to their reactivity with the OH radical. The model contains parameterisations for the emissions of dust from deserted regions (Vogel et al., 2009), sea salt (Lundgren, 2010) and biogenic VOCs (Vogel et al., 1995).

COSMO-ART uses a grid representation as latitude-longitude coordinates with a displaced north pole to minimize geometric distortion of the grid cells within the model domain (Schättler et al., 2008). As a limited area model, initial and boundary conditions are necessary, and they need to be provided on this rotated grid. Interpolation of the input data is performed by the preprocessor module INT2COSMO (Schättler, 2009), which is also used to interpolate emissions and initial and boundary conditions for chemical compounds (Appendix C) and is then called INT2COSMO-ART (Knote et al., 2011). This module has an input interface that is able to work with emission data in NetCDF (`http://www.unidata.ucar.edu/software/netcdf/`) or GRIB (WMO, 2010) format on regular or rotated latitude-longitude data providing emissions data for the species represented in COSMO-ART.

B.4 Emissions preprocessor

The emissions preprocessor developed in this work has the purpose to create a NetCDF representation of the emission amounts valid for a certain date and time for species as used in COSMO-ART so that they can be used as input to INT2COSMO-ART. It is written in Interactive Data Language (IDL, `http://www.exelisvis.com/language/en-US/ProductsServices/IDL.aspx`) and can be used on Windows, Linux and Macintosh systems. The methods used to translate TNO/MACC data into the model-specific format are described below in an abstracted manner. Not further mentioned are format conversion, data input/output and the convolution of the spatial representation of emission amounts with the time functions.

B.4.1 NO_2/NO_x split

Emission totals for oxidized nitrogen are given as total NO_x as the sum of NO + NO_2. The fraction of NO_x emitted as NO_2 (the mole fraction $NO_2/NO_x = f_{NO_2}$) differs between source categories, and can have important consequences on the resulting concentrations of secondary air pollutants like O_3. For all source categories except traffic, NO_x is emitted as 10 % (mass N) NO_2 and 90 % NO. For traffic,

estimates of f_{NO_2} are available for the largest European countries for the years 1995, 2000, 2005 and 2010 - as well as projections for 2015 and 2020 - from Fig. 2b in Grice et al. (2009). These fractions are linearly interpolated to the year to be processed. No distinction is made between SNAP subcategories for different vehicle types (7.1, 7.2 etc.). From TNO, only one time function for SNAP 7 is available. The total emission amount is summed up and treated as a whole. Differences e.g. in NO/NO_2 emission ratio between gasoline and diesel powered cars are already considered through the emissions estimates in Grice et al. (2009).

B.4.2 NMVOC speciation

The total mass of volatile organics needs to be mapped to the chemistry mechanism (RADMKA). This mechanism uses the lumped species approach, grouping organics according to their structure and reactivity with the OH radical (Stockwell et al., 1990). The mapping is divided in two steps: Firstly, the total NMVOC mass is distributed onto single chemical species according to mean NMVOC composition profiles from Passant (2002), which has compiled information about the composition of emissions from different SNAP source categories for the United Kingdom. This first step is called *speciation*. The masses of single chemical species created in the speciation step are grouped to model species, weighted by the difference between their OH reactivity and the one of the model species. This second step is called *lumping*. The correspondences and weightings are done using a program courtesy of Johannes Keller (PSI, Switzerland, personal communication 2010).

B.4.3 Particulate matter emissions

Particulate matter emissions are treated in COSMO-ART in a chemical- and size-resolved manner, so that the given PM totals need to be split into contributions of different chemical compounds, and further onto two size classes (Aitken and accumulation mode particles). Several species in different modes are possible targets for emissions.

The mapping onto the species available consists of putting the mass difference PM_{10} - $PM_{2.5}$ into the anthropogenic coarse mode, and distributing the remaining $PM_{2.5}$ emissions onto the remaining classes (fresh Aitken and accumulation modes, fresh soot mode). According to a speciation table received from TNO (personal communication, 2010) the mass total of $PM_{2.5}$ is distributed as presented in Table B.1. The emissions further need to be distributed on the different modes. In the original MADE description in Ackermann et al. (1998) the mass of each species (sulphate, organic carbon etc.) was distributed 80 % mas into the accumulation mode (J) and 20 % in the Aitken mode (I). Our preprocessing follows a newer study of Elleman and Covert (2010) resulting in a distribution of 90 % mass into the accumulation mode and 10 % mass into the Aitken mode. Soot has its own mode in COSMO-ART so not distribution is necessary here. Particulates contributions without a variable name in Table B.1 are not yet accounted for.

Only mass distributions need to be defined in the preprocessor itself. The definition of emission diameters (and hence the number concentrations) is made in COSMO-ART.

Table B.1: Contributions to $PM_{2.5}$ (TNO, personal communication, 2010). Percentages are mass contributions. The variable names indicate the target species in COSMO-ART.

SNAP	Desc.	% SO_4^{2-}	% OC	% BC	% Na	% other primary
1	Energy transformation	15.0	2.0	1.0	1.5	80.0
2	Small combustion sources	2.0	35.0	18.0	1.0	44.0
3	Industrial combustion	10.0	3.0	1.0	1.0	84.0
4	Industrial process emissions	3.0	3.0	5.0	1.5	88.0
5	Extraction of fossil fuels	0.0	0.0	0.0	0.5	99.5
6	Solvent and product use	0.0	0.0	0.0	0.0	0.0
7	Road transport	1.0	32.0	49.0	0.1	17.0
8	Non road transport (e.g. international shipping)	3.0	31.0	41.0	0.2	26.0
9	Waste handling and disposal	0.0	31.0	20.0	0.0	49.0
10	Agriculture	0.0	48.0	15.0	0.0	37.0
	Variable name	VSO4[IJ]	VORGPA[IJ]	VSOOT	-	VP25A[IJ]

B.4.4 Vertical distribution

No vertical distribution is provided by TNO. The emissions are distributed according to height distribution probability tables created during the COST728 action (`http://www.cost728.org/`, accessed Sept. 2011), which are also used in the EMEP unified modeling system. These SNAP category based tables distributes emissions onto 6 vertical ranges, from 0 - 990 m. Two tables are available, one for gases (`http://aqm.jrc.it/citydelta/EMEP_height.htm`, accessed Sept. 2011) and one for aerosols (`http://aqm.jrc.it/citydelta/emis_height_PM.html`, accessed Sept. 2011). The distributions for each category can be found in tables B.2 and B.3. The category "lowest level" is mapped onto an altitude range of 0 - 4 m, and the first height level category (0 - 90 m in the COST table) consequently starts at 4 m.

B.4.5 Yearly scaling

The TNO/MACC data is available for the years 2003 - 2007. Data for other years is created by scaling the emission amounts with reported and projected changes in country totals. For years before 2003, reported EMEP (Mareckova et al., 2008) totals give scaling factors per species and country. For years after 2007, projections from the International Institute for Applied Systems Analysis (IIASA, Laxenburg, Austria) are used. Therefrom, different projections of future emissions can be obtained on the per-country-total level. The PRIMES 2009 scenario is used for scaling here. Both, the scaling factors for EMEP as well as for the IIASA projections are calculated in the following manner: only relative changes between estimated IIASA / EMEP totals for the nearest year which also has TNO data available (i.e. 2003 for EMEP / 2007 for IIASA) and the year in question are used - the country total of the TNO/MACC data are then multiplied by this scaling factor.No extrapolation occurs - if no data is available for a certain target year, the closest year for which EMEP/IIASA data is available is used. No change in the time functions occurs. The f_{NO_2} is used as given in Grice et al. (2009) for the year in question.

B.5 Usage and output

The preprocessor consists of a number of routines of Integrated Data Language (IDL) source code, the ASCII input data from TNO, a number of ancillary data files and a shell script allowing for batch

Table B.2: Vertical distribution of gaseous emissions given as mass percentages (%). Level boundaries are given in meters.

SNAP	lowest level	4-90	90-170	170-310	310-470	470-710	710-990
1	0	0	0	8	46	29	17
2	0	50	50	0	0	0	0
3	0	0	4	19	41	30	6
4	0	90	10	0	0	0	0
5	0	90	10	0	0	0	0
6	100	0	0	0	0	0	0
7	100	0	0	0	0	0	0
8	100	0	0	0	0	0	0
9	0	10	15	40	35	0	0
10	100	0	0	0	0	0	0

Table B.3: Like Table B.2, but for particulate matter.

SNAP	lowest level	4-90	90-170	170-310	310-470	470-710	710-990
1	20	10	10	40	20	0	0
2	100	0	0	0	0	0	0
3	70	4	5	15	6	0	0
4	100	0	0	0	0	0	0
5	20	10	10	40	20	0	0
6	100	0	0	0	0	0	0
7	100	0	0	0	0	0	0
8	100	0	0	0	0	0	0
9	100	0	0	0	0	0	0
10	100	0	0	0	0	0	0

calculations. Paths to input, ancillary and output data are defined in a single environment script. The code is documented and tested.

Output are hourly NetCDF files containing 3D fields for each model species, describing the emissions as kg / h / cell. Table B.4 contains a comprehensive list of species created. Depending on the setup, the data is either on the original grid as delivered by TNO, or re-gridded e.g. on a certain COSMO rotated lat-lon grid. In case the vertical distribution option has been chosen the dataset has 7 height levels. Additionally to the data fields the file contains auxiliary variables to accommodate the input into the model (grid description, latitude and longitude values, time stamp).

Table B.4: Comprehensive list of species available as emissions after preprocessing of the TNO/MACC dataset.

gaseous species	
CO	carbon monoxide
NH3	ammonia
NO2	nitrogen dioxide
NO	nitric oxide
SO2	sulfur dioxide
gaseous species (not used in ART)	
CH4	methane
NMVOC	total NMVOC
lumped gaseous species	
ETH	ethane
HC3	alkanes (low OH rate constants)
HC5	alkanes (mean OH rate constants)
HC8	alkanes (high OH rate constants)
OL2	ethene
OLT	terminal alkenes
OLI	internal alkenes
TOL	toluene and less reactive aromatics
XYL	xylene and more reactive aromatics
CSL	cresol and other hydroxy substituted aromatics
HCHO	formaldehyde
ALD	acetaldehyde and higher aldehydes
KET	ketones
ORA2	acetic acid and higher acids
particulates	
VSOOT	elemental carbon ("soot") below 2.5 μm
VANTHA	coarse particulate matter between 2.5 and 10 μm (PM_{10} - $PM_{2.5}$)
VORGPA[IJ]	primary organics below 2.5 μm (Aitken / accumulation mode)
VP25A[IJ]	primary, unidentified anthropogenic particles below 2.5 μm (Aitken / accumulation mode)
VSO4[IJ]	primary sulfate particles below 2.5 μm (Aitken / accumulation mode)
particulates (not used in ART)	
PM25	total particulate matter mass below 2.5 μm
PM10	total particulate matter mass below 10 μm

Appendix C

INT2COSMO-ART documentation

C.1 Introduction

The limited area, regional numerical weather prediction (NWP) model of the Consortium on Small-scale MOdeling (COSMO, Baldauf et al., 2011) was extended by a treatment of Aerosols and Reactive Trace gases (COSMO-ART, Vogel et al., 2009). COSMO requires initial and boundary conditions (IC/BC) either from a global or coarser-grid regional model, and these data need to be interpolated and further preprocessed to be used. This is accomplished by the preprocessor INT2COSMO (historically called INT2LM, Schättler, 2009). In this work we have extended INT2COSMO by the ability to interpolate data from a global chemistry transport model (CTM) as initial and boundary conditions for trace gases and aerosols, further by the possibility to interpolate and combine multiple datasets representing emissions of trace gases and particulates, and finally by the ability to interpolate additional "external parameters", i.e. constant-in-time boundary conditions, which are used as input in several parameterisations used in the "-ART" part of COSMO-ART. This document describes the methods employed, the technical realization of the coupling and the usage of the extended preprocessor *INT2COSMO-ART*.

C.2 Methods

Three additional kinds of datasets can be used in INT2COSMO-ART: initial and boundary conditions for aerosols and trace gases, emissions datasets, and external parameters. The purpose of INT2COSMO-ART is to interpolate these datasets onto the rotated latitude-longitude (horizontal) / hybrid sigma (vertical) grid representation in COSMO(-ART), to derive additional variables and to create an output file which is then read in by COSMO(-ART) at run-time, providing all necessary information in such way that no additional computations have to be made then.

Horizontal interpolation using nearest neighbor or bi-linear interpolation methods is already included in INT2COSMO, and the same subroutines are used for the interpolation of the -ART datasets. Additionally, an aggregation-type "interpolation" has been included for the case that the input data might exist on a higher resolution than the simulation grid and it would become necessary to sum up all contributions within a cell. Emissions interpolation is realized in a globally mass conserving way irrespective of the interpolation method used.

In the vertical, a pressure-difference weighted interpolation was included to accurately distribute three-dimensional emissions (possibly on geometric heights or pressure levels) onto the hybrid-sigma discretised model levels. This procedure is briefly outlined in the following: The input level information is assumed to represent the mean geometric height of the emissions level. As COSMO uses a hybrid vertical coordinate system the height of each model level depends on topography. The interpolation routine takes care to distribute the emitted mass reasonably on the model levels by the following method:

If no level boundaries (variable *level_bnds* in the input file) are given: Each emission level height is assumed to represent the center of the corresponding height range. The upper and lower bounds are therefore calculated as the geometric mean between this level and the adjacent levels. In case that level boundaries are given, those are used. The relationship between the emission level and a model level can then fall into one of four categories:

- the model level falls completely in the emission level
- the emissions level falls completely in the model level
- the model level corresponds only partly to the emission level
  - the model level lower boundary is lower than the emission level lower boundary
  - the model level upper boundary is higher than the emission level upper boundary

It is necessary to distribute the emissions consistently according to their mass and the surrounding environment. Therefore, the pressure difference between two model levels is used as weight for the distribution. For model levels that fall only partly into the emission level, the pressure difference is weighted by the (linear) fraction of the model level geometric height that contributes to the emission level. All contributing pressure differences are scaled to one and the total emission mass is distributed according to these values.

Initial and boundary conditions are interpolated employing the same methods as are used for the interpolation of scalar quantities in the meteorological part. The input of data on (a different) hybrid sigma coordinate system is possible for initial and boundary conditions.

External parameters for COSMO-ART can include information about the fractional land-use per grid cell, a description of soil properties or information about the dimethyl sulfate (DMS) emission potential of oceans. Most of these datasets are already provided as the result of previous efforts and INT2COSMO-ART is solely used to interpolate the given fields onto the COSMO-ART grid, employing the existing interpolation methods. Which datasets are required depends on the setup for COSMO-ART.

All methods have been written in a general format such that they can be used with various input datasets. This might also make the use of additional pre-preprocessors necessary which transfer a particular (non-standard) model output into the file format expected by INT2COSMO-ART. Further preprocessing is also needed for more complex steps like the speciation of total non-methane volatile organic compounds on their representation in the chemical mechanism of COSMO-ART (see also Appendix B). INT2COSMO-ART expects initial and boundary conditions for trace gases to be volume mixing ratios (VMR), and micro-gram per meter cubed ($\mu g/m^3$) for aerosols. Emissions are expected to be kg/h/cell. Trivial unit conversions are implemented for ease of use.

C.3 Data format

INT2COSMO can read GRIB and NetCDF files. The extensions for -ART have only been implemented for NetCDF so far. Input file format requirements are in most cases identical for emission, initial/boundary condition and external parameter fields. The common aspects are described here, differences are mentioned later in the description of each type of input data.

The input file format is NetCDF (`http://www.unidata.ucar.edu/software/netcdf/`), the CF conventions (`http://cf-pcmdi.llnl.gov/`) for naming of dimensions, variables and attributes are expected. However, not all options possible in CF conventions are actually implemented.

Each file contains 2 (x,y) or 3 (x,y,z) dimensional representations of a variable, optionally (in case of time dependent data) valid for a single point / period in time. The horizontal grid has to be regular latitude-longitude, but the grid can have a rotated pole. See the COSMO documentation for information about rotated grids (Schättler et al., 2008). In the vertical, geometric height, pressure and hybrid-sigma-pressure levels can be given. In case the layer boundaries are known, an additional variable "level_bnds" can be included in the NetCDF with a size of (# layers,2), containing the lower and upper boundary height of each layer. In case of hybrid-sigma-pressure coordinates INT2COSMO-ART expects additional variables in the file: The hybrid A/B coefficients "hyam" and "hybm", the reference pressure "P0", and a surface pressure field "PS". A correct NetCDF CF time stamp is expected, defined as time since a reference date.

The file naming convention is simple, consisting of a freely selectable prefix and, in case of time dependent data, the start date of the period for which the data in the file is valid. The format of the date is YYYYmmddhh, hence a valid file name would be e.g.: "swiss_2009050400.nc".

C.4 Usage

INT2COSMO-ART is an extension to INT2COSMO, hence the setup for meteorology is identical to a normal COSMO simulation. The ART part consists of 4 different kinds of additional namelists, and 2 master switches to control the ART extensions in the CONTRL namelist (Table C.1):

l_chemistry is the master switch to turn on/off ART related processing. In case it is .FALSE., INT2COSMO-ART behaves like normal INT2COSMO, if it is .TRUE. additional fields for ART can be processed. The second switch, *l_chemistry_nested*, defines if a COSMO-ART to COSMO-ART nesting should happen, and consequently INT2COSMO-ART expects the coarse-grid (COSMO-ART) input data to contain *all* ART chemistry and aerosol fields.

The INT2COSMO-ART extension itself is controlled by 4 different namelists: *ARTCONTROL*, which provides overall settings for the run configuration, and (several) *ICBCDATASET* / *EMISSIONSDATASET* / *EXTPARSDATASET* namelists which describe single input datasets.

Table C.1: List of additional parameters for the CONTRL namelist

Name	Type	Definition / Purpose / Comments	Default
l_chemistry	LOG	main switch for the ART extension	.FALSE.
l_chemistry_nested	LOG	ART boundary data is provided from coarser COSMO run	.FALSE.

C.4.1 ARTCONTROL

The *ARTCONTROL* namelist (Table C.2, with an example in Listing 1) provides specifications for the overall run configuration and provides information about the number of input datasets for each category. Whether emissions, initial and boundary data, or external parameters are processed can be controlled by the *lemissions*, *licbc*, and *lextpars* switches. The switches *ndatasets_emissions*, *ndatasets_icbc* and *ndatasets_extpars* define the number of input datasets in each categories. For emissions and initial / boundary conditions, a time increment (in hours) can be specified additionally, describing the *output* frequency of the (combined) emissions / initial and boundary data: *hinc_emissions_lm* / *hinc_icbc_lm*.

Table C.2: List of parameters for the ARTCONTROL namelist.

Name	Type	Definition / Purpose / Comments	Default
lextpars	LOG	process external parameters (main switch)	.FALSE.
licbc	LOG	process boundary data (main switch)	.FALSE.
lemissions	LOG	process emissions (main switch)	.FALSE.
ndatasets_icbc	INT	number of input boundary datasets	1
ndatasets_emissions	INT	number of input emission datasets	1
ndatasets_extpars	INT	number of input ext. parameters datasets	1
hinc_icbc_lm	REAL	increment (hrs) for boundary data output	1.0
hinc_emissions_lm	REAL	increment (hrs) for emissions output	1.0

```
&ARTCONTROL
  lextpars   = .TRUE.,  ndatasets_extpars   = 2,
  lemissions = .TRUE.,  ndatasets_emissions = 1, hinc_emissions_lm = 1.0,
  licbc      = .TRUE.,  ndatasets_icbc      = 1, hinc_icbc_lm = 6.0,
/
```

Namelist example 1: ARTCONTROL

C.4.2 ICBCDATASET, EMISSIONSDATASET, EXTPARDATASET

Each input dataset is described in a *ICBCDATASET, EMISSIONSDATASET, EXTPARDATASET* namelist, which have an identical list of possible attributes (Table C.3, with an example in Listing 2). Besides the definition of the input grid, the input folder and file prefix can be given. Further options include the units of the input variables, the interpolation type used, an information about time dependency and a possible, artificial vertical distribution for 2D emission data. INT2COSMO-ART expects a data file for each time-step t = *ydate_ini* + x * *hinc_data*, unless the data is marked as time-invariant (*lconstant_in_time_data* = *.TRUE.*). In that case the data is read in only once at the beginning and then held constant, the name of the file expected consists only of *ylfn_prefix_data* plus ".nc", e.g. "swiss.nc".

Log-normal interpolation

Emission usually span several magnitudes and grid cells with very high emissions often lie beneath cells with low emissions. A normal bi-linear interpolation method would soften this gradient, which is not wanted. Therefore the interpolation can be done using the logarithm of the emission values. The logarithm

(base e) of the emission field is calculated, it is interpolated and the field is exponentiated afterwards. This feature can be controlled through the dataset namelist switch *llogtransform_data*.

Artificial vertical distribution

For 2D datasets that do not include a vertical distribution one can define an artificial vertical distribution which distributes the emission field on the model levels according to the distribution defined in *cvertdist_data*. To achieve this distribution, the switch *lvertdist_data* needs to be .TRUE. . *cvertdist_data* is a vector with a maximum of 10 values holding the relative amount each model level (starting from the bottom-most model level) gets from the emission field. It is scaled to a sum of 1, so percentages are also possible as values.

Table C.3: List of parameters for a EMISSIONSDATASET / ICBCDATASET / EXTPARDATASET namelist

Name	Type	Definition / Purpose / Comments	Default
startlon_tot_data	REAL	longitude of first grid point	-10.0
startlat_tot_data	REAL	latitude of first grid point	30.0
dlon_data	REAL	longitudinal grid spacing	0.5
dlat_data	REAL	latitudinal grid spacing	0.5
pollon_data	REAL	longitude of the rotated north pole	180.0
pollat_data	REAL	latitude of the rotated north pole	90.0
polgam_data	REAL	angle between the north poles of the systems	0.0
ie_tot_data	INT	number of grid points in longitude direction	80
je_tot_data	INT	number of grid points in latitude direction	80
ke_tot_data	INT	number of vertical levels	1
ylfn_prefix_data	CHAR	emission file name prefix	“file_”
yunits_data	CHAR	units of the data provided (“ppb”,”ppm”,”vmr”,”kg/m3”)	“ppm”
yvarlist_data(:)	CHAR	species to be read	all
yinterp_type	CHAR	interpolation type (“L” bilinear, “N”, nearest neighbour)	“L”
hinc_data	REAL	increment (hrs) for new data	1.0
lconstant_in_time_data	LOG	data do not vary over time	.FALSE.
ydirin_data	CHAR	emission data path	“input/”
llogtransform_data	LOG	log-normal interpolation	.FALSE.
lvertdist_data	LOG	artifical vertical distribution	.FALSE.
cvertdist_data(:)	REAL	percentages of artificial vertical distribution	[1.0,0.0,. . .]
yvertical_units_data	CHAR	units of the vertical axis (“m”,”pa”,”hyb_sig_pr”)	“m”

C.5 Memory considerations

Every trace gas or aerosol in COSMO-ART could be emitted or serve as IC/BC. Unless specified otherwise, each species is pre-allocated for reading. Therefore, around 170 3D fields with dimensions as defined in the DATASET namelist would be allocated. This can easily exceed the memory available on a machine. If only certain species are emitted / used as initial or boundary condition, defining them in the DATASET namelist via *yvarlist_data* greatly reduces the memory consumption, as only those species defined in the namelist are pre-allocated and processed.

```
&EMISSIONSDATASET
    startlon_tot_data=-44.5625, dlon_data=0.125,
    startlat_tot_data= 29.7812, dlat_data=0.0625,
    pollon_data=180.0, pollat_data=90.0,
    ie_tot_data=841, je_tot_data=778, ke_tot_data=7,
    ylfn_prefix_data = "macc_",  yunits_data="kg/m3",
    yvarlist_data= "CO", "NH3", "NO2", "NO", "SO2", "ETH", "HC3", "HC5", "HC8",
    "OL2", "OLT", "OLI", "TOL", "XYL", "CSL", "HCHO", "ALD", "KET", "ORA2",
    "VSOOT", "VANTHA", "VORGPAJ", "VORGPAI", "VP25AJ", "VP25AI",
    "VSO4I","VSO4J",
    yinterp_type="N", hinc_data=1.0,
    ydirin_data="<INPUT PATH TO EMISSION FILES>",
    llogtransform_data=.FALSE.,
/
```

Namelist example 2: EMISSIONSDATASET

C.6 Combining multiple datasets

It is often desirable to use more than one dataset and combine those. In the case of emission data for example, a coarser grid dataset for the surroundings and a higher resolution dataset for the focus region would be used. Or, for IC/BC, different data providers for different species deliver their data on different grids. In INT2COSMO-ART, both types of input data can have more than one dataset. They differ in the method data of a certain species are combined: while IC/BC are used from one dataset only, emissions are combined using the mask information within the datasets. The ordering of the datasets is reverse to their order in the namelist, i. e. for emissions the last EMISSIONSDATASET entry "lies on top" in the output file. An example: Two emission datasets, one for the whole European domain and one higher resolution for Switzerland are used. The namelists are defined in the following way:

```
In &ARTCONTROL : ... ndatasets_emissions=2 ...

&EMISSIONSDATASET
  European dataset definition ...
/
&EMISSIONSDATASET
  Switzerland dataset definition ...
/
```

Namelist example 3: multiple EMISSIONSDATASETs

Each pixel is then assigned the value of the uppermost dataset whose value is not set to the NetCDF _FillValue. Here, Switzerland emissions are only defined over the domain of Switzerland, and grid points outside are set to the NetCDF _FillValue. The result is an emission composite containing emission information from the Swiss dataset for grid points in the domain of Switzerland and from the European dataset for all other grid points. For initial and boundary conditions the dataset used is the last defined one which contains data for this species.

C.7 External parameters

Parameterisations in COSMO-ART, e.g. the emissions of biogenic volatile organic compounds need additional external parameters fields. INT2COSMO-ART can process raw datasets like land cover data and convert them into the format needed by COSMO-ART. Currently, two datasets are used and supported, but the method is written in a general way and can be extended easily. As for emissions and IC/BC, each input dataset is described by its own EXTPARSDATASET namelist. Depending on the fields that have been read, the respective COSMO-ART variables are calculated and written to the output. The usage section already presented the methods to include them into the INT2COSMO-ART namelists. The two main datasets used so far are:

C.7.1 GLC2000 land use classes

The GLC2000 land use classes dataset (`http://bioval.jrc.ec.europa.eu/products/glc2000/glc2000.php`) contains information about the coverage of Earth's surface and are provide as a gridded data set with high resolution, each cell containing the predominant land use class. Used in COSMO-ART are, however, are the fractional contributions of different land use types to each grid cell. This information is used directly in the calculation of dry deposition of gases. Additionally, emission fluxes for biogenic VOC are calculated from those contributions. Each of the GLC land use classes is attributed with a VOC emission factor at a reference temperature, thereby creating a mean emission factor for a grid cell. In COSMO-ART this factor is later weighted by the current temperature and radiation situation at a certain model time step. The first parts (calculating the contribution of a land use class to a grid cell, and deriving a VOC emission factor) are implemented in INT2COSMO-ART. GLC2000 raw data has been put into a simple NetCDF dataset. To reduce file sizes, subsets of the complete (global) dataset can be used as well. If no data is found for a certain grid cell, this cell is assumed to be water (class 20). See below for a definition of the EXTPARSDATASET namelist for a GLC2000 subset:

```
&EXTPARSDATASET
  startlon_tot_data =-20.0, dlon_data=0.008926392,
  startlat_tot_data =  9.973213, dlat_data=0.008926392,
  ie_tot_data=7841, je_tot_data=7291, ke_tot_data=1,
  ylfn_prefix_data="glc2000_europe",
  yvarlist_data="GLC2000",
  lconstant_in_time_data=.TRUE., ydirin_data="extPar/",
/
```

Namelist example 4: EXTPARSDATASET for GLC2000

C.7.2 Dust

The dust parametrization currently implemented in COSMO-ART uses additional input fields for more detailed description of soil parameters (Marticorena and Bergametti, 1995). These input data fields need to be rotated on the COSMO grid. The input dataset is provided as NetCDF by Empa. The corresponding EXTPARSDATASET namelist is shown below:

```
&EXTPARSDATASET
  startlon_tot_data =-17.0, dlon_data=1.0,
  startlat_tot_data = 12.0, dlat_data=1.0,
  ie_tot_data=95, je_tot_data=24, ke_tot_data=1,
  ylfn_prefix_data = "dust",
  lconstant_in_time_data=.TRUE., ydirin_data="extPar/",
/
```

Namelist example 5: EXTPARSDATASET for dust

C.8 Output files

INT2COSMO-ART creates three different types of output files:

- External parameters (land use/BVOC) ("laf⟨date⟩x.nc")
- External parameters (dust) ("laf⟨date⟩u.nc")
- ART boundary data ("l⟨prefix⟩⟨forecast hour⟩a.nc")
- Emission data ("l⟨prefix⟩⟨forecast hour⟩e.nc")

They are analogues to the meteorological input data for COSMO and need to be provided to the COSMO-ART simulation in the defined input directory (ydirin_art).

List of Tables

2.1 Contributions (in % mass) to $PM_{2.5}$ emissions as used in the TNO/GEMS emission inventory. Sodium (Na) is not used directly in the simulations, but added to the "other primary" category, representing the remaining, non-carbonaceous primary $PM_{2.5}$ part (including e.g., minerals, metal oxides, product emissions). Sulfate contributions have been calculated assuming 2% of total emitted SO_2 mass (IIASA RAINS emissions for 2000) is H_2SO_4 for all SNAP categories except SNAP 1 and 3. There, measured compositions of coal fly ash (as dominant contributor to source category) as reported by Lipsky et al. (2002) and Senior et al. (2000) are used as basis. OC depicts organic carbon, a ratio of 1.3 has been used to convert OC to organic aerosol (OA). 38

2.2 Normalized mean biases (%) in spring, summer, autumn and winter (SP,SU,AU,WI) for SYNOP and AIRBASE datasets, satellite comparisons and aerosol datasets. Satellite biases are the mean over all grid points, only land points and only sea points. AERONET comparison shows biases model - AERONET (AER), model - MODIS (MOD) at AERONET station, and MODIS - AERONET (DIF). AMS and EUSAAR biases are the mean over all stations presented in the evaluation, the number of stations in each period is given in the notes. 42

2.3 Comparison of number concentrations in different size ranges after Asmi et al. (2011) for number size distributions during the autumn 2008 simulation. N_{30to50}: 30 to 50 nm, N_{50}: above 50 nm, N_{100}: above 100 nm, N_{250}: above 250 nm. Note that the N_{250} parameter has a larger uncertainty than the others due to very low sampling rates. 58

2.4 Comparison of number concentration comparisons, like in Table 2.3, but for the spring 2009 simulation. 58

4.1 Simulations made and abbreviations used. 1990 and 2009 always refer to the simulation time frame in January of these years. Note that Δf_{NO_2} uses 2009 emissions as basis, instead of the remaining sensitivity studies that use emissions of 1990. 93

4.2 Regions used in analysis, their abbreviations, and the countries they are comprised of. Figure 4.1 gives a graphical overview. 104

B.1 Contributions to $PM_{2.5}$ (TNO, personal communication, 2010). Percentages are mass contributions. The variable names indicate the target species in COSMO-ART. 120

B.2 Vertical distribution of gaseous emissions given as mass percentages (%). Level boundaries are given in meters. 121

B.3 Like Table B.2, but for particulate matter. 122
B.4 Comprehensive list of species available as emissions after preprocessing of the TNO/MACC dataset. 123

C.1 List of additional parameters for the CONTRL namelist 127
C.2 List of parameters for the ARTCONTROL namelist. 128
C.3 List of parameters for a EMISSIONSDATASET / ICBCDATASET / EXTPARDATASET namelist 129

List of Figures

1.1 Schematic of the major daytime tropospheric gas-phase chemistry processes. Simplified from Staehelin et al. (2000). 3

1.2 Dependence of daily maximum O_3 concentrations (colored contours, concentrations in ppmv) on the NO_x / VOC precursor concentrations. NMVOC are all VOC except methane ("non-methane volatile organic compounds"). At a proportion of about 8 to 1 (solid black line), O_3 shows equal sensitivity to NMVOC and NO_x reductions. Adapted from Dodge (1977). 4

1.3 Schematic overview of the processes affecting aerosols during their lifetime in the atmosphere: emissions (A), transport (B), gas-phase chemistry (C), nucleation (D), condensation/evaporation (E), coagulation (F), activation/scavenging (G), evaporation/cloud processing (H), sedimentation (I), dry deposition (K), wet deposition (L). 7

1.4 Schematic of aerosol size ranges and associated processes. Black solid lines: number (top), surface area (middle) and volume (bottom) concentration size distributions of an aerosol population typically found at remote continental sites. Grey dashed lines delineate approximately the different *modes* (see text). Processes acting upon the aerosol and their size-dependent efficiency are shown as shaded areas / arrows, and annotated with the processes' names. Figure modified from Fig. 7.18 in Seinfeld and Pandis (2006). 8

1.5 Annual average chemical composition of $PM_{2.5}$ mass at selected stations in Europe. Figure modified from Fig. 3 in Putaud et al. (2004). 9

1.6 Illustration of the classical nucleation theory (CNT). The surface tension (blue curve) and the saturation-ratio (red curve) terms compete with each other, forming the black curve. The local maximum in the change in Gibbs free energy ΔG (intersection of the black curve with the dashed gray line) determines the critical radius r^*, above which the cluster is stable and further growth is not limited by nucleation any more. Surface tension, saturation-ratio and sum term calculations based on Fig. 14.3 in Jacobson (2005). 10

1.7 Particle growth rates as a function of relative humidity for a mixed sodium-chloride (NaCl) - sodium-sulfate (Na_2SO_4) particle. Figure based on Fig. 1 in Tang (1997). Solid black lines show the growth and evaporation curves for the mixed particle, blue lines for pure NaCl and orange lines for pure Na_2SO_4. Note the hysteresis between growth (particle grows once the deliquescence relative humidity (DRH) is reached) and evaporation (particle crystallizes only once the crystallization relative humidity (CRH) is reached). DRH and CRH are marked with circles, the mutual DRH / CRH with bold circles. 13

1.8 Fig. 1 in Jimenez et al. (2009): mass concentrations and chemical composition of non-refractory PM_1 ($PM_{1,NR}$) as measured by an aerosol mass spectrometer (AMS) during field campaigns at stations in the Northern Hemisphere. Statistical analysis was used to determine the fractions of primary (HOA + Other OA) and secondary organic aerosols (SV-OOA, LV-OOA)). In the inset the oxidation state of the different components is shown as the oxygen to carbon atoms ratio. 15

1.9 Schematic representation of the 2D-volatility basis set (2D-VBS), with the volatility on the x-axis and the oxidation state as y-axis. An arbitrary organic compound is shown with possible directions of movement through the different processes oligomerization, functionalisation and fragmentation. Further noted are regions of LV-OOA and SV-OOA. Fig. modified from Fig. 4c in Jimenez et al. (2009). 16

1.10 Effects of curvature and solutes on the critical saturation ratio S^* and the associated critical radius r^*. The dashed line represents the saturation ratio, i.e. a measure for the relative humidity necessary for activation. Fig. modified from Fig. 16.1 in Jacobson (2005). 16

1.11 Collection efficiency for impaction scavenging as used in SCAV. The different participating processes are shown as dashed lines (red is Brownian motion, green interception and violet impaction). The gray solid line shows the resulting total collection efficiency. Figure modified from Tost et al. (2006). 19

1.12 The components of the COSMO-ART (Vogel et al., 2009) modeling system, including the scavenging and wet-phase chemistry module added during this thesis (SCAV). 20

1.13 Schematic of typically used methods to represent a given (measured) aerosol distribution (gray solid line). For the modal approach: red solid lines show three log-normal distributions whose superposition is used to approximate the given distribution. For the sectional approach: blue boxes represent size bins. 25

1.14 Representation of aerosols in COSMO-ART: MADEsoot extended (Riemer et al., 2004; Vogel et al., 2009). 2 pairs of Aitken and accumulation modes, one with and one without soot core, a fresh soot mode, a primary coarse mode, 3 modes for mineral dust and 3 for sea salt. 27

1.15 The VBS, adapted from Fig. 1a of Donahue et al. (2006). "Partitioning of a collection of semi-volatile compounds, with total loadings (in $\mu g\,m^{-3}$) shown with full bars and the condensed-phase portion with filled (green) bars. Compounds are distributed according to their mass-equivalent effective saturation concentration (C*, also in $\mu g\,m^{-3}$), which is presented as a logarithmically distributed basis set. $C_{OA} = 10.45\ \mu g\,m^{-3}$, shown with an arrow, and so that bin is evenly split between the two phases" (Donahue et al., 2006). . . 30

2.1 Model domain and measurement station positions. AIRBASE/EMEP: gas-phase and bulk aerosol mass, AMS: aerosol chemical composition (EIMP/EUCAARI/EUSAAR), DMPS/SMPS: aerosol size distribution (EUSAAR/GUAN), AERONET: aerosol optical depth. The position of the column used for aerosol boundary conditions is marked with a red cross (aerosol IC/BC). Stations with AMS and/or DMPS/SMPS measurements: [a] Payerne (CH), [b] Aucencorth/Bush (UK), [c] Melpitz (DE), [d] Vavihill (SE), [e] Hyytiälä (FI), [f] K-Puszta (HU), [g] Cabauw (NL), [h] Helsinki (FI), [i] Barcelona (ES), [j] Montseny (ES), [k] Harwell (UK), [l] Kosetice (CZ), [m] Aspvreten (SE), [n] Birkenes (NO), [o] Mace Head (IE), [p] Ispra (IT), [q] Waldhof (DE). Several named stations measured both chemical composition and size distribution. 37

2.2 Boxplots of modelled (red) and measured (blue) median values of 2 m temperature (T_{2m}) and relative humidity (RH), and 10 m wind speed (WS). Note that 10 m wind direction (WD) are mean biases (green). Station RH was calculated from T_{2m} and Td_{2m}. Used are measurements from the SYNOP station nearest to each AIRBASE/EMEP station used in Figure 2.3. The number of stations used is shown at the top of each comparison. Simulations are ordered to represent an annual cyle: spring 2009, summer 2006, autumn 2008 and winter 2006. 41

2.3 Boxplots of modelled (red) and measured (blue) median concentrations for afternoon hours (12 - 18 LT) of several compounds, classified after Henne et al. (2010). The number of stations used is shown at the top of each comparison. Note that values for NO and NO_2 are on a logarithmic scale. Simulations are ordered to represent an annual cyle: spring 2009, summer 2006, autumn 2008 and winter 2006. 43

2.4 Maps of mean afternoon (12 -18) NO_x, O_3 and SO_2 concentrations for the summer 2006 period. Comparison with AIRBASE station concentrations is shown as points: Modelled mean in the outer ring and measured mean in the center. 45

2.5 Modelled and measured (AIRBASE) mean diurnal cycles of several compounds during the summer 2006 period, disaggregated after Henne et al. (2010). Measured values are shown as colored areas, modelled parameters as lines. Light blue areas show 90% range of station values, the range between dotted lines the same for modelled values. Blue colored areas compare to the area between dashed lines (70% range). The median of measured values is a solid, dark blue line, the median of modelled values a solid red line. If less than 5 stations report data, measured and modelled medians are reported as blue and red line pair per station, with different line styles for each pair. 47

2.6 Comparison of modelled NO_2 VTCs against OMI satellite data for (from top) the spring 2009, summer 2006, autumn 2008 and winter 2006 periods. Modelled values are found in the left column, OMI observations in the right one. Not the whole simulation domain could be compared due to missing coverage of the EOMINO dataset. 49

2.7 Comparison of modelled AOD (550 nm) against MODIS satellite data for (from top) the spring 2009, summer 2006, autumn 2008 and winter 2006 periods. Modelled values are found on the left, MODIS observations on the right hand side. 51

2.8 Timelines of aerosol optical depth (AOD) at selected AERONET stations in Europe for the different periods. Shown are AERONET measured values (black circles), MODIS derived AOD (blue asterisks) and the simulated AOD values (red lines). AERONET data has been cloud-screened by the data provider. MODIS data is also cloud screened. Modelled values are masked if simulated total cloud cover was above 25 %. 52

2.9 Timeline of chemical composition of $NR - PM_1$ (top: modelled, bottom: measured by AMS) during autumn 2008. Pie charts give mean over time period (size of pie relates total mass). Measured OA should be compared with the sum of modelled aPOA, aSOA and bSOA. Gray shaded areas mask times without measurement data. 54

2.10a Timeline of aerosol chemical composition as in Figure 2.9 but for stations measuring during the spring 2009 period (1 of 2). 55

2.10b Timeline of aerosol chemical composition as done in Figure 2.9 but for stations measuring during the spring 2009 period (2 of 2). 56

2.11 Modelled and measured aerosol size distributions at EUSAAR stations for the autumn 2008 period. Modelled distributions are shown as area shaded by mass contributions of different species, calculated as median over the simulation period. Measured values are a statistical size distribution from data of the whole season and are shown as lines. Solid lines depict median values, dashed lines the 67 % and dotted lines the 90 % percentile range. Grey background denotes areas with higher measurement uncertainty (Wiedensohler et al., 2010). 59

3.1 Cloud liquid water (A) and rain liquid water (B) concentrations (g/kg), and cloud pH (C). 75

3.2 Changes in gaseous SO_2 (A) and total SO_4^{2-} (B) aerosol mass as percent change against the reference simulation. 76

3.3 Distribution of of different groups of compounds between phases during passage of the cloud (between grid cells 90 and 110 of the idealized simulation). The three phases considered are gas (g), aerosol (a), and cloud water (l). The compound groups are sulfur "S" (plot A): SO_2 (g), H_2SO_4 (g), SO_4^{2-} (s), SO_2 (l), H_2SO_4 (l), HSO_4^- (l), SO_4^{2-} (l), HSO_3^- (l), SO_3^{2-}(l). Oxidized nitrogen "NO" (plot B): NO (g), NO_2 (g), HNO_3 (g), N_2O_5 (g), NO_3 (g), NO_3^- (s), HNO_3 (l), NO_3^- (l). Reduced nitrogen "NR" (plot C): NH_3 (g), NH_4^+ (s), NH_3 (l), NH_4^+ (l). Shown are column totals for grid columns above the mountain with its top at grid point 100. The percentage given at the top right shows the relative change in total aerosol mass between before (column total at grid point 90) and after cloud processing (at grid point 110). 77

3.4 Changes in mass concentrations of sulfate aerosols in the fresh Aitken mode (A) and the mixed accumulation mode (B) showing the effect of cloud processing. 78

3.5 Boxplots of mean trace gas and particulate matter concentrations over the simulations period. Shown are results from the reference simulation in Knote et al. (2011) (REF), results from a new simulation including aqueous-phase chemistry (SCAV), and measurement data from the AIRBASE network (meas.). Stations classified according to their representativeness following (Henne et al., 2010). 79

3.6 Accumulated precipitation (A), values below 10 kg/m^2 are masked out. Relative changes in SO_2 (B), and SO_4^{2-} (C) and NO_3^- (D) aerosol mass concentrations due to the inclusion of the new scavenging module. Shown are mean differences over the whole simulation period. 80

3.7a Timeline of aerosol chemical composition (top: reference simulation (Knote et al., 2011), middle: simulation with SCAV, bottom: measured by AMS) during autumn 2008. Pie charts give mean over time period (size of pie relates total mass). Measured OA should be compared with the sum of modeled aPOA, aSOA and bSOA. Gray shaded areas mask times without measurement data. While AMS measures non-refractory PM below 1 μm, we compare here with modeled PM below 2.5 μm, due to effects of the changes in size distribution mentioned in section 3.5. 81

3.7b As Figure 3.7a but for different stations. 82

3.8 Modeled aerosol volume concentration size distributions at selected stations for the autumn 2008 period. Modeled results for the reference simulation (red) and a simulation including SCAV and cloud processing (blue) are shown as thick solid lines. For reference the transmission functions of an AMS (dotted line), a $PM_{2.5}$ (dash-dotted line) and a PM_{10} (dashed line) inlet system as calculated in Knote et al. (2011)) are given as well. 83

3.9 Scatterplots of wet deposited mass of NO_3^- (A), NH_4^+ (B), and SO_4^{2-} (C). Each hollow symbol represents the comparison between the measured mass total over the simulation period against the modeled one at a single station. Symbols are categorized according to a station representativeness classification by Henne et al. (2010), which is shown by different colors / symbols. Filled black circles represent the arithmetic mean deposited mass. Lines are drawn to help estimate over/underestimation factors: solid = 1:1 , dashed = 2:1 and dotted = 5:1. 84

4.1 COSMO-ART model domain. A red X marks the position of the averaged vertical column that is used for initial and lateral boundary conditions for aerosols. Regions used in evaluation are color coded, see also Table 4.2. A frame of 30 grid points at the domain boundaries is not used as it is influenced by the relaxation against boundary values. EMEP stations used in analysis and their abbreviations (black circles): [1] Illmitz (AT02), [2] Payerne (CH02), [3] Svratouch (CZ01), [4] Kosetice (CZ03), [5] Westerland (DE01), [6] Langenbrügge (DE02), [7] Schauinsland (DE03), [8] Neuglobsow (DE07), [9] Schmücke (DE08), [10] Zingst (DE09), [11] Utö (FI09), [12] Virolahti II (FI17), [13] Oulanka (FI22), [14] Donon (FR08), [15] Revin (FR09), [16] Morvan (FR10), [17] Iraty (FR12), [18] Eskdalemuir (GB02), [19] K-puszta (HU02), [20] Ispra (IT04), [21] Rucava (LV10), [22] Birkenes (NO01), [23] Tustervatn (NO15), [24] Jarczew (PL02), [25] Sniezka (PL03), [26] Leba (PL04), [27] Diabla Gora (PL05), [28] Vavihill (SE11), [29] Chopok (SK02), [30] Stará Lesná (SK04), [31] Starina (SK06), [32] Deuselbach (DE04), [33] Brotjacklriegel (DE05), [34] Ähtäri (FI04), [35] Skreådalen (NO08), [36] Janiskoski (RU01), [37] Pinega (RU13). . 92

4.2 Observed yearly wet deposition (1990 - 2009) of SO_4^{2-} (A) and precipitation pH (B) for measurements within the EMEP network. Station abbreviations and statistical significance of the trend (*: 95%, **: 99%, ***: 99.9% level) at the left hand side of each row, mean yearly trends (mg S m^{-2} a^{-1}, pH a^{-1}) and total change between 1990 and 2009 (in % mass of 1990) as derived from least squares regression at the right-hand side of each row. Stations are sorted by mean wet deposition of SO_4^{2-}. 94

4.3 Like Figure 4.2, but for observed yearly wet deposition of NH_4^+ (A) and NO_3^- (B). Mean changes per year are mg N m^{-2} a^{-1} here. Stations are sorted by mean wet deposition of SO_4^{2-} (Fig. 4.2). 95

4.4 Trends in measured wet deposition of the major inorganic ions (filled circles), and trends in emissions of the respective precursors (country color) in Europe between 1990 and 2009 as percent mass differences for: NO_x emissions with NO_3^- wet deposition (A), NH_3 with NH_4^+ (B), and SO_2 with SO_4^{2-} (C). Measured trend estimated as linear regression on monthly aggregated data. Statistical significance of a monotonic trend (Mann-Kendall test, Mann, 1945; Kendall, 1975) marked by stars: significant on the 95% (-), 99% (+), or 99.9% (*) level. 96

4.5 Maps of the mean mass concentrations of SO_4^{2-} for the simulation with emissions of 1990 and 2009 (top row), and maps of absolute changes in this component considering all emission changes (Δbase) as well as due to changes in emissions of a single precursor (ΔSO_2, ΔNO_x, ΔNH_3, ΔVOC) and the change in f_{NO_2} (Δf_{NO_2}). Absolute changes are mean concentrations of the respective study minus base case with 1990 emissions (ΔX - 1990), except for Δf_{NO_2}, where the 2009 case is the reference. 98

4.6 Like Figure 4.5, but for NO_3^- 99

4.7 Differences in aerosol surface area density (left) and mean N_2O_5 concentration (right) between Δbase and ΔSO_2 in percent. 100

4.8 Like Figure 4.5, but for NH_4^+ 101

4.9 Like Figure 4.5, but for SOA 102

4.10a Modeled changes in mass of inorganic (NH_4^+, NO_3^-, SO_4^{2-}) and secondary organic (SOA) aerosol components (colored bars) between January 2009 and January 1990, the changes in annual precursor emissions (leftmost, white bar) and the changes in average annual wet deposition of all EMEP stations in the region if available (second from the left, gray bar) between 2009 and 1990 for all regions shown in Fig. 4.1 and listed in 4.2. All values are given as change in percent (emitted/wet deposited/ambient aerosol) mass of (January) 1990. 105

4.10b Like Fig. 4.10a, but for the remaining regions. 106

A.1 Overview of mean afternoon (hours 12 - 18) NO_x, O_3 and SO_2 concentrations like in Figure 2.4 but for the spring 2009 period. 112

A.2 Overview of mean afternoon (hours 12 - 18) NO_x, O_3 and SO_2 concentrations like in Figure 2.4 but for the autumn 2008 period. 112

A.3 Overview of mean afternoon (hours 12 - 18) NO_x, O_3 and SO_2 concentrations like in Figure 2.4 but for the winter 2006 period. 113

A.4 Statistics of mean diurnal cycles of several compounds for model and AIRBASE data. Like Figure 2.5 but for the spring 2009 period. 113

A.5 Statistics of mean diurnal cycles of several compounds for model and AIRBASE data. Like Figure 2.5 but for the autumn 2008 period. 114

A.6 Statistics of mean diurnal cycles of several compounds for model and AIRBASE data. Like Figure 2.5 but for the winter 2006 period. 114

A.8 Timeline of aerosol chemical composition. Like Figures 2.9 and 2.10a, 2.10a but for the summer 2006 period. 115

A.9 Comparison of modelled and measured aerosol size distributions at EUSAAR stations. Like Figure 2.11 but for the spring 2009 period. 115

A.7 Timelines of aerosol optical depth (AOD) at several AERONET stations in Europe. Like Figure 2.8 but for the remaining stations. 116

Bibliography

Aan de Brugh, J. M. J., M. Schaap, E. Vignati, F. Dentener, M. Kahnert, M. Sofiev, V. Huijnen, and M. C. Krol, 2011: The European aerosol budget in 2006. *Atmos. Chem. Phys.*, **11 (3)**, 1117–1139, doi:10.5194/acp-11-1117-2011.

Aas, W., et al., 1996: *EMEP manual for sampling and chemical analysis*. Norwegian Institute for Air Research, Kjeller, EMEP/CCC-Report 1/95 ed., http://www.nilu.no/projects/ccc/manual/.

Aas, W., et al., 2011: Transboundary acidification, eutrophication and ground level ozone in europe in 2009. Emep status report 2011, EMEP CCC, MSC-W, CEIP and CIAM. URL `http://www.emep.int/publ/common_publications.html`.

Abbatt, J., 1997: Interaction of HNO_3 with water-ice surfaces at temperatures of the free troposphere. *Geophys. Res. Lett.*, **24 (12)**, 1479–1482.

Ackerman, A., O. Toon, D. Stevens, A. Heymsfield, V. Ramanathan, and E. Welton, 2000: Reduction of tropical cloudiness by soot. *Science*, **288 (5468)**, 1042.

Ackermann, I. J., H. Hass, M. Memmesheimer, A. Ebel, F. S. Binkowski, and U. Shankar, 1998: Modal Aerosol Dynamics Model for Europe: Development and First Applications. *Atmos. Environ.*, **32 (17)**, 2981–2999.

Aiken, A. C., et al., 2010: Mexico city aerosol analysis during MILAGRO using high resolution aerosol mass spectrometry at the urban supersite (T0) - Part 2: Analysis of the biomass burning contribution and the non-fossil carbon fraction. *Atmos. Chem. Phys.*, **10 (12)**, 5315–5341, doi:10.5194/acp-10-5315-2010, URL `http://www.atmos-chem-phys.net/10/5315/2010/`.

Aksoyoglu, S., J. Keller, I. Barmpadimos, D. Oderbolz, V. A. Lanz, A. S. H. Prévôt, and U. Baltensperger, 2011: Aerosol modelling in Europe with a focus on Switzerland during summer and winter episodes. *Atmos. Chem. Phys.*, **11 (14)**, 7355–7373, doi:10.5194/acp-11-7355-2011.

Aktories, K., U. Förstermann, F. Hofmann, and K. Starke, 2009: *Allgemeine und spezielle Pharmakologie und Toxikologie*. 10th ed., Elsevier GmbH.

Albrecht, B., 1989: Aerosols, cloud microphysics, and fractional cloudiness. *Science*, **245 (4923)**, 1227.

Alexander, B., R. Park, D. Jacob, and S. Gong, 2009: Transition metal-catalyzed oxidation of atmospheric sulfur: Global implications for the sulfur budget. *J. Geophys. Res.*, **114**, D02 309.

Alfarra, M., et al., 2007: Identification of the mass spectral signature of organic aerosols from wood burning emissions. *Environ. Sci. Technol.*, **41 (16)**, 5770–5777.

Altieri, K., A. Carlton, H. Lim, B. Turpin, and S. Seitzinger, 2006: Evidence for oligomer formation in clouds: Reactions of isoprene oxidation products. *Environ. Sci. Technol.*, **40 (16)**, 4956–4960.

Andreae, M. and P. Crutzen, 1997: Atmospheric aerosols: Biogeochemical sources and role in atmospheric chemistry. *Science*, **276 (5315)**, 1052.

Andreae, M., et al., 1985: Dimethyl sulfide in the marine atmosphere. *J. Geophys. Res.*, **90 (D7)**, 12 891–12.

Andreae, M. O. and A. Gelencsér, 2006: Black carbon or brown carbon? The nature of light-absorbing carbonaceous aerosols. *Atmos. Chem. Phys.*, **6 (10)**, 3131–3148, doi:10.5194/acp-6-3131-2006, URL `http://www.atmos-chem-phys.net/6/3131/2006/`.

Andreani-Aksoyoglu, S., J. Keller, and A. Prévôt, 2008: *Air Pollution Modeling and Its Application XVII*, chap. Aerosol Modelling with CAMX4 and PMCAMX: A Comparison Study, 247–256. NATO Science for Peace and Security Series C: Environmental Security, Springer.

Andronache, C., 2003: Estimated variability of below-cloud aerosol removal by rainfall for observed aerosol size distributions. *Atmos. Chem. Phys.*, **3 (1)**, 131–143.

Andronache, C., 2004: Precipitation removal of ultrafine aerosol particles from the atmospheric boundary layer. *J. Geophys. Res.*, **109 (D16)**, D16S07.

Asmi, A., et al., 2011: Number size distributions and seasonality of submicron particles in Europe 2008 - 2009. *Atmos. Chem. Phys.*, **11 (11)**, 5505–5538, doi:10.5194/acp-11-5505-2011.

Atkinson, R., 2000: Atmospheric chemistry of VOCs and NO_x. *Atmos. Environ.*, **34 (12-14)**, 2063–2101.

Atkinson, R., S. Aschmann, J. Arey, and B. Shorees, 1992: Formation of OH radicals in the gas phase reactions of O_3 with a series of terpenes. *J. Geophys. Res.*, **97 (D5)**, 6065–6073.

Atkinson, R., et al., 2004: Evaluated kinetic and photochemical data for atmospheric chemistry: Volume I - gas phase reactions of O_x, HO_x, NO_x and SO_x species. *Atmos. Chem. Phys.*, **4 (6)**, 1461–1738, doi:10.5194/acp-4-1461-2004, URL `http://www.atmos-chem-phys.net/4/1461/2004/`.

Baer, M. and K. Nester, 1992: Parametrization of trace gas dry deposition velocities for a regional mesoscale diffusion model. *Annales Geophysicae*.

Baldauf, M. and J. Schulz, 2004: Prognostic precipitation in the Lokal Modell (LM) of DWD. 177–180 pp., COSMO Newsletter.

Baldauf, M., A. Seifert, J. Förstner, D. Majewski, M. Raschendorfer, and T. Reinhardt, 2011: Operational Convective-Scale Numerical Weather Prediction with the COSMO Model: Description and Sensitivities. *Mon. Weather Rev.*, **139 (12)**, 3887–3905, doi:10.1175/MWR-D-10-05013.1, URL `http://dx.doi.org/10.1175/MWR-D-10-05013.1`.

Baltensperger, U., H. Gäggeler, D. Jost, U. Nieveler, and M. Schwikowski, 1991: In-cloud scavenging by snow at a high-alpine site. *J. Aerosol Sci.*, **22**, S541–S544.

Bangert, M., C. Kottmeier, B. Vogel, and H. Vogel, 2011: Regional scale effects of the aerosol cloud interaction simulated with an online coupled comprehensive chemistry model. *Atmos. Chem. Phys.*, **11 (9)**, 4411–4423, doi:10.5194/acp-11-4411-2011.

Barmpadimos, I., C. Hueglin, J. Keller, S. Henne, and A. Prévôt, 2011: Influence of meteorology on PM_{10} trends and variability in Switzerland from 1991 to 2008. *Atmos. Chem. Phys.*, **11**, 1813–1835.

Barthlott, C., et al., 2011: Initiation of deep convection at marginal instability in an ensemble of mesoscale models: a case-study from COPS. *Q. J. R. Meteorol. Soc.*, **137 (S1)**, 118–136, doi:10.1002/qj.707, URL `http://dx.doi.org/10.1002/qj.707`.

Bartholomé, E. and A. Belward, 2005: GLC2000: a new approach to global land cover mapping from Earth observation data. *International Journal of Remote Sensing*, **26 (9)**, 1959–1977.

Bates, T., J. Cline, R. Gammon, and S. Kelly-Hansen, 1987: Regional and seasonal variations in the flux of oceanic dimethylsulfide to the atmosphere. *J. Geophys. Res.*, **92 (C3)**, 2930–2938.

Bäumer, D., U. Lohmann, G. Lesins, J. Li, and B. Croft, 2007: Parameterizing the optical properties of carbonaceous aerosols in the Canadian Centre for Climate Modeling and Analysis Atmospheric General Circulation Model with impacts on global radiation and energy fluxes. *J. Geophys. Res.*, **112 (D10)**, D10 207.

Bernstein, J., et al., 2004: Health effects of air pollution. *Journal of Allergy and Clinical Immunology*, **114 (5)**, 1116–1123.

Bessagnet, B., A. Hodzic, R. Vautard, M. Beekmann, S. Cheinet, C. Honoré, C. Liousse, and L. Rouil, 2004: Aerosol modeling with CHIMERE–preliminary evaluation at the continental scale. *Atmos. Environ.*, **38 (18)**, 2803–2817.

Binkowski, F. and U. Shankar, 1995: The regional particulate matter model 1. model description and preliminary results. *J. Geophys. Res.*, **100 (D12)**, 26 191–26.

Birmili, W., et al., 2009: Atmospheric aerosol measurements in the German Ultrafine Aerosol Network (GUAN): Part 1–soot and particle number size distributions. *Gefahrst. Reinh. Luft*, **69 (4)**, 137–145.

Bromley, L. A., 1973: Thermodynamic properties of strong electrolytes in aqueous solutions. *AIChE J.*, **19 (2)**, 313–320, doi:10.1002/aic.690190216, URL `http://dx.doi.org/10.1002/aic.690190216`.

Brown, D., et al., 2007a: An in vitro study of the potential of carbon nanotubes and nanofibres to induce inflammatory mediators and frustrated phagocytosis. *Carbon*, **45 (9)**, 1743–1756.

Brown, S., W. Dubé, H. Osthoff, D. Wolfe, W. Angevine, and A. Ravishankara, 2007b: High resolution vertical distributions of NO_3 and N_2O_5 through the nocturnal boundary layer. *Atmos. Chem. Phys.*, **7**, 139–149.

Brown, S., et al., 2004: Nighttime removal of NO_x in the summer marine boundary layer. *Geophys. Res. Lett.*, **31**, 7717.

Byun, D. and J. Ching, 1999: *Science algorithms of the EPA Models-3 community multiscale air quality (CMAQ) modeling system*. United States Environmental Protection Agency. Office of Research and Development and National Exposure Research Laboratory (US). Atmospheric Modeling Division.

Canagaratna, M., et al., 2007: Chemical and microphysical characterization of ambient aerosols with the Aerodyne aerosol mass spectrometer. *Mass Spectrometry Reviews*, **26 (2)**, 185–222.

Carlton, A., B. Turpin, K. Altieri, S. Seitzinger, A. Reff, H. Lim, and B. Ervens, 2007: Atmospheric oxalic acid and SOA production from glyoxal: Results of aqueous photooxidation experiments. *Atmos. Environ.*, **41 (35)**, 7588–7602.

Carlton, A., C. Wiedinmyer, and J. Kroll, 2009: A review of Secondary Organic Aerosol (SOA) formation from isoprene. *Atmos. Chem. Phys.*, **9**, 4987–5005.

Carroll, M., B. Ridley, D. Montzka, G. Hubler, J. Walega, R. Norton, B. Huebert, and F. Grahek, 1992: Measurements of nitric oxide and nitrogen dioxide during the Mauna Loa Observatory Photochemistry Experiment. *J. Geophys. Res.*, **97 (D10)**, 10 361–10.

Carter, W. P. L., 2010: Development of the SAPRC-07 chemical mechanism and updated ozone reactivity scales. Report to the California Air Resources Board Contracts No. 03-318, 06-408, and 07-730, California Air Resources Board.

Chameides, W. and J. Walker, 1973: A photochemical theory of tropospheric ozone. *J. Geophys. Res.*, **78 (36)**, 8751–8760.

Chang, T., 1984: Rain and snow scavenging of HNO_3 vapor in the atmosphere. *Atmos. Environ.*, **18 (1)**, 191–197.

Chapman, E., W. Gustafson Jr, R. Easter, J. Barnard, S. Ghan, M. Pekour, and J. Fast, 2009: Coupling aerosol-cloud-radiative processes in the WRF-Chem model: Investigating the radiative impact of elevated point sources. *Atmos. Chem. Phys.*, **9 (3)**, 945–964.

Choi, Y. and H. Fernando, 2008: Implementation of a windblown dust parameterization into MODELS-3/CMAQ: Application to episodic PM events in the US/Mexico border. *Atmos. Environ.*, **42 (24)**, 6039–6046.

Chou, M., M. Suarez, C. Ho, M. Yan, and K. Lee, 1998: Parameterizations for cloud overlapping and shortwave single-scattering properties for use in general circulation and cloud ensemble models. *J. Clim.*, **11 (2)**, 202–214.

Christensen, J., et al., 2007: *Climate Change 2007: The Physical Science Basis. Contribution of Working Group I to the Fourth Assessment Report of the Intergovernmental Panel on Climate Change*, chap. Regional Climate Projections, 996. Cambridge University Press, Cambridge, United Kingdom and New York, NY, USA.

Ciobanu, V., C. Marcolli, U. Krieger, U. Weers, and T. Peter, 2009: Liquid- liquid phase separation in mixed organic/inorganic aerosol particles. *J. Phys. Chem. A*, **113 (41)**, 10 966–10 978.

Claeys, M., et al., 2004: Formation of secondary organic aerosols through photooxidation of isoprene. *Science*, **303 (5661)**, 1173.

Clegg, S., J. Seinfeld, and E. Edney, 2003: Thermodynamic modelling of aqueous aerosols containing electrolytes and dissolved organic compounds. II. An extended Zdanovskii-Stokes-Robinson approach. *J. Aerosol Sci.*, **34 (6)**, 667–690.

Colberg, C., B. Luo, H. Wernli, T. Koop, and T. Peter, 2003: A novel model to predict the physical state of atmospheric $H_2SO_4/NH_3/H_2O$ aerosol particles. *Atmos. Chem. Phys.*, **3**, 909–924.

Corbett, J. and H. Koehler, 2003: Updated emissions from ocean shipping. *J. Geophys. Res.*, **108 (D20)**, 4650–64.

Cotton, W., G. Bryan, and S. van den Heever, 2011: Cumulonimbus clouds and severe convective storms. *International Geophysics*, **99**, 315–454.

Cross, E. S., et al., 2007: Laboratory and ambient particle density determinations using light scattering in conjunction with aerosol mass spectrometry. *Aerosol Sci. Technol.*, **41 (4)**, 343–359, doi:10.1080/02786820701199736.

Crutzen, P., 1970: The influence of nitrogen oxides on the atmospheric ozone content. *Q. J. R. Meteorol. Soc.*, **96 (408)**, 320–325.

Damian, V., A. Sandu, M. Damian, F. Potra, and G. Carmichael, 2002: The kinetic preprocessor KPP-a software environment for solving chemical kinetics. *Computers & chemical engineering*, **26 (11)**, 1567–1579.

De Gouw, J. and J. Jimenez, 2009: Organic aerosols in the Earth's atmosphere. *Environ. Sci. Technol.*, **43 (20)**, 7614–7618.

De Gouw, J., et al., 2005: Budget of organic carbon in a polluted atmosphere: Results from the New England Air Quality Study in 2002. *J. Geophys. Res.*, **110**.

de Meij, A., M. Krol, F. Dentener, E. Vignati, C. Cuvelier, and P. Thunis, 2006: The sensitivity of aerosol in Europe to two different emission inventories and temporal distribution of emissions. *Atmos. Chem. Phys.*, **6**, 4287–4309.

DeCaria, A., K. Pickering, G. Stenchikov, and L. Ott, 2005: Lightning-generated NO_x and its impact on tropospheric ozone production: A three-dimensional modeling study of a Stratosphere-Troposphere Experiment: Radiation, Aerosols and Ozone (STERAO-A) thunderstorm. *J. Geophys. Res.*, **110 (D14)**.

DeCarlo, P., J. Slowik, D. Worsnop, P. Davidovits, and J. Jimenez, 2004: Particle morphology and density characterization by combined mobility and aerodynamic diameter measurements. part 1: Theory. *Aerosol Sci. Technol.*, **38 (12)**, 1185–1205.

Denier van der Gon, H., A. Visschedijk, H. van der Brugh, and R. Dröge, 2010: A high resolution European emission data base for the year 2005, A contribution to UBA- Projekt PAREST: Particle Reduction Strategies. TNO-report TNO-034-UT-2010-01895_RPT-ML, TNO.

Dentener, F., G. Carmichael, Y. Zhang, J. Lelieveld, and P. Crutzen, 1996: Role of mineral aerosol as a reactive surface in the global troposphere. *J. Geophys. Res.*, **101 (D17)**, 22 869–22.

Dentener, F. and P. Crutzen, 1994: A three-dimensional model of the global ammonia cycle. *J. Atmos. Chem.*, **19 (4)**, 331–369.

Derwent, R., M. Jenkin, and S. Saunders, 1996: Photochemical ozone creation potentials for a large number of reactive hydrocarbons under European conditions. *Atmos. Environ.*, **30 (2)**, 181–199.

Dockery, D. and A. Pope, 1996: *Particles in Our Air: Concentrations and Health Effects*, chap. Epidemiology of acute health effects: Summary of time-scale studies, 123–148. Harvard University Press, Cambridge MA.

Dockery, D., et al., 1996: Health effects of acid aerosols on North American children: respiratory symptoms. *Environmental health perspectives*, **104 (5)**, 500.

Dodge, M., 1977: Effect of selected parameters on predictions of a photochemical model. Tech. rep., Environmental Protection Agency, Research Triangle Park, NC (USA). Environmental Sciences Research Lab.

Dodge, M., 2000: Chemical oxidant mechanisms for air quality modeling: critical review. *Atmos. Environ.*, **34 (12-14)**, 2103–2130.

Doms, G., 2011: A Description of the Nonhydrostatic Regional COSMO-Model, Part I: Dynamics and Numerics. Tech. rep., Deutscher Wetterdienst, Offenbach.

Doms, G., et al., 2011: A Description of the Nonhydrostatic Regional COSMO Model, Part II: Physical Parameterization. Tech. rep., Deutscher Wetterdienst, Offenbach.

Donahue, N., S. Epstein, S. Pandis, and A. Robinson, 2011: A two-dimensional volatility basis set: 1. organic-aerosol mixing thermodynamics. *Atmos. Chem. Phys.*, **11**, 3303–3318.

Donahue, N., A. Robinson, C. Stanier, and S. Pandis, 2006: Coupled partitioning, dilution, and chemical aging of semivolatile organics. *Environ. Sci. Technol.*, **40 (8)**, 2635–2643.

Donaldson, K., V. Stone, P. Gilmour, D. Brown, and W. MacNee, 2000: Ultrafine particles: mechanisms of lung injury. *Philosophical Transactions of the Royal Society of London. Series A: Mathematical, Physical and Engineering Sciences*, **358 (1775)**, 2741.

Donaldson, K. and C. Tran, 2004: An introduction to the short-term toxicology of respirable industrial fibres. *Mutation Research/Fundamental and Molecular Mechanisms of Mutagenesis*, **553 (1-2)**, 5 – 9, doi:10.1016/j.mrfmmm.2004.06.011, URL `http://www.sciencedirect.com/science/article/pii/S0027510704001915`.

Donaldson, K., L. Tran, L. Jimenez, R. Duffin, D. Newby, N. Mills, W. MacNee, and V. Stone, 2005: Combustion-derived nanoparticles: a review of their toxicology following inhalation exposure. *Particle and Fibre Toxicology*, **2 (1)**, 10.

Dunlea, E., et al., 2007: Evaluation of nitrogen dioxide chemiluminescence monitors in a polluted urban environment. *Atmos. Chem. Phys.*, **7 (10)**, 2691–2704.

Elbern, H., 1997: Parallelization and load balancing of a comprehensive atmospheric chemistry transport model. *Atmos. Environ.*, **31 (21)**, 3561–3574.

Elleman, R. and D. Covert, 2010: Aerosol size distribution modeling with the Community Multiscale Air Quality modeling system in the Pacific Northwest: 3. Size distribution of particles emitted into a mesoscale model. *J. Geophys. Res.*, **115 (D3)**, D03 204.

Ellis, R., J. Murphy, M. Markovic, T. VandenBoer, P. Makar, J. Brook, and C. Mihele, 2011: The influence of gas-particle partitioning and surface-atmosphere exchange on ammonia during BAQS-Met. *Atmos. Chem. Phys.*, **11**, 133–145.

EMEP/CORINAIR, 2001: Atmospheric emission inventory guidebook 3^{rd} edition. Technical Report 30, European Environmental Agency.

Emmons, L. K., et al., 2010: Description and evaluation of the Model for Ozone and Related chemical Tracers, version 4 (MOZART-4). *Geoscientific Model Development*, **3 (1)**, 43–67, doi:10.5194/gmd-3-43-2010.

Endresen, O., J. Bakke, E. Sorgard, T. Flatlandsmo Berglen, and P. Holmvang, 2005: Improved modelling of ship SO_2 emissions–a fuel-based approach. *Atmos. Environ.*, **39 (20)**, 3621–3628.

ENVIRON, 2004: User's guide - comprehensive air-quality model with extensions. Tech. rep., ENVIRON International Corporation, Novato, CA.

Ervens, B., A. Carlton, B. Turpin, K. Altieri, S. Kreidenweis, and G. Feingold, 2008: Secondary organic aerosol yields from cloud-processing of isoprene oxidation products. *Geophys. Res. Lett.*, **35 (L02816)**, L02 816.

Ervens, B., B. J. Turpin, and R. J. Weber, 2011: Secondary organic aerosol formation in cloud droplets and aqueous particles (aqSOA): a review of laboratory, field and model studies. *Atmos. Chem. Phys.*, **11 (21)**, 11 069–11 102, doi:10.5194/acp-11-11069-2011, URL `http://www.atmos-chem-phys.net/11/11069/2011/`.

Ervens, B., et al., 2003: CAPRAM 2.4 (MODAC mechanism): An extended and condensed tropospheric aqueous phase mechanism and its application. *J. Geophys. Res.*, **108 (D14)**, 4426.

Fagerli, H. and W. Aas, 2008: Trends of nitrogen in air and precipitation: Model results and observations at EMEP sites in Europe, 1980-2003. *Environ. Pollut. (Oxford, U. K.)*, **154 (3)**, 448–461.

Farmer, D., A. Matsunaga, K. Docherty, J. Surratt, J. Seinfeld, P. Ziemann, and J. Jimenez, 2010: Response of an aerosol mass spectrometer to organonitrates and organosulfates and implications for atmospheric chemistry. *Proc. Natl. Acad. Sci. U. S. A.*, **107 (15)**, 6670.

Fast, J., W. Gustafson Jr, R. Easter, R. Zaveri, J. Barnard, E. Chapman, G. Grell, and S. Peckham, 2006: Evolution of ozone, particulates, and aerosol direct radiative forcing in the vicinity of Houston using a fully coupled meteorology-chemistry-aerosol model. *J. Geophys. Res.*, **111 (D21)**, D21 305.

Fast, J., et al., 2009: Evaluating simulated primary anthropogenic and biomass burning organic aerosols during MILAGRO: implications for assessing treatments of secondary organic aerosols. *Atmos. Chem. Phys.*, **9 (16)**, 6191–6215, doi:10.5194/acp-9-6191-2009.

Feichter, J., E. Kjellström, H. Rodhe, F. Dentener, J. Lelieveldi, and G. Roelofs, 1996: Simulation of the tropospheric sulfur cycle in a global climate model. *Atmos. Environ.*, **30 (10-11)**, 1693–1707.

Feingold, G. and S. Kreidenweis, 2000: Does cloud processing of aerosol enhance droplet concentrations? *J. Geophys. Res.*, **105 (D19)**, 24 351–24.

Fountoukis, C. and A. Nenes, 2007: ISORROPIA II: a computationally efficient thermodynamic equilibrium model for $K^+ - Ca^{2+} - Mg^{2+} - NH_4^+ - Na^+ - SO_4^{2-} - NO_3^- - Cl^- - H_2O$ aerosols. *Atmos. Chem. Phys.*, **7**, 4639–4659.

Fowler, D., R. Smith, J. Muller, G. Hayman, and K. Vincent, 2005: Changes in the atmospheric deposition of acidifying compounds in the UK between 1986 and 2001. *Environ. Pollut. (Oxford, U. K.)*, **137 (1)**, 15–25.

Geiger, H., I. Barnes, I. Bejan, T. Benter, and M. Spittler, 2003: The tropospheric degradation of isoprene: an updated module for the regional atmospheric chemistry mechanism. *Atmos. Environ.*, **37 (11)**, 1503–1519.

Gelbard, F. and J. Seinfeld, 1980: Simulation of multicomponent aerosol dynamics. *Journal of Colloid and Interface Science*, **78 (2)**, 485–501.

Gondwe, M., M. Krol, W. Gieskes, W. Klaassen, and H. De Baar, 2003: The contribution of ocean-leaving DMS to the global atmospheric burdens of DMS, MSA, SO_2, and NSS $- SO_4^{2-}$. *Global Biogeochem. Cycles*, **17 (2)**, 1056.

Gong, S., et al., 2003: Canadian Aerosol Module: A size-segregated simulation of atmospheric aerosol processes for climate and air quality models 1. Module development. *J. Geophys. Res.*, **108 (D1)**.

Gong, W., C. Stroud, and L. Zhang, 2011: Cloud processing of gases and aerosols in air quality modeling. *Atmosphere*, **2 (4)**, 567–616.

Grell, G. and A. Baklanov, 2011: Integrated modeling for forecasting weather and air quality: A call for fully coupled approaches. *Atmos. Environ.*, **45 (38)**, 6845 – 6851, doi:10.1016/j.atmosenv.2011.01.017, URL `http://www.sciencedirect.com/science/article/pii/S1352231011000240`.

Grell, G., J. Dudhia, and D. Stauffer, 1994: A description of the fifth-generation Penn State/NCAR mesoscale model (MM5). Tech. rep., National Center for Atmospheric Research (NCAR). Mesoscale and Microscale Meteorology Divison.

Grell, G., S. Peckham, R. Schmitz, S. McKeen, G. Frost, W. Skamarock, and B. Eder, 2005: Fully coupled "online" chemistry within the WRF model. *Atmos. Environ.*, **39 (37)**, 6957–6975.

Grice, S., J. Stedman, A. Kent, M. Hobson, J. Norris, J. Abbott, and S. Cooke, 2009: Recent trends and projections of primary NO_2 emissions in Europe. *Atmos. Environ.*, **43 (13)**, 2154–2167.

Griffin, R., D. Cocker, R. Flagan, and J. Seinfeld, 1999: Organic aerosol formation from the oxidation of biogenic hydrocarbons. *J. Geophys. Res.*, **104 (D3)**, 3555–3567.

Guenther, A., T. Karl, P. Harley, C. Wiedinmyer, P. I. Palmer, and C. Geron, 2006: Estimates of global terrestrial isoprene emissions using MEGAN (Model of Emissions of Gases and Aerosols from Nature). *Atmos. Chem. Phys.*, **6 (11)**, 3181–3210, doi:10.5194/acp-6-3181-2006, URL `http://www.atmos-chem-phys.net/6/3181/2006/`.

Guerreiro, C., C. Hak, J. Horálek, P. Kurfürst, J. Ostatnická, F. de Leeuw, and C. Nagl, 2011: Status and trends of NO_2 ambient concentrations in Europe. ETC/ACC Technical Paper 2010/19, European Topic Centre on Air Pollution and Climate Change Mitigation.

Hairer, E. and G. Wanner, 2010: Numerical experiments. *Solving Ordinary Differential Equations II*, 143–166.

Hallquist, M., et al., 2009: The formation, properties and impact of secondary organic aerosol: current and emerging issues. *Atmos. Chem. Phys.*, **9 (14)**, 5155.

Hastie, T. and R. Tibshirani, 1990: *Generalized additive models*. Chapman & Hall/CRC.

Hayn, M., S. Beirle, F. Hamprecht, U. Platt, B. Menze, and T. Wagner, 2009: Analysing spatio-temporal patterns of the global NO_2-distribution retrieved from GOME satellite observations using a generalized additive model. *Atmos. Chem. Phys.*, **9**, 6459–6477.

Haywood, J. and O. Boucher, 2000: Estimates of the direct and indirect radiative forcing due to tropospheric aerosols: A review. *Rev. Geophys.*, **38 (4)**, 513–543.

Hegg, D. and P. Hobbs, 1978: Oxidation of sulfur dioxide in aqueous systems with particular reference to the atmosphere. *Atmos. Environ.*, **12 (1-3)**, 241–253.

Heinemann, G. and M. Kerschgens, 2005: Comparison of methods for area-averaging surface energy fluxes over heterogeneous land surfaces using high-resolution non-hydrostatic simulations. *International Journal of Climatology*, **25 (3)**, 379–403.

Henne, S., D. Brunner, D. Folini, S. Solberg, J. Klausen, and B. Buchmann, 2010: Assessment of parameters describing representativeness of air quality in-situ measurement sites. *Atmos. Chem. Phys.*, **10 (8)**, 3561–3581.

Hesstvedt, E., Ø. Hov, and I. Isaksen, 1978: Quasi-steady-state approximations in air pollution modeling: Comparison of two numerical schemes for oxidant prediction. *International Journal of Chemical Kinetics*, **10 (9)**, 971–994.

Higgins, J., 2004: *An introduction to modern nonparametric statistics*. Brooks/Cole Pacific Grove (California).

Hindmarsh, A., 1972: Gear: Ordinary differential equation system solver. Tech. rep., California Univ., Livermore (USA). Lawrence Livermore Lab.

Hodzic, A., J. L. Jimenez, S. Madronich, M. R. Canagaratna, P. F. DeCarlo, L. Kleinman, and J. Fast, 2010: Modeling organic aerosols in a megacity: potential contribution of semi-volatile and intermediate volatility primary organic compounds to secondary organic aerosol formation. *Atmos. Chem. Phys.*, **10 (12)**, 5491–5514, doi:10.5194/acp-10-5491-2010.

Hodzic, A., et al., 2009: Modeling organic aerosols during MILAGRO: importance of biogenic secondary organic aerosols. *Atmos. Chem. Phys.*, **9 (18)**, 6949–6981, doi:10.5194/acp-9-6949-2009.

Hoek, G., B. Brunekreef, S. Goldbohm, P. Fischer, and P. van den Brandt, 2002: Association between mortality and indicators of traffic-related air pollution in the Netherlands: a cohort study. *Lancet*, **360 (9341)**, 1203–1209.

Hohenegger, C., P. Brockhaus, and C. Schar, 2008: Towards climate simulations at cloud-resolving scales. *Meteorol. Z.*, **17 (4)**, 383–394.

Holben, B., et al., 1998: AERONET–A federated instrument network and data archive for aerosol characterization. *Remote Sensing of Environment*, **66 (1)**, 1–16.

Holst, J., H. Mayer, and T. Holst, 2008: Effect of meteorological exchange conditions on PM_{10} concentration. *Meteorol. Z.*, **17 (3)**, 273–282.

Hoppel, W., J. Fitzgerald, G. Frick, R. Larson, and E. Mack, 1990: Aerosol size distributions and optical properties found in the marine boundary layer over the Atlantic Ocean. *J. Geophys. Res.*, **95 (D4)**, 3659–3686.

Hov, Ø., I. Isaksen, and E. Hesstvedt, 1978: A numerical method to predict secondary air pollutants with an application on oxidant generation in an urban atmosphere. *Boundary Layer Phys. Appl. to Specific Probl. of Air Pollution*, WMO, Vol. Boundary Layer Phys. Appl. to Specific Probl. of Air Pollution, 219–226.

Hůnova, I., J. Šantroch, and J. Ostatnická, 2004: Ambient air quality and deposition trends at rural stations in the Czech Republic during 1993-2001. *Atmos. Environ.*, **38 (6)**, 887–898.

Hüglin, C., B. Buchmann, and R. Weber, 2006: Long-term observation of real-world road traffic emission factors on a motorway in Switzerland. *Atmos. Environ.*, **40 (20)**, 3696–3709.

Huijnen, V., et al., 2010: Comparison of OMI NO_2 tropospheric columns with an ensemble of global and European regional air quality models. *Atmos. Chem. Phys.*, **10**, 3273–3296.

Jacobson, M., 2005: *Fundamentals of atmospheric modeling*. Cambridge Univ Pr.

Jacobson, M. Z., 1994: Developing, Coupling, and Applying a Gas, Aerosol, Transport, and Radiation Model to Study Urban and Regional Air Pollution. Ph.D. thesis, University of California, Los Angeles.

Jaeger, E. and S. Seneviratne, 2010: Impact of soil moisture–atmosphere coupling on European climate extremes and trends in a regional climate model. *Climate Dynamics*, 1–21.

Jimenez, J., et al., 2009: Evolution of organic aerosols in the atmosphere. *Science*, **326 (5959)**, 1525.

Jöckel, P., R. Sander, A. Kerkweg, H. Tost, and J. Lelieveld, 2005: Technical Note: The Modular Earth Submodel System (MESSy)–a new approach towards Earth System Modeling. *Atmos. Chem. Phys.*, **5**, 433–444.

Jonson, J., D. Simpson, H. Fagerli, S. Solberg, et al., 2006: Can we explain the trends in european ozone levels? *Atmos. Chem. Phys.*, **6 (1)**, 51–66.

Kalberer, M., et al., 2004: Identification of polymers as major components of atmospheric organic aerosol. *Science*, **303**.

Kanakidou, M., et al., 2005: Organic aerosol and global climate modelling: a review. *Atmos. Chem. Phys.*, **5 (4)**, 1053–1123, URL `http://www.atmos-chem-phys.net/5/1053/2005/`.

Kendall, M., 1975: Rank correlation measures. *Charles Griffin, London*, **202**.

Kerminen, V. and A. Wexler, 1994: Post-fog nucleation of $H_2SO_4^{2-} - H_2O$ particles in smog. *Atmos. Environ.*, **28 (15)**, 2399–2406.

Kerminen, V.-M., et al., 2010: Atmospheric nucleation: highlights of the EUCAARI project and future directions. *Atmos. Chem. Phys.*, **10 (22)**, 10 829–10 848, doi:10.5194/acp-10-10829-2010, URL `http://www.atmos-chem-phys.net/10/10829/2010/`.

Kirkby, J., et al., 2011: Role of sulphuric acid, ammonia and galactic cosmic rays in atmospheric aerosol nucleation. *Nature*, **476 (7361)**, 429–433.

Kleinman, L., et al., 1997: Dependence of ozone production on no and hydrocarbons in the troposphere. *Geophys. Res. Lett.*, **24 (18)**, 2299–2302.

Knote, C., et al., 2011: Towards an online-coupled chemistry-climate model: evaluation of trace gases and aerosols in COSMO-ART. *Geoscientific Model Development*, **4 (4)**, 1077–1102, doi:10.5194/gmd-4-1077-2011, URL `http://www.geosci-model-dev.net/4/1077/2011/`.

Köhler, H., 1936: The nucleus in and the growth of hygroscopic droplets. *Trans. Faraday Soc.*, **32**, 1152–1161.

Korhonen, P., M. Kulmala, A. Laaksonen, Y. Viisanen, R. McGraw, and J. Seinfeld, 1999: Ternary nucleation of H_2SO_4, NH_3, and H_2O in the atmosphere. *J. Geophys. Res.*, **104 (D21)**, 26 349–26.

Korsholm, U., A. Baklanov, A. Gross, A. Mahura, B. Sass, and E. Kaas, 2008: Online coupled chemical weather forecasting based on HIRLAM–overview and prospective of Enviro-HIRLAM. HIRLAM Newsletter 54.

Kreidenweis, S., et al., 2003: Modification of aerosol mass and size distribution due to aqueous-phase SO_2 oxidation in clouds: Comparisons of several models. *J. Geophys. Res.*, **108 (D7)**, 4213.

Kroll, J., J. Smith, D. Che, S. Kessler, D. Worsnop, and K. Wilson, 2009: Measurement of fragmentation and functionalization pathways in the heterogeneous oxidation of oxidized organic aerosol. *Phys. Chem. Chem. Phys.*, **11 (36)**, 8005–8014.

Kuenen, J., H. Denier van der Gon, A. Visschedijk, and H. van der Brugh, 2011: High resolution European emission inventory for the years 2003 - 2007. Tno-report tno-060-ut-2011-00588, TNO.

Kulmala, M., L. Pirjola, and J. Mäkelä, 2000: Stable sulphate clusters as a source of new atmospheric particles. *Nature*, **404 (6773)**, 66–69.

Kulmala, M., H. Vehkamäki, T. Petäjä, M. Dal Maso, A. Lauri, V. Kerminen, W. Birmili, and P. McMurry, 2004: Formation and growth rates of ultrafine atmospheric particles: a review of observations. *J. Aerosol Sci.*, **35 (2)**, 143–176.

Kulmala, M., et al., 2009: Introduction: European Integrated Project on Aerosol Cloud Climate and Air Quality interactions (EUCAARI)-integrating aerosol research from nano to global scales. *Atmos. Chem. Phys.*, **9 (8)**, 2825–2841.

Kusik, C. and H. Meissner, 1978: Electrolyte activity coefficients in inorganic processing. *Fundamental Aspects of Hydrometallurgical Processes, Proc. Conf., Chicago (IL), USA*, Chicago (IL), USA, AIChE Symposium Series, Vol. 74, 14–20.

Laden, F., J. Schwartz, F. E. Speizer, and D. W. Dockery, 2006: Reduction in Fine Particulate Air Pollution and Mortality: Extended Follow-up of the Harvard Six Cities Study. *Am. J. Respir. Crit. Care Med.*, **173 (6)**, 667–672, doi:10.1164/rccm.200503-443OC.

Lanz, V., M. Alfarra, U. Baltensperger, B. Buchmann, C. Hueglin, and A. Prevot, 2007: Source apportionment of submicron organic aerosols at an urban site by factor analytical modelling of aerosol mass spectra. *Atmos. Chem. Phys.*, **7 (6)**, 1503–1522.

Lanz, V., et al., 2010: Characterization of aerosol chemical composition with aerosol mass spectrometry in central europe: an overview. *Atmos. Chem. Phys.*, **10**, 10 453–10 471.

Lawrence, M. and P. Crutzen, 1998: The impact of cloud particle gravitational settling on soluble trace gas distributions. *Tellus B*, **50 (3)**, 263–289.

Levy, R., L. Remer, S. Mattoo, E. Vermote, and Y. Kaufman, 2007: Second-generation operational algorithm: Retrieval of aerosol properties over land from inversion of Moderate Resolution Imaging Spectroradiometer spectral reflectance. *J. Geophys. Res.*, **112 (D13211)**.

Li, G., W. Lei, M. Zavala, R. Volkamer, S. Dusanter, P. Stevens, and L. Molina, 2010: Impacts of HONO sources on the photochemistry in Mexico City during the MCMA-2006/MILAGO Campaign. *Atmos. Chem. Phys.*, **10**, 6551–6567.

Lieber, M. and R. Wolke, 2008: Optimizing the coupling in parallel air quality model systems. *Environmental Modelling & Software*, **23 (2)**, 235–243.

Lim, H., A. Carlton, and B. Turpin, 2005: Isoprene forms secondary organic aerosol through cloud processing: Model simulations. *Environ. Sci. Technol.*, **39 (12)**, 4441–4446.

Lim, Y., Y. Tan, M. Perri, S. Seitzinger, and B. Turpin, 2010: Aqueous chemistry and its role in secondary organic aerosol (SOA) formation. *Atmos. Chem. Phys.*, **10**, 10 521–10 539.

Lipsky, E., C. Stanier, S. Pandis, and A. Robinson, 2002: Effects of sampling conditions on the size distribution of fine particulate matter emitted from a pilot-scale pulverized-coal combustor. *Energy & fuels*, **16 (2)**, 302–310.

Liu, J. and D. L. Mauzerall, 2007: Potential influence of inter-continental transport of sulfate aerosols on air quality. *Environmental Research Letters*, **2 (4)**, 045 029.

Lohmann, U., 2002: A glaciation indirect aerosol effect caused by soot aerosols. *Geophys. Res. Lett.*, **29 (4)**, 11–1.

Lohmann, U. and J. Feichter, 2005: Global indirect aerosol effects: a review. *Atmos. Chem. Phys.*, **5 (5)**, 715–737.

Lovejoy, E., J. Curtius, and K. Froyd, 2004: Atmospheric ion-induced nucleation of sulfuric acid and water. *J. Geophys. Res.*, **109 (D8)**, D08 204.

Lundgren, K., 2006: Numerical simulation of the spatial and temporal distribution of sea salt particles on the regional scale. M.S. thesis, Department of Meteorology Stockholm University, Stockholm, Sweden.

Lundgren, K., 2010: Direct radiative effects of sea salt on the regional scale. Ph.D. thesis, Fakultät für Physik des Karlsruher Instituts für Technologie (KIT), Karlsruhe, Germany.

Mann, H., 1945: Nonparametric tests against trend. *Econometrica: Journal of the Econometric Society*, 245–259.

Marcolli, C., B. Luo, and T. Peter, 2004: Mixing of the organic aerosol fractions: Liquids as the thermodynamically stable phases. *J. Phys. Chem. A*, **108 (12)**, 2216–2224.

Mareckova, K., R. Wankmueller, M. Anderl, B. Muik, S. Poupa, and M. Wieser, 2008: Inventory review 2008. Emission Data reported under the LRTAP Convention and NEC directive. Stage 1 and 2 review. Status of gridded data. Tech. rep., CEIP - Centre on Emission Inventories and Projections. CEIP 1/2008.

Marticorena, B. and G. Bergametti, 1995: Modeling the atmospheric dust cycle: 1. design of a soil-derived dust emission scheme. *J. Geophys. Res.*, **100 (16)**, 415–16.

McKeen, S., et al., 2007: Evaluation of several $PM_{2.5}$ forecast models using data collected during the ICARTT/NEAQS 2004 field study. *J. Geophys. Res.*, **112 (D10)**, D10S20.

Meehl, G., et al., 2007: Global Climate Projections. Climate Change 2007: The Physical Basis, Contribution of Working Group I to the Fourth Assessment Report of the Intergovernmental Panel on Climate Change. Cambridge University Press, UK.

Metzger, S., F. Dentener, S. Pandis, and J. Lelieveld, 2002: Gas/aerosol partitioning: 1. a computationally efficient model. *J. Geophys. Res.*, **107 (10.1029)**.

Metzger, S., B. Steil, L. Xu, J. E. Penner, and J. Lelieveld, 2011: Description of EQSAM4: gas-liquid-solid partitioning model for global simulations. *Geoscientific Model Development Discussions*, **4 (4)**, 2791–2847, doi:10.5194/gmdd-4-2791-2011, URL `http://www.geosci-model-dev-discuss.net/4/2791/2011/`.

Minguillón, M., et al., 2011: Fossil versus contemporary sources of fine elemental and organic carbonaceous particulate matter during the DAURE campaign in Northeast Spain. *Atmos. Chem. Phys.*, **11**, 23 573–23 618.

Mlawer, E., S. Taubman, P. Brown, M. Iacono, and S. Clough, 1997: Radiative transfer for inhomogeneous atmospheres: RRTM, a validated correlated-k model for the longwave. *J. Geophys. Res.*, **102 (D14)**, 16 663–16.

Morcrette, J., H. Barker, J. Cole, M. Iacono, and R. Pincus, 2008: Impact of a new radiation package, McRad, in the ECMWF Integrated Forecasting System. *Mon. Weather Rev.*, **136 (12)**, 4773–4798.

Murphy, B., N. Donahue, C. Fountoukis, and S. Pandis, 2011: Simulating the oxygen content of ambient organic aerosol with the 2D volatility basis set. *Atmos. Chem. Phys.*, **11**, 7859–7873.

Nenes, A., S. Pandis, and C. Pilinis, 1998: ISORROPIA: A new thermodynamic equilibrium model for multiphase multicomponent inorganic aerosols. *Aquat. Geochem.*, **4 (1)**, 123–152.

Neu, J. and M. Prather, 2011: Toward a more physical representation of precipitation scavenging in global chemistry models: cloud overlap and ice physics and their impact on tropospheric ozone. *Atmos. Chem. Phys.*, **11**, 24 413–24 466.

Odum, J., T. Hoffmann, F. Bowman, D. Collins, R. Flagan, and J. Seinfeld, 1996: Gas/particle partitioning and secondary organic aerosol yields. *Environ. Sci. Technol.*, **30 (8)**, 2580–2585.

Orlanski, I., 1975: A rational subdivision of scales for atmospheric processes. *Bull. Am. Meteorol. Soc.*, **56 (5)**, 527–530.

Paatero, P. and U. Tapper, 1994: Positive matrix factorization: A non-negative factor model with optimal utilization of error estimates of data values. *Environmetrics*, **5 (2)**, 111–126.

Pankow, J., 1994: An absorption model of gas/particle partitioning of organic compounds in the atmosphere. *Atmos. Environ.*, **28 (2)**, 185–188.

Park, K., D. Kittelson, M. Zachariah, and P. McMurry, 2004: Measurement of inherent material density of nanoparticle agglomerates. *Journal of Nanoparticle Research*, **6 (2)**, 267–272.

Passant, N. R., 2002: Speciation of UK emissions of non-methane volatile organic compounds. Tech. rep., AEA Technology. AEAT/ENV/R/0545.

Paulot, F., J. Crounse, H. Kjaergaard, A. Kürten, J. St Clair, J. Seinfeld, and P. Wennberg, 2009: Unexpected epoxide formation in the gas-phase photooxidation of isoprene. *Science*, **325 (5941)**, 730.

Pearce, J., J. Beringer, N. Nicholls, R. Hyndman, and N. Tapper, 2010: Quantifying the influence of local meteorology on air quality using generalized additive modeling. *Atmos. Environ.*

Peters, T. M., R. W. Vanderpool, and R. W. Wiener, 2001: Design and Calibration of the EPA PM2.5 Well Impactor Ninety-Six (WINS). *Aerosol Sci. Technol.*, **34 (5)**, 389–397, doi:10.1080/02786820120352.

Pincus, R. and M. Baker, 1994: Effect of precipitation on the albedo susceptibility of clouds in the marine boundary layer. *Nature*, **372 (6503)**, 250–252.

Pitzer, K., 1973: Thermodynamics of electrolytes. I. Theoretical basis and general equations. *J. Phys. Chem.*, **77 (2)**, 268–277.

Platt, U. and F. Heintz, 1994: Nitrate radicals in tropospheric chemistry. *Israel Journal of Chemistry*, **34 (3-4)**, 289–300.

Poland, C., et al., 2008: Carbon nanotubes introduced into the abdominal cavity of mice show asbestos-like pathogenicity in a pilot study. *Nature nanotechnology*, **3 (7)**, 423–428.

Prank, M., M. Sofiev, H. van der Gon, M. Kaasik, T. Ruuskanen, and J. Kukkonen, 2010: A refinement of the emission data for kola peninsula based on inverse dispersion modelling. *Atmos. Chem. Phys.*, **10**, 10 849–10 865.

Price, C., J. Penner, and M. Prather, 1997: NO_x from lightning 1. Global distribution based on lightning physics. *J. Geophys. Res.*, **102 (D5)**, 5929–5941.

Pruppacher, H. and R. Jaenicke, 1995: The processing of water vapor and aerosols by atmospheric clouds, a global estimate. *Atmos. Res.*, **38 (1-4)**, 283–295.

Putaud, J., et al., 2004: A European aerosol phenomenology - 2: chemical characteristics of particulate matter at kerbside, urban, rural and background sites in Europe. *Atmos. Environ.*, **38 (16)**, 2579–2595.

Radhakrishnan, K., A. Hindmarsh, U. S. N. Aeronautics, and S. Administration, 1993: *Description and use of LSODE, the Livermore solver for ordinary differential equations*. National Aeronautics and Space Administration, Office of Management, Scientific and Technical Information Program.

Rasch, P., M. Barth, J. Kiehl, S. Schwartz, and C. Benkovitz, 2000: A description of the global sulfur cycle and its controlling processes in the National Center for Atmospheric Research Community Climate Model, Version 3. *J. Geophys. Res.*, **105 (D1)**, 1367–1385.

Reidy, B., et al., 2009: Comparison of models used for national agricultural ammonia emission inventories in europe: Litter-based manure systems. *Atmos. Environ.*, **43 (9)**, 1632–1640, cited By (since 1996): 2.

Riemer, N., 2002: Numerische Simulationen zur Wirkung des Aerosols auf die troposphärische Chemie und die Sichtweite. Ph.D. thesis, Fakultät für Physik - Universität Karlsruhe.

Riemer, N., H. Vogel, and B. Vogel, 2004: Soot aging time scales in polluted regions during day and night. *Atmos. Chem. Phys.*, **4 (7)**, 1885–1893.

Riemer, N., H. Vogel, B. Vogel, T. Anttila, A. Kiendler-Scharr, and T. Mentel, 2009a: Relative importance of organic coatings for the heterogeneous hydrolysis of N_2O_5 during summer in Europe. *J. Geophys. Res.*, **114 (D17)**, D17 307.

Riemer, N., H. Vogel, B. Vogel, and F. Fiedler, 2003a: Modeling aerosols on the mesoscale-γ: Treatment of soot aerosol and its radiative effects. *J. Geophys. Res.*, **108**, 4601.

Riemer, N., H. Vogel, B. Vogel, B. Schell, I. Ackermann, C. Kessler, and H. Hass, 2003b: Impact of the heterogeneous hydrolysis of N_2O_5 on chemistry and nitrate aerosol formation in the lower troposphere under photosmog conditions. *J. Geophys. Res.*, **108 (D4)**, 4144.

Riemer, N., M. West, R. Zaveri, and R. Easter, 2009b: Simulating the evolution of soot mixing state with a particle-resolved aerosol model. *J. Geophys. Res.*, **114 (D9)**, D09 202.

Rinke, R., 2008: Parametrisierung des Auswaschens von Aerosolpartikeln durch Niederschlag. Ph.D. thesis, Inst. für Meteorol. und Klimaforsch. der Univ. Karlsruhe (TH), Karlsruhe, Germany.

Ritter, B. and J. Geleyn, 1992: A comprehensive radiation scheme for numerical weather prediction models with potential applications in climate simulations. *Mon. Weather Rev.*, **120 (2)**, 303–325.

Robinson, A. L., et al., 2007: Rethinking organic aerosol: Semivolatile emissions and photochemical aging. *Science*, **315**.

Rockel, B., A. Will, and A. Hense, 2008: The regional climate model COSMO-CLM (CCLM). *Meteorol. Z.*, **17 (4)**, 347–348.

Rosenbrock, H., 1963: Some general implicit processes for the numerical solution of differential equations. *The Computer Journal*, **5 (4)**, 329.

Russell, A., A. Perring, L. Valin, E. Bucsela, E. Browne, K. Min, P. Wooldridge, and R. Cohen, 2011: A high spatial resolution retrieval of NO_2 column densities from OMI: method and evaluation. *Atmos. Chem. Phys.*, **11**, 8543–8554.

Sander, R., A. Kerkweg, P. Jöckel, and J. Lelieveld, 2005: Technical Note: The new comprehensive atmospheric chemistry module MECCA. *Atmos. Chem. Phys.*, **5**, 445–450.

Sandu, A. and R. Sander, 2006: Technical note: Simulating chemical systems in Fortran90 and Matlab with the Kinetic PreProcessor KPP-2.1. *Atmos. Chem. Phys.*, **6 (1)**, 187–195.

Sandu, A., J. Verwer, J. Blom, E. Spee, G. Carmichael, and F. Potra, 1997a: Benchmarking stiff ODE solvers for atmospheric chemistry problems II: Rosenbrock solvers. *Atmos. Environ.*, **31 (20)**, 3459–3472.

Sandu, A., J. Verwer, M. Van Loon, G. Carmichael, F. Potra, D. Dabdub, and J. Seinfeld, 1997b: Benchmarking stiff ODE solvers for atmospheric chemistry problems I: implicit vs explicit. *Atmos. Environ.*, **31 (19)**, 3151–3166.

Sausen, R., 2010: Global Chemistry-Climate Modelling with EMAC. *High Performance Computing in Science and Engineering, Garching/Munich 2009*, Springer, 663–674.

Schaap, M., R. Timmermans, M. Roemer, G. Boersen, P. Builtjes, F. Sauter, G. Velders, and J. Beck, 2008: The LOTOS-EUROS model: description, validation and latest developments. *International Journal of Environment and Pollution*, **32 (2)**, 270–290.

Schättler, U., 2009: A description of the nonhydrostatic regional COSMO-Model Part V. Preprocessing: Initial and boundary data for the COSMO-Model. Tech. rep., Deutscher Wetterdienst, Offenbach. Available at http://www.cosmo-model.org.

Schättler, U., G. Doms, and C. Schraff, 2008: A description of the nonhydrostatic regional COSMO-Model, Part VII: User's Guide. Tech. rep., Deutscher Wetterdienst, Offenbach.

Schell, B., I. Ackermann, H. Hass, F. Binkowski, and A. Ebel, 2001: Modeling the formation of secondary organic aerosol within a comprehensive air quality model system. *J. Geophys. Res.*, **106 (D 22)**, 28 275–28 293.

Schlünzen, K. and J. Katzfey, 2003: Relevance of sub-grid-scale land-use effects for mesoscale models. *Tellus A*, **55 (3)**, 232–246.

Schmidt, H., C. Derognat, R. Vautard, and M. Beekmann, 2001: A comparison of simulated and observed ozone mixing ratios for the summer of 1998 in Western Europe. *Atmos. Environ.*, **35 (36)**, 6277–6297.

Schumann, U. and H. Huntrieser, 2007: The global lightning-induced nitrogen oxides source. *Atmos. Chem. Phys.*, **7**, 3823–3907.

Seifert, A. and K. Beheng, 2006: A two-moment cloud microphysics parameterization for mixed-phase clouds. Part 1: Model description. *Meteorology and Atmospheric Physics*, **92 (1)**, 45–66.

Seinfeld, J. and S. Pandis, 2006: *Atmospheric chemistry and physics: from air pollution to climate change.* A Wiley-Intersciencie publications, Wiley.

Senior, C., L. Bool III, and J. Morency, 2000: Laboratory study of trace element vaporization from combustion of pulverized coal. *Fuel Processing Technology*, **63 (2-3)**, 109–124.

Sillman, S., 1995: The use of NO_y, H_2O_2, and HNO_3 as indicators for ozone-NO_x-hydrocarbon sensitivity in urban locations. *J. Geophys. Res.*, **100 (D7)**, 14 175–14.

Sillman, S. and D. He, 2002: Some theoretical results concerning O_3-NO_x-VOC chemistry and NO_x-VOC indicators. *J. Geophys. Res.*, **107 (10.1029)**.

Simmons, A., S. Uppala, D. Dee, and S. Kobayashi, 2007: ERA-Interim: New ECMWF reanalysis products from 1989 onwards. 25–35 pp., ECMWF Newsletter.

Skamarock, W. C., et al., 2008: A description of the Advanced Research WRF version 3. Tech. rep., NCAR Tech. Note NCAR/TN-475+ STR.

Slinn, W., 1984: Precipitation scavenging. *Atmospheric science and power production*, 466–532.

Sorooshian, A., et al., 2006: Oxalic acid in clear and cloudy atmospheres: Analysis of data from International Consortium for Atmospheric Research on Transport and Transformation 2004. *J. Geophys. Res., [Atmos.]*, **111**.

Spracklen, D. V., et al., 2010: Explaining global surface aerosol number concentrations in terms of primary emissions and particle formation. *Atmos. Chem. Phys.*, **10 (10)**, 4775–4793, doi:10.5194/acp-10-4775-2010.

Staehelin, J., A. Prévôt, and I. Barnes, 2000: *Handbuch der Umweltveränderungen und Oekotoxikologie–Atmosphäre*, chap. Photochemie der Troposphäre. Springer Verlag, Berlin.

Stanelle, T., B. Vogel, H. Vogel, D. Bäumer, and C. Kottmeier, 2010: Feedback between dust particles and atmospheric processes over West Africa during dust episodes in March 2006 and June 2007. *Atmos. Chem. Phys.*, **10 (22)**, 10 771–10 788, doi:10.5194/acp-10-10771-2010.

Steinbacher, M., C. Zellweger, B. Schwarzenbach, S. Bugmann, B. Buchmann, C. Ordonez, A. Prevot, and C. Hueglin, 2007: Nitrogen oxide measurements at rural sites in Switzerland: Bias of conventional measurement techniques. *J. Geophys. Res.*, **112 (D11)**, D11 307.

Stern, R., et al., 2008: A model inter-comparison study focussing on episodes with elevated PM_{10} concentrations. *Atmos. Environ.*, **42 (19)**, 4567–4588.

Stier, P., et al., 2005: The aerosol-climate model ECHAM5-HAM. *Atmos. Chem. Phys.*, **5 (4)**, 1125–1156.

Stockwell, W., P. Middleton, J. Chang, and X. Tang, 1990: The second generation regional acid deposition model chemical mechanism for regional air quality modeling. *J. Geophys. Res.*, **95 (D10)**, 16 343.

Stokes, R. and R. Robinson, 1966: Interactions in aqueous nonelectrolyte solutions. I. Solute-solvent equilibria. *J. Phys. Chem.*, **70 (7)**, 2126–2131.

Suklitsch, M., A. Gobiet, A. Leuprecht, and C. Frei, 2008: High resolution sensitivity studies with the regional climate model CCLM in the Alpine Region. *Meteorol. Z.*, **17 (4)**, 467–476.

Tang, I. and H. Munkelwitz, 1993: Composition and temperature dependence of the deliquescence properties of hygroscopic aerosols. *Atmos. Environ.*, **27 (4)**, 467–473.

Tang, I. N., 1997: Thermodynamic and optical properties of mixed-salt aerosols of atmospheric importance. *J. Geophys. Res.*, **102 (D2)**, 1883–1893.

Theloke, J. and R. Friedrich, 2007: Compilation of a database on the composition of anthropogenic VOC emissions for atmospheric modeling in Europe. *Atmos. Environ.*, **41 (19)**, 4148–4160.

Tost, H., P. Jöckel, A. Kerkweg, R. Sander, and J. Lelieveld, 2006: Technical note: A new comprehensive SCAVenging submodel for global atmospheric chemistry modelling. *Atmos. Chem. Phys.*, **6**, 565–574.

Tuovinen, J., T. Laurila, H. Lattila, A. Ryaboshapko, P. Brukhanov, and S. Korolev, 1993: Impact of the sulphur dioxide sources in the Kola Peninsula on air quality in northernmost Europe. *Atmos. Environ.*, **27 (9)**, 1379–1395.

Turpin, B., P. Saxena, and E. Andrews, 2000: Measuring and simulating particulate organics in the atmosphere: problems and prospects. *Atmos. Environ.*, **34 (18)**, 2983–3013.

Twomey, S., 1974: Pollution and the planetary albedo. *Atmos. Environ.*, **8 (12)**, 1251–1256.

Uppala, S., et al., 2005: The ERA-40 re-analysis. *Q. J. R. Meteorol. Soc.*, **131 (612)**, 2961–3012.

Vaden, T. D., D. Imre, J. Beránek, M. Shrivastava, and A. Zelenyuk, 2011: Evaporation kinetics and phase of laboratory and ambient secondary organic aerosol. *Proc. Natl. Acad. Sci. U. S. A.*, **108 (6)**, 2190–2195, doi:10.1073/pnas.1013391108.

van der Werf, G. R., et al., 2010: Global fire emissions and the contribution of deforestation, savanna, forest, agricultural, and peat fires (1997-2009). *Atmos. Chem. Phys.*, **10 (23)**, 11 707–11 735, doi:10.5194/acp-10-11707-2010, URL `http://www.atmos-chem-phys.net/10/11707/2010/`.

Vautard, R., M. Beekmann, J. Roux, and D. Gombert, 2001: Validation of a hybrid forecasting system for the ozone concentrations over the Paris area. *Atmos. Environ.*, **35 (14)**, 2449–2461.

Vautard, R., et al., 2003: Paris emission inventory diagnostics from ESQUIF airborne measurements and a chemistry transport model. *J. Geophys. Res.*, **108 (D17)**, 8564.

Vautard, R., et al., 2007: Evaluation and intercomparison of Ozone and PM_{10} simulations by several chemistry transport models over four European cities within the CityDelta project. *Atmos. Environ.*, **41 (1)**, 173–188.

Vestreng, V., G. Myhre, H. Fagerli, S. Reis, and L. Tarrasón, 2007: Twenty-five years of continuous sulphur dioxide emission reduction in Europe. *Atmos. Chem. Phys.*, **7 (13)**, 3663–3681, doi:10.5194/acp-7-3663-2007, URL `http://www.atmos-chem-phys.net/7/3663/2007/`.

Vestreng, V., L. Ntziachristos, A. Semb, S. Reis, I. S. A. Isaksen, and L. Tarrasón, 2009: Evolution of NO_x emissions in Europe with focus on road transport control measures. *Atmos. Chem. Phys.*, **9 (4)**, 1503–1520, doi:10.5194/acp-9-1503-2009, URL `http://www.atmos-chem-phys.net/9/1503/2009/`.

Vignati, E., J. Wilson, and P. Stier, 2004: M7: An efficient size-resolved aerosol microphysics module for large-scale aerosol transport models. *J. Geophys. Res.*, **109 (D22)**.

Visschedijk, A., P. Zandveld, and H. Denier van der Gon, 2007: High resolution gridded European emission database for the EU Integrate Project GEMS. TNO-report 2007-A-R0233/B, TNO.

Vogel, B., F. Fiedler, and H. Vogel, 1995: Influence of topography and biogenic volatile organic compounds emission in the state of Baden-Württemberg on ozone concentrations during episodes of high air temperatures. *J. Geophys. Res.*, **100 (D11)**, 22 907.

Vogel, B., C. Hoose, H. Vogel, and C. Kottmeier, 2006: A model of dust transport applied to the Dead Sea area. *Meteorol. Z.*, **15 (6)**, 611–624.

Vogel, B., H. Vogel, D. Bäumer, M. Bangert, K. Lundgren, R. Rinke, and T. Stanelle, 2009: The comprehensive model system COSMO-ART–Radiative impact of aerosol on the state of the atmosphere on the regional scale. *Atmos. Chem. Phys.*, **9**, 8661–8680.

Volkamer, R., et al., 2006: Secondary organic aerosol formation from anthropogenic air pollution: Rapid and higher than expected. *Geophys. Res. Lett.*, **33**, 17.

Wagstrom, K. and S. Pandis, 2011: Contribution of Long Range Transport to Local Fine Particulate Matter Concerns. *Atmos. Environ.*

Walcek, C. and G. Taylor, 1986: A theoretical method for computing vertical distributions of acidity and sulfate production within cumulus clouds. *J. Atmos. Sci.*, **43 (4)**, 339–355.

Wang, C., J. J. Corbett, and J. Firestone, 2008: Improving Spatial Representation of Global Ship Emissions Inventories. *Environ. Sci. Technol.*, **42 (1)**, 193–199, doi:10.1021/es0700799.

Weisman, M. and J. Klemp, 1982: The dependence of numerically simulated convective storms on vertical wind shear and buoyancy. *Mon. Weather Rev.*, **110 (6)**, 504–520.

Went, F., 1960: Organic matter in the atmosphere, and its possible relation to petroleum formation. *Proc. Natl. Acad. Sci. U. S. A.*, **46 (2)**, 212.

Wexler, A. and S. Clegg, 2002: Atmospheric aerosol models for systems including the ions H^+, NH_4^+, Na^+, SO_4^{2-}, NO_3^-, Cl^-, Br^-, and H_2O. *J. Geophys. Res.*, **107 (10.1029)**.

Wexler, A. and J. Seinfeld, 1991: Second-generation inorganic aerosol model. *Atmos. Environ.*, **25 (12)**, 2731–2748.

Whitby, E. and P. McMurry, 1997: Modal aerosol dynamics modeling. *Aerosol Sci. Technol.*, **27 (6)**, 673–688.

Wichmann, H.-E., C. Spix, T. Tuch, G. Wölke, A. Peters, J. Heinrich, W. G. Kreyling, and J. Heyder, 2000: Daily mortality and fine and ultrafine particles in Erfurt, Germany. Part I: Role of particle number and particle mass. Research report 98, Health Effects Institute.

Wiedensohler, A., et al., 2010: Particle mobility size spectrometers: harmonization of technical standards and data structure to facilitate high quality long-term observations of atmospheric particle number size distributions. *Atmos. Meas. Tech.*, **3 (6)**, 5521–5587, doi:10.5194/amtd-3-5521-2010.

WMO, 2010: Manual on codes, International Codes, Volume I.2. Tech. Rep. 306, World meteorological organization, Geneva, Switzerland.

Wolke, R., O. Knoth, O. Hellmuth, W. Schroder, and J. Weickert, 2001: Load-balancing in the parallel model system LM-MUSCAT for multiscale chemistry-transport simulations. *Proceedings of the 5-th GLOREAM Workshop, Wengen (Switzerland, September 2001).*

Wurzler, S., T. Reisin, and Z. Levin, 2000: Modification of mineral dust particles by cloud processing and subsequent effects on drop size distributions. *J. Geophys. Res.*, **105 (D4)**, 4501–4512.

Yarwood, G., S. Rao, M. Yocke, and G. Whitten, 2005: Updates to the carbon bond chemical mechanism: CB05. Final report to the US EPA, RT-0400675, US EPA.

Yin, Y., D. J. Parker, and K. S. Carslaw, 2001: Simulation of trace gas redistribution by convective clouds - Liquid phase processes. *Atmos. Chem. Phys.*, **1 (1)**, 19–36, doi:10.5194/acp-1-19-2001, URL `http://www.atmos-chem-phys.net/1/19/2001/`.

Zaveri, R., R. Easter, J. Fast, and L. Peters, 2008: Model for simulating aerosol interactions and chemistry (MOSAIC). *J. Geophys. Res.*, **113**, D13 204.

Zaveri, R., R. Easter, and L. Peters, 2005a: A computationally efficient multicomponent equilibrium solver for aerosols (MESA). *J. Geophys. Res.*, **110 (D24)**, D24 203.

Zaveri, R., R. Easter, and A. Wexler, 2005b: A new method for multicomponent activity coefficients of electrolytes in aqueous atmospheric aerosols. *J. Geophys. Res.*, **110 (D2)**, D02 201.

Zhang, K. and A. Wexler, 2002: A hypothesis for growth of fresh atmospheric nuclei. *J. Geophys. Res.*, **107 (D21)**, 4577.

Zhang, Q., M. Alfarra, D. Worsnop, J. Allan, H. Coe, M. Canagaratna, and J. Jimenez, 2005a: Deconvolution and quantification of hydrocarbon-like and oxygenated organic aerosols based on aerosol mass spectrometry. *Environ. Sci. Technol.*, **39 (13)**, 4938–4952.

Zhang, Q., D. Worsnop, M. Canagaratna, and J. Jimenez, 2005b: Hydrocarbon-like and oxygenated organic aerosols in Pittsburgh: Insights into sources and processes of organic aerosols. *Atmos. Chem. Phys.*, **5**, 3289–3311.

Zhang, Q., et al., 2007: Ubiquity and dominance of oxygenated species in organic aerosols in anthropogenically-influenced Northern Hemisphere midlatitudes. *Geophys. Res. Lett.*, **34 (13)**, L13 801.

Zhang, Y., 2008: Online-coupled meteorology and chemistry models: history, current status, and outlook. *Atmos. Chem. Phys.*, **8 (11)**, 2895–2932, URL `http://www.atmos-chem-phys.net/8/2895/2008/`.

Zhang, Y., S. Kreidenweis, and G. Feingold, 1999: Stratocumulus processing of gases and cloud condensation nuclei 2. Chemistry sensitivity analysis. *J. Geophys. Res.*, **104 (D13)**, 16 061–16.

Zhang, Y., Y. Pan, K. Wang, J. Fast, and G. Grell, 2010: WRF/Chem-MADRID: Incorporation of an aerosol module into WRF/Chem and its initial application to the TexAQS2000 episode. *J. Geophys. Res.*, **115 (D18)**, D18 202.

Zhang, Y., S. Wu, S. Krishnan, K. Wang, A. Queen, V. Aneja, and S. Arya, 2008: Modeling agricultural air quality: Current status, major challenges, and outlook. *Atmos. Environ.*, **42 (14)**, 3218–3237.

Zhao, M. and P. Austin, 2005: Life Cycle of Numerically Simulated Shallow Cumulus Clouds. Part I: Transport. *J. Atmos. Sci.*, **62 (5)**, 1269–1290.

Zhou, Y., D. Brunner, K. Boersma, R. Dirksen, and P. Wang, 2009: An improved tropospheric NO_2 retrieval for OMI observations in the vicinity of mountainous terrain. *Atmos. Meas. Tech.*, **2**, 401–416.

Zhou, Y., D. Brunner, C. Hueglin, S. Henne, and J. Staehelin, 2011: Changes in OMI tropospheric NO_2 columns over Europe from 2004 to 2009 and the influence of meteorological variability. *Atmos. Environ.*

Zhou, Y., D. Brunner, R. J. D. Spurr, K. F. Boersma, M. Sneep, C. Popp, and B. Buchmann, 2010: Accounting for surface reflectance anisotropy in satellite retrievals of tropospheric NO_2. *Atmos. Meas. Tech.*, **3 (5)**, 1185–1203, doi:10.5194/amt-3-1185-2010.

Zimmermann, F., H. Lux, W. Maenhaut, J. Matschullat, K. Plessow, F. Reuter, and O. Wienhaus, 2003: A review of air pollution and atmospheric deposition dynamics in southern Saxony, Germany, Central Europe. *Atmos. Environ.*, **37 (5)**, 671–691.

Zuend, A., C. Marcolli, B. Luo, and T. Peter, 2008: A thermodynamic model of mixed organic-inorganic aerosols to predict activity coefficients. *Atmos. Chem. Phys.*, **8**, 4559–4593.

Curriculum vitae

Christoph Knote
born 13 January 1981 in Weiden i. d. Opf., Germany

Education

01/2009-02/2012	PhD student at Empa, Laboratory for Air Pollution / Env. Technology, Dübendorf, Switzerland, under supervision of Dr. Dominik Brunner and Prof. Dr. Ulrike Lohmann. PhD thesis within the Center for Climate Systems Modeling (C_2SM), a collaboration with the Institute for Atmospheric and Climate sciences at ETH Zürich, MeteoSwiss and Agroscope Tänikon/Reckenholz.
05/2004-12/2008	Applied Environmental Sciences (German Diploma) at Universtät Trier, Germany. Diploma thesis written at GKSS Forschungszentrum Geesthacht, Germany, supervised by Dr. Burkhardt Rockel and Prof. Dr. Günther Heinemann.
10/2001-08/2003	Political Sciences (M. A.) at Ludwig-Maximilian Universität München, Germany, until intermediate examination.
07/2000-05/2001	Civilian Service at Malteser Hilfsdienst, Weiden, Germany.
06/2000	Abitur (german university entrance qualification), Augustinus Gymnasium Weiden, Germany.

Conferences, workshops and summer schools

10/2011	CMAS annual conference (presentation), Chapel Hill (NC), United States of America
10/2011	PhD symposium (poster), Empa, St. Gallen, Switzerland
09/2011	European aerosol conference (presentation), Manchester, United Kingdom
05/2011	EMEP TFMM meeting (presentation), Empa, Dübendorf, Switzerland
01/2011	Scalable performance analysis tools for HPC applications (workshop),ETH Zürich, Switzerland
01/2011	GLOREAM-EURASAP air quality workshop (presentation), Copenhagen, Denmark

12/2010	Multi-threaded programming, tuning and optimization on multi-core MPP platforms (workshop), EPFL, Lausanne, Switzerland
12/2010	C_2SM COSMO user workshop (presentation), ETH Zürich, Switzerland
10/2010	PhD symposium (presentation), Empa, Dübendorf, Switzerland
09/2010	International Aerosol Conference (poster), Helsinki, Finland
07/2010	International Global Atmospheric Chemistry conference (poster), Halifax, Canada
06/2010	Aerosol train (workshop), PSI, Villigen, Switzerland
05/2010	UPC and CAF, Parallel programming workshop, HLRS, Stuttgart, Germany
11/2009	PhD Symposium (poster), Empa, Dübendorf, Switzerland
10/2009	CLIMPOL interdisciplinary PhD colloquium (presentation), ETH Zürich, Switzerland
08/2009	Parallel programming workshop, CSCS, Manno (TI), Switzerland
08/2009	IfT summer school on aerosols and climate, Rabenberg, Germany

Publications

Knote, C., Brunner, D., Vogel, H., Allan, J., Asmi, A., Äijälä, M., Carbone, S., van der Gon, H. D., Jimenez, J. L., Kiendler-Scharr, A., Mohr, C., Poulain, L., Prévôt, A. S. H., Swietlicki, E., and Vogel, B., 2011: Towards an online-coupled chemistryclimate model: evaluation of trace gases and aerosols in COSMO-ART, Geosci. Model Dev., 4, 1077-1102, http://dx.doi.org/10.5194/gmd-4-1077-2011.

Knote, C., G. Heinemann and B. Rockel, 2010: Changes in weather extremes: Assessment of return values using high resolution climate simulations at convection resolving scale. Meteorologische Zeitschrift, 19 (1), 11-23, http://dx.doi.org/10.1127/0941-2948/2010/0424.

Knote, C., G. Bonafé, and F. Di Giuseppe, 2009: Leaf Area Index Specification for Use in Mesoscale Weather Prediction Systems, Monthly Weather Review, 137, 3535-3550, http://dx.doi.org/10.1175%2F2009MWR2891.1.

Acknowledgments

First of all I am grateful to my supervisor Dominik Brunner, who has provided unconditional support for my work and ideas. Discussions with him and his suggestions have always proven to be most fruitful. Ulrike Lohmann is thanked for her supervision during my thesis and the interest in my work. Martijn Schaap kindly agreed to act as external co-examiner. I am grateful to Brigitte Buchmann, head of our section, who was always very supportive and created a very comfortable working atmosphere. It has been instrumental for my thesis to have a good collaboration with Heike and Bernhard Vogel at KIT Karlsruhe, and also the other members of the Vogel group, which I am also very thankful for. Stephan Henne is kindly acknowledge for the answers to thousands of small questions that came during the course of my thesis, and for fruitful discussions as well. Oliver Fuhrer and Pirmin Kaufmann of MeteoSwiss were always willing to provide help with the model or observation data. Finally thanks to my office colleagues over time, Christoph, Roman, Yipin, Patrick, as well as my fellow doctoral students Christoph, Matthias and Steven.